UNIVERSIDADE FEDERAL DO CEARÁ
CENTRO DE CIÊNCIAS
DEPARTAMENTO DE BIOQUÍMICA E BIOLOGIA MOLECULAR
PROGRAMA DE PÓS-GRADUAÇÃO EM BIOQUÍMICA

VALÉRIA FREITAS LIMA

UNDERSTANDING THE REGULATION OF PLANT PRIMARY METABOLISM BY INTEGRATING METABOLOMICS AND PHYSIOLOGICAL APPROACHES

FORTALEZA
2023

VALÉRIA FREITAS LIMA

UNDERSTANDING THE REGULATION OF PLANT PRIMARY METABOLISM BY INTEGRATING METABOLOMICS AND PHYSIOLOGICAL APPROACHES

Thesis presented to the Graduate Program in Biochemistry of the Federal University of Ceará and to the Doctoral Programme in Plant Biology of the University of the Balearic Islands as part of the requirements to obtain the title of Doctor in Biochemistry and Doctor of Philosophy, respectively, as a partnership agreement between both universities covering a program for the joint supervision. Field of research: Plant Science.

Supervisors: Prof. Dr. Danilo de Menezes Daloso; Prof. Dr. Jorge Gago Mariño.

FORTALEZA

2023

Dados Internacionais de Catalogação na Publicação
Universidade Federal do Ceará
Sistema de Bibliotecas
Gerada automaticamente pelo módulo Catalog, mediante os dados fornecidos pelo(a) autor(a)

L711u Lima, Valéria Freitas.
Understanding the regulation of plant primary metabolism by integrating metabolomics and physiological approaches / Valéria Freitas Lima. – 2023.
212 f. : il. color.

Tese (doutorado) – Universidade Federal do Ceará, Centro de Ciências, Programa de Pós-Graduação em Bioquímica , Fortaleza, 2023.
Orientação: Prof. Dr. Danilo de Menezes Daloso.
Coorientação: Prof. Dr. Jorge Gago Mariño.

1. 13C-metabolic flux analysis. 2. Guard cells. 3. Mass spectrometry. 4. Metabolic regulation. 5. Metabolomics. I. Título.

CDD 572

VALÉRIA FREITAS LIMA

UNDERSTANDING THE REGULATION OF PLANT PRIMARY METABOLISM BY INTEGRATING METABOLOMICS AND PHYSIOLOGICAL APPROACHES

Thesis presented to the Graduate Program in Biochemistry of the Federal University of Ceará and to the Doctoral Programme in Plant Biology of the University of the Balearic Islands as part of the requirements to obtain the title of Doctor in Biochemistry and Doctor of Philosophy, respectively, as a partnership agreement between both universities covering a program for the joint supervision. Field of research: Plant Science.

Accepted on 31 Aug. 2023

OPPONENTS

_____

Prof. Dr. Danilo de Menezes Daloso (Supervisor)
Universidade Federal do Ceará (UFC)

_____

Prof. Dr. Joaquim Albenísio Gomes da Silveira
Universidade Federal do Ceará (UFC)

_____

Prof. Dr. Humberto Henrique de Carvalho
Universidade Federal do Ceará (UFC)

_____

Dra. Ana Karla Moreira Lobo
Lancaster University (LU-UK)

_____

Dra. Rachel Hellen Vieira de Sousa Lima
Universidade Federal do Cariri (UFCA)

To my family

ACKNOWLEDGMENTS

This study was financed in part by the Brazilian Federal Agency for Support and Evaluation of Graduate Education (CAPES-Brazil) – Finance Code 001. This work was also supported by the MCIN/AEI (Spain, project PID2019-107434GA-100).

Thanks to the Federal University of Ceará (Universidade Federal do Ceará - UFC), especially to the Graduate Program in Biochemistry and the Department of Biochemistry and Molecular Biology. Also, thanks to the University of the Balearic Islands (Universitat de les Illes Balears - UIB), specially to the research group on Plant Biology under Mediterranean Conditions. Thanks for providing the necessary resources, facilities, and a conducive research environment. Their administrative support and academic resources have been essential in the pursuit of my research goals.

More importantly, my thesis was only made possible due to the invaluable help and involvement of friends, colleagues, and other notable people from both sides of the Atlantic Ocean.

I am immensely grateful to all my supervisors, whose pivotal and dedicated involvement extended far beyond the responsibilities of mere guidance. I consider myself fortunate to have had their support throughout my PhD journey.

I would like to express my deepest gratitude to my supervisor, **Danilo Daloso**, for his invaluable guidance throughout my master and doctoral journey. In addition to the enriching conversations, laughs shared amid academic stress, beers and barbecues, his dedication, expertise and unconditional support were essential in shaping the direction of my research and fostering my academic and personal growth. I am also truly grateful for his commitment and encouragement in my “drama” moments. All of this, propelled me to overcome challenges and move forward. Therefore, his willingness to be there not just as a supervisor, but as a friend, made this academic journey even more special and memorable. I've learned a lot from you. Thank you so much for everything!

I would also like to extend my heartfelt appreciation to my Spain supervisor, **Xurxo Gago**, for their collaboration and invaluable contributions to my research since my master. Thanks for promptly and kindly accepting me in his group. The opportunity to engage in a cotutela under his supervision has enriched my academic experience, provided me with a broader international perspective, and gave me the chance of living a dream, which was living in the Mallorca’s Paradise.

I would like to extend my sincere gratitude to my friends in the lab at Brazil, **LabPlant**. Specially to Rikaely, Bruno, Eva, Vicente, Silvio, Paulo, Danny, Raissa, Raysa, Nicole, Ricardo, Analu, Ana Karla and Fabrício. Their camaraderie, intellectual discussions, and shared experiences have made the research environment enjoyable and stimulating. Their support and collaboration have been instrumental in the successful completion of this Thesis.

I am also indebted to my friends in the lab at Spain, **Ca'n Boom**. Thanks to Maria Sueiro, Miquel Angel, Pere A, Dino, Pedro, Aina, Toni Joseph, Pere Miquel, and specially to my dear Neus Cubo and Joan Pons. Their friendship, scientific insights during coffee time, and cultural exchange have enriched my research experience and broadened my horizons. I am grateful for their camaraderie, collaboration, and unwavering support. A tots vosaltres, moltes gràcies!

I extend my heartfelt gratitude to all co-authors who collaborated on the publications I during my PhD journey, with special acknowledgment to those whose work is included in this Thesis.

Last but not least, I am immensely thankful to **my family** for their unconditional love, encouragement, and unwavering support. First, my parents Auxiliadora (*Mãe*) and Alberto (*Pai*). Their constant belief in me and their sacrifices have been a source of motivation throughout my doctoral journey. Also, thanks to all my relatives, especially my brothers Lucas and Sylvio. I am grateful for their understanding, patience, and presence in my life. I love you all. I extend my deep appreciation to Roberto for all his support and understanding. His constant presence and encouragement words were essential for me to face challenges with courage and determination. His affection and understanding in moments of stress were a true refuge, and I am forever grateful for having you in my life.

Finally, I would like to express my gratitude to **God** for His blessings, guidance, and strength throughout this journey. His unwavering presence and faithfulness have been a source of inspiration and motivation in overcoming challenges and pursuing excellence.

I am sincerely grateful to all those mentioned above and to countless others who have contributed to my academic and personal growth. Their support and encouragement have been invaluable, and I am truly humbled and thankful for their presence in my life.

“If I have seen further, it is by standing on the shoulders of giants.”

(Isaac Newton)

RESUMO

Nos últimos anos, a pesquisa sobre a regulação metabólica das plantas avançou consideravelmente graças à metabolômica, especialmente com o desenvolvimento da ^{13}C-análise de fluxo metabólico (^{13}C-MFA). Apesar dos avanços significativos, o mapeamento preciso dos padrões de fluxo metabólico *in vivo* ainda é um desafio. Enquanto as abordagens baseadas em ressonância magnética nuclear elucidaram redes metabólicas pequenas com grande precisão, os métodos com espectrometria de massas foram prejudicados pela falta de informação posicional a nível atômico. Esta Tese aborda essa limitação através de uma nova abordagem que utiliza cromatografia gasosa (GC) acoplada à espectrometria de massas (MS) para determinar com precisão a marcação ^{13}C-posicional em metabólitos chave do metabolismo central. Esta abordagem, validada com substâncias de referência marcadas posicionalmente com ^{13}C via GC-impacto eletrônico-MS e GC-ionização química a pressão atmosférica-MS, demonstrou eficácia na análise de dados prévios de ^{13}C-MFA em folhas e células-guarda. Novas informações foram obtidas sobre a glicose, revelando que seus átomos de carbono são preferencialmente marcados pela fotossíntese e gliconeogênese. Além disso, foi estabelecida uma plataforma para investigar a incorporação de ^{13}C em malato e glutamato derivados da enzima fosfo*enol*piruvato carboxilase (PEPc). Nossos resultados revelaram que a gliconeogênese e a assimilação de CO_2 mediada por PEPc em malato são ativadas de maneira independente à luz nas células-guarda, enquanto que os fluxos de glicólise e PEPc em direção ao glutamato são restringidos pelo sistema de tiorredoxina mitocondrial em folhas iluminadas. Também exploramos a dinâmica metabólica das células-guarda após a assimilação de CO_2 mediada por PEPc, tanto no escuro quanto durante a transição do escuro para a luz. Embora as mudanças metabólicas tenham sido consistentes de modo geral, a influência da luz nas estruturas da rede metabólica foi evidente, resultando em um aumento do enriquecimento de ^{13}C em açúcares e metabólitos associados ao ciclo do ácido tricarboxílico (TCA). Além disso, dada a influência do clima nas plantas em todo o mundo, também investigamos os efeitos da seca, altas temperaturas e alta concentração de CO_2 em uma samambaia (*Nephrolepis exaltata*) e uma angiosperma típica, *Brassica oleracea*. Enquanto *B. oleracea* mostrou respostas fisiológicas significativas à alta concentração de CO_2, independentemente de outras condições de estresse, *N. exaltata* exibiu uma resposta limitada a todos os estresses a nível fisiológico. Os níveis de lipídios e metabólitos primários em *B. oleracea* mudaram em resposta ao estresse, o que não ocorreu na *N. exaltata*. Nossos resultados sugerem que as mudanças climáticas impactam diferencialmente samambaias e angiospermas. Em resumo, a integração de análises

metabolômicas e fisiológicas proporciona uma visão detalhada dos mecanismos subjacentes à regulação e adaptação metabólica das plantas. Estas abordagens não apenas oferecem estratégias inovadoras para a análise metabolômica, mas também contribuem para o entendimento das respostas ambientais das plantas, de diferentes grupos, em um mundo em constante mudança climática.

Palavras-chave: ^{13}C-análise de fluxo metabólico; células-guarda; espectrometria de massas; metabolômica; regulação metabólica.

ABSTRACT

In recent years, research on the plant metabolic regulation has significantly advanced thanks to metabolomics, mainly by the emergence of ^{13}C-metabolic flux analysis (^{13}C-MFA), which is revealing complex network patterns of metabolic pathways. Despite significant progress, accurately mapping patterns of *in vivo* metabolic flux remains challenging. While approaches based on nuclear magnetic resonance have resolved small networks with high accuracy, mass spectrometry methods have been hindered by the lack of atomic-level positional information. This Thesis addresses this limitation through an establishment of a novel approach using gas chromatography (GC) coupled with mass spectrometry (MS) to precisely determine ^{13}C-positional labeling in key metabolites of central metabolism. Validated with reference substances positionally labeled with ^{13}C via GC-electron impact-MS and GC-atmospheric pressure chemical ionization-MS, this approach showcases efficacy in analyzing previous ^{13}C-MFA data in leaves and guard cells. New insights were obtained into glucose, which has carbon atoms preferentially labeled by photosynthesis and gluconeogenesis. Additionally, we provide a platform to investigate ^{13}C-incorporation into malate and glutamate derived from phosphoenolpyruvate carboxylase (PEPc). Our findings revealed that gluconeogenesis and PEPc-mediated CO_2 assimilation into malate are activated in a light-independent manner in guard cells, while fluxes from glycolysis and PEPc towards glutamate are restricted by the mitochondrial thioredoxin system in illuminated leaves. We also explored the metabolic dynamics of guard cells after PEPc-mediated CO_2 assimilation, under darkness or during dark-to-light transition. Although metabolic changes were largely consistent between dark-exposed and illuminated guard cells, the influence of light on metabolic network structures was evidenced by increased ^{13}C-enrichment in sugars and metabolites associated with the tricarboxylic acid (TCA) cycle. Additionally, given the impact of climate change on plants performance worldwide, we investigated the effects of drought, high temperatures, and high CO_2 concentration on a fern (*Nephrolepis exaltata*) and a typical angiosperm, *Brassica oleracea*. While *B. oleracea* exhibited significant physiological responses to high CO_2 concentration, independent of other stress conditions, the fern was mostly unresponsive to all stresses at the physiological level. Lipid and primary metabolite levels in *B. oleracea* changed in response to stress, whereas these metabolic responses were absent in the fern. Our findings suggest differential impacts of climate change on ferns and angiosperms. Collectively, the integration of metabolomics and physiological analyses used in our studies provides comprehensive insights into mechanisms underlying plant metabolic regulation and adaptation,

offering innovative strategies for metabolomics analysis and contributing to knowledge of the environmental responses of plants, from different groups, to the conditions of a world undergoing climate change.

Keywords: guard cells; mass spectrometry; metabolic regulation; ^{13}C-metabolic flux analysis; metabolomics.

RESUMEN

En los últimos años, la investigación de la regulación metabólica de las plantas ha avanzado notablemente gracias a la metabolómica, especialmente con el desarrollo del ^{13}C-análisis de flujo metabólico (^{13}C-MFA). A pesar de los avances significativos, el mapeo preciso de los patrones de flujo metabólico *in vivo* sigue siendo un desafío. Mientras que los enfoques basados en la resonancia magnética nuclear han resuelto redes pequeñas con gran precisión, los métodos de espectrometría de masas se han visto obstaculizados por la falta de información posicional a nivel atómico. Esta Tesis aborda esta limitación mediante un nuevo enfoque que utiliza cromatografía de gases (GC) acoplada a la espectrometría de masas (MS) para determinar con precisión el marcado ^{13}C-posicional en metabolitos clave del metabolismo central. Este enfoque, validado con sustancias de referencia marcadas posicionalmente con ^{13}C vía GC-impacto electrónico-MS y GC-ionización química a presión atmosférica-MS, ha demostrado eficacia en el análisis de datos previos de ^{13}C-MFA en hojas y células guardas. Se ha obtenido información novedosa sobre la glucosa, revelando que sus átomos de carbono son preferentemente marcados por la fotosíntesis y la gluconeogénesis. Además, se ha establecido una plataforma para investigar la incorporación de ^{13}C en malato y glutamato derivados de la enzima fosfoenolpiruvato carboxilasa (PEPc). Nuestros resultados revelaron que la gluconeogénesis y la asimilación de CO_2 mediada por PEPc en malato se activan de manera independiente a la luz en las células guardas, mientras que los flujos de glucólisis y PEPc hacia el glutamato están restringidos por el sistema de tiorredoxina mitocondrial en hojas iluminadas. También exploramos la dinámica metabólica de las células guardas, después de la asimilación de CO_2 mediada por PEPc, tanto en la oscuridad como durante la transición de la oscuridad a la luz. Aunque los cambios metabólicos fueron mayormente consistentes en general, se evidenció la influencia de la luz en las estructuras de la red metabólica, resultando en un aumento del enriquecimiento de ^{13}C en azúcares y metabolitos asociados al ciclo del ácido tricarboxílico (TCA). Además, dado que el cambio climático está afectando el rendimiento de las plantas en todo el mundo, también investigamos los efectos de la sequía, altas temperaturas y alta concentración de CO_2 en un helecho (*Nephrolepis exaltata*) y una angiosperma típica, *Brassica oleracea*. Mientras que *B. oleracea* mostró respuestas fisiológicas significativas a la alta concentración de CO_2, independientemente de otras condiciones de estrés, el helecho exhibió una respuesta limitada a todos los estreses a nivel fisiológico. Los niveles de lípidos y metabolitos primarios en *B. oleracea* cambiaron inducidos por estrés, lo que no sucedió en el helecho. Nuestros hallazgos sugieren impactos diferenciales del cambio climático en helechos

y angiospermas. En resumen, la integración de análisis metabolómicos y fisiológicos proporciona una visión detallada de los mecanismos subyacentes a la regulación y adaptación metabólica de las plantas. Este enfoque no solo ofrece estrategias innovadoras para el análisis metabolómico, sino que también contribuye al entendimiento de las respuestas ambientales de las plantas, de diferentes grupos, en un mundo en constante cambio climático.

Palabras clave: ^{13}C-análisis de flujo metabólico; células guarda; espectrometría de masas, metabolómica; regulación metabólica.

RESUM

En els darrers anys, la recerca sobre la regulació metabòlica de les plantes ha avançat notablement gràcies a la metabolòmica, especialment amb el desenvolupament de l'anàlisi de flux metabòlic amb carboni-13 (^{13}C-MFA). Malgrat els avenços significatius, el mapeig precís dels patrons de flux metabòlic *in vivo* continua sent un repte. Mentre que els enfocaments basats en la resonància magnètica nuclear han resolt xarxes petites amb gran precisió, els mètodes d'espectrometria de masses s'han vist obstaculitzats per la manca d'informació posicional a nivell atòmic. Aquesta tesi aborda aquesta limitació mitjançant un nou enfocament que utilitza la cromatografia de gasos (GC) acoblada a l'espectrometria de masses (MS) per determinar amb precisió el marcatge ^{13}C-posicional en metabòlits clau del metabolisme central. Aquest enfocament, validat amb substàncies de referència marcades posicionalment amb ^{13}C via GC-impacte electrònic-MS i GC-ionització química a pressió atmosfèrica-MS, ha demostrat eficàcia en l'anàlisi de dades prèvies de ^{13}C-MFA en fulles i cèl·lules guarda. S'ha obtingut informació nova sobre la glucosa, revelant que els seus àtoms de carboni són preferentment marcats per la fotosíntesi i la gluconeogènesi. A més, s'ha establert una plataforma per investigar la incorporació de ^{13}C en malat i glutamat derivats de l'enzim fosfoenolpiruvat carboxilasa (PEPc). Els nostres resultats van revelar que la gluconeogènesi i l'assimilació de CO_2 mediada per PEPc en malat s'activen de manera independent a la llum a les cèl·lules guarda, mentre que els fluxos de glucòlisi i PEPc cap al glutamat estan restringits pel sistema de tiorredoxina mitocondrial en fulles il·luminades. També vam explorar la dinàmica metabòlica de les cèl·lules guarda, després de l'assimilació de CO_2 mitjançant per PEPc, tant a la foscor com durant la transició de la foscor a la llum. Tot i que els canvis metabòlics van ser majoritàriament consistents en general, es va evidenciar la influència de la llum en les estructures de la xarxa metabòlica, resultat en un augment de l'enriquiment de ^{13}C en sucres i metabòlits associats al cicle de l'àcid tricarboxílic (TCA). A més, donat que el canvi climàtic està afectant el rendiment de les plantes a tot el món, també vam investigar els efectes de la sequera, altes temperatures i alta concentració de CO_2 en una falguera (*Nephrolepis exaltata*) i una angiosperma típica, *Brassica oleracea*. Mentre que *B. oleracea* va mostrar respostes fisiològiques significatives a la alta concentració de CO_2, independentment d'altres condicions d'estrès, la falguera va exhibir una resposta limitada a tots els estressos a nivell fisiològic. Els nivells de lípids i metabòlits primaris a *B. oleracea* van canviar induïts per estrès, cosa que no va succeir a la falguera. Els nostres resultats suggereixen impactes diferencials del canvi climàtic en falgueres i angiospermes. En resum, la integració d'anàlisis metabolòmiques i fisiològiques proporciona

una visió detallada dels mecanismes subjacents a la regulació i adaptació metabòlica de les plantes. Aquest enfocament no només ofereix estratègies innovadores per a l'anàlisi metabolòmica, sinó que també contribueix a la comprensió de les respostes ambientals de les plantes, de diferents grups, en un món en constant canvi climàtic.

Paraules clau: ^{13}C-anàlisi de flux metabòlic; cèl·lules guarda; espectrometria de masses; metabolòmica; regulació metabòlica.

LIST OF ABBREVIATIONS AND ACRONYMS

Ac-CoA	acetyl-CoA
$_{A}CO_2$	ambient CO_2 concentration
AlaAT	alanine aminotransferase
A_N	net photosynthetic rate
APCI	atmospheric pressure chemical ionization
AspAT	aspartate aminotransferase
AT	ambient temperature
CA	carbonic anhydrase
C_c	chloroplastic CO_2 concentration
C_i	sub-stomatal CO_2 concentration
Cit	Citrate
CS	citrate synthase
D	Drought
DA^{13}C	dual atomic ^{13}C-enrichment
DGDG	digalactosyl diacylglycerol
EI	electron impact
ETR	electron transport rate
F^{13}C	fractional ^{13}C-enrichment
f_{ias}	fraction of mesophyll intercellular air spaces
FUM	Fumarase
FW	Fresh weight
GABA	gamma-aminobutyric acid
GC-MS	gas chromatography coupled to mass spectrometry
Glc	Glucose
g_m	mesophyll conductance
g_s	stomatal conductance
$_{H}CO_2$	high CO_2 concentration
HT	high temperature
IDH	isocitrate dehydrogenase
ILE	isotope labelling experiment
J_{max}	maximum electron transport rate

L_{betch}	distance between chloroplasts
L_{chl}	chloroplast length
LC-MS	liquid chromatography coupled to mass spectrometry
LMA	leaf mass per area
Mal	Malate
MDH	malate dehydrogenase
ME	malic enzyme
MEOX	Methoxyaminated
MFA	metabolic flux analysis
MGDG	monogalactosyl diacylglycerol
MS	mass spectrometry
MSTFA	*N*-Methyl-*N*-(trimethylsilyl) trifluoroacetamide
m/z	mass-to-charge ratio
NMR	nuclear magnetic resonance
OAA	Oxaloacetate
$P^{13}C$	positional ^{13}C-enrichment
Pc	pyruvate carboxylase
PC	phosphatidyl choline
PCA	principal component analysis
PDH	pyruvate dehydrogenase
PE	phosphatidyl ethanolamine
PEP	Phospho*enol*pyruvate
PEPc	phospho*enol*pyruvate carboxylase
PEPCK	phospho*enol*pyruvate carboxykinase
PK	pyruvate kinase
PLS-DA	partial least square-discriminant analysis
PPDK	pyruvate phosphate dikinase
P_r,	Photorespiration
Pyr	Pyruvate
$R^{13}C$	relative ^{13}C-enrichment
R_d	dark respiration
RIA	relative isotopologue abundance
RMC	relative metabolite content

RWC	relative water content
S_c	chloroplast surface area exposed to intercellular air spaces per area
S_c/S_m	ratio between chloroplasts and mesophyll surface areas exposed to intercellular air spaces
SD	stomatal density
SDH	succinate dehydrogenase
S_m	mesophyll area exposed to intercellular air spaces per area
Suc	Sucrose
$T^{13}C$	total ^{13}C-enrichment
TAG	Triacylglycerol
TCA	tricarboxylic acid
T_{chl}	chloroplast thickness
T_{cw}	cell wall thickness
T_{cyt}	cytosol thickness
T_L	leaf thickness
T_{LE}	lower epidermis thickness
T_{MES}	mesophyll thickness
T_{MES_pal}	palisade mesophyll thickness
T_{MES_spo}	spongy mesophyll thickness
TMS	Trimethylsilylated
TOF	time-of-flight
TP	triose-phosphates
T_{UE}	upper epidermis thickness
V_{cmax}	maximum velocity of Rubisco carboxylation
2-OG	2-oxoglutarate
$\delta^{13}C$	carbon isotopic composition
$\Delta^{13}C$	carbon isotope discrimination

TABLE OF CONTENTS

1 GENERAL INTRODUCTION

Recent decades have been characterized by the rapid evolution of several Omics approaches, especially genomics, transcriptomics, proteomics and metabolomics. These technologies have substantially enhanced the precision and efficiency to obtain detailed molecular information that aid to improve our understanding on the functioning of diverse biological systems, including plants. Importantly, the integration of metabolomics with plant physiology approaches has established its immense relevance to understanding the processes that govern the functioning of plants. Plant metabolomics, by allowing a comprehensive analysis of the metabolites present within any plant cell or tissue, offers important information on the metabolic status, stress levels, and responses to different stimuli and environmental conditions (Fiehn, 2002; Bino et al., 2004). Complementarily, plant physiology studies investigate fundamental physiological processes, such as photosynthesis, transpiration, and respiration, allowing a deeper understanding on the plant mechanisms of acclimation and adaptation to changes in environmental conditions (Xu et al., 2015; Kumar et al., 2021; Lobo et al., 2022).

The integration of both metabolomics and plant physiology analyses has been used as an instrument to revealing in details the complex network of metabolic and physiological interactions that occur in plants (Fernie and Morgan, 2013). Indeed, metabolite profiling analysis have allowed researches to access a large-scale data sets of metabolites in an unprecedented way. In parallel, ^{13}C-metabolic flux analysis (^{13}C-MFA) allow plant scientists to quantify the rate of metabolic fluxes in specific metabolic pathways as well as identify key metabolic pathways that are affected by environmental factors (Allen et al., 2009; Verslues and Juenger, 2011; Szecowka et al., 2013; Ma et al., 2014; Arrivault et al., 2017; Robaina-Estévez et al., 2017; Liu et al., 2022). This provides not only a more dynamic and functional view of plant metabolism but also contributes to the understanding of plant adaptation and defense responses to environmental stresses at metabolic flux level, which is highly closed to the phenotype observed. Moreover, plant metabolomics can be applied for the identification of biomarkers and potential targets for genetic improvement, aimed at increasing tolerance and or optimizing the performance of agricultural crops under adverse conditions (Liu et al., 2022; Zandalinas et al., 2022).

Research studies using metabolomics and physiology approaches have provided importance advances for several fields of plant biology, including agriculture and applied

biotechnology. They are providing essential information and new insights towards solutions to global challenges in terms of food security and adaptation of crop plants to foreseen climate change (Fernie and Schauer, 2009; Verslues and Juenger, 2011). These advances enable the development of practical applications as well as the management of strategies to improve crop yield and/or resilience (Roessner and Bowne, 2009). In addition, these studies are also contributing to advance the basic knowledge in plant biology, while enabling a better comprehension of the complex relationships among molecular components and physiological mechanisms that underpin the development, growth, environmental responses, and evolution of plants.

In summary, although plant metabolomics represents a powerful approach to investigate the mechanisms of metabolic regulation in plants and to understand their ecophysiological responses to different environmental conditions, is still little explored in combination with other omics, mainly in some plant cells and/or in basal lineages of vascular plants. However, new methodologies for data acquisition and metabolite annotation are now emerging, taking advantage of progress in analytical techniques and computer science field, which generates a new range of possibilities to be explored. In this context, this Thesis aims to contribute to the advance of metabolomics approaches, and to the understanding of the physiological and metabolic regulation mechanisms across species, highlighting their importance for adapting to environmental change conditions.

2 GENERAL REVIEW

2.1 Plant metabolism

Plants are able to generate a huge number of metabolites varying in structure and function, that help them acclimate to variable challenging environments (Weng et al., 2014; Liu et al., 2020). It is estimated that more than 200 000 metabolites exist in the Plant Kingdom (Dixon and Strack, 2003), divided into two general categories: primary and secondary metabolisms (Pott et al., 2019). Among these, only a subset of these compounds are produced in any given tissue or species (Schwab, 2003; Fernie, 2007; Pichersky and Lewinsohn, 2011; Luo, 2015; Fang et al., 2019; Venegas-Molina et al., 2021).

Primary metabolites are constitutively accumulated in plant cells (Sulpice and Mckeown, 2015), and directly involved in the plant growth, development, and reproduction (Fiehn, 2002; Fernie and Tohge, 2017). On the other hand, secondary metabolites play a major role in plant defense to biotic and abiotic stresses, being often restricted to specific tissues or specific development stages of plants (Obata and Fernie, 2012; Sulpice and Mckeown, 2015; Fernie and Tohge, 2017; Zaynab et al., 2018; Fang et al., 2019; Pott et al., 2019). Interestingly, both classes of metabolisms are intrinsically linked. For instance, metabolites from primary metabolic pathways (e.g., glycolysis and the tricarboxylic acid (TCA) cycle) act as carbon skeletons for the synthesis of secondary metabolites. Additionally, beyond aiding nitrogen assimilation, amino acids act as precursors for specialized compounds including pigments and phytohormones. Therefore, plant metabolism involves dynamic process across species, with many metabolites displaying accumulation induced by external stimuli (Kusano et al., 2011; Clemente-Moreno et al., 2019; Lima et al., 2019), and often acting as a bridge between the genotype and phenotype of a plant (Fiehn, 2002).

2.2 Plant metabolomics

Over the past two decades, a vast number of studies have been performed to investigate the regulation of plant metabolism, given their importance to plant growth, development, environmental adaptation, and evolution (Fernie et al., 2004; Obata and Fernie, 2012; Weng, 2013; Fernie and Tohge, 2017). In recent years, the development of broad large-scale approaches in Omics field, such as genomics, transcriptomics, proteomics, and metabolomics has contributed to plant metabolism diversity exploration as well as to the current understanding

of the molecular mechanisms by which plants controls its own chemical composition (Fernie and Tohge, 2017). Hence, metabolomics is a comprehensive analysis of the set of metabolites in a given biological system, with measurement of these metabolites at a given time (Fiehn, 2002; Nicholson and Lindon, 2008; Maltese and Verpoorte, 2010; Okazaki and Saito, 2012). This tool focus on a better systematic understanding of biological networks through precise and extensive research on metabolism, and contributes to decoding the functions of genes (Hall et al., 2002; Bino et al., 2004; Fiehn, 2008; Hagel and Facchini, 2008).

Metabolomics studies have analyzed a wide range of compounds, ranging from small molecules to complex metabolites, such as amino acids, sugars, organic acids, lipids, nucleic acids, amines, ketones, aldehydes, vitamins, steroids, signaling molecules, polyphenols, and hormones (Bino et al., 2004; Hirai et al., 2004; Pramai et al., 2017; Wang et al., 2019). By examining variations in metabolism, it is possible to better understanding how gene expression and metabolic pathways respond to different environmental conditions, providing insights into metabolic regulation in plants (Fiehn, 2002; Saito and Matsuda, 2010). Therefore, the use of metabolomics on plants has leading to significant crop improvement, once metabolites not only contribute to plant growth, development, and adaptation to environmental changes but also to advances in the fields of food and agriculture (Chen et al., 2016; Hong et al., 2016; Ma and Qi, 2021).

2.3 Analytical techniques used on metabolomics

The analysis of metabolites is complex and laborious, both experimentally and computationally, due to the huge chemical diversity of compounds and also by the large variations in the relative levels of metabolites. Therefore, a comprehensive coverage of plant metabolism can only be achieved by using multiple approaches for extraction, separation and detection of metabolites. To detect subsets of metabolites covering a range of metabolome of plants or any other organism (Hall, 2006), some analytical techniques, such as gas chromatography coupled to mass spectrometry (GC-MS), liquid chromatography-MS (LC-MS) and/or nuclear magnetic resonance (NMR) spectroscopy (Fiehn, 2002; Sumner et al., 2007) are generally performed (Krishnan et al., 2005; Dettmer et al., 2007; Eisenreich and Bacher, 2007; Dunn, 2008). The integration of them enables a more detailed view of part of the plant metabolome and allow robust investigations of small metabolic variations in response to different experimental conditions. Among these, GC-MS method has been one of the most

popular metabolomics techniques used, combining the advantages of two strong complementary technologies, which results in a high-resolution separation with precise detection in a broad dynamic range to characterize small molecules (Yuan et al., 2022). Through this platform, GC can separate molecular compounds, including metabolites that have almost identical structure and consequently mass spectra. These compounds are subsequently transferred to the mass spectrometer for further detection. MS also provides fragmentation patterns that enables the differentiation of chemically diverse, but co-eluting metabolites. This process has six component steps (extraction, derivatization, separation by GC, ionization, detection by MS, and evaluation) (Kopka et al., 2004; Lisec et al., 2006).

Two major approaches of metabolomic analysis are current extensively used, metabolite profiling and metabolic flux analysis (Sauer, 2004). Both approaches shared the intermediate experimental analytical set-up. However, according to the biological question, the chosen analytical technologies can vary. In general, a typical metabolomics analysis requires general steps of sample collection, sample extraction, data acquisition and data analysis (Kopka et al., 2004; Shen et al., 2023). As stated above, different strategies can be used, depending on the experiment. Metabolite profiling, for example, is one of the most common tools applied in laboratories for the analysis of plant metabolism. It allows the identification and the relative quantification of changes in metabolite pool size, that represents the biochemical state of the chosen sample at a specific point in time. This approach also shows a great potential of discovery of novel metabolites (Fernie et al., 2004; Kopka et al., 2004).

In turn, metabolic flux analysis (MFA) is a simultaneous identification and estimation of the intracellular flux of a compound through a metabolic network, interpreted numerically as the relative fraction of a specific metabolite, that result from genetic and/or environmental interventions (Lee et al., 1999; Ratcliffe and Shachar-Hill, 2006; Antoniewicz, 2015). This information provides insights into the regulation of specific metabolic pathways, contributing to the suggestion of new targets for further metabolic engineering. Indeed, several flux analyses have been performed to elucidate the metabolism in a wide of biological system, ranging from simple to complex systems, such as *Escherichia coli* (Maier et al., 2008), *Saccharomyces cerevisiae* (Moxley et al., 2009), plants (Szecowka et al., 2013; Dethloff et al., 2017; Robaina-Estévez et al., 2017; Medeiros et al., 2018), mammalian cells (Hiller and Metallo, 2013; Mueller and Heinzle, 2013; Young, 2013), and other cellular systems (Au et al., 2014; Adebiyi et al., 2015).

In contrast to metabolite profiling, MFA often requires an extra step at the initial approach: the application of an isotope tracer, whether metabolic steady state is not assumed for the system, that leads to a partial incorporation and distribution of isotopes into metabolite pools (Szyperski, 1998; Wiechert, 2001; Wittmann, 2001). For instance, ^{13}C-based metabolic flux analysis (^{13}C-MFA) is one of the most advanced and informative technique used for determining intercellular fluxes of central metabolism in biological systems (Wiechert, 2001; Zamboni, 2011; Antoniewicz, 2015; Lima et al., 2018). In this case, the use of a specifically labelled ^{13}C-substrate added in the medium for a period of time, results in an incorporation of ^{13}C-atoms into metabolic intermediates of a metabolic network of interest. In the last decade, the use of stable isotopes, mainly ^{13}C, became important to determine and integrate *in vivo* measurements of metabolic reactions in systems biology (Robaina-Estévez et al., 2017).

2.4 Applications of plant metabolomics

Over recent years, the application of metabolomics research has expanded to various fields. This approach is not only providing information of previously unknown and/or poorly studied responses in specific metabolic networks, but is being also a useful tool for quantitatively predicting physiological traits (Putri et al., 2012). In plant science, specifically, metabolomics have been increasingly used the screening of apparent or up to now unknown metabolic phenotypes in functional genomic studies of plants (Fiehn et al., 2000; Roessner et al., 2001; Fiehn, 2002; Fernie et al., 2004), for investigate regulatory networks involved across species (Weckwerth et al., 2004; Gago et al., 2016; Lima et al., 2019; Cândido-Sobrinho et al., 2022), evaluation of mutant plants (Baker et al., 2006; Ricroch et al., 2011; Daloso et al., 2016), understanding of guard cell metabolism (Robaina-Estévez et al., 2017; Medeiros et al., 2018; Lima et al., 2019); measurement of circadian rhythms (Gibon et al., 2006; Espinoza et al., 2010), for characterize physiological and biochemical responses to different types of environmental stress conditions (Caldana et al., 2011; Kusano et al., 2011; Obata and Fernie, 2012), and to unveil relationships between metabolites associated with carbon and nitrogen metabolism (Stitt and Fernie, 2003).

Moreover, the analyses of plant systems have also been mostly carried out on bulked tissues (i.e., whole roots, leaves, or shoots), which are providing important biological information about plant tolerance and avoidance mechanisms to abiotic stresses. Overall, studies on plant metabolomics have been contributing to a comprehensive understanding of organisms at

individual level and, at the same time, providing important links that further helps to explain the organism-environment interactions (Luo, 2015; Fang et al., 2019). However, it is worth noting that integrating information from different molecular entities within a cell remains challenging due to their distinct temporal dynamics and regulatory complexities (Fernie and Stitt, 2012).

3 HYPOTHESIS

This thesis involved three main hypotheses:

1. The identification of the chemical structures of the fragments of the metabolites identified by GC-EI-MS allows the establishment of a positional ^{13}C-isotopomer approach, which in turn permit a detailed and accurate understanding of plant metabolic fluxes in response to different environmental conditions.

2. Guard cells exhibit strong metabolic modifications following PEPc-mediated CO_2 assimilation in the dark, but light exposure leads to more drastic metabolic changes, including an increase in the metabolic fluxes throughout the TCA cycle as a mechanism to underpin the specific metabolic requirements of the stomatal opening process.

3. Ferns and angiosperms present distinct physiological and metabolic responses to climate change conditions due to the evolution and specific characteristics of these two plant groups.

4 OBJECTIVES

4.1 General objectives

This Thesis was focused on three General Objectives:

4.1.1. To establish a GC-MS-based ^{13}C-positional isotopomer approach to improve the resolution of flux maps from ^{13}C-metabolic flux analysis (^{13}C-MFA).

4.1.2. To unveil the metabolic changes following PEPc-mediated CO_2 assimilation in dark-exposed guard cells as well as to identify those associated to the transition from dark-to-light condition.

4.1.3. To investigate ecophysiological and metabolic responses of angiosperms and ferns subjected to conditions associated to the climate change scenario, such as increased CO_2, high temperatures and drought.

4.2 Specific objectives

The previous General Objectives were approached by four Specific Objectives:

4.2.1. To evaluate the accuracy and limitations of mass spectrometry-based ^{13}C-metabolic flux analysis (^{13}C-MFA) compared to ^{13}C-isotope labelling experiments (^{13}C-ILE) in assessing metabolic fluxes in plant primary metabolism.

4.2.2. To develop and validate an approach based on gas chromatography coupled to mass spectrometry (GC-MS) to obtain information on the ^{13}C-positional labeling in key metabolites of plant systems.

4.2.3. To apply ^{13}C-MFA to investigate metabolic carbon fluxes in guard cells and leaves in response different light conditions, identifying redirected metabolic fluxes following phosphoenolpyruvate carboxylase (PEPc)-mediated CO_2 assimilation.

4.2.4. To evaluate the physiological, anatomical and metabolic responses of one fern and one angiosperm to climate change conditions, including drought, high temperatures and high CO_2 concentrations.

CHAPTER I

Mass spectrometry-based ^{13}C-metabolic flux analysis should go deeper at atomic level

5 CHAPTER I – MASS SPECTROMETRY-BASED ^{13}C-METABOLIC FLUX ANALYSIS SHOULD GO DEEPER AT ATOMIC LEVEL

Valéria F. Lima[1], Danilo M. Daloso[1*]

[1] LabPlant, Departamento de Bioquímica e Biologia Molecular, Universidade Federal do Ceará, 60451-970, Fortaleza, Ceará, Brasil.

* Corresponding author.

Submitted to *Journal of Experimental Botany* (Viewpoint).

Keywords: ^{13}C-positional labelling analysis, isotopologues, isotopomers, metabolic fluxes, metabolic network, metabolite fragmentation.

Introduction

^{13}C-metabolic flux analysis (^{13}C-MFA) is an approach to measure the flux of ^{13}C throughout a metabolic network, involving mathematical modelling and/or ^{13}C-isotope labelling experiments (^{13}C-ILE). The accuracy of modelling is much higher than ^{13}C-ILE, meaning that several predictions obtained by the first are experimentally difficult to confirm. Overcoming the major bottlenecks of ^{13}C-ILE, such as the low atomic resolution of mass spectrometry (MS)-based ^{13}C-MFA approaches is thus needed. Here, we highlight that increasing the capacity to obtain positional ^{13}C-labelling information from MS approaches is crucial to improve the power of ^{13}C-MFA and reduce the gap between modelling and ^{13}C-ILE.

Metabolomics approaches used in ^{13}C-labelling experiments

Metabolomics is separated in targeted and untargeted analyses. Whilst the first requires metabolite identification, the untargeted analysis (also called *metabolic fingerprinting*) use the features (peaks identified in the chromatograms) to discriminate different samples (Perez de Souza *et al.*, 2019). The main targeted metabolomics analyses are metabolite profiling and ^{13}C-MFA. Nuclear magnetic resonance (NMR) and gas and liquid chromatography's coupled to MS (GC/MS, LC/MS) are the major approaches used in ^{13}C-MFA. The identification of metabolites via LC/MS or GC/MS considers two parameters: the retention time obtained in the chromatography and the fragments obtained at the MS. LC/MS is the most versatile MS platform and have been used to identify lipids, phytohormones and primary and secondary metabolites, depending on the MS type and the LC column used. By contrast, GC/MS is mostly restricted to small and polar metabolites. Although there is an overlap in the type of compounds detected by GC/MS and LC/MS, the metabolite fragmentation obtained from these approaches differs substantially. This is due to the methods used to prepare the samples and the different ionization sources used in the MS in each of these approaches. For instance, GC/MS analysis generally includes a step called derivatization, which consists of adding certain chemicals to the samples to simplify the structure and increase the volatility of the compounds. This substantially increase the size of the metabolites, rendering fragments with different mass-to-charge ratio (*m/*z) than the expected for a non-derivatized metabolite (Figure 1A). Additionally, GC/MS is usually carried out with strong ionization sources (e.g., electron impact (EI)), that

produce a stable fragmentation pattern, facilitating targeted metabolomics analysis. The opposite is observed in LC/MS approaches, in which weaker ionization sources are commonly used (e.g., electrospray (ESI)). This means that the fragmentation pattern obtained by LC-ESI/MS is not stable as those obtained by GC-EI/MS, making the metabolite identification detected by LC-ESI/MS more laborious. Furthermore, information from the fragmentation of a certain metabolite obtained from GC-EI/MS is not useful for LC-ESI/MS analysis, and *vice-versa*. It is clear therefore that the establishment of new methods to obtain MS-based ^{13}C-positional information may be restricted to a specific MS platform.

By contrast to MS approaches, ^{13}C-NMR allows the precise quantification of the ^{13}C incorporation at atomic level in a relatively easier manner. This is an outstanding advantage of ^{13}C-NMR over MS and make NMR a key approach to unveil how branches of specific metabolic pathways are regulated (Kruger and Ratcliffe, 2021). However, NMR is much less sensitive than MS and requires a considerable amount of tissues to be analysed, hampering its use for large metabolic networks and for single cell metabolomics studies (Medeiros *et al.*, 2019). By contrast, MS approaches offer greater sensitivity and can be applied to a wider range of compounds (Batista Silva *et al.*, 2016). However, the chemical structure of the metabolite fragments used in MS-based ^{13}C-MFA has been surprisingly neglected, i.e., most of the ^{13}C-labelling information obtained by MS approaches has been obtained by analysing isotopologues, not isotopomers (Box I). Therefore, positional ^{13}C-labelling information is currently obtained predominantly from ^{13}C-NMR approaches. This is one of the main reasons that explain the enormous gap between metabolic modelling and ^{13}C-ILE.

Mass spectrometry-based ^{13}C-MFA

The main obstacle to improve MS-based ^{13}C-MFA is to increase the number of metabolites identified in the network. For this, different tools for metabolite annotation are currently available (Misra, 2021). However, the identification of metabolites does not necessarily require the elucidation of the chemical structure of all fragments obtained (Figure 1B). This means that metabolite profiling analysis can be improved by simply identifying the fragments generated after metabolite fragmentation. By contrast, ^{13}C-MFA requires two additional steps than metabolite profiling: (i) the labelling of the tissue with a ^{13}C-tracer, to be chosen according to the aim of the work and the tissue under investigation, and (ii) the quantification of the ^{13}C incorporation in the metabolites. For this, is important to know the chemical structure of the fragment used to quantify the ^{13}C-enrichment in a metabolite (Box II).

Among the MS platforms, GC/MS has tremendous advantages to obtain positional ^{13}C-labelling information due to the highly predictable metabolite fragmentation obtained by strong ionization sources such as EI and APCI (atmospheric pressure chemical ionization). GC/MS is perhaps the best platform to start solving the problem of small resolution of metabolic fluxes at atomic level. However, an enormous effort is needed from the metabolomics community to unveil the chemical structure of the fragments (Okahashi *et al.*, 2019) and to validate whether they can (or not) be used in ^{13}C-MFA (Lima *et al.*, 2021). The chemical structure of each fragment can be revealed by combining *in silico* simulations of metabolite fragmentation and their confirmation by analysing positionally ^{13}C-labelled standards (Box II). This first step will require a great effort from ^{13}C-labelling commercial suppliers and laboratories that have the expertise to synthesize positionally ^{13}C-labelled standards, as demonstrated for organic acids (Okahashi *et al.*, 2019).

By analysing a standard in a GC-EI/MS, the researcher will obtain which fragments have been detected by the MS and how many carbons is likely presented in each fragment. For example, the fragment *m/z* 233 is the major detected in malate derivatized by of *N*-Methyl-*N*-(trimethylsilyl) trifluoroacetamide (MSTFA) and analysed by GC-EI/MS (Lisec *et al.*, 2006). Leaf malate *m/z* 233 has three adjacent peaks (*m/z* 234, *m/z* 235 and *m/z* 236) with a typical natural ^{13}C isotope abundance, indicating that this fragment contains three carbons of the malate backbone (Figure 1C). The peaks *m/z* 234, *m/z* 235 and *m/z* 236 are the M1, M2 and M3 **isotopologues** of *m/z* 233. Increases in the intensity of these peaks indicate the incorporation of 1, 2 and 3 ^{13}C into malate. Whilst the intensity of the peak *m/z* 233 is sufficient to metabolite profiling analysis, the intensities of M1, M2 and M3 are needed to determine the ^{13}C-enrichment in malate from ^{13}C-ILE. Given that the isotopologues usually have lower intensities than their parental ion (M), MS approaches with high sensitivity facilitate the acquisition of mass spectral data and thus optimize ^{13}C-MFA. However, information's from isotopologues do not demonstrate which carbons of the molecule have been labelled. For instance, the intensity of malate M1 indicates the incorporation of one ^{13}C into malate, but it does not discriminate in which carbons of the malate backbone (1, 2, 3 or 4) the ^{13}C has been incorporated (Figure 1C). Such positional ^{13}C-labelling information requires the identification and quantification of the **isotopomers**, not only **isotopologues**.

From isotopologues to isotopomers

Isotopologues (M1, M2, M3 etc) differs only in their isotopic composition (i.e. in the number of isotopic substitutions), while isotopomers have the same number of each isotopic atom but differing in their positions (Stoll, 2007). For instance, the incorporation of one or two ^{13}C into malate leads to the formation of two isotopologues, M1 and M2, respectively. However, M1 can be observed when the ^{13}C is incorporated at the carbons 1, 2, 3 or 4 of the malate backbone. This preconizes that isotopomers have the same molecular mass, whilst isotopologues do not (Stoll, 2007). In this context, NMR approaches can easily distinguish the isotopomers, thanks to the different signals obtained when the ^{13}C is incorporated in different carbons of the molecule. By contrast, the incorporation of one ^{13}C in malate leads to the very same M1 signal, no matter which carbon of the malate backbone (1, 2, 3 or 4) this ^{13}C has been incorporated (Ratcliffe and Shachar-Hill, 2006). The identification of the isotopomers by MS requires the knowledge of the chemical structure of the fragments obtained, a careful mass spectral analysis and a mathematical approach to determine ^{13}C-enrichment at atomic level.

Advantages in obtaining positional ^{13}C-labelling information

The benefits of increasing the atomic resolution of MS-based ^{13}C-MFA are vast (Wieloch, 2021; Wieloch *et al.*, 2021, 2022). For instance, disentangling the structure of metabolite fragments will avoid erroneous metabolic flux calculations and thus inaccurate conclusions from ^{13}C-ILE (Figure 2). The identification of fragments at both nominal and high mass resolutions may also aid the distinction of metabolites with similar retention time and chemical structure, a long bottleneck of targeted metabolomics. It is noteworthy that the identification of fragments at high mass resolution, which can be obtained by very sensitive MS platforms (e.g. GC-APCI/MS), is primordial to validate information's obtained at nominal mass resolution, for example by GC-EI/MS (Lima *et al.*, 2021). Positional ^{13}C-labelling information from MS approaches may substantially increase the resolution of flux maps by facilitating the distinction between previously stored carbons (^{12}C) and those derived from the ^{13}C-tracer that are incorporated into the metabolites, which can unveil which pathways contribute to the synthesis of a particular metabolite (Abadie *et al.*, 2017; Lima *et al.*, 2021) and be used to determine enzyme activity *in vivo* (Abadie and Tcherkez, 2019). Increasing the atomic resolution of MS-based ^{13}C-MFA will certainly strength the power of this approach for functional genomics and systems biology studies, which, in turn, can pave the way for plant metabolic engineering. In all scenarios, a multi-disciplinary team is required.

BOX I: Isotopologues *vs* Isotopomers

Malate is a metabolite with 4 carbons (Figure IA). After extraction and derivatization by *N*-Methyl-*N*-(trimethylsilyl) trifluoroacetamide (MSTFA), the molecule of malate acquires 3TMS (Figure IB). Analysis of this molecule by GC-EI/MS produce several fragments, in which *m/z* 233 and *m/z* 245 are those with higher intensity and are thus good markers for the identification of malate in a biological sample derivatized by MSTFA (Figure IC). The fragment *m/z* 245 refers to a loss of a TMS group, meaning that the fragment contains all four carbons of the molecule, whilst the fragment *m/z* 233 contains the carbons 2, 3 and 4 of the malate backbone (Figure ID), as confirmed by GC-EI/MS analysis using purified compounds (Okahashi *et al.*, 2019). Increases in the intensity of the peaks *m/z* 246, *m/z* 247, *m/z* 248 and *m/z* 249 indicate the incorporation of one, two, three and four ^{13}C into malate. These adjacent peaks of *m/z* 245 (i.e. *m/z* 246, *m/z* 247, *m/z* 248 and *m/z* 249) are called isotopologues, and can be represented by the letter M followed by the number of ^{13}C that have been incorporated (M1, M2, M3 and M4) (Figure IE). Thus, isotopologues refers to the number of ^{13}C that have been incorporated into the fragment. In this case, given that the fragment contains all carbons of the molecule, the analysis of the isotopologues provide great insights concerning the number of ^{13}C that have been incorporated into the molecule. However, isotopologues do not provide information on which carbon of the molecule the ^{13}C has been incorporated. For example, increases in malate *m/z* 246 (M1) indicates that one ^{13}C has been incorporated into the fragment *m/z* 245, but this information does not allow the researcher to identify in which of the four carbons of the fragment this ^{13}C has been incorporated (Figure IF). Therefore, although the information from isotopologues can be used to calculate the amount of ^{13}C incorporated into a metabolite, no positional ^{13}C-labelling information is obtained from fragments in which the chemical structure is unknown or unclear.

BOX II: Unveiling the chemical structure of fragments obtained by GC-EI/MS

The fragments detected in a mass spectrum can be characterized in terms of their elemental and isotopic composition. However, some laborious steps are needed to acquire ^{13}C-positional information from fragments obtained by GC-EI/MS (Figure II). Initially, it is necessary to identify the chemical structure of the metabolite of interest, considering the method used for derivatization and the major fragments detected in the MS. The structures of TMS and (in part) methoxyaminated metabolites is described in several metabolome databases, such as Golm, NIST, PubChem, MassBank, MoNA, etc (Figure IIA). Once the chemical structure is known, an *in silico* analysis can be performed to simulate the metabolite fragmentation. However, this

can generate one or a subset of fragments containing the same *m/z* but with different carbon atoms of the molecule. For example, *in silico* fragmentation of malate 3TMS originates a fragment *m/z* 117, which, among several possibilities, could represent the loss of a TMS group, containing the carbon 1 or 4 of the malate backbone (Figure IIB). Therefore, an additional step can be required to unveil the chemical structure of the fragment, which involves the validation of the *in silico* simulation by analysing positionally ^{13}C-labelled reference substances. However, this is highly limited by the availability of such positionally labelled compounds. Furthermore, recent evidence suggests that information from nominal mass (GC-EI/MS) should be confirmed at high mass resolution (GC-APCI/MS) to avoid erroneous interpretation (Figure IIC). Moreover, it is important to test the viability of the fragments unveiled by using reference substances in complex samples from ^{13}C-MFA studies, given that it is not unusual that certain fragments show low intensity or overlapped with near fragments, being thus not suitable for ^{13}C-MFA (Figure IID).

Acknowledgements

This work was partially supported by the National Institute of Science and Technology in Plant Physiology under Stress Conditions (INCT Plant Stress Physiology – Grant: 406455/2022-8) and the National Council for Scientific and Technological Development (CNPq, Grant No. 404817/2021-1). The authors gratefully acknowledge the CNPq for the research fellowship to Danilo M. Daloso (303709/2020-0) and the scholarship granted by the Brazilian Federal Agency for Support and Evaluation of Graduate Education (CAPES-Brazil) to Valéria F. Lima (88882.454529/2019-01).

References

Abadie C, Lothier J, Boex-Fontvieille E, Carroll A, Tcherkez G. 2017. Direct assessment of the metabolic origin of carbon atoms in glutamate from illuminated leaves using ^{13}C-NMR. New Phytologist **216**, 1079–1089.

Abadie C, Tcherkez G. 2019. In vivo phosphoenolpyruvate carboxylase activity is controlled by CO_2 and O_2 mole fractions and represents a major flux at high photorespiration rates. New Phytologist **221**, 1843–1852.

Batista Silva W, Daloso DM, Fernie AR, Nunes-Nesi A, Araújo WL. 2016. Can stable isotope mass spectrometry replace radiolabelled approaches in metabolic studies? Plant Science **249**, 59–69.

Kruger NJ, Ratcliffe RG. 2021. Whither metabolic flux analysis in plants? Journal of Experimental Botany **72**, 7653–7657.

Lima VF, Erban A, Daubermann AG, *et al.* 2021. Establishment of a GC-MS-based ^{13}C-positional isotopomer approach suitable for investigating metabolic fluxes in plant primary metabolism. The Plant Journal **108**, 1213–1233.

Lisec J, Schauer N, Kopka J, Willmitzer L, Fernie AR. 2006. Gas chromatography mass spectrometry-based metabolite profiling in plants. Nature Protocols **1**, 387–396.

Medeiros DB, da Luz LM, de Oliveira HO, Araújo WL, Daloso DM, Fernie AR. 2019. Metabolomics for understanding stomatal movements. Theoretical and Experimental Plant Physiology **9**, 91–102.

Misra BB. 2021. New software tools, databases, and resources in metabolomics: updates from 2020. Metabolomics **17**, 49.

Okahashi N, Kawana S, Iida J, Shimizu H, Matsuda F. 2019. Fragmentation of dicarboxylic and tricarboxylic acids in the Krebs Cycle using GC-EI-MS and GC-EI-MS/MS. Mass Spectrometry **8**, A0073–A0073.

Perez de Souza L, Alseekh S, Naake T, Fernie A. 2019. Mass spectrometry-based untargeted plant metabolomics. Current protocols in plant biology **4**, e20100.

Ratcliffe RG, Shachar-Hill Y. 2006. Measuring multiple fluxes through plant metabolic networks. Plant Journal **45**, 490–511.

Stoll S. 2007. Isotopomers and isotopologues: the History behind the confusion. Chem. Educator **12**, 1–3.

Wieloch T. 2021. The next phase in the development of ^{13}C isotopically non-stationary metabolic flux analysis. Journal of Experimental Botany **72**, 6087–6090.

Wieloch T, Sharkey TD, Werner RA, Schleucher J. 2022. Intramolecular carbon isotope signals reflect metabolite allocation in plants. Journal of Experimental Botany **73**, 2558–2575.

Wieloch T, Werner RA, Schleucher J. 2021. Carbon flux around leaf-cytosolic glyceraldehyde-3-phosphate dehydrogenase introduces a ^{13}C signal in plant glucose. Journal of Experimental Botany **72**, 7136–7144.

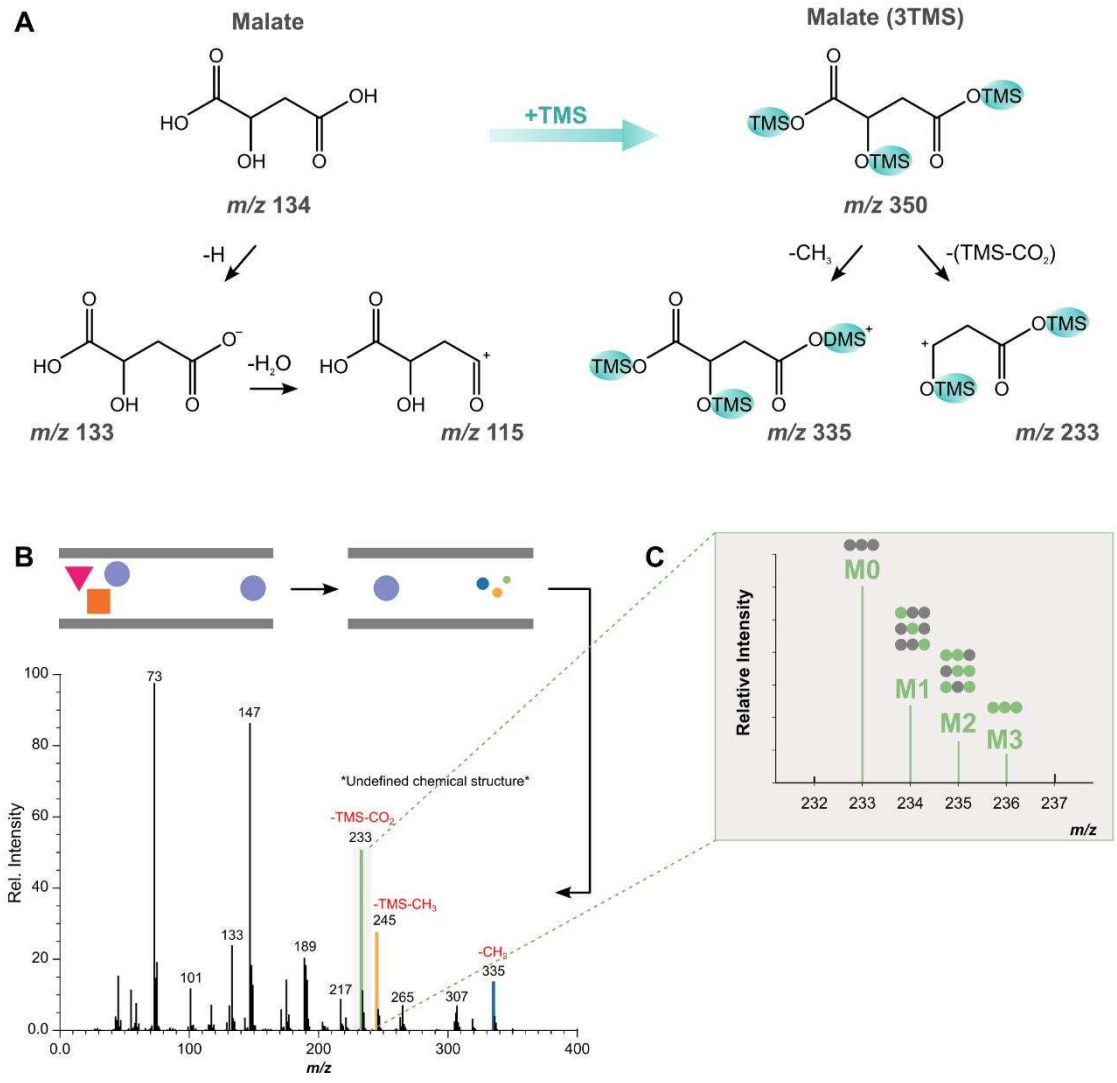

Figure 1. (A) Proposed fragmentation of malic acid before and after its derivatization, which results in the addition of 3TMS into the malate backbone. The mass-to-charge ratio (*m/z*) of each fragment is provided under the chemical formula. (B) Schematic representation of the molecule separation carried out by gas chromatography (GC) and the fragmentation obtained latter by an ionization source in the mass spectrometer (MS) (upper figure). Strong ionization sources, such as electron impact (EI), commonly used in GC/MS, leads to a stable fragmentation pattern. For instance, the mass spectrum of malate (3TMS) obtained by GC-EI/MS includes *m/z* 233, *m/z* 245 and *m/z* 335. These fragments are then used to identify this metabolite in a complex mixture of compounds, even if the chemical structure of these fragments is unknown. (C) Schematic representation highlighting the different isotopologues of the fragment *m/z* 233. Grey and green spheres represent ^{12}C and ^{13}C, respectively. The knowledge of how many carbons contains each fragment can be obtained by analysing standard (reference) substances in a GC-MS. For instance, the chemical structure of the fragment *m/z* 233 was identified by analysing ^{13}C-positionally labelled malate standards (Okahashi et al. 2019).

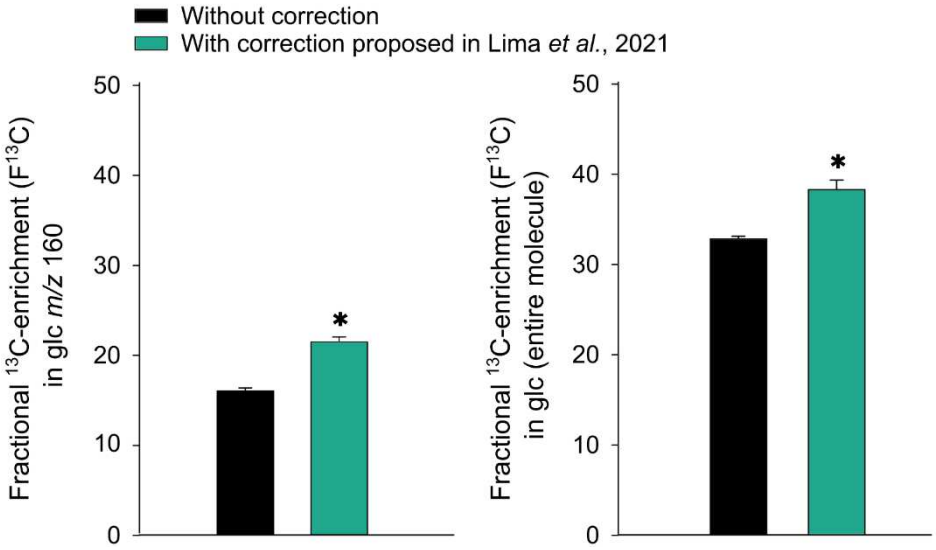

Figure 2. Fractional ^{13}C-enrichment ($F^{13}C$) in the fragment with mass-to-charge ratio (*m/z*) 160 of glucose from Arabidopsis rosettes subjected to 60 min under $^{13}CO_2$. Analysis of ^{13}C-positionally labelled glucose indicates that the fragment *m/z* 160 contains the carbons 1 and 2 of the glucose backbone and have an overlap with the fragment *m/z* 157 that contain 4 carbons, i.e. the isotopologues of the fragment *m/z* 157 range from *m/z* 158 (M1) to *m/z* 161 (M4). Thus, the ^{13}C-enrichment in the fragment *m/z* 160 did not reflects the ^{13}C-enrichment in the entire molecule of glucose and can be underestimated by considering the ^{13}C-enrichment in M3 and M4 of the fragment *m/z* 157. A recent ^{13}C-positional isotopomer approach suggests an alternative to subtract the intensities of the M3 and M4 isotopologues of the *m/z* 157 fragment from the $F^{13}C$ calculation of the *m/z* 160 fragment (Lima *et al.*, 2021). The corrected $F^{13}C$ in the glucose fragment *m/z* 160 (left figure) allows the calculation of the $F^{13}C$ in the entire molecule of glucose (right figure), which represents the sum of the $F^{13}C$ in the fragments *m/z* 160 (carbons 1 and 2) and *m/z* 319 (carbons 3, 4, 5 and 6). The original data is derived from Szecowka *et al*. (2013). The Plant Cell, 25(2), 694-714. For more details about the $F^{13}C$ calculations, see Lima *et al*., 2021. The Plant Journal, 108(4), 1213-1233.

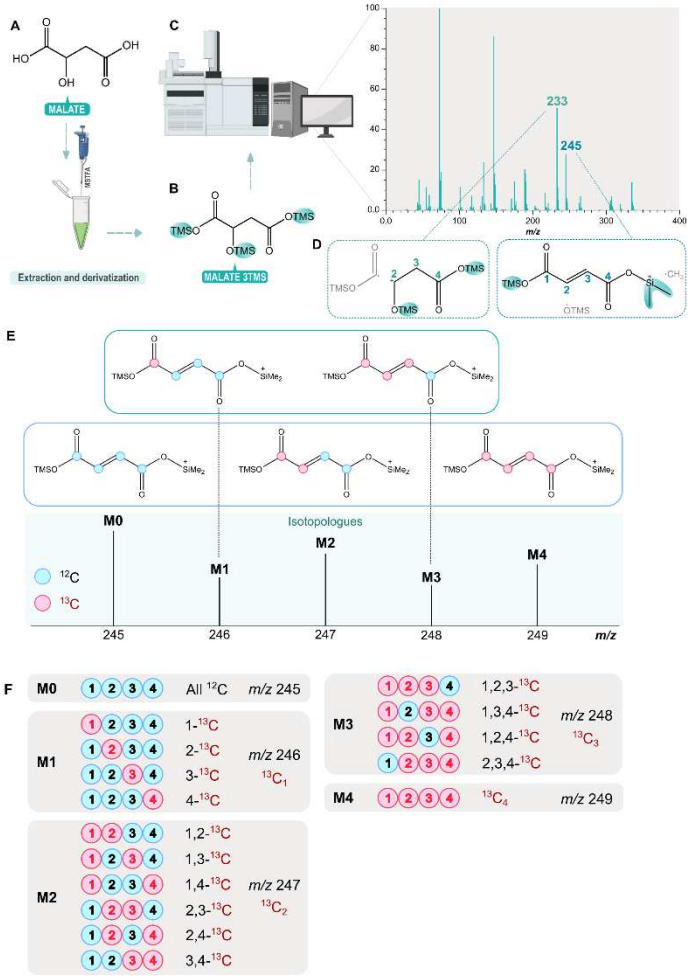

Figure I. Schematic representation on the workflow and the procedures to extract, derivatize and investigate the ^{13}C-enrichment into malate by gas chromatography coupled to electron impact mass spectrometry (GC-EI/MS). Most of the GC/MS-based metabolomics analysis requires the derivatization of the metabolites, which can be carried out by adding chemicals such as *N*-Methyl-*N*-(trimethylsilyl) trifluoroacetamide (MSTFA) to increase the volatility of the compounds (A). After this process, the molecule of malate typically shows 3TMS added to its chemical structure (B). The fragmentation of malate 3TMS by EI generates a specific pattern in terms of *m/z* values and intensities, in which the fragments *m/z* 233 and *m/z* 245 are the most abundants (C). These fragments have specific chemical structures, with the presence of different carbons of the malate backbone (D). Thus, the researcher may choose which fragment will be used to investigate the ^{13}C-enrichment into malate. After that, it is necessary to identify all isotopologues of the fragment, which refers to the number of ^{13}C atoms that has been incorporated, regardless of the atomic position. The fragment containing only ^{12}C is called the monoisotopic peak, represented as M0 (*m/z* 245). Subsequently, the incorporation of one, two, three or four ^{13}C into the malate backbone are represented by the letter M followed by the number of ^{13}C that has been incorporated (M1 - *m/z* 246, M2 - *m/z* 247, M3 - *m/z* 248, M4 - *m/z* 249) (E). It is important to highlight that the intensity of the isotopologues did not discriminate which carbon of the malate backbone has been labelled. For instance, the intensity of *m/z* 246 (M1) represents the incorporation of one ^{13}C, which could be observed at the positions 1, 2, 3 or 4 of the malate backbone (F). Thus, the ^{13}C-analysis at isotopologue level did not provide information about the atomic position.

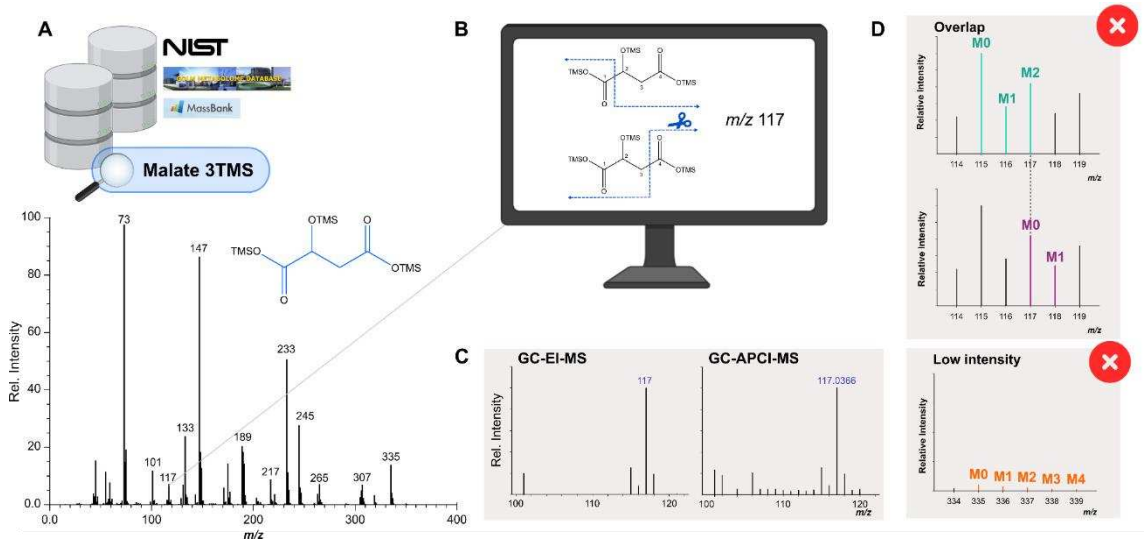

Figure II. Schematic representation on the procedures required to unveil the chemical structure of the fragments and to obtain positional ^{13}C-labelling information from gas chromatography coupled to electron impact mass spectrometry (GC-EI/MS)-based ^{13}C-metabolic flux analysis (^{13}C-MFA). The typical mass spectrum, the major fragments obtained and the chemical structure of the fragments of a metabolite of interest can be obtained by assessing different metabolome databases, which depends on the derivatization method used (A). Alternatively, *in silico* fragmentation methods can be carried out to propose possible chemical structures of each fragment of interest. However, different fragments with the same *m/z* can be obtained. For instance, two different fragments with *m/z* 117 can be obtained after malate 3TMS fragmentation by GC-EI/MS analysis (B). The undoubted description of the chemical structure of the fragments is thus only unveiled by using ^{13}C-positionally labelled reference substances. Recent evidence suggests that this analysis should be performed by using GC/MS platforms that provide information at nominal and high-mass resolution, for example by GC-EI/MS and GC-APCI (atmospheric pressure chemical ionization)/MS, respectively (C). The use of high-mass resolution platforms facilitates the distinction of fragments with the same nominal *m/z*, such as the two *m/z* 117 fragments highlighted in the figure B. It is important to highlight that not all fragments identified are suitable to be used in ^{13}C-MFA, given that several of then shows very low intensity or have overlap with other fragments (D). The use of fragments overlapping with a near one may leads to erroneous ^{13}C-enrichment calculations, as demonstrated in the figure 2.

CHAPTER II

Establishment of a GC-MS-based ^{13}C-positional isotopomer approach suitable for investigating metabolic fluxes in plant primary metabolism

6 CHAPTER II – ESTABLISHMENT OF A GC-MS-BASED ^{13}C-POSITIONAL ISOTOPOMER APPROACH SUITABLE FOR INVESTIGATING METABOLIC FLUXES IN PLANT PRIMARY METABOLISM

Valéria F. Lima[1], Alexander Erban[2], André G. Daubermann[3], Francisco Bruno S. Freire[1], Nicole P. Porto[1], Silvio A. Cândido-Sobrinho[1], David B. Medeiros[2], Markus Schwarzländer[4], Alisdair R. Fernie[2], Leticia dos Anjos[3#], Joachim Kopka[2], Danilo M. Daloso[1*]

[1] LabPLant, Departamento de Bioquímica e Biologia Molecular, Universidade Federal do Ceará, 60451-970, Fortaleza-CE, Brasil.
[2] Max-Planck-Institute of Molecular Plant Physiology, D-14476 Potsdam-Golm, Germany.
[3] Departamento de Biologia, Setor de Fisiologia Vegetal, Universidade Federal de Lavras, 37200-900, Lavras-MG, Brasil.
[4] Institute of Plant Biology and Biotechnology, Westfälische-Wilhelms-Universität Münster, D-48143 Münster, Germany.
[#] Current address: Departamento de Bioquímica e Biologia Molecular, Universidade Federal do Ceará, 60451-970, Fortaleza-CE, Brasil.

*Corresponding author.

Published manuscript in *The Plant Journal* in 2021.

Summary

^{13}C-Metabolic flux analysis (^{13}C-MFA) has greatly contributed to our understanding of plant metabolic regulation. However, the generation of detailed *in vivo* flux maps remains a major challenge. Flux investigations based on nuclear magnetic resonance have resolved small networks with high accuracy. Mass spectrometry (MS) approaches have broader potential but have hitherto been limited in their power to deduce flux information due to lack of atomic level position information. Herein we established a gas chromatography (GC) coupled to MS-based approach that provides ^{13}C-positional labelling information in glucose, malate and glutamate. A map of electron impact (EI)-mediated mass spectral fragmentation was created and validated by ^{13}C-positionally labelled references via GC-EI-MS and GC-atmospheric pressure chemical ionization (APCI)-MS technologies. The power of the approach was revealed by analysing previous ^{13}C-MFA data from leaves and guard cells and ^{13}C-HCO_3 labelling of guard cells harvested in the dark and after the dark-to-light transition. We demonstrated that the approach is applicable to established GC-EI-MS-based ^{13}C-MFA without the need for experimental adjustment but will benefit in the future from paired analyses by the two GC-MS platforms. We identified specific glucose carbon atoms that are preferentially labelled by photosynthesis and gluconeogenesis and provide an approach to investigate the phospho*enol*pyruvate carboxylase (PEPc)-derived ^{13}C-incorporation into malate and glutamate. Our results suggest that gluconeogenesis and the PEPc-mediated CO_2 assimilation into malate are activated in a light-independent manner in guard cells. We further highlight that the fluxes from glycolysis and PEPc toward glutamate are restricted by the mitochondrial thioredoxin system in illuminated leaves.

Keywords: ^{13}C-metabolic flux analysis, gluconeogenesis, guard cells, metabolic regulation, PEPc, TCA cycle, isotopomer analysis.

Introduction

Identifying the fate of carbon released into the metabolic network by a certain compound is one of the major challenges in plant metabolomics (Silva *et al.*, 2016). This is due to both the intrinsic complexity of plant cell metabolism and to technical limitations of the commonly used ^{13}C-metabolic flux analysis (^{13}C-MFA) (Sweetlove and Fernie, 2013). ^{13}C-MFA is an extremely powerful approach to unveil pathway activation rather than merely the accumulation of particular metabolites in a specific time (Fernie and Morgan, 2013; Schwender *et al.*, 2004). This is important given that metabolic fluxes do not necessarily correlate either with the accumulation of metabolites or with the level of pathway associated transcripts and proteins (Williams *et al.*, 2008; Fernie and Stitt, 2012). ^{13}C-MFA represents therefore an important component of functional genomics and metabolic engineer (Nielsen and Keasling, 2016). However, experimental and technical challenges currently limit the use of ^{13}C-MFA in plant biology.

^{13}C-MFA presupposes the use of a ^{13}C-labeled tracer and a sensitive technique to measure the ^{13}C incorporation into the metabolites. Given the possibility to identify ^{13}C-labelling at atom position, ^{13}C-nuclear magnetic resonance (^{13}C-NMR) is one of the best approaches for ^{13}C-MFA (Zamboni *et al.*, 2009; Kim *et al.*, 2010). However, NMR is less sensitive than mass spectrometry (MS), which restricts its use to small metabolic networks (Ratcliffe and Shachar-Hill, 2006) and renders the use of NMR for single cell MFA non-feasible, given that an enormous amount of cells would be required for such analysis (Medeiros *et al.*, 2019). Metabolite separation by gas (GC), liquid (LC) or capillary (CE) chromatography coupled to MS appear as important techniques to overcome the sensitivity limitation of ^{13}C-NMR approaches (Antoniewicz, 2013a). However, the reduced power of MS approaches to deduce flux information at defined atom positions restricts its use in ^{13}C-MFA and consequently limits our understanding of how metabolic pathways are regulated.

The ^{13}C-positional isotopomer labelling information obtained by ^{13}C-NMR is not only key to understand the regulation of metabolic pathways but can also be used to estimate enzyme activity *in vivo* (Abadie and Tcherkez, 2019). This is a critical advantage of NMR over MS approaches (Antoniewicz, 2013b). The analysis of positional isotopomers refers to the differentiation of not only the mass difference but also the atomic level resolution of where the label has been incorporated into a given molecule (Antoniewicz, 2013a). Information from ^{13}C-positional labelling analysis allows the discrimination of which pathways contribute to the

synthesis of a particular metabolite. For instance, ^{13}C-NMR has recently been used to investigate the source of carbon for glutamate (Glu) synthesis in *Helianthus annuus* L. leaves following provision of $^{13}CO_2$ (Abadie *et al.*, 2017). The results of this study indicate that there is incorporation of one carbon from the anaplerotic CO_2 assimilation catalysed by phospho*enol*pyruvate carboxylase (PEPc) activity into the carbon 1 (1-C) of the Glu backbone and that no carbon from glycolysis is incorporated into Glu following short time $^{13}CO_2$ labelling (Abadie *et al.*, 2017). This result corroborates previous modelling and ^{13}C-labelling studies indicating that the fluxes throughout the tricarboxylic acid (TCA) cycle are inhibited in illuminated leaves (Tcherkez *et al.*, 2012; Gauthier *et al.*, 2010; Cheung *et al.*, 2014).

By contrast to illuminated leaves, evidence highlights that a high ^{13}C incorporation into Glu and glutamine (Gln) and in tricarboxylic acid (TCA) cycle metabolites is observed in illuminated guard cells following provision of ^{13}C-sucrose and ^{13}C-HCO_3, respectively (Daloso *et al.*, 2015a; Robaina-Estévez *et al.*, 2017; Medeiros *et al.*, 2018; Daloso *et al.*, 2016a). Furthermore, ^{14}C- and ^{13}C-labelling experiments highlight that malate and aspartate are strongly labelled in illuminated guard cells (Brown and Outlaw, 1982; Daloso *et al.*, 2015a; Robaina-Estévez *et al.*, 2017; Daloso *et al.*, 2016b). This characteristic resemble those of C4 and CAM cell types, in which a high PEPc activity is observed (O'Leary *et al.*, 2011). However, given the lack of a MS-based ^{13}C-positional labelling approach, none of these works directly investigated the PEPc-mediated ^{13}C-incorporation into malate or aspartate. Taken together, these observations suggest that the metabolic fluxes toward the TCA cycle, Glu, and Gln synthesis are differentially regulated in mesophyll cells and guard cells under illumination and highlights the need for cell specific investigations.

The carbon assimilated by PEPc is directly incorporated into the 4-C of oxaloacetate (OAA) and subsequently incorporated into the 4-C of malate or aspartate by malate dehydrogenase (MDH) and aspartate amino transferase (AspAT), respectively (Melzer and O'Leary, 1987). It is thus reasonable to hypothesize that the ^{13}C-incorportion into the 4-C of malate and/or aspartate reflects PEPc activity (Abadie and Tcherkez, 2019). In this vein, a recent study elegantly provided a map of fragmentation of trimethylsilyl (TMS)-derivatized TCA cycle metabolites obtained by GC-MS using electron impact (EI) as ionization source (Okahashi *et al.*, 2019). The results from this study suggest that the fragment with mass-to-charge ratio (*m*/*z*) 117 contains the 4-C of malate, offering a great possibility to investigate the PEPc-mediated ^{13}C incorporation into malate. However, the work from Okahashi and colleagues is solely based on ^{13}C-positionally labelled reference compounds, i.e., no biological

sample has been used. Therefore, the feasibility of the use of the mass fragment (in the following: fragment) *m/z* 117 to investigate the PEPc-mediated ^{13}C incorporation into malate remains to be determined.

Here we established an *in silico* fragmentation map of TMS-derivatized compounds with further validation by analysing positionally ^{13}C-labelled reference substances with both GC-EI-MS at nominal mass resolution and high-mass-resolution GC-MS coupled to atmospheric pressure chemical ionization (APCI). We aimed to investigate the PEPc-mediated ^{13}C incorporation into malate and glutamate. Given the importance of glucose metabolism for guard cells (Flütsch *et al.*, 2020a; Flütsch *et al.*, 2020b; Lawson and Matthews, 2020) and the difficulty to distinguish ^{13}C-label incorporation into glucose from different metabolic pathways, especially in source tissues, we extended current analytical limitations by establishing a ^{13}C-positional labelling approach that determines the ^{13}C-incorporation into glucose at atomic level. The power of the approach was revealed by analysing previous GC-MS data from ^{13}C-labelling studies carried out in leaves and guard cells (Szecowka *et al.*, 2013; Arrivault *et al.*, 2017; Daloso *et al.*, 2015a; Daloso *et al.*, 2015b) together with ^{13}C-HCO_3 kinetic labelling using guard cells harvested in the dark and after the dark-to-light transition.

Results

Establishment of a GC-MS-based ^{13}C-positional labelling approach

To identify the ^{13}C-positional labelling information from mass spectral analyses of glucose, malate and glutamate, we first assembled a mass spectral fragmentation map by identifying the chemical structures of the trimethylsilylated and – in part – methoxyaminated metabolites deposited in the Golm Metabolome Database (http://gmd.mpimp-golm.mpg.de/) (Kopka *et al.*, 2005) and by searches of metabolite fragmentation patterns in previously published studies (Souza *et al.*, 2018; De Jongh *et al.*, 1969; Antoniewicz *et al.*, 2007; Okahashi *et al.*, 2019; Petersson, 1972; Abadie *et al.*, 2017; Leimer *et al.*, 1977) (Figure 1 – Step 1). We additionally performed an *in silico* simulation of metabolite fragmentation and identified fragments that represented one or a subset of the metabolites´ carbon atoms (Figure 1 – Step 2). These predictions were validated by analysing commercially available ^{13}C-positionally labelled reference substances by GC-EI-MS at nominal mass resolution and by GC-APCI-MS at high mass resolution (Figure 1 – Step 3) (Strehmel *et al.*, 2014). Fragments with low intensity and/or those indistinguishably overlapping with other fragments were discarded from the analysis (see

Data S1 for detailed description of the fragments analysed here). The feasibility of the remaining fragments for retrieving carbon position information was investigated using GC-MS data from previous plant ^{13}C-labelling studies (Figure 1 – Step 4) (Daloso *et al.*, 2015a; Daloso *et al.*, 2015b; Arrivault *et al.*, 2017; Szecowka *et al.*, 2013; Ishihara *et al.*, 2015; Medeiros *et al.*, 2018; Dethloff *et al.*, 2017). In parallel, we established different mathematical frameworks to estimate positional ^{13}C-enrichment in glucose, malate and glutamate (Figure 1 – Step 5). To that end, we calculated the **relative (%) isotopologue abundance (RIA)** using the **relative metabolite content (RMC)** (Eqn 1), which was then used to derive the **fractional ^{13}C-enrichment (F^{13}C)** of each fragment (Eqn 2) (Lima *et al.*, 2018).

Eqn 1: Relative (%) isotopologue abundance (RIA)

$RIA(Mn) = [RMC(Mn) \times 100] / \Sigma [M0, M1...Mn]$

$RMC = [(Mn - noise) / R] / FW$

Mn = intensity of the isotopologue with n ^{13}C incorporation.

noise = intensity of the fragment detected in an empty tube.

R = intensity of the fragment *m/z* 319 of ribitol, used as an internal quantitative control

FW = fresh weight.

Eqn 2: Fractional ^{13}C-enrichment (F^{13}C)

$F^{13}C = [\Sigma (RIA(Mn) \times n)] / N$

N = number of carbon atoms of the molecule present in the fragment

To allow comparison between samples and to obtain the ^{13}C-positional labelling information, the F^{13}C of each fragment was normalized by the control (time 0) of each experiment. The values obtained from this normalization are denominated here as **relative ^{13}C-enrichment (R^{13}C)** (Eqn 3).

Eqn 3: Relative ^{13}C-enrichment (R^{13}C)

$R^{13}C = F^{13}C_{(time\ n)} / F^{13}C_{(time\ 0)}$

Time n = samples harvested after n min of ^{13}C-labelling.

$F^{13}C_{(time\ 0)}$ = average of the F^{13}C obtained in samples not subjected to ^{13}C-labelling.

After that, the R^{13}C was multiplied by the number of carbon atoms of the metabolite present in the fragment (N) to obtain the **total ^{13}C-enrichment (T^{13}C)** (Eqn 4).

Eqn 4: Total ^{13}C-enrichment (T^{13}C)

$T^{13}C = R^{13}C \times N$

The **positional ^{13}C-enrichment (P^{13}C)** was then calculated by subtracting the $T^{13}C$ of different fragments (for details see equations 5-to-13 below).

^{13}C-positional labelling analysis of glutamate

It has previously been demonstrated that the PEPc-derived ^{13}C is incorporated into the 1-C of Glu in illuminated leaves (Abadie *et al.*, 2017). We searched for fragments that contain the 1-C of the Glu backbone. Our *in silico* analysis showed that the fragmentation at the TMS-carboxyl group between the 1-C and 2-C of Glu results in the fragments *m/z* 117 and *m/z* 246, with monoisotopic *m/z* of 117.0366 and 246.1339, respectively (Figure 2a). Similarly, glutamine (Gln) fragmentation at the TMS-carboxyl group between the 1-C and 2-C results in the fragments *m/z* 117 (117.0372) and *m/z* 245 (245.1505) (Figure 2b). Both Glu and Gln have a common fragment with *m/z* 156 (*m/z* 156.0839), that also contains 2,3,4,5-C of their backbone (Figures 2c,d). Given that the incorporation of ^{13}C atoms in a fragment causes a shift in the *m/z* ratio observed in the mass spectra, we deduced that the Gln fragments *m/z* 156 and *m/z* 245 should change to 160 and 249, respectively, and confirmed this by analysing a fully labelled Gln reference (U-^{13}C Gln) (Figures 2e,f). GC-EI-MS analysis of a 1-^{13}C Gln reference validated that the fragments *m/z* 156 and *m/z* 245 lack the 1-C of the Gln backbone (Figure 2e,f). Analyses of 1-^{13}C Glu and 5-^{13}C Glu confirmed that the fragment *m/z* 156 does not contain 1-C but 5-C of the Glu backbone (Figure 2g). The fragment *m/z* 347 of Gln shifted to *m/z* 352 in U-^{13}C Gln analysis (Figure 2h), highlighting that this fragment and its analogue in Glu (*m/z* 348) provide information of the complete carbon backbones of Gln and Glu, respectively.

The relative abundance of *m/z* 118 increased substantially in 1-^{13}C Glu and was 2.7-fold more abundant than non-labelled Glu with natural, *i.e.,* ambient, composition of carbon isotopes (Figure 2i). Apparently, *m/z* 117 contain the 1-C of Glu, but the intensity of labelled *m/z* 118 did not fully match the abundance of the non-labelled *m/z* 117, suggesting a possible contribution of mass fragments with equal or very similar nominal mass and their respective isotopologues. Indeed, detailed mass spectral analysis highlights the presence of the mass fragments *m/z* 114-118 at similar abundance in non-labelled Glu (Figure S1). Therefore, the *m/z* 117 abundance can be a potential composite of isotopologues of the fragments *m/z* 115 and *m/z* 116, which explain the higher intensity of ambient *m/z* 117 compared to the intensity of *m/z* 118 from 1-^{13}C Glu analysis (Figure 2i). We then established a mathematical framework to estimate

the $P^{13}C$ in the 1-C of Glu by using the $T^{13}C$ of the fragments *m/z* 348 (1,2,3,4,5-C) and *m/z* 246 (2,3,4,5-C) (Eqn 5).

Eqn 5: $P^{13}C$ in 1-C of Glu

$$P^{13}C(\text{1-C Glu}) = T^{13}C_{[m/z\ 348\ (1,2,3,4,5\text{-C})]} - T^{13}C_{[m/z\ 246\ (2,3,4,5\text{-C})]}$$

The $P^{13}C$ in the 1-C of Glu obtained from this calculation was linearly correlated with the $T^{13}C$ of the fragment *m/z* 117 in Arabidopsis rosettes following provision of $^{13}CO_2$ (Figure 2j). This reinforces the observation that the fragment *m/z* 117 provides positional information of the 1-C of Glu. Therefore, the $T^{13}C$ in the fragment *m/z* 246 (or *m/z* 156) coupled to the $P^{13}C$ at the 1-C of Glu obtained by either the mathematical framework or the $T^{13}C$ of the fragment *m/z* 117 can be used to distinguish the relative contribution of glycolysis and TCA cycle pathways (see Glu carbons highlighted in red and black in the Figure 3a) from that of the CO_2 fixation via PEPc to the synthesis of Glu (see Glu carbon highlighted in blue in the Figure 3a).

Analysis of the PEPc-mediated ^{13}C incorporation into malate

Analysis of positionally labelled organic acids by GC-EI-MS suggests that the malate fragment *m/z* 117 contains the 4-C of the malate backbone (Okahashi *et al.*, 2019). The *m/z* 117 is a common fragment of trimethylsilylated carboxylic acid moieties obtained after EI-fragmentation of TCA cycle metabolites (see blue atoms in the Figure 3a), suggesting that this fragment could be used to investigate the PEPc-mediated ^{13}C-incorporation into malate (Figure 3b). However, our GC-APCI-MS analysis indicates the existence of two fragments with common nominal mass (*m/z* 117) but different monoisotopic masses (*m/z* 117.0366 and *m/z* 117.0731) (Figure 4a). These fragments correspond to 66 % and 34 % of the total *m/z* 117 abundance, respectively. Analysis of 1-^{13}C malate and 2-^{13}C malate references indicate that the fragment 117.0366 does not contain 1-C and 2-C, whilst the fragment *m/z* 117.0730 contains the 2-C but not 1-C of the malate backbone (Figure 4a). According to our fragmentation simulation and the data from Okahashi and collaborators (Okahashi *et al.*, 2019), the fragment *m/z* 117.0366 contains the 4-C of the malate backbone ($TMS\text{-}COO^{\cdot+}$) whilst the fragment *m/z* 117.0730 possibly contains the 2,3-C ($TMS\text{-}OCH2CH2^{\cdot+}$) (Figure 4b). Importantly, our GC-APCI-MS analysis confirmed unequivocally that 1-C does not contribute to *m/z* 117.0366 (Figure 4a) and therefore is specific to 4-C (Figure 4b) as well as that the fragment *m/z* 265 contains the 2-C of the malate backbone (Figure S2), as suggested previously (Okahashi *et al.*,

2019). Whilst the chemical structure of the fragments *m/z* 233 (2,3,4-C) and *m/z* 245 (1,2,3,4-C) was identified (Figure 4c), the composition of the fragment *m/z* 265 is yet non-interpreted.

We next used the mathematical framework described above for $P^{13}C$ analysis to estimate the $P^{13}C$ in each carbon atom of malate (Eqn's 6-9). For this purpose, we used the $T^{13}C$ of the GC-EI-MS fragments *m/z* 245 (1,2,3,4-C), *m/z* 233 (2,3,4-C), *m/z* 265 (2-C) and *m/z* 117 (4-C). Given that the monoisotopic mass that contains the 4-C of malate backbone (*m/z* 117.0366) corresponds to 66% of the total *m/z* 117 abundance, the $T^{13}C$ of *m/z* 117 was then multiplied by 0.66 in the $P^{13}C$ calculation of 3-C and 4-C of malate.

Eqn 6: $P^{13}C$ in the 1-C of malate

$$P^{13}C(\text{1-C Mal}) = T^{13}C_{[m/z\ 245\ (1,2,3,4\text{-C})]} - T^{13}C_{[m/z\ 233\ (2,3,4\text{-C})]}$$

Eqn 7: $P^{13}C$ in the 2-C of malate

$$P^{13}C(\text{2-C Mal}) = T^{13}C_{[m/z\ 265\ (2\text{-C})]}$$

Eqn 8: $P^{13}C$ in the 3-C of malate

$$P^{13}C(\text{3-C Mal}) = T^{13}C_{[m/z\ 233\ (2,3,4\text{-C})]} - T^{13}C_{[m/z\ 265\ (2\text{-C})]} - \{T^{13}C_{[m/z\ 117\ (4\text{-C})]} \times 0.66\}$$

Eqn 9: $P^{13}C$ in the 4-C of malate

$$P^{13}C(\text{4-C Mal}) = T^{13}C_{[m/z\ 117\ (4\text{-C})]} \times 0.66$$

Determination of ^{13}C-enrichment in glucose at single and dual atomic level

The fragmentation map of glucose 1MEOX 5TMS was obtained by *in silico* simulation and confirmed by previous GC-MS studies (Desage *et al.*, 1989; Beylot *et al.*, 1993; MacLeod *et al.*, 2001) and by analysing naturally (i.e. containing ~1.1% of ^{13}C), uniformly (U-^{13}C) and positionally ^{13}C-labelled glucose using both GC-EI-MS and GC-APCI-MS. The composition of fifteen glucose fragments was determined. However, it is important to emphasize that several of them are not suitable for ^{13}C-MFA. This is due to either low intensity of the fragments or isotopologues and/or to complex overlaps between isotopologue sets of two fragments with close nominal masses. For instance, the fragment *m/z* 259 has five carbons of the glucose backbone (2,3,4,5,6-C), whose three isotopologues, M3 (*m/z* 262), M4 (*m/z* 263) and M5 (*m/z* 264), overlay the fragment *m/z* 262 that has three carbons of the glucose backbone (1,2,3-C) (Data S1). Additionally, both fragments have low intensity and several other yet non-interpreted

fragments are found near them in the mass spectrum (Figure S3). These fragments, and others with similar caveats, were discarded from the analysis.

The composition of the fragments *m/z* 129 (4,5,6-C), *m/z* 205 (5,6-C), *m/z* 217 (4,5,6-C) and *m/z* 319 (3,4,5,6-C) was clearly identified by both GC-EI-MS and GC-APCI-MS analyses (Figures 5a-d) and, therefore, can be used in ^{13}C-MFA without restriction (see Figures S4-S8 for detailed information regarding ^{13}C-positionally labelled glucose analyses). The fragments *m/z* 103 and *m/z* 133 contain one carbon of the glucose backbone, as evidenced by the increases in the intensity of *m/z* 104, *m/z* 104.0605 and *m/z* 134.0716 when analysing U-^{13}C glucose reference by GC-EI-MS and GC-APCI-MS (Figures S4a-d). GC-APCI-MS analyses identified two fragments with nominal mass *m/z* 103 but different monoisotopic masses (*m/z* 103.0570 and *m/z* 103.0532) and three fragments with nominal mass *m/z* 133 but different monoisotopic masses (*m/z* 133.0132, *m/z* 133.0503 and *m/z* 133.0676). The fragments *m/z* 103.0570 and *m/z* 133.0676 contain the 6-C of the glucose backbone, as evidenced by U-^{13}C and 6-^{13}C glucose analyses (Figure S4b,d). Whilst the composition of the *m/z* 103.0570 is clear (Figure 5e), which represents 40% of the *m/z* 103 intensity, the chemical structure of the fragment *m/z* 133 is yet to be determined. Thus, we calculate P^{13}C at the 6-C of glucose by 40 % of the T^{13}C of *m/z* 103 from GC-EI-MS analysis (Eqn 10).

Eqn 10: P^{13}C in the 6-C of glucose

$$P^{13}C(\text{6-C Glc}) = T^{13}C_{[m/z\ 103\ (6\text{-C})]} \times 0.4$$

Surprisingly, none of the fragments suitable for ^{13}C-MFA described so far contain the 1,2-C of the glucose backbone. These carbons could be investigated by using the fragment's *m/z* 160 (1,2-C) (Figure 5f), *m/z* 259 (2-C), *m/z* 262 (1,2-C) and the molecular ions *m/z* 554, *m/z* 569 and *m/z* 570. However, the intensity of the fragment *m/z* 554 is low in GC-EI-MS analysis and the other fragments overlap with a close fragment (Data S1). We then established another mathematical framework to estimate the F^{13}C of the overlapping fragments *m/z* 157 and *m/z* 160 (Figure 5g). Given that the fragments *m/z* 157 and *m/z* 319 have the same carbons of the glucose backbone (3,4,5,6-C), it is expected that the F^{13}C is identical or highly similar between these fragments. We then correlated the NI of the isotopologues M0, M1 and M2 of these fragments, which do not overlap other fragments, to verify whether our assumption is correct. The results showed that the correlation between M0 (*m/z* 319 *vs m/z* 157), M1 (*m/z* 320 *vs m/z* 158) and M2 (*m/z* 321 *vs m/z* 159) of these fragments is linear ($R^2 > 0.9$; $P < 0.05$) (Figure 5h), confirming our prediction. Given that no other compound was coeluted with glucose, we

assume that the correlation between M3 and M4 of the fragments *m/z* 319 and *m/z* 157 should have similar values in terms of absolute and/or relative abundance. To test whether this assumption is justified, we investigated the relationship between isotopologues of other fragments that contain redundant information of identical carbon atoms from the glucose backbone. The correlation between isotopologues of the fragments *m/z* 129 (4,5,6-C) and *m/z* 217 (4,5,6-C) was higher when using NI rather than RIA data. The opposite was observed when comparing isotopologues of the fragments *m/z* 103 (6-C) and *m/z* 133 (6-C). In both cases, the $F^{13}C$ is highly correlated between the fragments ($R^2 > 0.98$) (Table S1). Thus, although slight differences may be observed in the RIA between fragments that contain the same carbons of the glucose backbone, these differences do not seem to affect the $F^{13}C$ calculation. We then assumed that the RIA of M3 (*m/z* 160) and M4 (*m/z* 161) of the fragment *m/z* 157 is equal to the RIA of M3 (*m/z* 322) and M4 (*m/z* 323) of the fragment *m/z* 319. These values were used to calculate the $F^{13}C$ of the fragment *m/z* 160 (Eqn 11).

Eqn 11: $F^{13}C$ of glucose *m/z* 160

$$F^{13}C_{(Glc\text{ - }m/z\ 160)} = [(RIA^{*}_{m/z\ 160\ (M0)} \times 0) + (RIA^{*}_{m/z\ 161\ (M1)} \times 1) + (RIA^{*}_{m/z\ 162\ (M2)} \times 2)] / 2$$

$$RIA^{*}_{m/z\ 160\ (M0)} = RIA_{m/z\ 160\ (M0)} - RIA_{m/z\ 322\ (M3)}$$

$$RIA^{*}_{m/z\ 161\ (M1)} = RIA_{m/z\ 161\ (M1)} - RIA_{m/z\ 323\ (M4)}$$

$$RIA^{*}_{m/z\ 162\ (M2)} = 100 - [RIA^{*}_{m/z\ 160\ (M0)} + RIA^{*}_{m/z\ 161\ (M1)}]$$

Next, we used different fragments of glucose and established a mathematical framework to provide three novel possibilities to analyse the ^{13}C-enrichment into glucose: (i) to estimate the $P^{13}C$ in each atom of glucose, with exception of the 1,2-C that could not be distinguished (Eqn's 12-15), (ii) to estimate the ^{13}C-enrichment in pairs of carbon atoms, 1,2-C, 3,4-C and 5,6-C (Eqn's 16-18), and (iii) to estimate the ^{13}C-enrichment in the entire glucose molecule (Eqn 19).

Eqn 12: $P^{13}C$ in 1,2-C of glucose

$$P^{13}C(1,2\text{-C Glc}) = T^{13}C_{[m/z\ 160\ (1,2\text{-C})]}$$

Eqn 13: $P^{13}C$ in the 3-C of glucose

$$P^{13}C(3\text{-C Glc}) = T^{13}C_{[m/z\ 319\ (3,4,5,6\text{-C})]} - T^{13}C_{[m/z\ 129\ (4,5,6\text{-C})]}$$

Eqn 14: $P^{13}C$ in the 4-C of glucose

$$P^{13}C(4\text{-C Glc}) = T^{13}C_{[m/z\ 217\ (4,5,6\text{-C})]} - T^{13}C_{[m/z\ 205\ (5,6\text{-C})]}$$

Eqn 13: $P^{13}C$ in the 5-C of glucose

$$P^{13}C(5\text{-C Glc}) = T^{13}C_{[m/z\ 205\ (5,6\text{-C})]} - \{T^{13}C_{[m/z\ 103\ (6\text{-C})]} \times 0.4\}$$

The factor 0.4 was used to estimate the $P^{13}C$ in the 5-C of glucose given that the monoisotopic mass that contains the 6-C of glucose backbone (*m/z* 103.0570) corresponds to 40% of the total *m/z* 103 abundance, as estimated by GC-APCI-MS analysis.

Eqn 16: Dual atomic ^{13}C-enrichment ($DA^{13}C$) in 1,2-C of glucose

$$DA^{13}C(1,2\text{-C Glc}) = P^{13}C(1,2\text{-C Glc})$$

Eqn 17: $DA^{13}C$ in 3,4-C of glucose

$$DA^{13}C(3,4\text{-C Glc}) = P^{13}C(3\text{-C Glc}) + P^{13}C(4\text{-C Glc})$$

Eqn 18: $DA^{13}C$ in 5,6-C of glucose

$$DA^{13}C(5,6\text{-C Glc}) = P^{13}C(5\text{-C Glc}) + P^{13}C(6\text{-C Glc})$$

Eqn 19: ^{13}C-enrichment in the entire molecule of glucose

$$U^{13}C\ Glc = T^{13}C_{[m/z\ 160\ (1,2\text{-C})]} + T^{13}C_{[m/z\ 319\ (3,4,5,6\text{-C})]}$$

Validation of the ^{13}C-positional isotopomer labelling approaches

To further test the power of our approaches, we applied the mathematical framework described above to investigate ^{13}C-metabolic distribution through the TCA cycle and associated pathways as well as toward glucose synthesis using previous GC-MS data from Arabidopsis rosettes and maize leaves following provision of $^{13}CO_2$, from Arabidopsis leaves following provision of ^{13}C-malate, ^{13}C-glucose or ^{13}C-pyruvate and from tobacco guard cells following provision of ^{13}C-HCO_3 (Daloso *et al.*, 2015a; Daloso *et al.*, 2015b; Arrivault *et al.*, 2017; Szecowka *et al.*, 2013). We additionally carried out a ^{13}C-HCO_3 kinetic labelling experiment harvesting guard cells after 0, 10, 20 and 60 min of labelling under continuous dark or after the dark-to-light transition. In the next sections, we describe the main results obtained from these analyses.

Guard cells do assimilate CO_2 in the dark, but illumination increases PEPc-derived ^{13}C incorporation into malate

The $P^{13}C$ in the 4-C of malate was 2.3-fold higher in maize leaves than Arabidopsis rosettes following provision of $^{13}CO_2$ (Figure 6a). This is in agreement with the current understanding of C3 and C4 cells, in which a higher PEPc activity is expected to occur in C4 cells (Bowyer and Leegood, 1997). It is noteworthy however that no statistical comparison could be performed in this case, given that GC-MS analysis of the maize experiment was carried out using a single replicate (Arrivault *et al.*, 2017). All malate fragments analysed here were labelled in illuminated Arabidopsis rosettes (Figure 6b). We next estimated the $P^{13}C$ in each of the carbon atom positions of malate. Whilst 1-C remained unlabelled throughout the experiment, increased $P^{13}C$ into 2-C, 3-C and 4-C labelling was observed (Figure 6c). A comparison of guard cells in the dark and in the light, showed that guard cells assimilate CO_2 in the dark, as evidenced by the increased $R^{13}C$ in malate *m/z* 117 (4-C). This was the only fragment labelled in guard cells in either light or dark conditions (Figure 6d). Interestingly, illumination led to higher $R^{13}C$ in malate *m/z* 117 after 60 min, when compared to the corresponding dark-exposed control, suggesting a higher PEPc activity in the light (Figure 6e).

Glucose is rapidly labelled by gluconeogenesis in the dark, but light exposure increased the ^{13}C-enrichment in the entire glucose molecule

Practically all glucose fragments investigated here have been labelled in guard cells, with exception of the fragments *m/z* 129 (4,5,6-C) and *m/z* 133 (6-C) in dark-exposed guard cells (Figure 7a). Notably, light exposure increased the $R^{13}C$ in different glucose fragments, which leads to a higher ^{13}C-enrichment in the entire glucose molecule after 10 and 60 min of labelling in illuminated guard cells, when compared to guard cells in the dark (Figure 7b). Interestingly, glucose levels dropped in guard cells after the start of the experiment in a light-independent manner. In contrast, the level of glucose in Arabidopsis rosettes remained unchanged 60 min after provision of $^{13}CO_2$ (Figure 7c).

Carbon positions 1 and 2 of glucose are preferentially labelled in the light mirroring photosynthetic carbon flux

^{13}C-positional labelling analysis revealed that 1,2-C, 3,4-C and 5,6-C are labelled in guard cells in a light-independent manner after 10 min of label exposure. All positions were labelled after 10 min of label exposure to guard cells, with exception of 3-C and 4-C of darkened

and illuminated guard cells, respectively (Figure 8a). By contrast, in Arabidopsis rosettes only the 5-C and the pair 3,4-C differed after 10 min of labelling (Figure 8a). Notably, the ^{13}C-enrichment in glucose is continuously increasing in Arabidopsis rosettes over time, reaching full labelling after 20 min of label exposure (Figure 8a). By contrast, the ^{13}C-enrichment in guard cell glucose fluctuates, which may be related to the strong decrease in the glucose content (Figure 7c) and/or to a dilution of the labelling derived from starch degradation (Horrer *et al.*, 2016; Flütsch *et al.*, 2020b). At 60 min of labelling, only illuminated tissues showed increased ^{13}C-enrichment in glucose carbons, especially in 1,2-C (Figure 8a). Comparing the percentage of ^{13}C-enrichment in the carbon pairs of glucose, Arabidopsis rosettes showed higher percentages of ^{13}C-enrichment in the 1,2-C than dark-exposed guard cells after 10 min of labelling and illuminated guard cells after 20 and 60 min of labelling (Figure 8b). These results suggest that the 1,2-C are preferentially labelled by photosynthesis (Figure 8c), which is consistent with the higher photosynthetic capacity of mesophyll cells, as compared to guard cells (Gotow *et al.*, 1988; Lawson, 2009), and corroborates modelling and NMR-based ^{13}C-positional labelling analysis (Wieloch *et al.*, 2018; Wieloch *et al.*, 2021).

Gluconeogenesis is active in guard cells

It has been shown that glucose from rat livers, in which gluconeogenesis is highly active, is solely labelled in 3,4-C following provision of ^{13}C-HCO_3 (Beylot *et al.*, 1993). Similarly, evidence from anaplerotic CO_2 fixation of non-illuminated *Cucurbita pepo* L. cotyledons following provision of $^{14}CO_2$ indicates that these carbons are preferentially labelled, although label is also incorporated into the carbon positions 1, 2, 5 and 6 (Leegood and ap Rees, 1978). The gluconeogenesis-derived ^{13}C-incorporation into the 3,4-C of glucose is explained by a set of biochemical reactions involving the anaplerotic CO_2 assimilation and the fumarase (FUM) symmetrisation reaction, which culminates in phospho*enol*pyruvate (PEP) labelled at 1,3-C (Figure 9a). Based on this rationale, we explored whether the label incorporation into 3,4-C could be used to investigate the presence of gluconeogenic fluxes in tissues fed with ^{13}C-HCO_3 or $^{13}CO_2$. Analysis of the ^{13}C-enrichment into 3,4-C reveals that they are labelled in guard cells in a light-independent manner (Figures 8a). The percentage of ^{13}C-incorporation into these carbons is higher than 1,2-C and 5,6-C in guard cells (Figure S9). Higher ^{13}C-enrichment at the carbon positions 3 and 4 was observed in guard cells when compared to Arabidopsis rosettes in both relative (%) and absolute terms (Figure 9b). Those observations strongly suggest that guard

cells operate flux through gluconeogenesis and that this flux is much less pronounced in mesophyll cells as the dominant cell type in rosette tissues.

PEPc-mediated ^{13}C-incorporation into the carbon 1 of glutamate is negatively regulated by the mitochondrial NTR/TRX system in Arabidopsis leaves

We next analysed the ^{13}C-enrichment in Glu in Arabidopsis leaves of wild type (WT) and in plants impaired in their thioredoxin system using a *trxo1* line and a *ntra ntrb* line fed with U-^{13}C glucose, U-^{13}C malate or U-^{13}C pyruvate (Daloso *et al.*, 2015b). The R^{13}C in 2,3,4,5-C of Glu increased following provision of ^{13}C-pyruvate, showing active label incorporation, while ^{13}C-glucose and ^{13}C-malate provision did not cause any change. No difference in labelling was observed between the genotypes for the same ^{13}C-tracer treatment, however (Figures 10a-c). Assessing 1-C a contrasting picture emerged. No ^{13}C-enrichment in 1-C of Glu was observed following provision of ^{13}C-malate; ^{13}C-pyruvate gave rise to labelling that was similar in all three genetic backgrounds, however. Strikingly, provision of ^{13}C-glucose resulted in ^{13}C-enrichment in the 1-C of Glu exclusively in the mutants (Figures 10d-f). This suggests that the NTR/TRX system suppresses flux through PEPc through a mechanism that operates in the mitochondrial matrix (Figure 10g).

Discussion

Feasibility and potential of the GC-MS-based ^{13}C-positional isotopomer approach

The GC-EI-MS platform offers high resolution/sensitivity and a stable fragmentation pattern due to the strong energy used in EI ionization (Huege *et al.*, 2007). Thus, GC-EI-MS-based ^{13}C-MFA is a promising alternative to overcome the limitation of the lack of positional ^{13}C-labelling information of MS-based ^{13}C-MFA (Choi *et al.*, 2012). However, the lack of a clear fragmentation map has restricted the use of data from this platform in ^{13}C-MFA. Aiming to overcome this technical limitation, we established a specific fragmentation map of glucose, malate and glutamate that allowed us to investigate the ^{13}C incorporation into glucose at atom position and the ^{13}C distribution from PEPc activity into malate and Glu. The results are in overall agreement with recent NMR-based ^{13}C-MFA (Abadie *et al.*, 2017; Abadie *et al.*, 2018), validating suitability of the approach for high resolution flux analysis.

The feasibility of our approach is further supported by the fact that malate labelled specifically at the 4-C shows a shift from *m/z* 117 to *m/z* 118 when injected solely in a GC-EI-MS (Okahashi *et al.*, 2019). Following the intensity of the fragments *m/z* 117 and *m/z* 118, we

could obtain insight into the ^{13}C incorporation into malate, which relates to the *in vivo* PEPc activity. Our analyses showed that the $R^{13}C$ in malate *m/z* 117 is higher in maize than Arabidopsis leaves following provision of $^{13}CO_2$ (Figure 6a), evidencing a higher PEPc-mediated ^{13}C incorporation into malate in C4 as compared to C3 cells. Interestingly, this approach allowed us to confirm that guard cells do assimilate CO_2 in the dark, but light imposition likely increased PEPc activity in this cell (Figure 6e). These results highlight the effectiveness of the ^{13}C-positional isotope labelling approach, which can be further applied to establish a method for PEPc activity measurements *in vivo* using GC-MS data. An alternative approach for the determination of PEPc activity *in vivo* has recently been established by NMR-based ^{13}C-MFA (Abadie and Tcherkez, 2019). Here, we provide proof-of-concept for a particularly versatile and powerful approach through the analysis of GC-EI-MS-based ^{13}C-MFA. The approach is not limited to plant cells, given that GC-MS is one of the most common platforms used in metabolomics (Garcia and Barbas, 2011), offering a possibility to improve the resolution of metabolic flux maps across organisms. It is also important to highlight that our approach can theoretically be applied to any metabolite of interest. However, the availability of positionally ^{13}C-labelled reference compounds and the establishment of the fragmentation map of chemically complex metabolites can limit this achievement. Furthermore, our GC-APCI-MS analysis indicates that a careful validation using positionally ^{13}C-labelled references and different MS platforms is required to ensure appropriate interpretation and construction of valid flux maps.

Guard cell gluconeogenesis is stimulated in a light-independent manner

Gluconeogenesis is an important metabolic pathway which has been extensively studied in microorganisms and animal models (Sauer and Eikmanns, 2005). In plants, however, ^{13}C-MFA and modelling studies involving gluconeogenesis have been largely restricted to seedlings and seed embryos (Allen *et al.*, 2009; Lonien and Schwender, 2009; Clark *et al.*, 2020; Moreira *et al.*, 2019). This is particularly due to the fact that gluconeogenesis is pivotal for seed germination and seedling establishment (Eastmond *et al.*, 2015; Cornah *et al.*, 2004; Rylott *et al.*, 2003; Penfield *et al.*, 2004). However, the lack of an approach to estimate gluconeogenic fluxes under non-steady state conditions has limited our understanding of the significance of this pathway, particularly in other developmental stages and tissues. In this vein, the methods used to estimate gluconeogenic fluxes in plants are largely indirect, either through determination of gene expression or the activity of gluconeogenic enzymes and/or by metabolic

models and ^{13}C-MFA that have steady-state condition as prerequisite (Walker *et al.*, 2018; Alonso *et al.*, 2011; Robaina-Estévez *et al.*, 2017; Lonien and Schwender, 2009; Chung *et al.*, 2015). A major challenge to measure gluconeogenic fluxes in source tissues is the difficulty in distinguishing the ^{13}C-labelling in glucose that is provided by different metabolic pathways. Consequently, our understanding of the role and regulation of gluconeogenesis in photosynthetic tissues remains very limited. To overcome this hurdle, we established an approach that allows to determine the ^{13}C positional incorporation into the 3,4-C of glucose, which are preferentially labelled by gluconeogenesis (Figure 9a).

The labelling incorporation into the 3,4-C of glucose by gluconeogenesis is explained by the anaplerotic CO_2 fixation mediated by pyruvate carboxylase (PC) and/or PEPc followed by activity of TCA cycle enzymes (Merritt *et al.*, 2011; Jitrapakdee *et al.*, 2008). These reactions produce organic acids labelled at the 1-C and 4-C given the symmetrisation reaction of fumarase (FUM) (Abadie and Tcherkez, 2019; Jin *et al.*, 2005). In turn, it results in OAA labelled at the 1-C and 4-C. Whilst the 4-C is lost as CO_2 in the OAA to phospho*enol*pyruvate (PEP) conversion catalysed by phospho*enol*pyruvate carboxykinase (PEPCK), the 1-C is then incorporated into 3,4-C of glucose by gluconeogenesis (Beylot *et al.*, 1993; Heath, 1968; Stark *et al.*, 2009; Jin *et al.*, 2005). Our results support the concept that the ^{13}C-enrichment in 3,4-C of glucose derived from ^{13}C-HCO_3 can be used to estimate gluconeogenic fluxes and that guard cells run this pathway in a light-independent manner. Several independent lines of argument derived from our analysis support the interpretation of active gluconeogenesis. Firstly, assuming that no CO_2 is assimilated by RuBisCO in the dark and given the fact that guard cells do fix CO_2 by PEPc in the dark either, the increased R^{13}C in different glucose fragments (Figure 7a) strongly support activity of gluconeogenesis. Secondly, the proportion of ^{13}C-incorporation into the 3,4-C is higher than that at the other glucose carbon positions in guard cells, including in the dark (Figure S9). Thirdly, dark-exposed guard cells show a higher ^{13}C-enrichment in these carbons in relative (%) and absolute terms, when compared to illuminated Arabidopsis rosettes following provision of $^{13}CO_2$ (Figure 9b). Thus, beyond providing important insights on the role of gluconeogenesis for glucose synthesis in guard cells, our study highlights the possibility of using GC-MS-based ^{13}C-MFA to investigate gluconeogenic fluxes in photosynthetic tissues. Given that several gluconeogenesis-related genes are either highly expressed in guard cells or have been demonstrated to be important for stomatal movement regulation (Penfield *et al.*, 2012; Daloso *et al.*, 2016b), our method paves the way to unveil the

role of gluconeogenesis for both guard cell glucose homeostasis and stomatal movement regulation.

Our results further highlight that 1,2,5,6-C of glucose are also labelled in guard cells in the dark. This could be an indication of label incorporation into glucose derived from fully labelled PEP (Heath, 1968; Jin *et al.*, 2005). This idea is supported by the finding that provision of U-^{13}C pyruvate to rat livers results in labelling of all carbon positions of glucose, but with a preference for 1,2,5,6-C (Beylot *et al.*, 1993). It seems likely therefore that the PEPc-mediated $^{13}CO_2$ assimilation is simultaneously used to activate the TCA cycle and gluconeogenesis in guard cells, as evidenced by the increased relative ^{13}C-enrichment in malate *m/z* 117 (4-C) and in different glucose fragments.

Intriguingly, guard cell glucose content is strongly reduced under both dark and light conditions (Figure 7c), raising the question on why gluconeogenesis has been stimulated. A possible explanation for that is the important metabolic control exerted by both hexokinase and the metabolite fructose-2,6-biphosphate for the regulation of glycolysis and gluconeogenesis (Daloso *et al.*, 2017; Granot and Kelly, 2019; Stitt, 1990). It has been proposed that sugar degradation within guard cells is a mechanism that occurs under both stomatal opening and closure conditions (Kelly *et al.*, 2013; Medeiros *et al.*, 2018; Flütsch *et al.*, 2020b). Given that gluconeogenesis seems to be stimulated in a light-independent manner, this suggests that a sophisticated metabolic control would be responsible to either stimulate gluconeogenesis and starch synthesis during dark-induced stomatal closure (Raschke and Dittrich, 1977; Schnabl, 1980; Outlaw and Manchester, 1979; Penfield *et al.*, 2012) or to activate glycolysis and metabolic pathways associated to the TCA cycle during light-induced stomatal opening (Daloso *et al.*, 2015a; Daloso *et al.*, 2016a; Robaina-Estévez *et al.*, 2017; Medeiros *et al.*, 2018; Hedrich *et al.*, 1985; Zhao and Assmann, 2011). Further modelling and instationary ^{13}C-MFA using gluconeogenic mutants and different ^{13}C-positionally labelled gluconeogenic substrates such as pyruvate and PEP will be important to unveil the dynamic of labelling incorporation into glucose derived from different gluconeogenic substrates.

Glycolytic flux toward glutamate synthesis is repressed by the mitochondrial TRX system in illuminated Arabidopsis leaves

Several lines of evidence indicate that the metabolic fluxes toward the TCA cycle are inhibited in illuminated leaves, which is particularly due to the inhibition of key components of mitochondrial metabolism through transcriptional and post-translational mechanisms (Fonseca-

Pereira *et al.*, 2021; Møller *et al.*, 2020; Tcherkez *et al.*, 2012; Nunes-Nesi *et al.*, 2013; Xu *et al.*, 2021). Among these mechanisms, the light-dependent, phosphorylation-mediated inhibition of mitochondrial PDH is a clear barrier to the entrance of carbon to the TCA cycle (Tovar-Méndez *et al.*, 2003; Tcherkez *et al.*, 2005; Zhang *et al.*, 2021). Our analysis reinforces this concept and provides further insight into how light inhibition of the mitochondrial PDH restrict the metabolic fluxes from PEPc and glycolysis toward Glu synthesis. This idea is supported by the fact that the 2,3,4,5-C of Glu were labelled to a greater extent following provision of ^{13}C-pyruvate, when compared to the other ^{13}C-tracers, suggesting an induction of PDH activity by increased substrate availability. Furthermore, the PEPc-mediated ^{13}C incorporation into the 1-C of Glu was only observed in illuminated WT Arabidopsis leaves following provision of ^{13}C-pyruvate, and not following provision of ^{13}C-malate and ^{13}C-glucose. It seems likely therefore that PEPc frequently uses the CO_2 released by PDH and/or isocitrate dehydrogenase (IDH).

The ^{13}C-enrichment in the 1-C of Glu following provision of ^{13}C-glucose exclusively observed in *trxo1* and *ntra ntrb* mutants suggests that the mitochondrial TRX system restricts the fluxes throughout this pathway *in vivo*, as previously suggested (Florez-Sarasa *et al.*, 2019; Daloso *et al.*, 2015b; Nietzel *et al.*, 2020). In this scenario, the lack of TRX *o1* or both NTRA/NTRB lifts the inhibition upon PDH and/or IDH activity, increasing therefore the rate of labelled CO_2 released from mitochondria and fixed by PEPc. However, mitochondrial IDH is known to be activated by TRXs *in vitro* (Yoshida and Hisabori, 2014) and the lack of *trxo1* did not change the activity of IDH in mitochondrial extracts (Daloso *et al.*, 2015b). In contrast, it has been recently shown that both TRX *o1* is able to inhibit the activity of the mitochondrial dihydrolipoamide dehydrogenase (mtLPD) *in vitro* (Reinholdt *et al.*, 2019), which corresponds to the E3 subunit of PDH that has been suggested to be redox regulated (Balmer *et al.*, 2004; Nietzel *et al.*, 2020). Thus, it is possible that the ^{13}C-enrichment in the 1-C of Glu in the absence of TRX *o1* or of both NTRA and NTRB would be mainly due to an increase in PDH activity. Alternatively, given that mitochondrial MDH is not redox regulated (Yoshida and Hisabori, 2016), TRX/NTR mutants may have higher export rates of malate to the cytosol, where decarboxylation by malic enzyme may increase the amount of CO_2 for PEPc. This scenario appears unlikely, however, given that no ^{13}C-enrichment in the 1-C of Glu following provision of ^{13}C-malate was observed. Taken together, these results provide evidence that the mitochondrial TRX/NTR system serves as an important control point to modulate metabolic fluxes through matrix carbon metabolism and thereby affecting primary metabolism also beyond the mitochondria.

Experimental procedures

Data acquisition from previous published ^{13}C-labelling studies

We obtained GC-EI-MS chromatograms from previous published ^{13}C-labelling studies (Daloso *et al.*, 2015a; Daloso *et al.*, 2015b; Medeiros *et al.*, 2018; Arrivault *et al.*, 2017; Szecowka *et al.*, 2013; Dethloff *et al.*, 2017; Ishihara *et al.*, 2015) that comprise primary metabolites extracted from plant material following a well-established protocol for GC-MS analysis (Lisec *et al.*, 2006).

Plant material and growth condition

Seeds of *Nicotiana tabacum* (L.) cv. Havana 425 were germinated and cultivated in a substrate composed by a mixture of vermiculite, sand and soil (2:1:0.5) for 30 days. Plants were kept well-watered and nourished with Hoagland nutrient solution every week (Hoagland and Arnon, 1950) under non-controlled greenhouse conditions with natural 12 h of photoperiod, ambient temperature 30 ± 4 °C, relative humidity 62 ± 10% and photosynthetic photon flux density which reached a maximum value of 500 μmol photons m^{-2} s^{-1}.

Guard cell isolation

A pool of guard cell-enriched epidermal fragments (simply referred here as guard cells) was isolated following a protocol that was optimized for metabolite profiling analysis (Daloso *et al.*, 2015a). Guard cells were isolated at pre-dawn by blending approximately three expanded leaves per replicate in a Warring blender (Philips, RI 2044 B.V. International Philips, Amsterdam, The Netherlands), that contains an internal filter to remove excess mesophyll cells, fibres and other cellular debris. All guard cell isolations were carried out in the dark to maintain closed stomata and simulate opening upon illumination, following the natural stomatal circadian rhythm.

^{13}C-isotope labelling kinetic experiment in isolated guard cells

After isolation, guard cells were transferred to light or dark conditions and incubated in a solution containing 50 μM $CaCl_2$ and 5 mM MES-Tris (pH 6.15) in the presence of ^{13}C-$NaHCO_3$ (Sigma-Aldrich®, Germany). The experiment was initiated at the beginning of the light period of the day. Guard cell samples were rapidly harvested on a nylon membrane (220 μM) and snap-frozen in liquid nitrogen after 0, 10, 20 and 60 minutes under white light or dark conditions.

Extraction of metabolites and mass spectrometry analysis

The extraction of polar metabolites and their derivatization was carried out as described previously (Lisec *et al.,* 2006), except that 1 ml of the polar (upper) phase, instead of 150 µl, was collected and reduced to dryness (Lima *et al.*, 2019). Metabolites were derivatized by methoxyamination, with subsequent addition of TMS and finally analysed by GC-EI-TOF-MS (Lisec *et al.,* 2006). The mass spectral analysis were performed using the software Xcalibur® 2.1 (Thermo Fisher Scientific, Waltham, MA, USA) (Lima *et al.*, 2018). Metabolites were identified using the Golm Metabolome Database (http://gmd.mpimp-golm.mpg.de/) (Kopka *et al.*, 2005) and reported as described previously (Data S2) (Fernie *et al.*, 2011; Alseekh *et al.*, 2021).

Establishment of the ^{13}C-positional isotopomer labelling approach

The chemical structure of the major well-known chemically derivatized fragments was obtained by revisiting previous published publications reporting fragmentation and by *in silico* simulations using the software ChemBioDraw 12.0 (CambridgeSoft, Cambridge, MA, USA). To confirm the fragmentation simulation, we compared our data with those obtained from Okahashi and collaborators, in which positionally labelled TMS-derivatized organic acids were analysed via GC-EI-MS (Okahashi *et al.*, 2019), and with the fragmentation obtained by analysing positionally labelled reference substances via nominal mass resolution GC-EI-TOF-MS and high mass resolution GC-APCI-TOF-MS with previously established methods and settings (Kopka *et al.*, 2017; Erban *et al.*, 2020). The complete list of reference substances used here is found at the Table S2.

^{13}C-enrichment analysis

The RIA and F^{13}C were obtained as described previously (Lima *et al.*, 2018). In detail, in a fragment of three carbons, the sum of the raw intensities (normalized by ribitol and fresh weight) of the isotopologues M, M1, M2 and M3 was set to 100%. The intensity of each isotopologue is then relative (in %) to this sum (Eqn 1). The RIA was then used to obtain the F^{13}C (Eqn 2), the R^{13}C (Eqn 3) and the T^{13}C (Eqn 4).

Estimation of positional ^{13}C-enrichment in glucose, malate and glutamate

We estimated the P^{13}C at different carbons of glucose, malate and Glu by using a previous established mathematical framework (Beylot *et al.*, 1993), with modifications.

Positional labelling determination was obtained by using the $T^{13}C$ from different fragments (see Eqn's 5-18 for details).

Statistical analysis

The $F^{13}C$ throughout time was compared to the time zero by ANOVA and Dunnet's test ($P < 0.05$), which allow multiple comparison with a specific control (Dunnett, 1955). Exception is made for the data from maize laves following provision of $^{13}CO_2$, which contains only one biological replicate and, thus, did not allow statistical comparisons. The $F^{13}C$ in Glu of Arabidopsis leaves under different labelled substrates was compared using ANOVA and Tukey test ($P < 0.05$). Regression analyses were carried out using a linear model. All these analyses were carried out using SIGMAPLOT 14 (Systat Software Inc., San Jose, CA, USA). Punctual comparisons between dark and light treatments or different cell types were carried out by Student's *t* test ($P < 0.05$) by using Microsoft Excel (Microsoft, Redmond, WA, USA).

Acknowledgments

This work was made possible through financial support from the National Council for Scientific and Technological Development (CNPq, Grant 428192/2018-1). JK and AE acknowledge funding of the German science foundation (DFG) grant (KO 2329/7-1) that is part of the SCyCode research consortium (FOR2816). We also thank the research fellowship granted by CNPq to DMD and the scholarships granted by the Brazilian Federal Agency for Support and Evaluation of Graduate Education (CAPES-Brazil) to VFL, AGD, SACS and NPP and CNPq to FBSF. We thank the authors who kindly provided their mass spectral data from published work and Dr. Leonardo P. Souza, Dr. Isabel Orf and Dr. Thomas C.R. Williams for helpful discussions about metabolic flux analysis.

Conflict of interest

The authors declare no potential conflict of interest.

List of author contributions

VFL and DMD designed the experiments. VFL, FBSF, NPP and SACS performed the ^{13}C-labelling experiment. Mass spectrometry analysis were performed by DBM and AE under the supervision of ARF and JK. Data analysis was performed by VFL, AGD, AE, LA and DMD. All authors contributed to the establishment of the method and to write the final manuscript; DMD obtained funding and is responsible for this article.

References

Abadie, C., Bathellier, C. and Tcherkez, G. (2018) Carbon allocation to major metabolites in illuminated leaves is not just proportional to photosynthesis when gaseous conditions (CO_2 and O_2) vary. *New Phytol.*, **218**, 94–106.

Abadie, C., Lothier, J., Boex-Fontvieille, E., Carroll, A. and Tcherkez, G. (2017) Direct assessment of the metabolic origin of carbon atoms in glutamate from illuminated leaves using ^{13}C-NMR. *New Phytol.*, **216**, 1079–1089.

Abadie, C. and Tcherkez, G. (2019) *In vivo* phospho*enol*pyruvate carboxylase activity is controlled by CO_2 and O_2 mole fractions and represents a major flux at high photorespiration rates. *New Phytol.*, **221**, 1843–1852.

Allen, D.K., Ohlrogge, J.B. and Shachar-Hill, Y. (2009) The role of light in soybean seed filling metabolism. *Plant J.*, **58**, 220–234.

Alonso, A.P., Val, D.L. and Shachar-Hill, Y. (2011) Central metabolic fluxes in the endosperm of developing maize seeds and their implications for metabolic engineering. *Metab. Eng.*, **13**, 96–107.

Alseekh, S., Aharoni, A., Brotman, Y., et al. (2021) Mass spectrometry-based metabolomics: A guide for annotation, quantification and best reporting practices. *Nat. Methods*, **18**, 747–756.

Antoniewicz, M.R. (2013a) Tandem mass spectrometry for measuring stable-isotope labeling. *Curr. Opin. Biotechnol.*, **24**, 48–53.

Antoniewicz, M.R. (2013b) ^{13}C metabolic flux analysis: Optimal design of isotopic labeling experiments. *Curr. Opin. Biotechnol.*, **24**, 1116–1121.

Antoniewicz, M.R., Kelleher, J.K. and Stephanopoulos, G. (2007) Accurate assessment of amino acid mass isotopomer distributions for metabolic flux analysis. *Anal. Chem.*, **79**, 7554–7559.

Arrivault, S., Obata, T., Szecówka, M., Mengin, V., Guenther, M., Hoehne, M., Fernie, A.R. and Stitt, M. (2017) Metabolite pools and carbon flow during C4 photosynthesis in maize: $^{13}CO_2$ labeling kinetics and cell type fractionation. *J. Exp. Bot.*, **68**, 283–298.

Balmer, Y., Vensel, W.H., Tanaka, C.K., et al. (2004) Thioredoxin links redox to the regulation of fundamental processes of plant mitochondria. *Proc. Natl. Acad. Sci.*, **101**, 2642–2647.

Beylot, M., Previs, S.F., David, F. and Brunengraber, H. (1993) Determination of the ^{13}C-labeling pattern of glucose by gas chromatography-mass spectrometry. *Anal. Biochem.*, **212**, 526–531.

Bowyer, J.R. and Leegood, R.C. (1997) Photosynthesis. In *Plant Biochemistry*. Elsevier, pp. 49-104.

Brown, P.H. and Outlaw, W.H. (1982) Effect of fusicoccin on dark $^{14}CO_2$ fixation by *Vicia faba* guard-cell protoplasts. *Plant Physiol.*, **70**, 1700–1703.

Cheung, C.Y.M., Poolman, M.G., Fell, D.A., Ratcliffe, R.G. and Sweetlove, L.J. (2014) A diel flux balance model captures interactions between light and dark metabolism during day-night cycles in C3 and Crassulacean Acid Metabolism leaves. *Plant Physiol.*, **165**, 917–929.

Choi, J., Grossbach, M.T. and Antoniewicz, M.R. (2012) Measuring complete isotopomer distribution of aspartate using gas chromatography/tandem mass spectrometry. *Anal. Chem.*, **84**, 4628–4632.

Chung, S.T., Chacko, S.K., Sunehag, A.L. and Haymond, M.W. (2015) Measurements of gluconeogenesis and glycogenolysis: A methodological review. *Diabetes*, **64**, 3996–4010.

Clark, T.J., Guo, L., Morgan, J. and Schwender, J. (2020) Modeling plant metabolism: From network reconstruction to mechanistic models. *Annu Rev Plant Biol*, **71**, 1–24.

Cornah, J.E., Germain, V., Ward, J.L., Beale, M.H. and Smith, S.M. (2004) Lipid utilization, gluconeogenesis, and seedling growth in Arabidopsis mutants lacking the glyoxylate cycle enzyme malate synthase. *J. Biol. Chem.*, **279**, 42916–42923.

Daloso, D.M., Antunes, W.C., Pinheiro, D.P., Waquim, J.P., Araújo, W.L., Loureiro, M.E., Fernie, A.R. and Williams, T.C.R. (2015a) Tobacco guard cells fix CO_2 by both Rubisco and PEPcase while sucrose acts as a substrate during light-induced stomatal opening. *Plant Cell Environ.*, **38**, 2353–2371.

Daloso, D.M., Müller, K., Obata, T., et al. (2015b) Thioredoxin, a master regulator of the tricarboxylic acid cycle in plant mitochondria. *Proc. Natl. Acad. Sci. U. S. A.*, **112**, E1392–E1400.

Daloso, D.M., Williams, T.C.R., Antunes, W.C., Pinheiro, D.P., Müller, C., Loureiro, M.E. and Fernie, A.R. (2016a) Guard cell-specific upregulation of *sucrose synthase 3* reveals that the role of sucrose in stomatal function is primarily energetic. *New Phytol.*, **209**, 1470–1483.

Daloso, D.M., Anjos, L. dos and Fernie, A.R. (2016b) Roles of sucrose in guard cell regulation. *New Phytol.*, **211**, 809–818.

Daloso, D.M., Medeiros, D.B., Anjos, L. dos, Yoshida, T., Araújo, W.L. and Fernie, A.R. (2017) Metabolism within the specialized guard cells of plants. *New Phytol.*, **216**, 1018–1033.

Desage, M., Guilluy, R., Brazier, J. -L, Riou, J. -P, Beylot, M., Normand, S. and Vidal, H. (1989) Positional isotopic analysis of ^{13}C-labelled glucose by mass spectrometry: Applications

to the study of gluconeogenesis in liver cells. *Biomed. Environ. Mass Spectrom.*, **18**, 1010–1015.

Dethloff, F., Orf, I. and Kopka, J. (2017) Rapid in situ ^{13}C tracing of sucrose utilization in Arabidopsis sink and source leaves. *Plant Methods*, **13**, 1–19.

Dunnett, C.W. (1955) A multiple comparison procedure for comparing several treatments with a control. *J. Am. Stat. Assoc.*, **50**, 1096–1121.

Eastmond, P.J., Astley, H.M., Parsley, K., et al. (2015) Arabidopsis uses two gluconeogenic gateways for organic acids to fuel seedling establishment. *Nat. Commun.*, **6**, 1–8.

Erban, A., Martinez-Seidel, F., Rajarathinam, Y., Dethloff, F., Orf, I., Fehrle, I., Alpers, J., Beine-Golovchuk, O. and Kopka, J. (2020) Multiplexed profiling and data processing methods to identify temperature-regulated using gas chromatography coupled to mass spectrometry. In D. K. Hincha and E. Zuther, eds. *Plant Cold Acclimation*. New York, NY: Humana Press, pp. 203–239.

Fernie, A.R., Aharoni, A., Willmitzer, L., et al. (2011) Recommendations for reporting metabolite data. *Plant Cell*, **23**, 2477–2482.

Fernie, A.R. and Morgan, J.A. (2013) Analysis of metabolic flux using dynamic labelling and metabolic modelling. *Plant, Cell Environ.*, **36**, 1738–1750.

Fernie, A.R. and Stitt, M. (2012) On the discordance of metabolomics with proteomics and transcriptomics: Coping with increasing complexity in logic, chemistry, and network interactions scientific correspondence. *Plant Physiol.*, **158**, 1139–1145.

Florez-Sarasa, I., Obata, T., Del-Saz, N.F., Reichheld, J.-P., Meyer, E.H., Rodriguez-Concepcion, M., Ribas-Carbo, M. and Fernie, A.R. (2019) The lack of mitochondrial thioredoxin TRXo1 affects *in vivo* alternative oxidase activity and carbon metabolism under different light conditions. *Plant Cell Physiol.,* **60**, 2369–2381.

Flütsch, S., Nigro, A., Conci, F., Fajkis, J., Thalmann, M., Trtílek, M., Panzarová, K. and Santelia, D. (2020a) Glucose uptake to guard cells via STP transporters provides carbon sources for stomatal opening and plant growth. *EMBO reports Press*, **21**, e49719.

Flütsch, S., Wang, Y., Takemiya, A., et al. (2020b) Guard cell starch degradation yields glucose for rapid stomatal opening in Arabidopsis. *Plant Cell*, **32**, 2325–2344.

Fonseca-Pereira, P. da, Souza, P.V.L., Fernie, A.R., Timm, S., Daloso, D.M. and Araújo, W.L. (2021) Thioredoxin-mediated regulation of (photo)respiration and central metabolism. *J. Exp. Bot.* erab098.

Garcia, A. and Barbas, C. (2011) Gas chromatography-mass spectrometry (GC-MS)-based

metabolomics. *Methods Mol. Biol.*, **708**, 191–204.

Gauthier, P.P.G., Bligny, R., Gout, E., Mahé, A., Nogués, S., Hodges, M. and Tcherkez, G.G.B. (2010) *In folio* isotopic tracing demonstrates that nitrogen assimilation into glutamate is mostly independent from current CO_2 assimilation in illuminated leaves of *Brassica napus*. *New Phytol.*, **185**, 988–999.

Gotow, K., Taylor, S. and Zeiger, E. (1988) Photosynthetic carbon fixation in guard cell protoplasts of *Vicia faba* L.: Evidence from radiolabel experiments. *Plant Physiol.*, **86**, 700–705.

Granot, D. and Kelly, G. (2019) Evolution of guard-cell theories : The story of sugars. *Trends Plant Sci.*, **24**, 507–518.

Heath, D.F. (1968) The interaction of glycolysis, gluconeogenesis and the tricarboxylic acid cycle in rat liver *in vivo*. *Biochem. J.*, **110**, 337–362.

Hedrich, R., Raschke, K. and Stitt, M. (1985) A role for fructose 2,6-bisphosphate in regulating carbohydrate metabolism in guard cells. *Plant Physiol.*, **79**, 977–982.

Hoagland, D.R. and Arnon, D.I. (1950) The water-culture method for growing plants without soil. *Calif. Agric. Exp. Stn. Circ.*, **347**, 1–32.

Horrer, D., Flütsch, S., Pazmino, D., Matthews, J.S.A., Thalmann, M., Nigro, A., Leonhardt, N., Lawson, T. and Santelia, D. (2016) Blue light induces a distinct starch degradation pathway in guard cells for stomatal opening. *Curr. Biol.*, **26**, 362–370.

Huege, J., Sulpice, R., Gibon, Y., Lisec, J., Koehl, K. and Kopka, J. (2007) GC-EI-TOF-MS analysis of *in vivo* carbon-partitioning into soluble metabolite pools of higher plants by monitoring isotope dilution after $^{13}CO_2$ labelling. *Phytochemistry*, **68**, 2258–2272.

Ishihara, H., Obata, T., Sulpice, R., Fernie, A.R. and Stitt, M. (2015) Quantifying protein synthesis and degradation in Arabidopsis by dynamic $^{13}CO_2$ labeling and analysis of enrichment in individual amino acids in their free pools and in protein. *Plant Physiol.*, **168**, 74–93.

Jin, E.S., Jones, J.G., Burgess, S.C., Merritt, M.E., Sherry, A.D. and Malloy, C.R. (2005) Comparison of [3,4-^{13}C2]glucose to [6,6- $^{2}H_2$]glucose as a tracer for glucose turnover by nuclear magnetic resonance. *Magn. Reson. Med.*, **53**, 1479–1483.

Jitrapakdee, S., St Maurice, M., Rayment, I., Cleland, W.W., Wallace, J.C. and Attwood, P. V. (2008) Structure, mechanism and regulation of pyruvate carboxylase. *Biochem. J.*, **413**, 369–387.

Jongh, D.C. De, Radford, T., Hribar, J.D., Hanessian, S., Bieber, M., Dawson, G. and Sweeley, C.C. (1969) Analysis of trimethylsilyl derivatives of carbohydrates by gas

chromatography and mass spectrometry. *J. Am. Chem. Soc.*, **91**, 1728–1740.

Kelly, G., Moshelion, M., David-Schwartz, R., Halperin, O., Wallach, R., Attia, Z., Belausov, E. and Granot, D. (2013) Hexokinase mediates stomatal closure. *Plant J.*, **75**, 977–988.

Kim, H.K., Choi, Y.H. and Verpoorte, R. (2010) NMR-based metabolomic analysis of plants. *Nat. Protoc.*, **5**, 536–549.

Kopka, J., Schauer, N., Krueger, S., et al. (2005) GMD@CSB.DB: The Golm metabolome database. *Bioinformatics*, **21**, 1635–1638.

Kopka, J., Schmidt, S., Dethloff, F., et al. (2017) Systems analysis of ethanol production in the genetically engineered cyanobacterium Synechococcus sp. PCC 7002. *Biotechnol. Biofuels*, **10**, 1–21.

Lawson, T. (2009) Guard cell photosynthesis and stomatal function. *New Phytol.*, **181**, 13–34.

Lawson, T. and Matthews, J. (2020) Guard cell metabolism and stomatal function. *Annu. Rev. ofPlant Biol.*, **71**, 273–302.

Leegood, R.C. and ap Rees, T. (1978) Dark fixation of CO_2 during gluconeogenesis by the cotyledons of *Cucurbita pepo* L. *Planta*, **140**, 275–282.

Leimer, K.R., Rice, R.H. and Gehrke, C.W. (1977) Complete mass spectra of the per-trimethylsilylated amino acids. *J. Chromatogr. A*, **141**, 355–375.

Lima, V.F., Anjos, L. dos, Medeiros, D.B., Cândido-Sobrinho, S.A., Souza, L.P., Gago, J., Fernie, A.R. and Daloso, D.M. (2019) The sucrose-to-malate ratio correlates with the faster CO_2 and light stomatal responses of angiosperms compared to ferns. *New Phytol.,* **223**, 1873–1887.

Lima, V.F., Souza, L.P. de, Williams, T.C.R., Fernie, A.R. and Daloso, D.M. (2018) Gas chromatography–mass spectrometry-based ^{13}C-labeling studies in plant metabolomics. In *Plant Metabolomics*. pp. 47–58.

Lisec, J., Schauer, N., Kopka, J., Willmitzer, L. and Fernie, A.R. (2006) Gas chromatography mass spectrometry-based metabolite profiling in plants. *Nat. Protoc.*, **1**, 387–396.

Lonien, J. and Schwender, J. (2009) Analysis of metabolic flux phenotypes for two arabidopsis mutants with severe impairment in seed storage lipid synthesis. *Plant Physiol.*, **151**, 1617–1634.

MacLeod, J.K., Flanigan, I.L., Williams, J.F. and Grant Collins, J. (2001) Mass spectrometric studies of the path of carbon in photosynthesis: Positional isotopic analysis of

^{13}C-labelled C4 to C7 sugar phosphates. *J. Mass Spectrom.*, **36**, 500–508.

Medeiros, D.B., Luz, L.M. da, Oliveira, H.O. de, Araújo, W.L., Daloso, D.M. and Fernie, A.R. (2019) Metabolomics for understanding stomatal movements. *Theor. Exp. Plant Physiol.*, **9**, 91–102.

Medeiros, D.B., Perez Souza, L., Antunes, W.C., Araújo, W.L., Daloso, D.M. and Fernie, A.R. (2018) Sucrose breakdown within guard cells provides substrates for glycolysis and glutamine biosynthesis during light-induced stomatal opening. *Plant J.*, **94**, 583–594.

Melzer, E. and O'Leary, M.H. (1987) Anapleurotic CO_2 fixation by phosphoenolpyruvate carboxylase in C3 plants. *Plant Physiol.*, **84**, 58–60.

Merritt, M.E., Harrison, C., Sherry, A.D., Malloy, C.R. and Burgess, S.C. (2011) Flux through hepatic pyruvate carboxylase and phosphoenolpyruvate carboxykinase detected by hyperpolarized ^{13}C magnetic resonance. *Proc. Natl. Acad. Sci.*, **108**, 19084–19089.

Møller, I.M., Igamberdiev, A.U., Bykova, N. V, Finkemeier, I., Rasmusson, A.G. and Schwarzländer, M. (2020) Matrix redox physiology governs the regulation of plant mitochondrial metabolism through posttranslational protein modifications. *Plant Cell*, **32**, 573–594.

Moreira, T.B., Shaw, R., Luo, X., Ganguly, O., Kim, H.S., Coelho, L.G.F., Cheung, C.Y.M. and Williams, T.C.R. (2019) A genome-scale metabolic model of soybean (*Glycine max*) highlights metabolic fluxes in seedlings. *Plant Physiol.*, **180**, 1912–1929.

Nielsen, J. and Keasling, J.D. (2016) Engineering cellular metabolism. *Cell*, **164**, 1185–1197.

Nietzel, T., Mostertz, J., Ruberti, C., et al. (2020) Redox-mediated kick-start of mitochondrial energy metabolism drives resource-efficient seed germination. *Proc. Natl. Acad. Sci. U. S. A.*, **117**, 741–751.

Nunes-Nesi, A., Araújo, W.L., Obata, T. and Fernie, A.R. (2013) Regulation of the mitochondrial tricarboxylic acid cycle. *Curr. Opin. Plant Biol.*, **16**, 335–343.

O'Leary, B., Park, J. and Plaxton, W.C. (2011) The remarkable diversity of plant PEPC (phosphoenolpyruvate carboxylase): Recent insights into the physiological functions and post-translational controls of non-photosynthetic PEPCs. *Biochem. J.*, **436**, 15–34.

Okahashi, N., Kawana, S., Iida, J., Shimizu, H. and Matsuda, F. (2019) Fragmentation of dicarboxylic and tricarboxylic acids in the Krebs cycle using GC-EI-MS and GC-EI-MS/MS. *Mass Spectrom.*, **8**, A0073–A0073.

Outlaw, W.H. and Manchester, J. (1979) Guard cell starch concentration quantitatively related to stomatal aperture. *Plant Physiol.*, **64**, 79–82.

Penfield, S., Clements, S., Bailey, K.J., Gilday, A.D., Leegood, R.C., Gray, J.E. and Graham, I.A. (2012) Expression and manipulation of *PHOSPHOENOLPYRUVATE CARBOXYKINASE 1* identifies a role for malate metabolism in stomatal closure. *Plant J.*, **69**, 679–688.

Penfield, S., Rylott, E.L., Gilday, A.D., Graham, S., Larson, T.R. and Graham, I.A. (2004) Reserve mobilization in the Arabidopsis endosperm fuels hypocotyl elongation in the dark, is independent of abscisic acid, and requires *PHOSPHOENOLPYRUVATE CARBOXYKINASE 1*. *Plant Cell*, **16**, 2705–2718.

Petersson, G. (1972) Mass spectrometry of hydroxy dicarboxylic acids as trimethylsilyl derivatives. Rearrangement fragmentations. *Org. Mass Spectrom.*, **6**, 565–576.

Raschke, K. and Dittrich, P. (1977) [^{14}C]Carbon-dioxide fixation by isolated leaf epidermes with stomata closed or open. *Planta*, **134**, 69–75.

Ratcliffe, R.G. and Shachar-Hill, Y. (2006) Measuring multiple fluxes through plant metabolic networks. *Plant J.*, **45**, 490–511.

Reinholdt, O., Schwab, S., Zhang, Y., Reichheld, J.-P., Fernie, A.R., Hagemann, M. and Timm, S. (2019) Redox-regulation of photorespiration through mitochondrial thioredoxin o1. *Plant Physiol.*, **181**, 442–457.

Robaina-Estévez, S., Daloso, D.M., Zhang, Y., Fernie, A.R. and Nikoloski, Z. (2017) Resolving the central metabolism of Arabidopsis guard cells. *Sci. Rep.*, **7**, 1–13.

Rylott, E.L., Gilday, A.D. and Graham, I.A. (2003) The gluconeogenic enzyme phosphoenolpyruvate carboxykinase in Arabidopsis is essential for seedling establishment. *Plant Physiol.*, **131**, 1834–1842.

Sauer, U. and Eikmanns, B.J. (2005) The PEP-pyruvate-oxaloacetate node as the switch point for carbon flux distribution in bacteria. *FEMS Microbiol. Rev.*, **29**, 765–794.

Schnabl, H. (1980) CO_2 and malate metabolism in starch-containing and starch-lacking guard-cell protoplasts. *Planta*, **149**, 52–58.

Schwender, J., Ohlrogge, J. and Shachar-Hill, Y. (2004) Understanding flux in plant metabolic networks. *Curr. Opin. Plant Biol.*, **7**, 309–317.

Silva, W.B., Daloso, D.M., Fernie, A.R., Nunes-Nesi, A. and Araújo, W.L. (2016) Can stable isotope mass spectrometry replace radiolabelled approaches in metabolic studies? *Plant Sci.*, **249**, 59–69.

Souza, L.P. de, Fernie, A.R. and Tohge, T. (2018) Carbon atomic survey for identification of selected metabolic fluxes. In C. António, ed. *Plant Metabolomics*. Methods in Molecular

Biology. New York, NY: Springer New York, pp. 59–67.

Stark, R., Pasquel, F., Turcu, A., Pongratz, R.L., Roden, M., Cline, G.W., Shulman, G.I. and Kibbey, R.G. (2009) Phosphoenolpyruvate cycling via mitochondrial phosphoenolpyruvate carboxykinase links anaplerosis and mitochondrial GTP with insulin secretion. *J. Biol. Chem.*, **284**, 26578–26590.

Stitt, M. (1990) Fructose-2,6-bisphosphate as a regulatory molecule in plants. *Annu. Rev. Plant Physiol. Plant Mol. Biol.*, **41**, 153–185.

Strehmel, N., Kopka, J., Scheel, D. and Böttcher, C. (2014) Annotating unknown components from GC/EI-MS-based metabolite profiling experiments using GC/APCI(+)-QTOFMS. *Metabolomics*, **10**, 324–336.

Sweetlove, L.J. and Fernie, A.R. (2013) The spatial organization of metabolism within the plant cell. *Annu. Rev. Plant Biol.*, **64**, 723–746.

Szecowka, M., Heise, R., Tohge, T., et al. (2013) Metabolic fluxes in an illuminated Arabidopsis rosette. *Plant Cell*, **25**, 694–714.

Tcherkez, G., Boex-Fontvieille, E., Mahé, A. and Hodges, M. (2012) Respiratory carbon fluxes in leaves. *Curr. Opin. Plant Biol.*, **15**, 308–314.

Tcherkez, G., Cornic, G., Bligny, R., Gout, E. and Ghashghaie, J. (2005) *In Vivo* respiratory metabolism of illuminated leaves. *Plant Physiol.*, **138**, 1596–1606.

Tovar-Méndez, A., Miernyk, J.A. and Randall, D.D. (2003) Regulation of pyruvate dehydrogenase complex activity in plant cells. *Eur. J. Biochem.*, **270**, 1043–1049.

Walker, R.P., Benincasa, P., Battistelli, A., Moscatello, S., Técsi, L., Leegood, R.C. and Famiani, F. (2018) Gluconeogenesis and nitrogen metabolism in maize. *Plant Physiol. Biochem.*, **130**, 324–333.

Wieloch, T., Ehlers, I., Yu, J., Frank, D., Grabner, M., Gessler, A. and Schleucher, J. (2018) Intramolecular ^{13}C analysis of tree rings provides multiple plant ecophysiology signals covering decades. *Sci. Rep.*, **8**, 1–10.

Wieloch, T., Werner, R.A. and Schleucher, J. (2021) Carbon flux around leaf-cytosolic glyceraldehyde-3-phosphate dehydrogenase introduces a ^{13}C signal in plant glucose. *J. Exp. Bot.,* erab316.

Williams, T.C.R., Miguet, L., Masakapalli, S.K., Kruger, N.J., Sweetlove, L.J. and Ratcliffe, R.G. (2008) Metabolic network fluxes in heterotrophic Arabidopsis cells: Stability of the flux distribution under different oxygenation conditions. *Plant Physiol.*, **148**, 704–718.

Xu, Y., Fu, X., Sharkey, T.D., Shachar-Hill, Y. and Walker, B.J. (2021) The metabolic origins

of non-photorespiratory CO_2 release during photosynthesis: A metabolic flux analysis. *Plant Physiol.*, **186**, 297–314.

Yoshida, K. and Hisabori, T. (2016) Adenine nucleotide-dependent and redox-independent control of mitochondrial malate dehydrogenase activity in *Arabidopsis thaliana*. *Biochim. Biophys. Acta - Bioenerg.*, **1857**, 810–818.

Yoshida, K. and Hisabori, T. (2014) Mitochondrial isocitrate dehydrogenase is inactivated upon oxidation and reactivated by thioredoxin-dependent reduction in Arabidopsis. *Front. Environ. Sci.*, **2**, 1–7.

Zamboni, N., Fendt, S.-M., Rühl, M. and Sauer, U. (2009) ^{13}C-based metabolic flux analysis. *Nat. Protoc.*, **4**, 878–892.

Zhang, Y., Giese, J., Mae-Lin Kerbler, S., et al. (2021) Two mitochondrial phosphatases, PP2c63 and Sal2, are required for posttranslational regulation of the TCA cycle in Arabidopsis. *Mol. Plant*., **14**, 1104–1118.

Zhao, Z. and Assmann, S.M. (2011) The glycolytic enzyme, phosphoglycerate mutase, has critical roles in stomatal movement, vegetative growth, and pollen production in *Arabidopsis thaliana*. *J. Exp. Bot.*, **62**, 5179–5189.

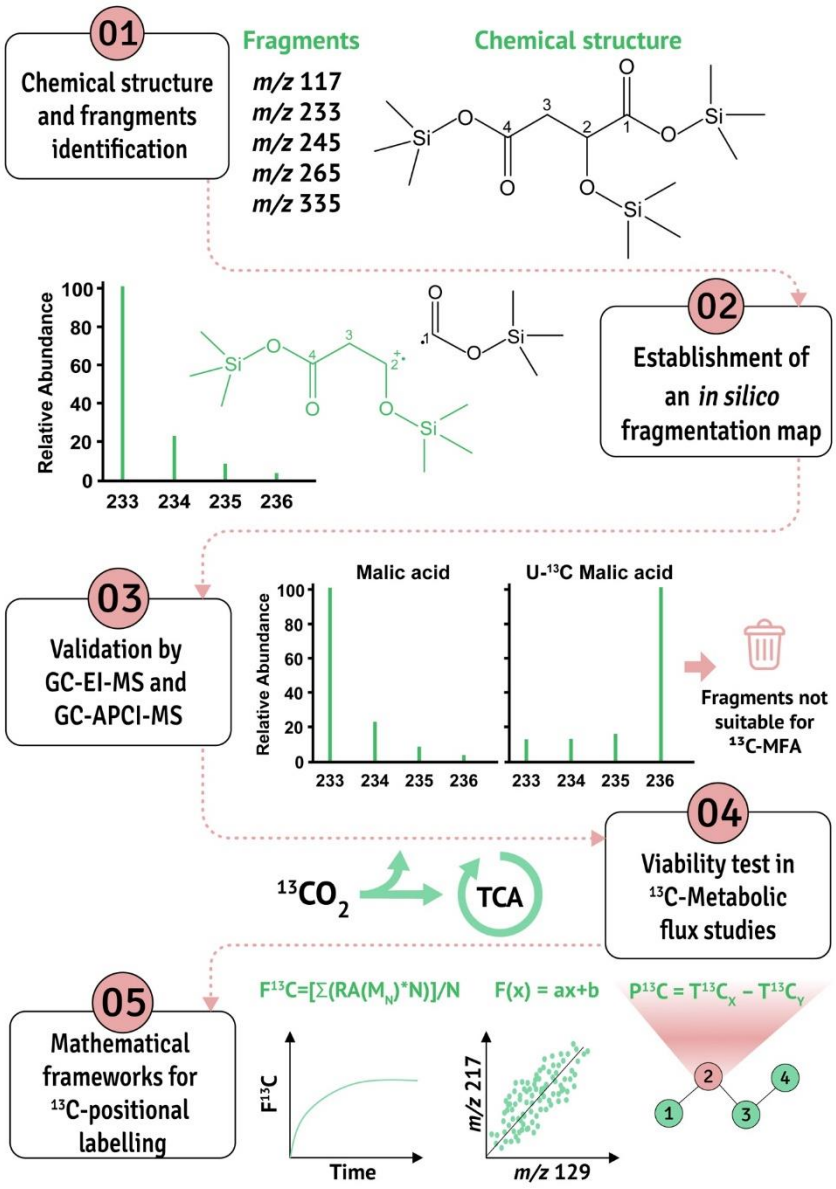

Figure 1. Schematic representation of the steps toward ^{13}C-positional isotopomer labelling approach establishment. We first identified the chemical structure and the major fragments of chemically derivatized metabolites for GC-MS analysis by revisiting previous published works and the Golm Metabolome Database (Step 1). After that, an *in silico* simulation of metabolite fragmentation was performed and a map of fragments, containing one or a subset of carbon atoms, was constructed (Step 2). The predictions were then validated by analysing commercially available ^{13}C-positionally labelled reference substances by both GC-EI-MS and GC-APCI-MS analyses (Step 3). Fragments with undetermined chemical structure and not validated by ^{13}C-positionally labelled reference substances analysis were discarded from the analysis. The viability of the remaining fragments for retrieving carbon position information was investigated using data from previous plant ^{13}C-metabolic flux analysis (^{13}C-MFA). (Step 4). Fragments with low intensity or overlapping with near fragments were further excluded from the analysis. Limitations involving overlapping fragments were overcome by establishing different mathematical frameworks to finally obtain ^{13}C-positional labelling information (Step 5).

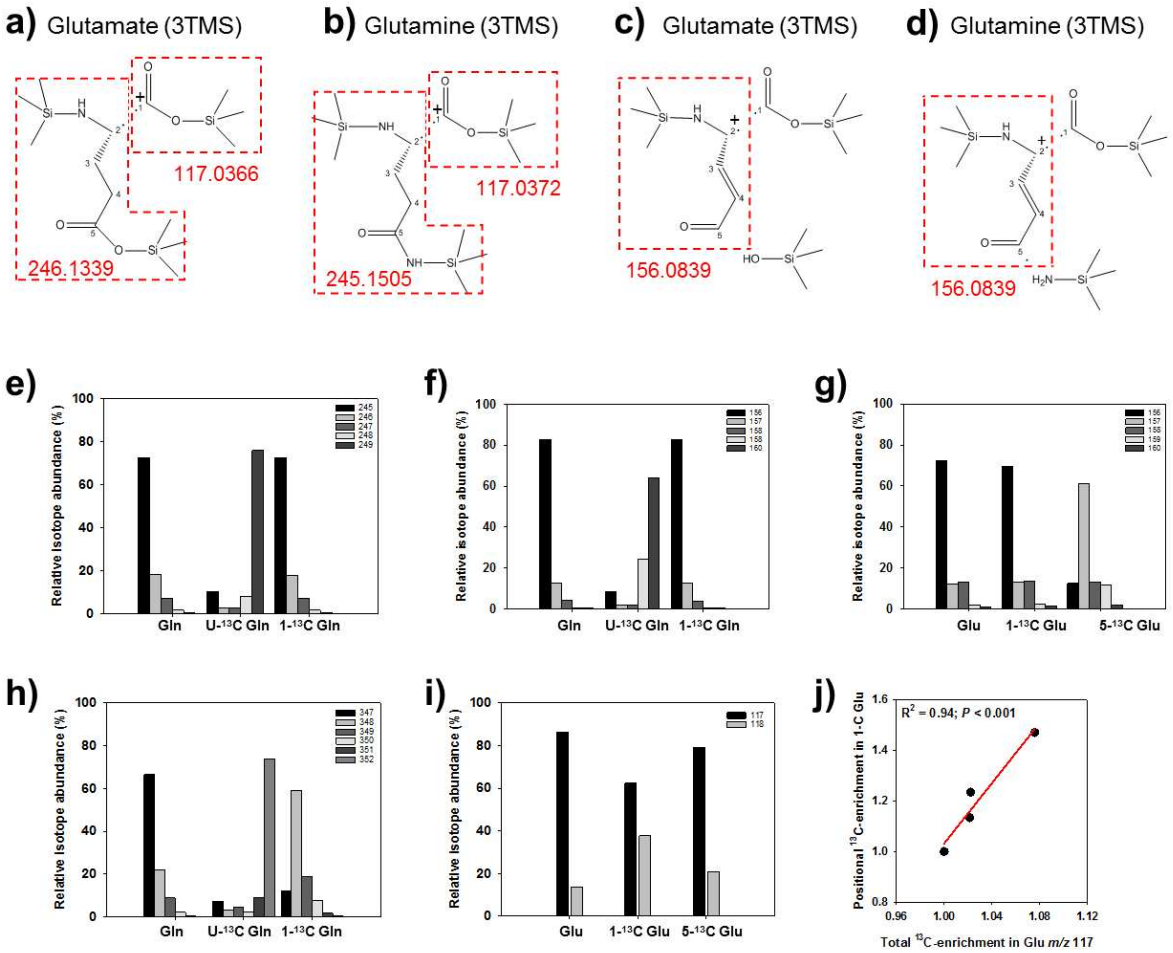

Figure 2. Fragmentation map of trimethylsilylated (TMS) and methoxyaminated (MEOX) glutamate (Glu) and glutamine (Gln) obtained by gas chromatography coupled to mass spectrometry analysis using atmospheric pressure chemical ionization (APCI) as ionization source. a-d) Fragmentation map with expected exact mass values assembled by *in silico* analysis using the software ChemBioDraw 12.0. In order to simplify, just one of several possible dissociative cleavages from the diverse TMS or MEOX moieties were represented here. e-i) GC-MS analysis of reference substances of Glu and Gln non-labelled, fully labelled (U-^{13}C) and labelled at the carbons 1 (1-^{13}C) or 5 (5-^{13}C). For simplification, only GC-EI-MS data, and not GC-APCI-MS, is showed. j) Relationship between the positional ^{13}C-enrichment in the carbon 1 (1-C) of Glu obtained by the difference between the total ^{13}C-enrichment of the fragment *m/z* 348 (1,2,3,4,5-C) minus the total ^{13}C-enrichment of the fragment *m/z* 246 (2,3,4,5-C) (see eqn 5) with the total ^{13}C-enrichment of the fragment *m/z* 117. This analysis was performed using data from Arabidopsis rosettes following provision of $^{13}CO_2$ (Szecowka *et al.*, 2013). This relationship was best fitted into a linear model.

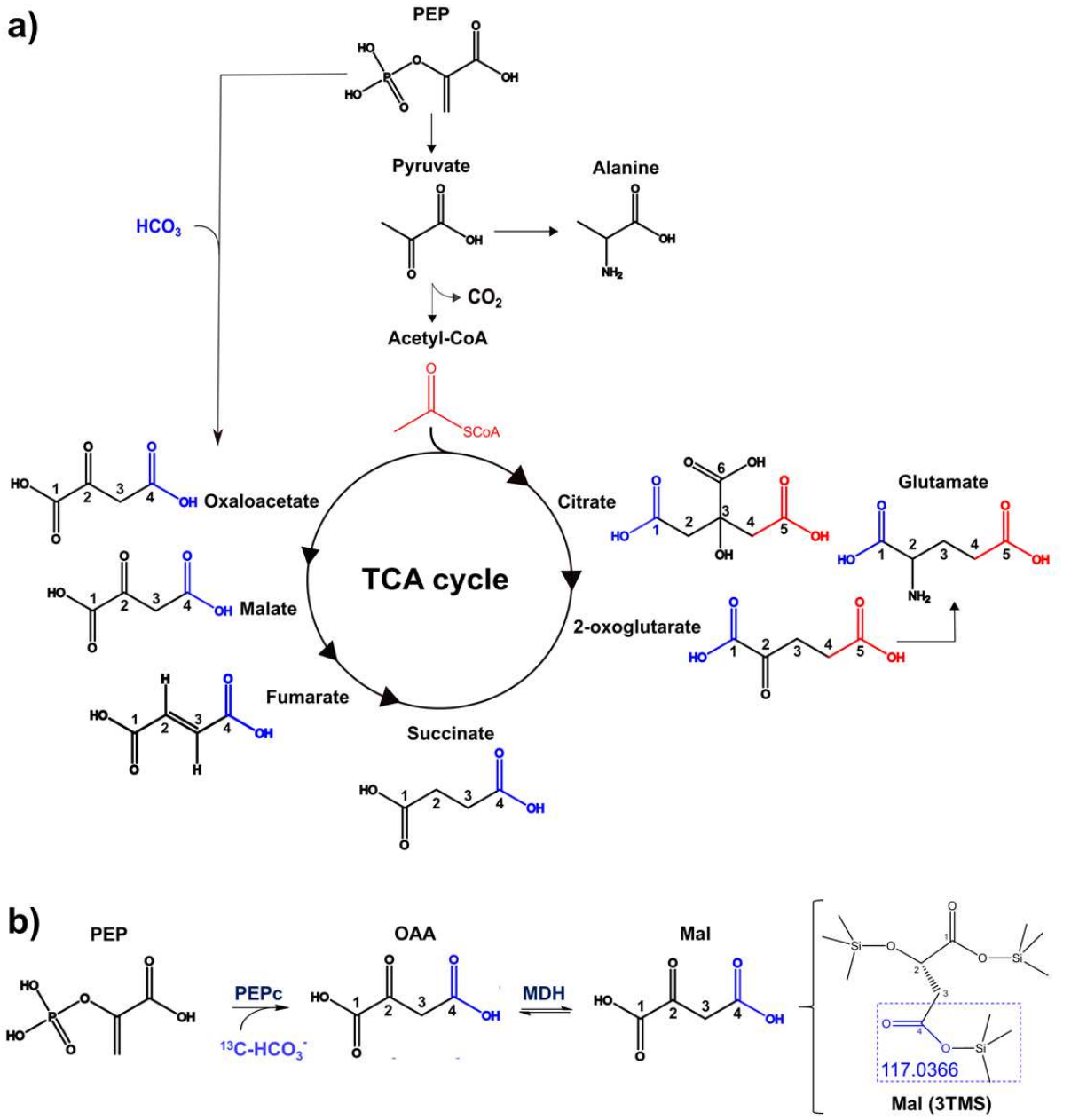

Figure 3. Simplified diagram of the TCA cycle and associated pathways distinguishing the carbon fluxes from PEPc activity and glycolysis toward the TCA cycle and the synthesis of Glu. a) Carbons in blue and red types highlight the carbon derived from the PEPc-mediated anaplerotic CO_2 fixation and those from acetyl-CoA, respectively, according to a ^{13}C-nuclear magnetic resonance metabolic flux study (Abadie *et al.*, 2017). b) Diagram showing the carbon tracking from PEPc-mediated ^{13}C-HCO_3 assimilation to the synthesis of OAA and Mal with detailed schematic representation of Mal 3TMS demonstrating the composition of the fragment *m/z* 117.0366 containing the carbon 4 of the Mal backbone. All molecules were represented in fully protonated form to simplify the structures. Abbreviations: Glu, glutamate; Mal, malate; MDH, malate dehydrogenase; OAA, oxaloacetate; PEP, phospho*enol*pyruvate; PEPc, phospho*enol*pyruvate carboxylase; TCA, tricarboxylic acid, TMS, trimethylsilylated.

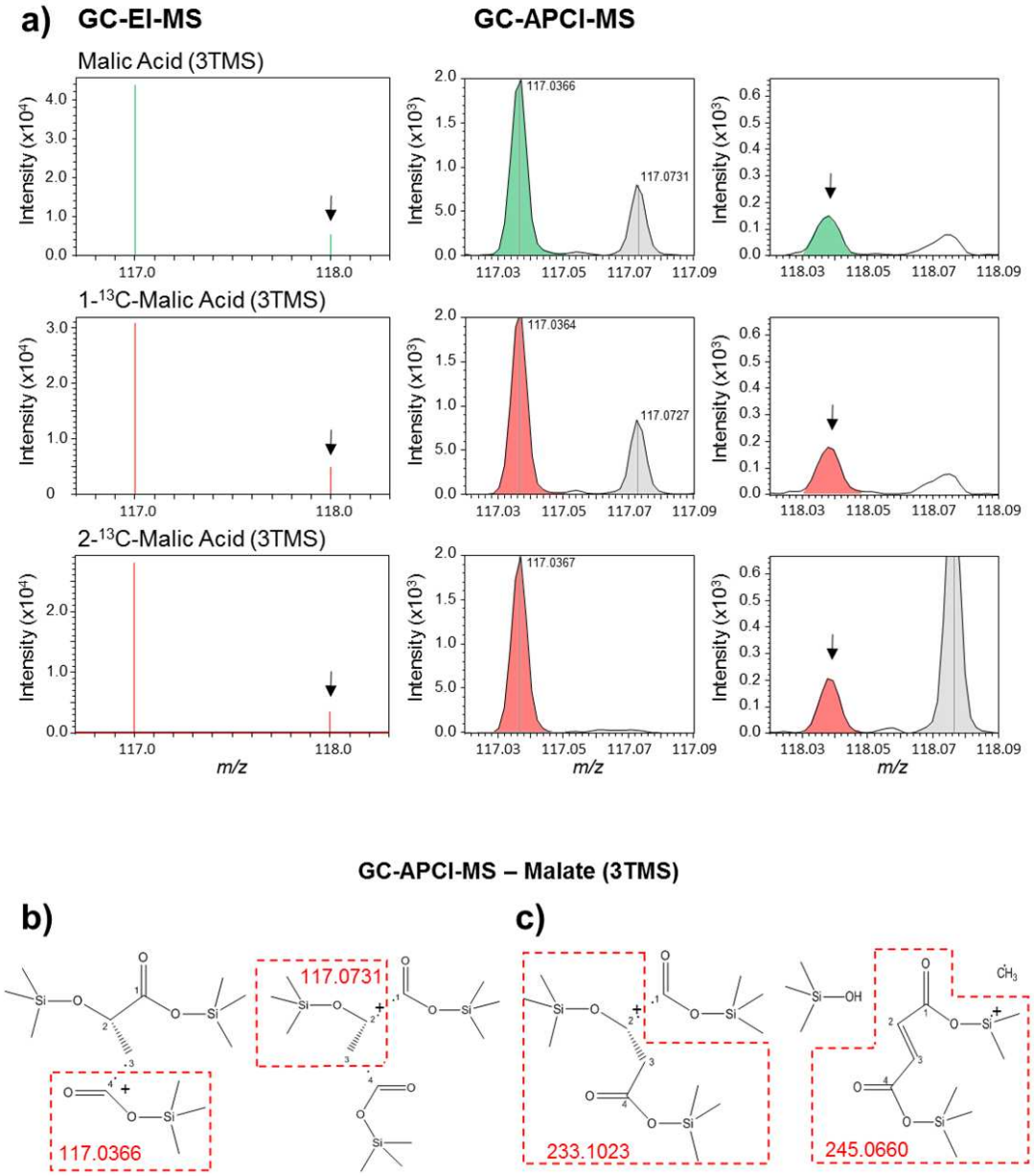

Figure 4. Analysis of ^{13}C-positionally labelled malic acid references and fragmentation map of malic acid (3TMS) obtained by GC-MS analysis. **a)** Detailed mass spectral analyses of the malic acid fragment *m/z* 117 by GC-EI-MS and by high mass resolution GC-APCI-MS analyses of non-labelled (green), 1-^{13}C, and 2-^{13}C positional labelled (red) malic acids. These analyses demonstrate that the contribution of the 1-C carboxyl group of malate to mass fragment [TMS-COO$^{\cdot+}$] of expected exact mass *m/z* 117.0366 can be neglected. Note the approximately constant abundance of isotopologue 118 and 118.0399, respectively (black arrows). We verify observations of Okahashi and co-authors (2019) and conclude that respective ^{13}C-enrichment analyses are a suitable proxy for positional labelling analyses of the malate 4-C atom. A second mass fragment (grey) with exact mass ~117.0730 [TMS-OCH2CH2$^{\cdot+}$] can be distinguished by GC-APCI-MS. This fragment is predicted to contain 2-C (hereby verified) and 3-C of malate. **b)** Chemical structure of malic acid (3TMS) fragments proposed by *in silico* simulations and confirmed by GC-APCI-MS analysis. Abbreviation: APCI, atmospheric pressure chemical ionization (APCI); EI, electron impact; GC-MS, gas chromatography coupled to mass spectrometry; *m/z*, mass-to-charge ratio; TMS, trimethylsilylated.

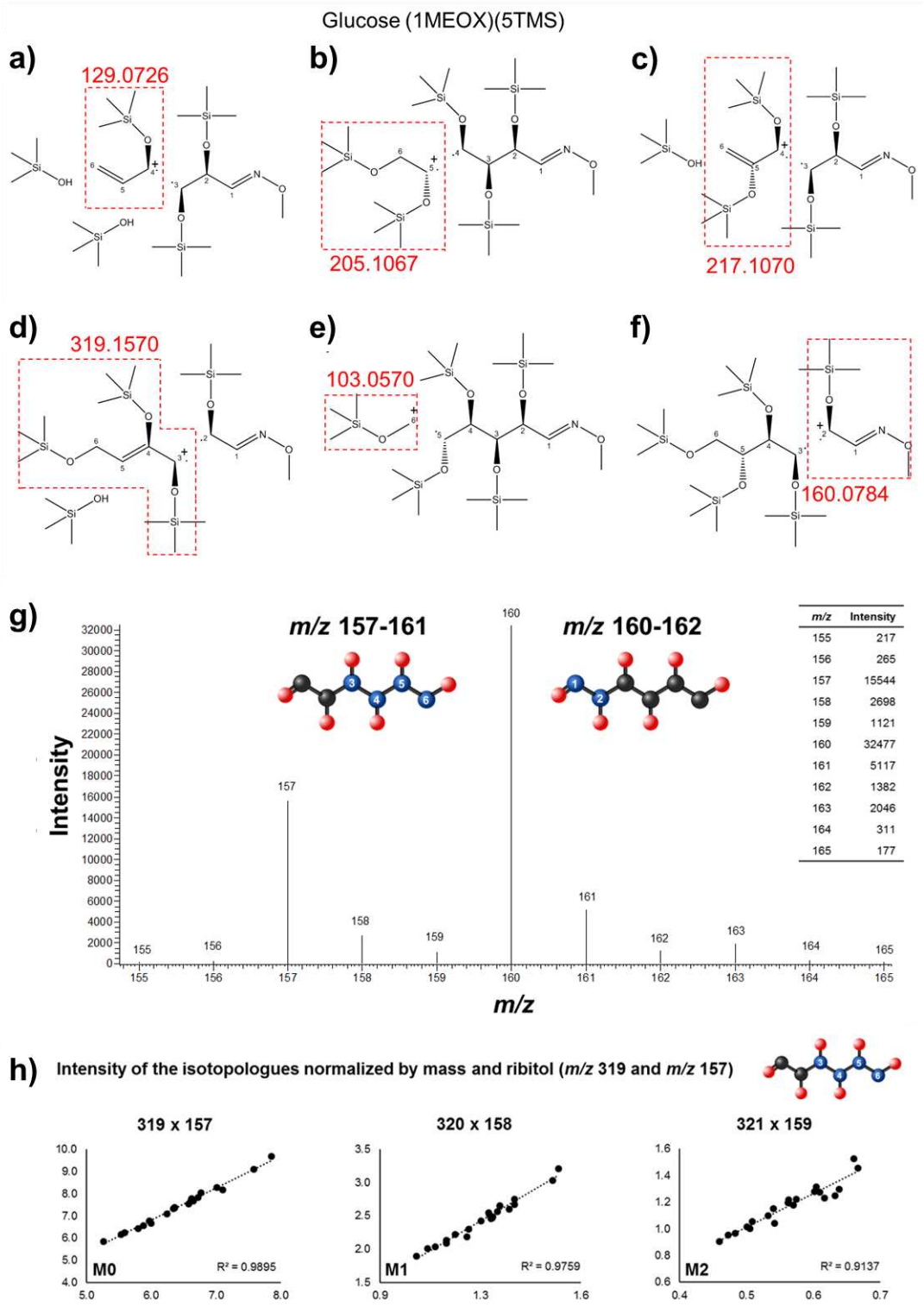

Figure 5. Establishment of ^{13}C-positionally labelled glucose analysis. a-f) Fragmentation map of glucose (1MEOX) (5TMS) obtained by GC-MS analysis. g) Mass spectral visualization of the fragments *m/z* 157 (3,4,5,6-C) and *m/z* 160 (1,2-C) of glucose, highlighting the composition of them and the intensity of their isotopologues. h) Relationship between the isotopologues (M0, M1 and M2) of the fragments *m/z* 157 and *m/z* 319 (3,4,5,6-C) of glucose. Regression analyses were carried out using a linear model and in each graph is indicated the corresponding R^2 and the regression line.

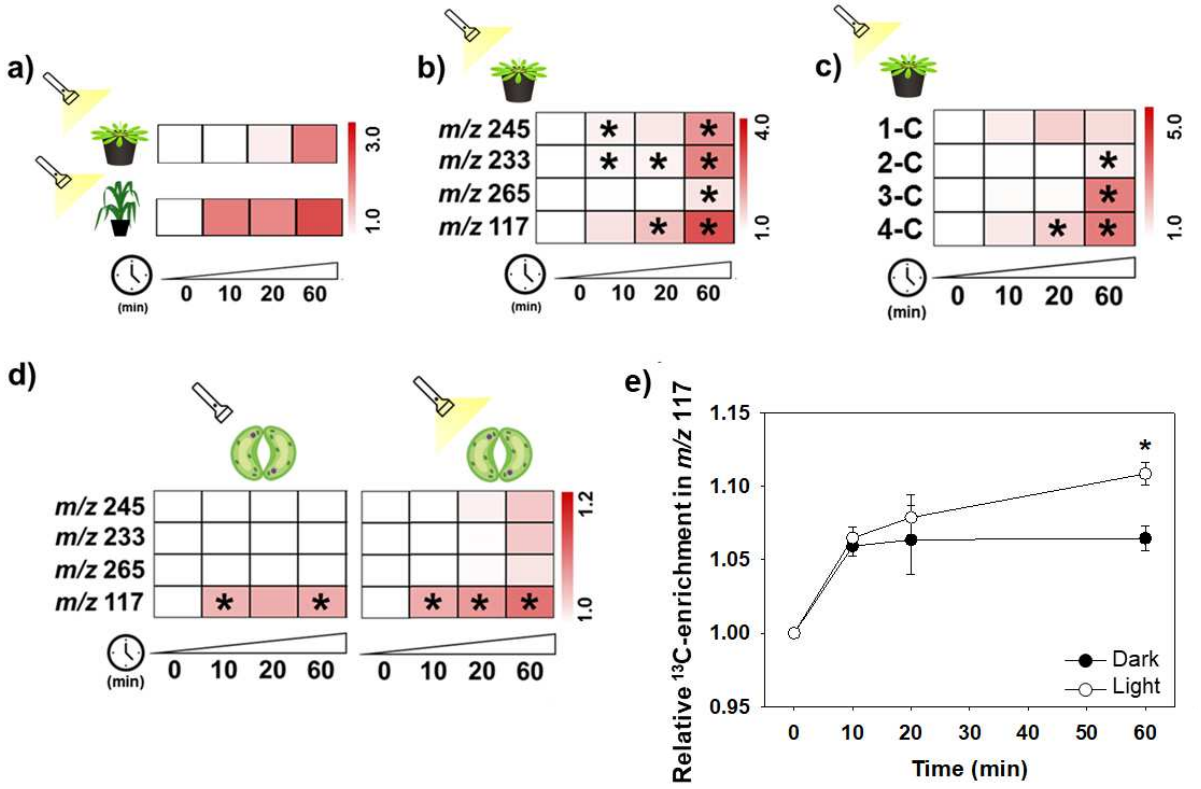

Figure 6. Relative ^{13}C-enrichment in malate from illuminated Arabidopsis rosettes and maize leaves following provision of $^{13}CO_2$ and tobacco guard cells under dark and light conditions following provision of ^{13}C-HCO_3. a) Relative ^{13}C-enrichment in the carbon 4 (4-C) of malate from illuminated Arabidopsis rosettes and maize leaves following provision of $^{13}CO_2$. b-c) Relative ^{13}C-enrichment in different fragments (b) and in each carbon (c) of malate from illuminated Arabidopsis rosettes following provision of $^{13}CO_2$. d) Relative ^{13}C-enrichment in different fragments of malate from tobacco guard cells under dark and light conditions following provision of ^{13}C-HCO_3. e) Relative ^{13}C-enrichment in the fragment *m/z* 117 (4-C) of malate highlighting the difference between darkened and illuminated guard cells following provision of ^{13}C-HCO_3. The data from these figures were normalized to the time 0 of each experiment. Asterisks in the figures a-d indicate significant difference compared to the time 0 of each experiment, whilst in the figure e the asterisk indicates significant difference between light and dark treatments by Student's *t*-test ($P < 0.05$). Values are presented as mean ± SE (n = 3 and 4 for Arabidopsis rosettes and guard cells, respectively). Abbreviations: *m/z*, mass-to-charge ratio.

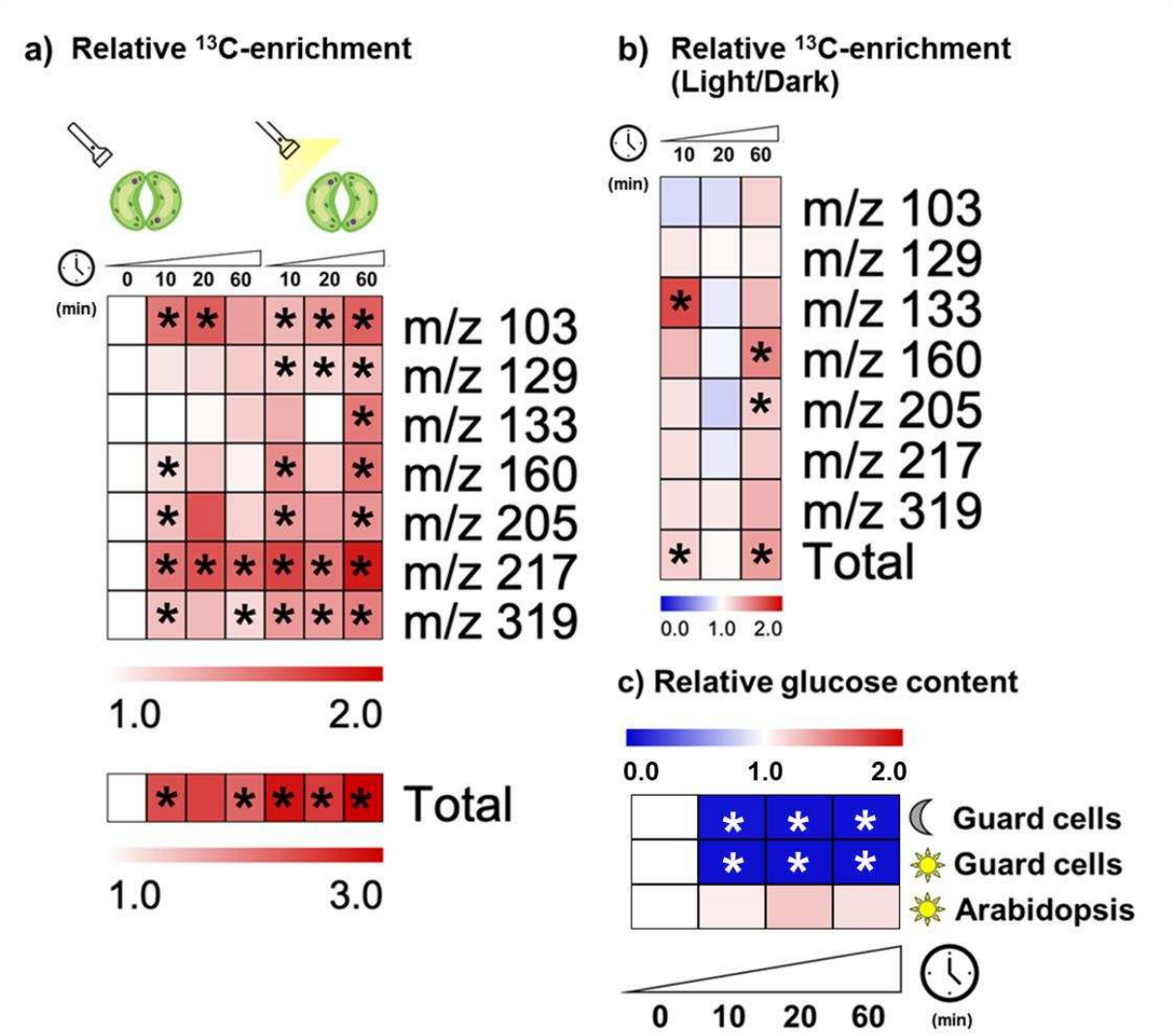

Figure 7. ^{13}C-enrichment analysis in glucose. a) Relative ^{13}C-enrichment in different fragments and in the entire molecule of glucose (Total) in darkened and illuminated guard cells following provision of ^{13}C-HCO_3. The heat map represents data relative to the time 0 of the experiment. b) Relative ^{13}C-enrichment comparison between darkened and illuminated guard cells. The heat map represents data from illuminated guard cells relative to the values obtained in darkened guard cells in each time point. c) Relative glucose content in guard cells under dark or light conditions following provision of ^{13}C-HCO_3 and illuminated Arabidopsis rosettes following provision of $^{13}CO_2$. Illuminated Arabidopsis rosettes was abbreviated to Arabidopsis in order to simplify the figure. The total data considered in (a-b) were obtained by the sum of the relative ^{13}C-enrichment in *m/z* 160 and *m/z* 319. Asterisks indicate significant difference compared to the time 0 of each experiment. Values are presented as mean ± SE (n = 3 and 4 for Arabidopsis rosettes and guard cells, respectively). Abbreviation: *m/z*, mass-to-charge ratio.

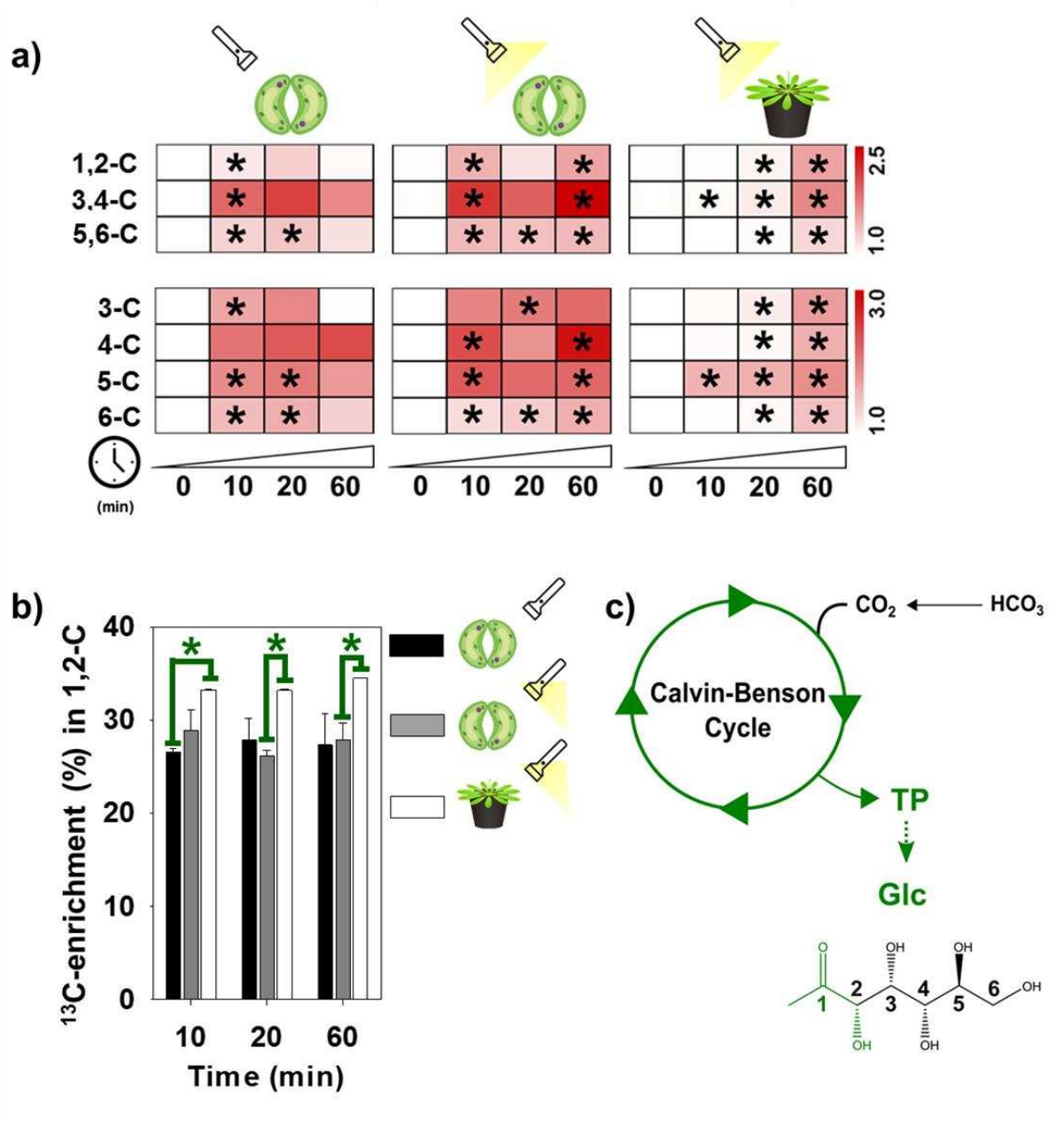

Figure 8. Positional ^{13}C-enrichment analysis in glucose from tobacco guard cells under dark and light conditions following provision of ^{13}C-HCO_3 and from illuminated Arabidopsis rosettes following provision of $^{13}CO_2$. a) Positional ^{13}C-labelling incorporation in glucose at dual atomic (upper panel) and atomic (lower panel) levels. Asterisks indicate significant difference compared to the time 0 of each experiment. b) Percentage (%) of the ^{13}C-labelling incorporation into the carbons 1 and 2 (1,2-C) of glucose. This % refers to the proportion of ^{13}C-labelling incorporation into the 1,2-C as compared to the pair of carbon atoms 3,4 and 5,6-C in each sample. Asterisks indicate significant difference between the samples in each time point by Student's *t*-test ($P < 0.05$). Values are presented as mean ± SE (n = 3 and 4 for Arabidopsis rosettes and guard cells, respectively). c) Schematic representation highlighting the glucose carbons (1,2-C - in green) preferentially labelled by photosynthesis.

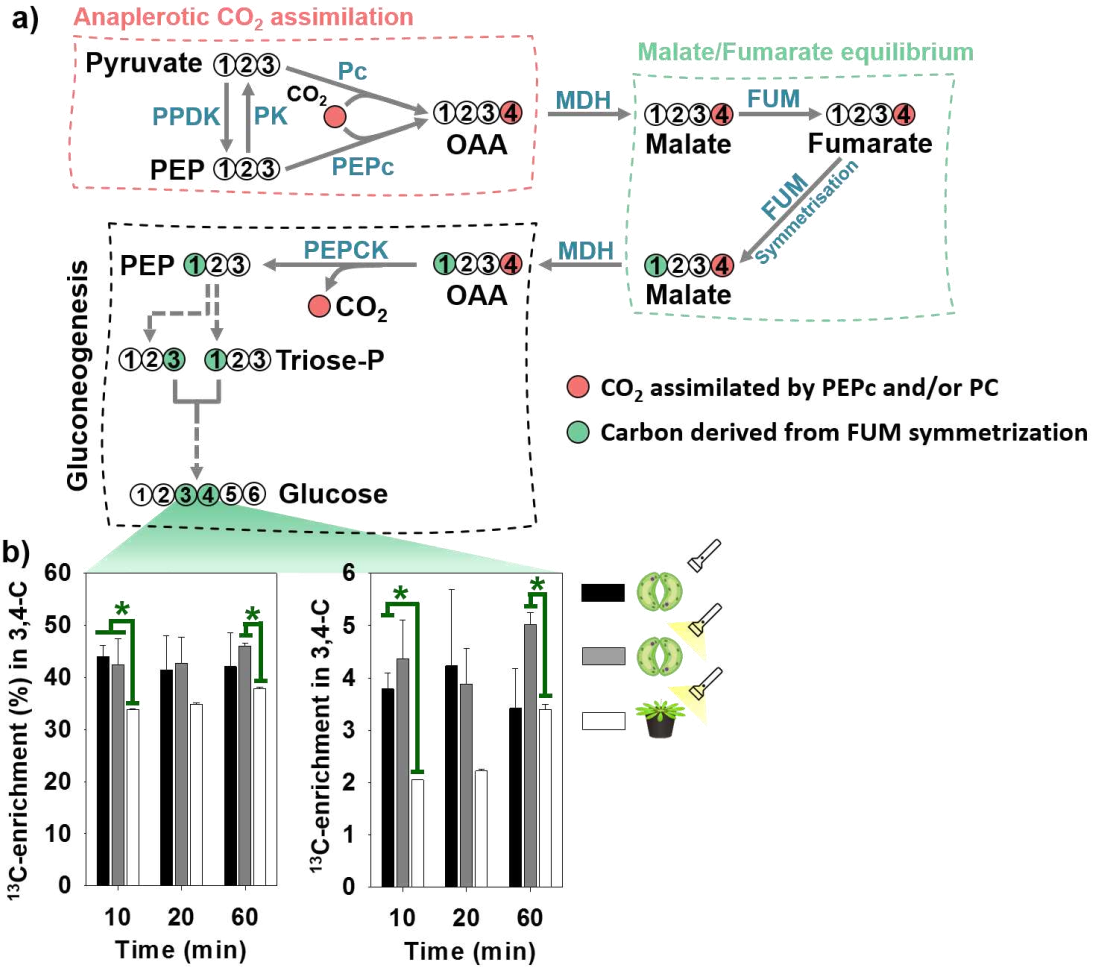

Figure 9. Gluconeogenesis-mediated ^{13}C-labelling of the carbons 3 and 4 (3,4-C) of glucose. a) Schematic representation of gluconeogenesis-mediated ^{13}C-incorporation into 3,4-C of glucose highlighting the CO_2 assimilation by anaplerotic reactions catalysed by either PC or PEPc. The CO_2 incorporated into the 4-C of OAA by Pc or PEPc (red circles) is subsequently transferred to the 4-C of malate and fumarate by MDH and FUM, respectively. Given that malate and fumarate are constantly at equilibrium, the 1-C of both metabolites is labelled by the symmetrisation reaction of FUM (green circles), resulting in OAA labelled at both 1-C and 4-C. The activity of PEPCK converts OAA to PEP labelled only at the 1-C (1-^{13}C), given that the 4-C is lost as CO_2. Following several reactions (dashed lines), 1-^{13}C PEP results in triose phosphates (triose-P) labelled at both 1-C and 3-C, which are then combined to produce glucose labelled at both 3-C and 4-C. b) Percentage (%) of the ^{13}C-labelling incorporation into the 3,4-C of glucose from tobacco guard cells under dark and light conditions following provision of ^{13}C-HCO_3 and from illuminated Arabidopsis rosettes following provision of $^{13}CO_2$. This % refers to the proportion of ^{13}C-labelling incorporation into the 3,4-C as compared to the pair of carbon atoms 1,2 and 5,6-C in each sample. Asterisks indicate significant difference between the samples in each time point by Student's *t*-test ($P < 0.05$). Values are presented as mean ± SE (n = 3 and 4 for Arabidopsis rosettes and guard cells, respectively). Abbreviations: Metabolites (OAA, oxaloacetate; PEP, phospho*enol*pyruvate; Triose-P, triose phosphates). Enzymes (FUM, fumarase; MDH, malate dehydrogenase; Pc, pyruvate carboxylase; PEPc, phospho*enol*pyruvate carboxylase; PEPCK, phospho*enol*pyruvate carboxykinase; PK, pyruvate kinase; PPDK, pyruvate, orthodiphosphate dikinase).

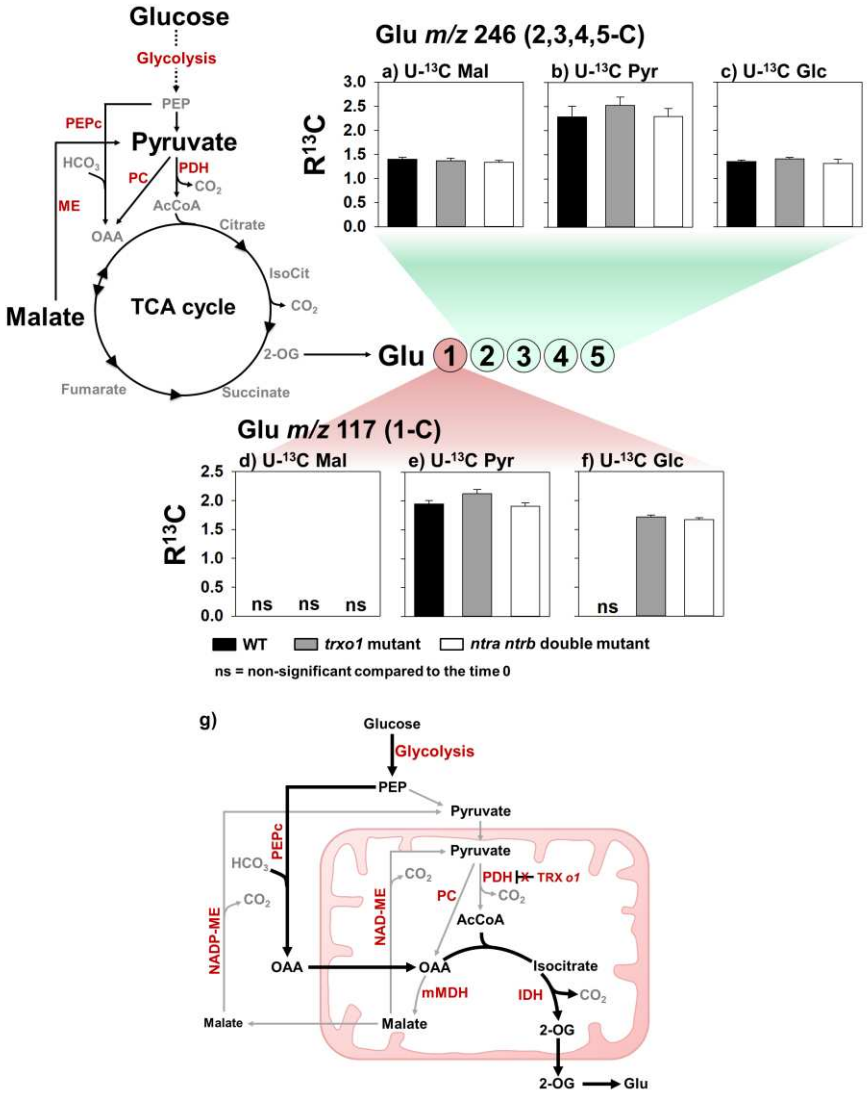

Figure 10. Relative ^{13}C-enrichment ($R^{13}C$) in glutamate (Glu) in illuminated Arabidopsis leaves from wild type (WT), *trxo1* mutant and *ntra ntrb* double mutant following provision of uniformly ^{13}C-labelled (U-^{13}C) glucose, malate or pyruvate for 240 minutes. a-c) $R^{13}C$ in the fragment *m/z* 246 (2,3,4,5-C) of Glu. d-f) $R^{13}C$ in the fragment *m/z* 117 (1-C) of Glu. The presence of bar graphs indicates significant $R^{13}C$ in the fragment under the respective ^{13}C-tracer when compared to the time 0 of each experiment; whilst ns indicates non-significant $R^{13}C$ over time. The $R^{13}C$ in Glu *m/z* 246 following provision of ^{13}C-pyruvate was different from those observed following provision of ^{13}C-glucose and ^{13}C-malate in each genotype by ANOVA and Tukey's test ($P < 0.05$). Values are presented as mean ± SE (n=6). g) Schematic representation of the differential TCA-cycle metabolic fluxes in *trxo*1 mutant. In this scenario, the lack of TRX *o1* lifts the inhibition upon PDH, increasing the carbon fluxes toward Glu synthesis from glycolysis and PEPc activity. Black and thicker arrows indicate higher carbon fluxes. Abbreviations: Metabolites: AcCoA, acetyl-coenzyme A; Glc, glucose; Glu, glutamate; IsoCit, isocitrate; Mal, malate; OAA, oxaloacetate; PEP, phospho*enol*pyruvate; Pyr, pyruvate; 2-OG, 2-oxoglutarate. Enzymes, highlighted in light red: IDH, isocitrate dehydrogenase; mMDH, mitochondrial malate dehydrogenase; NAD-ME, NAD-malic enzyme; NADP-ME, NADP-malic enzyme; PC, pyruvate carboxylase; PDH, pyruvate dehydrogenase; PEPc, phospho*enol*pyruvate carboxylase.

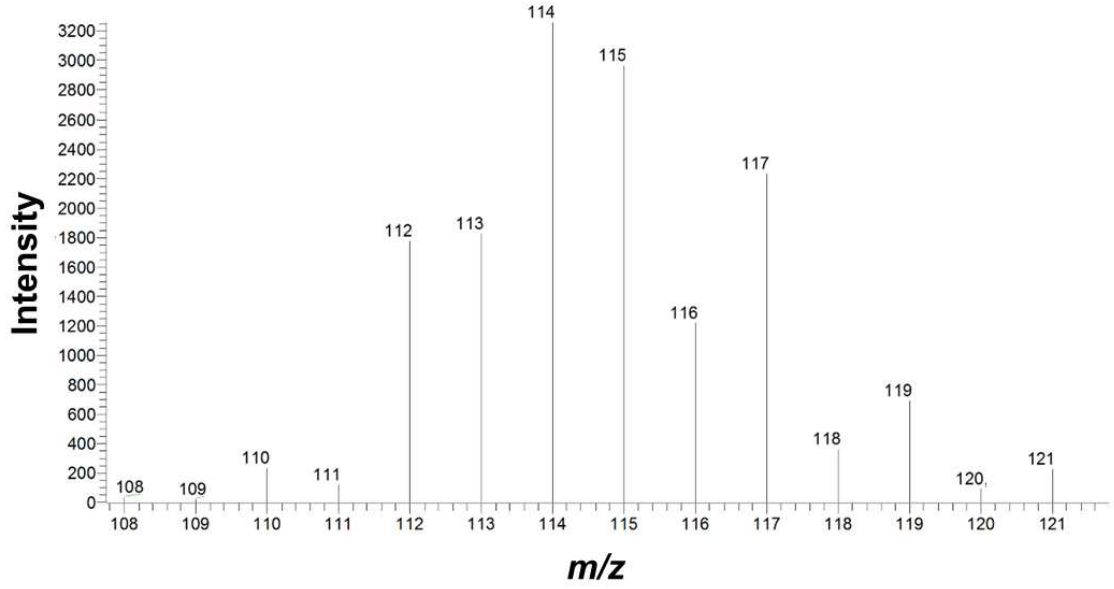

Supplemental Figure 1 Mass spectrum of EI-induced fragmentation of TMS-derivatized glutamate highlighting the peaks around the fragment *m/z* 117. Abbreviations: EI, electron impact; *m/z*, mass-to-charge ratio; TMS, trimethylsilylated.

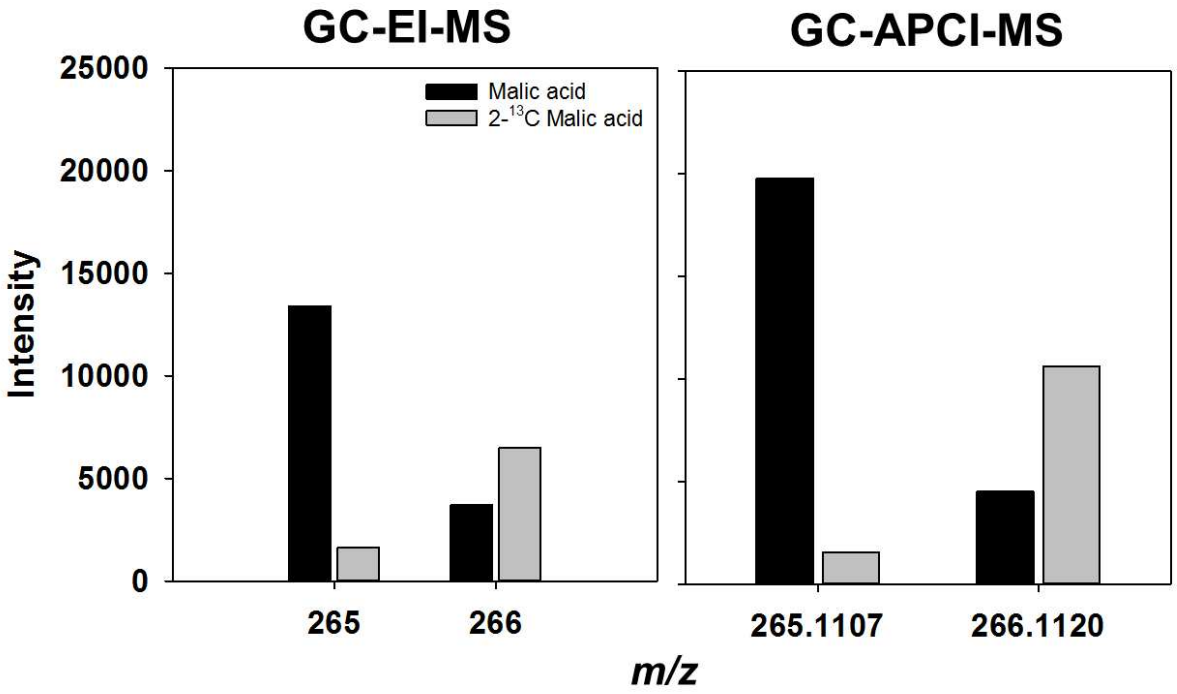

Supplemental Figure 2 Intensity of the isotopologues *m/z* 265 and *m/z* 266 of malic acid (3TMS) obtained by both GC-EI-MS and GC-APCI-MS using naturally (black bars) and positionally ^{13}C-labelled at the carbon 2 (2-C) (grey bars). Abbreviations: APCI, atmospheric pressure chemical ionization; EI, electron impact; GC-MS, gas chromatography coupled to mass spectrometry; *m/z*, mass-to-charge ratio; TMS, trimethylsilylated

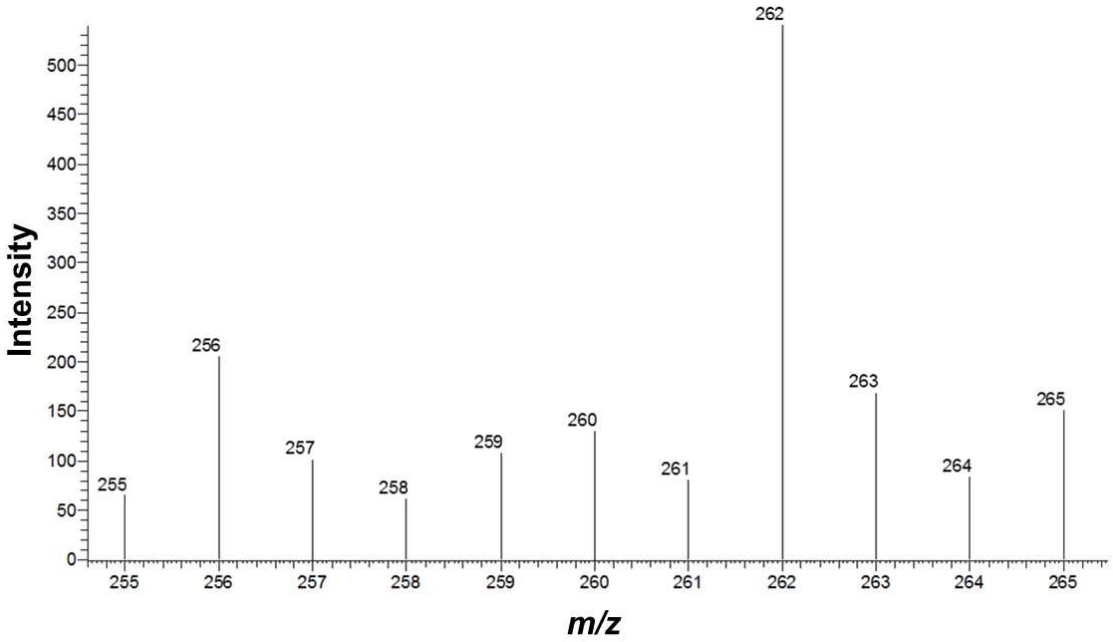

Supplemental Figure 3 Mass spectrum of EI-induced fragmentation of MEOX/TMS-derivatized glucose highlighting the low intensity of *m/z* 259 and *m/z* 262 as well as the overlap between the isotopologues M3 (*m/z* 262), M4 (*m/z* 263) and M5 (*m/z* 264) of the fragment *m/z* 259 with the isotopologues M0 (*m/z* 262), M1 (*m/z* 263), M2 (*m/z* 264) and M3 (*m/z* 264) of the fragment *m/z* 262. Abbreviations: EI, electron impact; MEOX, methoxyaminated; *m/z*, mass-to-charge ratio; TMS, trimethylsilylated.

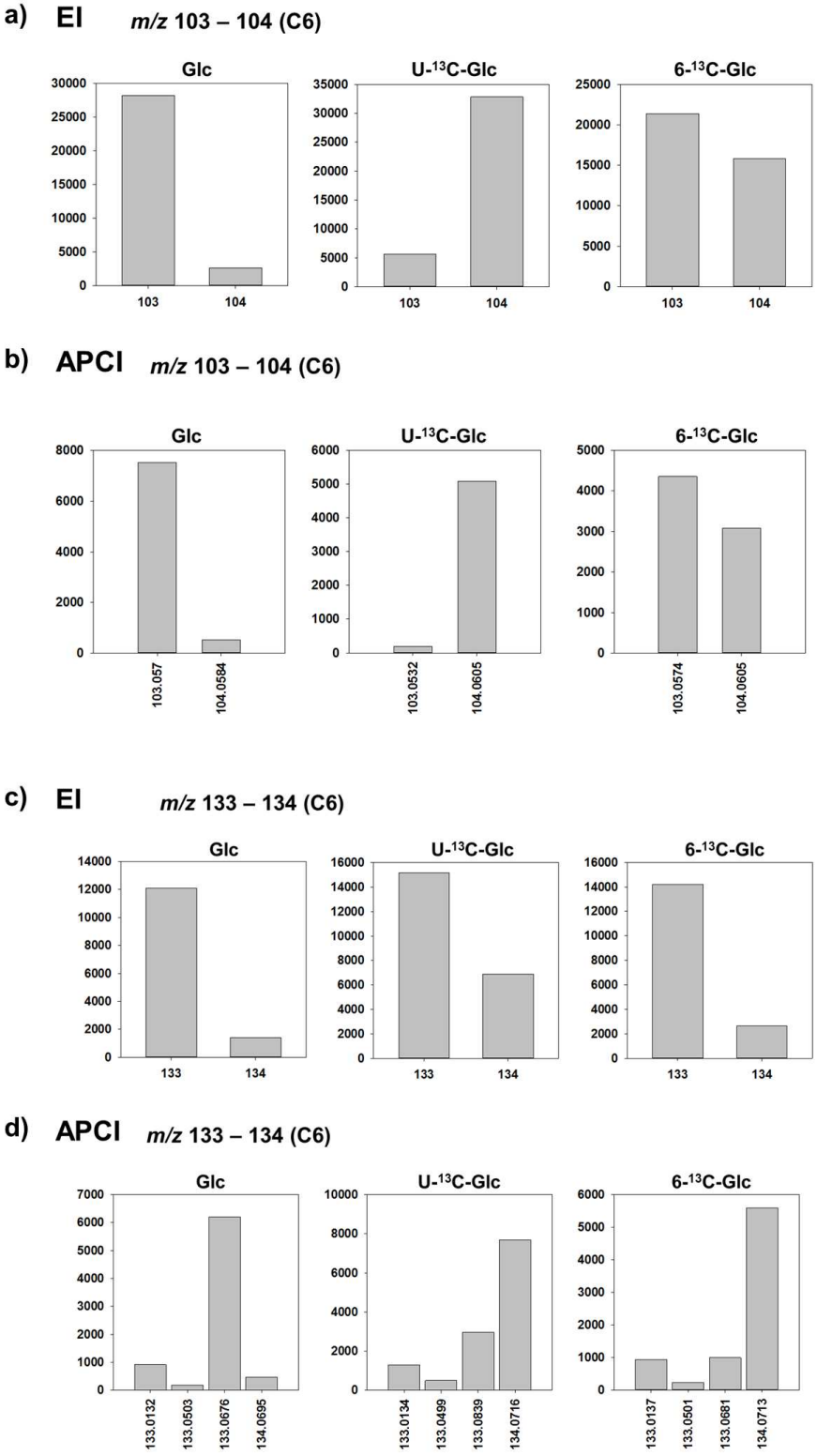

Supplemental Figure 4 Intensity of the fragments *m/z* 103 (6-C) and *m/z* 133 (6-C) of MEOX/TMS-derivatized glucose obtained by both GC-EI-MS and GC-APCI-MS using naturally, uniformly (U-^{13}C) and 6-^{13}C positionally labelled glucose (Glc) references. The increases observed in the monoisotopic mass of isotopologues M1 (*m/z* 104 and *m/z* 134) from APCI-MS analysis indicates that both fragments likely contain the carbon 6 of the glucose backbone. Abbreviations: APCI, atmospheric pressure chemical ionization; EI, electron impact; MEOX, methoxyaminated; *m/z*, mass-to-charge ratio; TMS, trimethylsilylated.

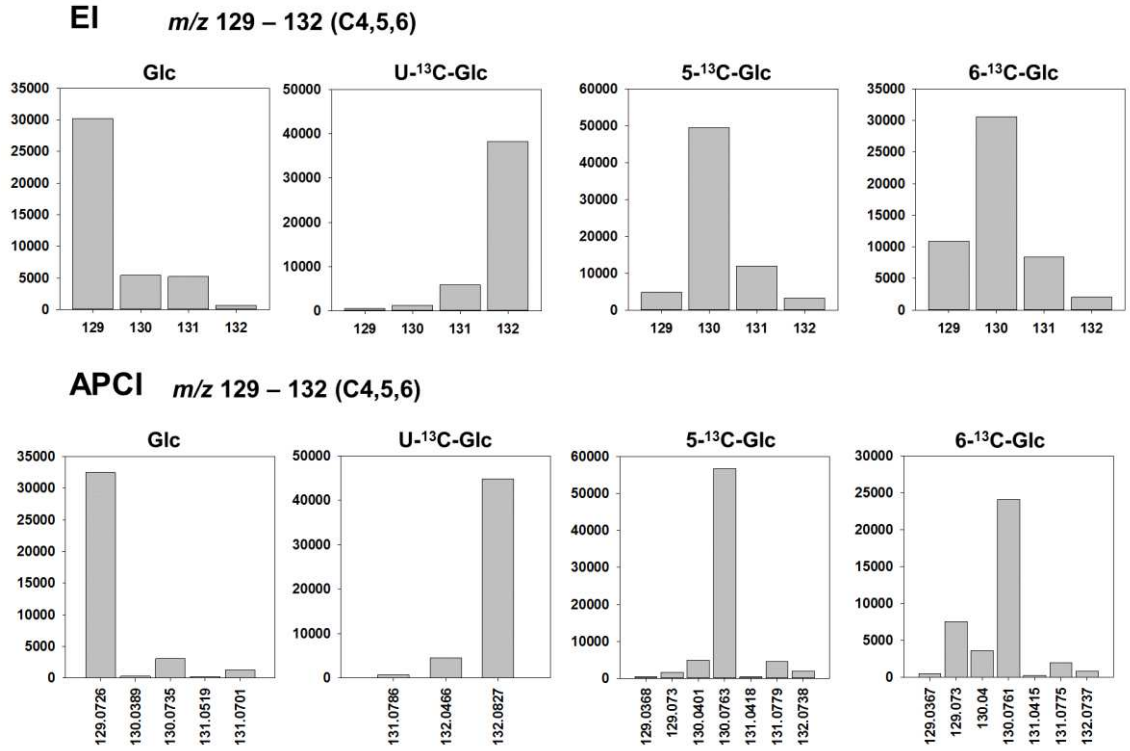

Supplemental Figure 5 Intensity of the fragments *m/z* 129 (4,5,6-C) and *m/z* 217 (4,5,6-C) of MEOX/TMS-derivatized glucose obtained by both GC-EI-MS and GC-APCI-MS using naturally, uniformly (U-^{13}C) and 5-^{13}C and 6-^{13}C positionally labelled glucose (Glc) references. U-^{13}C glucose analysis indicates that these fragments contain three carbons of the glucose backbone. The increases in *m/z* 130 and *m/z* 218 in both 5-^{13}C and 6-^{13}C analyses indicate that these fragments contain the carbons 5 and 6 of the glucose backbone. Abbreviations: APCI, atmospheric pressure chemical ionization; EI, electron impact; MEOX, methoxyaminated; *m/z*, mass-to-charge ratio; TMS, trimethylsilylated.

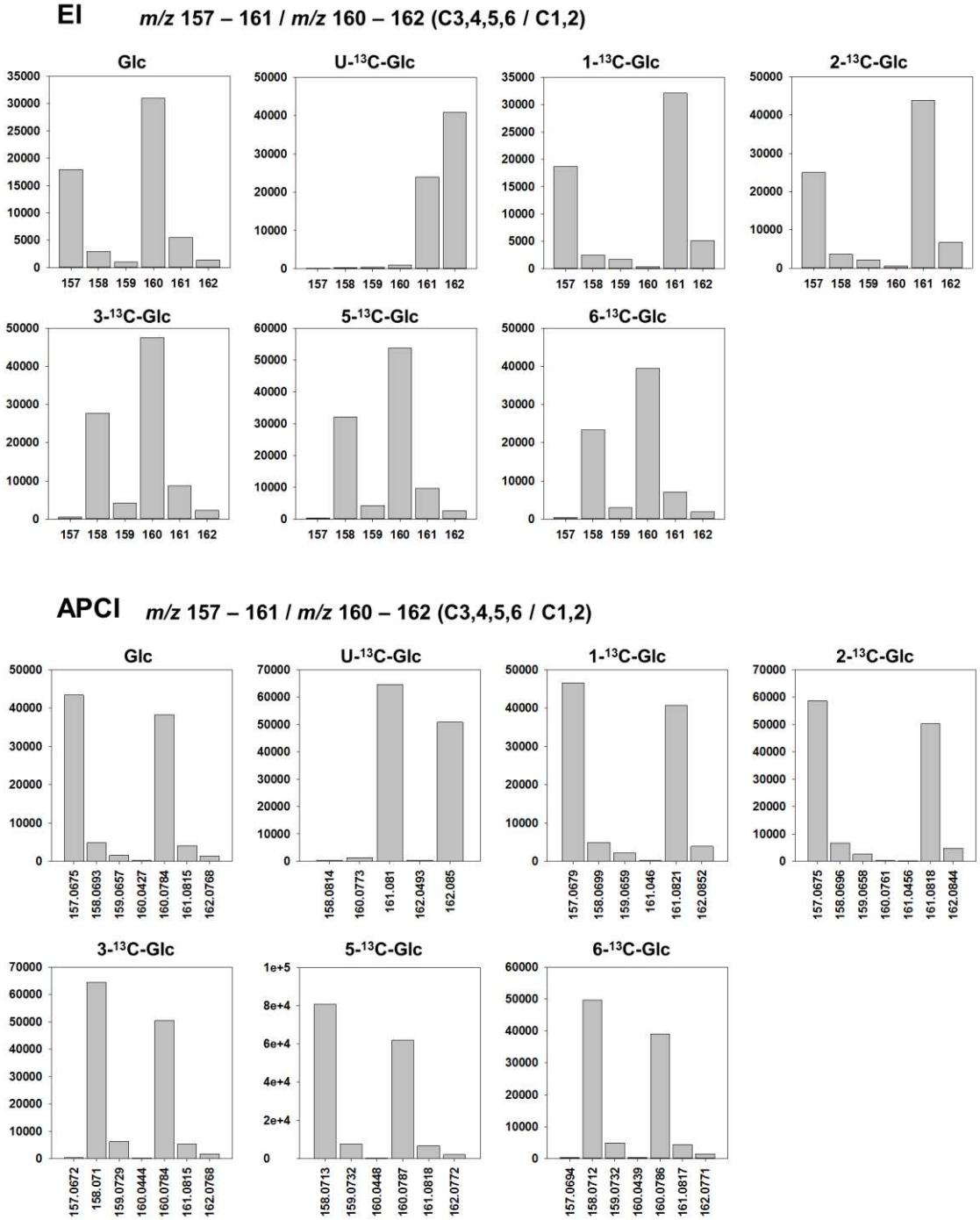

Supplemental Figure 6 Intensity of the fragments *m/z* 157 (3,4,5,6-C) and *m/z* 160 (1,2-C) of MEOX/TMS-derivatized glucose obtained by both GC-EI-MS and GC-APCI-MS using naturally, uniformly (U-^{13}C) and 1-^{13}C, 2-^{13}C, 3-^{13}C, 5-^{13}C and 6-^{13}C positionally labelled glucose (Glc) references. U-^{13}C glucose analysis indicates that the fragments *m/z* 157 and *m/z* 160 contain four and two carbons of the glucose backbone, respectively, as evidenced by the increases in *m/z* 161 and *m/z* 162. The composition of these fragments suggested by our *in silico* analysis is confirmed by positionally labelled glucose references. Abbreviations: APCI, atmospheric pressure chemical ionization; EI, electron impact; MEOX, methoxyaminated; *m/z*, mass-to-charge ratio; TMS, trimethylsilylated.

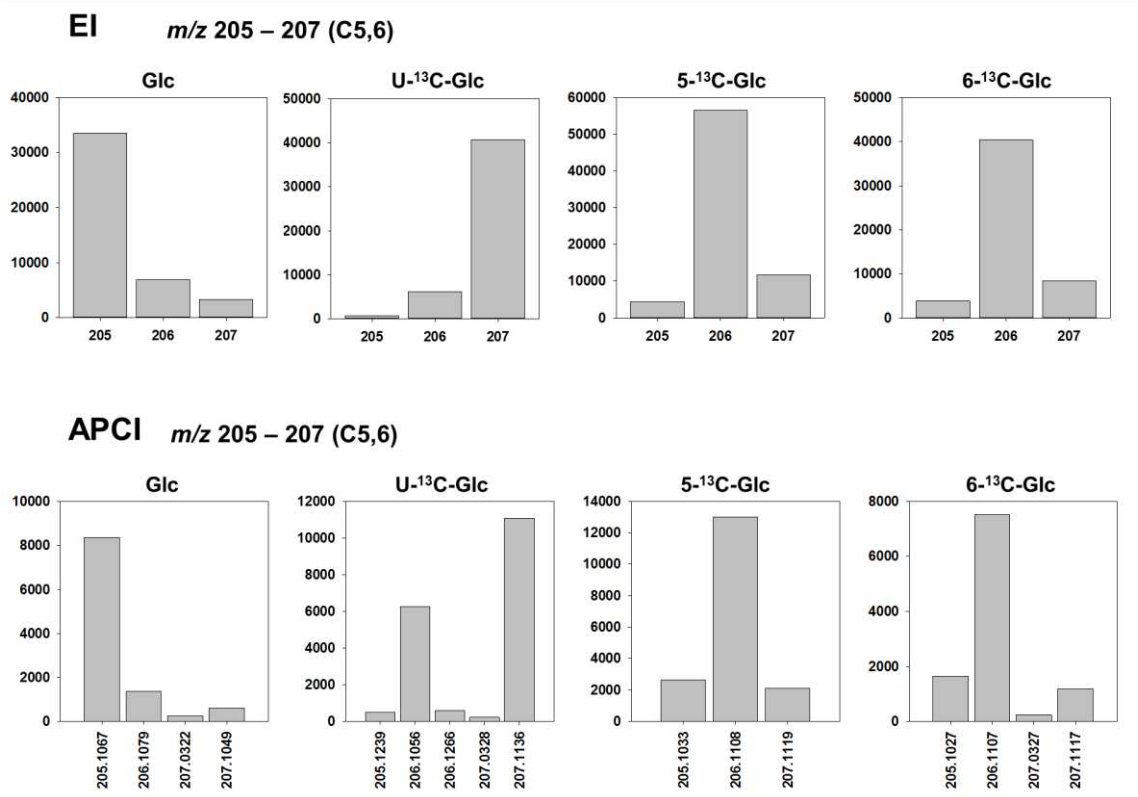

Supplemental Figure 7 Intensity of the fragment *m/z* 205 (5,6-C) of MEOX/TMS-derivatized glucose obtained by both GC-EI-MS and GC-APCI-MS using naturally, uniformly (U-^{13}C) and 5-^{13}C and 6-^{13}C positionally labelled glucose (Glc) references. U-^{13}C glucose analysis indicates that this fragment contains two carbons of the glucose backbone, as evidenced by the increased intensity of *m/z* 207 and *m/z* 207.1136. Positionally labelled glucose analysis clearly identified that this fragment contains the 5-C and 6-C of the glucose backbone. Abbreviations: APCI, atmospheric pressure chemical ionization; EI, electron impact; MEOX, methoxyaminated; *m/z*, mass-to-charge ratio; TMS, trimethylsilylated.

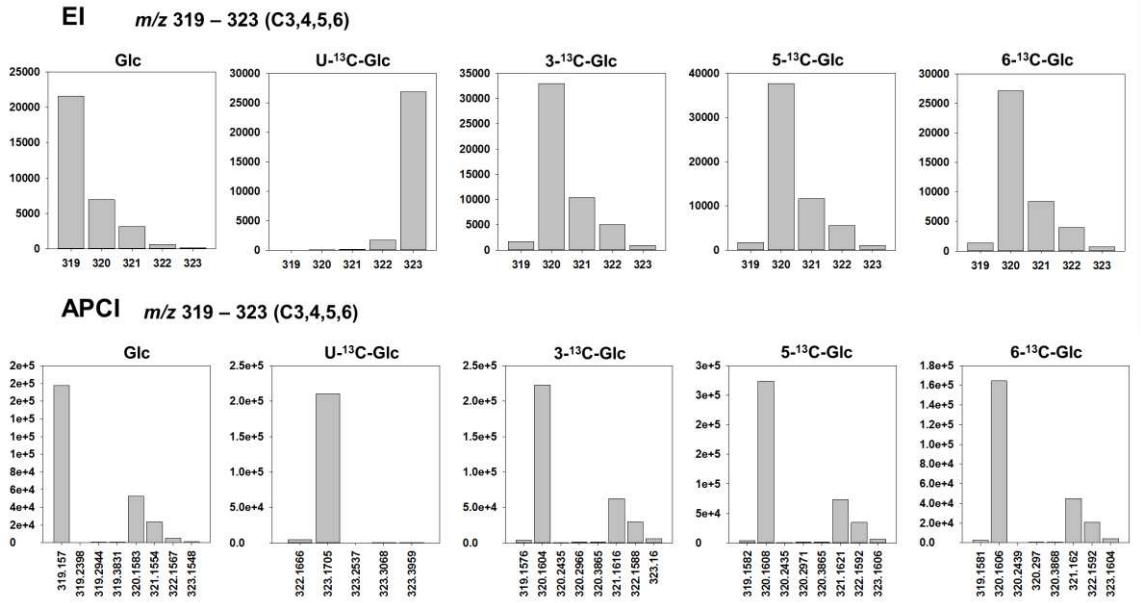

Supplemental Figure 8 Intensity of the fragment *m/z* 319 (3,4,5,6-C) of MEOX/TMS-derivatized glucose obtained by both GC-EI-MS and GC-APCI-MS using naturally, uniformly (U-^{13}C) and 3-^{13}C, 5-^{13}C and 6-^{13}C positionally labelled glucose (Glc) references. U-^{13}C glucose analysis indicates that this fragment contains four carbons of the glucose backbone, as evidenced by the increased intensity of *m/z* 323 and *m/z* 323.1705. Positionally labelled glucose analysis strongly suggests that this fragment contains the 3,4,5,6-C of the glucose backbone. Abbreviations: APCI, atmospheric pressure chemical ionization; EI, electron impact; MEOX, methoxyaminated; *m/z*, mass-to-charge ratio; TMS, trimethylsilylated.

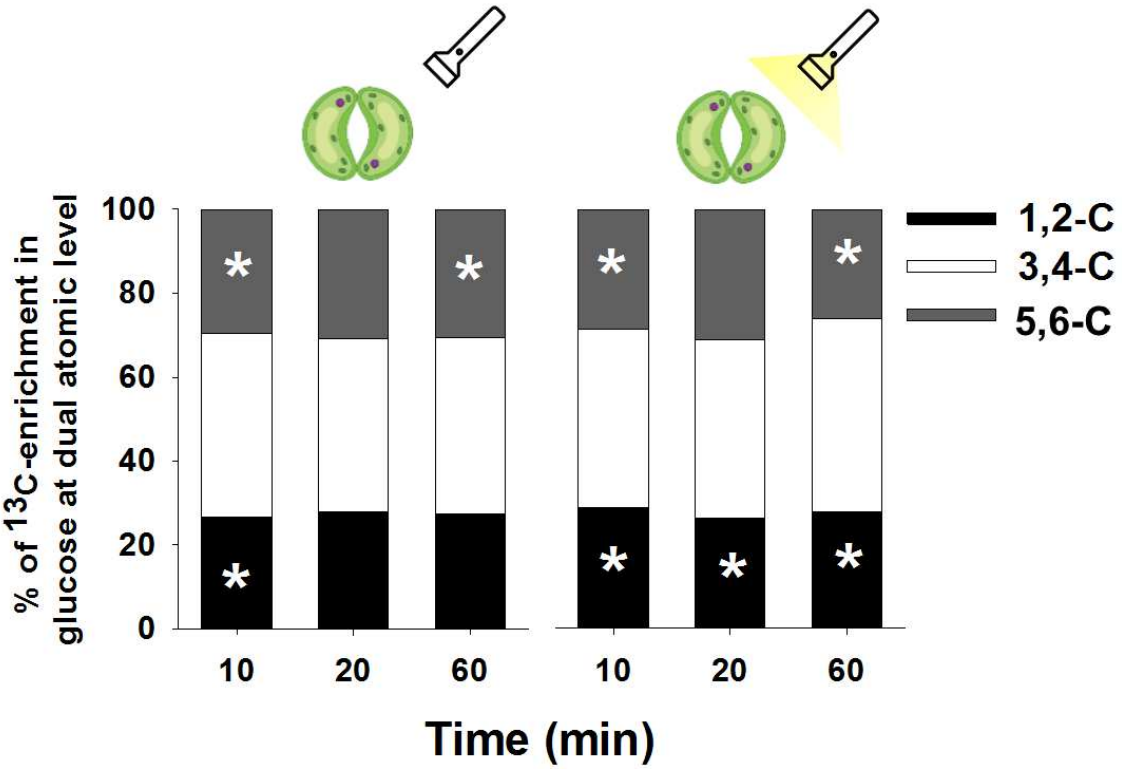

Supplemental Figure 9 Percentage (%) of the ^{13}C-labelling incorporation into glucose carbons at dual atomic level in darkened and illuminated guard cells following provision of ^{13}C-HCO_3. Asterisks indicate that the % of ^{13}C-enrichment in that carbon pair is lower than those observed in the 3,4-C in the same sample and at the same time point. The % of ^{13}C-labelling between the pair of glucose carbons was compared by Student's *t*-test ($P < 0.05$). Values are presented as mean ± SE (n = 4).

Table S1 Pearson correlation analysis between isotopologues from fragments that contain the same carbons of the glucose backbone. The analysis was carried out using both normalized intensity (NI) and relative (%) isotopologue abundance (RIA) data. We further compared the fractional ^{13}C-enrichment of these fragments, which consider both NI and RIA data. The fragments *m/z* 129 and *m/z* 217 contain 4,5,6-C of the glucose backbone, whereas the fragments *m/z* 103 and *m/z* 133 contain the 6-C of the glucose backbone. These relationships were obtained using data from Arabidopsis rosettes following provision of $^{13}CO_2$.

	NI	RIA
***m/z* 129 vs *m/z* 217**		
m/z 129 vs *m/z* 217	1.00	0.99
m/z 130 vs *m/z* 218	1.00	0.27
m/z 131 vs *m/z* 219	0.97	0.69
m/z 132 vs *m/z* 220	0.99	1.00
***m/z* 103 vs *m/z* 133**		
m/z 103 vs *m/z* 133	0.98	0.98
m/z 104 vs *m/z* 134	0.87	0.98

	Fractional ^{13}C-enrichment
m/z 129 vs *m/z* 217	0.99
m/z 103 vs *m/z* 133	0.98

Table S2 List of positionally ^{13}C-labelled references used in this study.

Positionally labelled reference substances analysed	
Glucose (1MEOX)(5TMS)	Glucose (1MEOX)(5TMS) U-^{13}C-Glucose (1MEOX)(5TMS) 1-^{13}C-Glucose (1MEOX)(5TMS) 2-^{13}C-Glucose (1MEOX)(5TMS) 3-^{13}C-Glucose (1MEOX)(5TMS) 5-^{13}C-Glucose (1MEOX)(5TMS) 6-^{13}C-Glucose (1MEOX)(5TMS)
Glutamic Acid (3TMS)	Glutamic Acid (3TMS) 1-^{13}C-Glutamic Acid (3TMS) 5-^{13}C-Glutamic Acid (3TMS) 2,3,3,4,4-D_5-Glutamic Acid (3TMS)
Glutamine (3TMS)	Glutamine (3TMS) U-^{13}C-Glutamine (3TMS) 1-^{13}C-Glutamine (3TMS) amine-^{15}N-Glutamine (3TMS) amide-^{15}N-Glutamine (3TMS) 2,3,3,4,4-D_5-Glutamine (3TMS)
Malic Acid (3TMS)	Malic Acid (3TMS) 1-^{13}C-Malic Acid (3TMS) 2-^{13}C-Malic Acid (3TMS)

CHAPTER III

Unveiling the dark side of guard cell metabolism

7 CHAPTER III – UNVEILING THE DARK SIDE OF GUARD CELL METABOLISM

Valéria F. Lima[1], Francisco Bruno S. Freire[1], Silvio A. Cândido-Sobrinho[1], Nicole P. Porto[1], David B. Medeiros[2], Alexander Erban[2], Joachim Kopka[2], Markus Schwarzländer[3], Alisdair R. Fernie[2], Danilo M. Daloso[1*]

[1] LabPlant, Departamento de Bioquímica e Biologia Molecular, Universidade Federal do Ceará, 60451-970, Fortaleza, Ceará, Brasil.

[2] Max-Planck-Institute of Molecular Plant Physiology, 14476 Potsdam-Golm, Germany.

[3] Institute of Plant Biology and Biotechnology, Westfälische-Wilhelms-Universität Münster, D-48143 Münster, Germany.

*Corresponding author.

Published manuscript in *Plant Physiology and Biochemistry* in 2023.

Abstract

Evidence suggests that guard cells have higher rate of phospho*enol*pyruvate carboxylase (PEPc)-mediated dark CO_2 assimilation than mesophyll cells. However, it is unknown which metabolic pathways are activated following dark CO_2 assimilation in guard cells. Furthermore, it remains unclear how the metabolic fluxes throughout the tricarboxylic acid (TCA) cycle and associated pathways are regulated in illuminated guard cells. Here we carried out a ^{13}C-HCO_3 labelling experiment in tobacco guard cells harvested under continuous dark or during the dark-to-light transition to elucidate principles of metabolic dynamics downstream of CO_2 assimilation. Most metabolic changes were similar between dark-exposed and illuminated guard cells. However, illumination altered the metabolic network structure of guard cells and increased the ^{13}C-enrichment in sugars and metabolites associated to the TCA cycle. Sucrose was labelled in the dark, but light exposure increased the ^{13}C-labelling and leads to more drastic reductions in the content of this metabolite. Fumarate was strongly labelled under both dark and light conditions, while illumination increased the ^{13}C-enrichment in pyruvate, succinate and glutamate. Only one ^{13}C was incorporated into malate and citrate in either dark or light conditions. Our results indicate that several metabolic pathways are redirected following PEPc-mediated CO_2 assimilation in the dark, including gluconeogenesis and the TCA cycle. We further showed that the PEPc-mediated CO_2 assimilation provides carbons for gluconeogenesis, the TCA cycle and glutamate synthesis and that previously stored malate and citrate are used to underpin the specific metabolic requirements of illuminated guard cells.

Keywords: ^{13}C-labelling analysis, glutamate, gluconeogenesis, metabolic network, metabolic regulation, phospho*enol*pyruvate carboxylase, TCA cycle.

Introduction

Guard cell metabolism has been studied for over a century. From the starch-sugar conversion hypothesis to the discovery that inorganic ions such as potassium (K^+) modulate guard cell osmotic potential during light-induced stomatal opening (Lloyd, 1908; Fischer, 1968), the understanding of how guard cell metabolism regulates stomatal movements has evolved dramatically over the decades (Granot and Kelly, 2019). Breakdown of sugars, starch and lipids within guard cells are important mechanisms to sustain the speed of light-induced stomatal opening (Antunes *et al.*, 2012, 2017; Ni, 2012; Daloso *et al.*, 2015*a*; Horrer *et al.*, 2016; McLachlan *et al.*, 2016; Medeiros *et al.*, 2018; Flütsch *et al.*, 2020*a*). Given the sink characteristics of guard cells (Hite *et al.*, 1993; Ritte *et al.*, 1999), the import of ATP, organic acids and sugars from mesophyll cells contributes to the stomatal opening upon illumination (Hedrich and Marten, 1993; Araújo *et al.*, 2011; Kelly *et al.*, 2013; Wang *et al.*, 2014*b*, 2019; Lugassi *et al.*, 2015; Medeiros *et al.*, 2016; Antunes *et al.*, 2017; Flütsch *et al.*, 2020*a*). Thus, light mediates stomatal opening by both, perception directly in the guard cells (Kinoshita *et al.*, 2001; Wang *et al.*, 2010; Ando and Kinoshita, 2018) and indirectly through signals derived from mesophyll cells (Mott, 2009; Fujita *et al.*, 2019; Flütsch and Santelia, 2021). For the latter mode the respiratory activity seems to be of great importance (Nunes-Nesi *et al.*, 2007; Araújo *et al.*, 2011; Vialet-Chabrand *et al.*, 2021). Taken together, these works have substantially improved our understanding of light-induced changes in guard cell metabolism. However, light is just one out of several stimuli that affects stomatal aperture and how guard cell metabolism operates in the dark remains unexplored.

As the main energy source for plants, folial illumination activates photosynthesis alongside other mechanisms that sustain plant metabolism (Buchanan, 2016). Photosynthetic ATP production and CO_2 assimilation mediated by ribulose-1,5-bisphosphate carboxylase/oxygenase (RuBisCO) are pivotal for the functioning of photoautotrophic cells. This is especially true for C3 and C4 plants, in which the vast majority of carbon assimilation occurs in the light period (Hohmann-Marriott and Blankenship, 2011; Matthews *et al.*, 2020). Additionally, given the capacity of plant cells to store and transport photoassimilates, the remobilisation of photosynthesis-derived products such as starch and sucrose is an important mechanism that sustains both metabolism and growth during the night period (Sulpice *et al.*, 2014; Apelt *et al.*, 2017; Mengin *et al.*, 2017). By contrast to C3- and C4-plants, a special group of plants that evolved Crassulaceae Acid Metabolism (CAM) can also fix CO_2 through the activity of phospho*enol*pyruvate carboxylase (PEPc) in the dark (Ranson and Thomas, 1960;

O'Leary *et al.*, 2011). In these plants, the stomata open in the dark and close in the light. Whilst the stomatal opening in the dark favours the PEPc-mediated CO_2 fixation, stomatal closure in the light avoids water loss, leading to the highest water use efficiency (WUE) observed in plants. Curiously, several C3 and C4 plants maintain a substantial transpiration stream during the night period (Caird *et al.*, 2007; Costa *et al.*, 2015). Furthermore, nocturnal stomatal conductance (g_{sn} - the rate of stomatal opening in the night) was positively correlated with relative growth rate in a multi-species meta-analysis (Resco de Dios *et al.*, 2019). However, the regulation of g_{sn} remains insufficiently understood (Gago *et al.*, 2020). Given the role of guard cell metabolism in regulating stomatal opening (Daloso *et al.*, 2017; Lawson and Matthews, 2020), unveiling how guard cell metabolism operates in the dark will be a prerequisite for a mechanistic understanding of g_{sn} regulation.

Radiotracer experiments suggest that guard cells can incorporate CO_2 in the dark at higher rates than mesophyll cells (Gotow *et al.*, 1988). Furthermore, ^{13}C-labelling results using mesophyll and guard cell protoplasts highlight that guard cells have faster and higher ^{13}C-incorporation into malate under illuminated conditions (Robaina-Estévez *et al.*, 2017). These results suggest a high PEPc activity in guard cells under either dark or light conditions. Indeed, recent ^{13}C-positional labelling analysis confirmed that guard cells are able to assimilate CO_2 in the dark, as evidenced by the increases in the ^{13}C-enrichment in the carbon 4 (4-C) of malate (Lima *et al.*, 2021), which is derived from PEPc activity (Abadie and Tcherkez, 2019). High dark CO_2 fixation rates are typically found in CAM cell types (Cockburn, 1983). However, the idea that guard cells have CAM-like metabolism is not fully supported by transcriptome studies (Wang *et al.*, 2011; Bates *et al.*, 2012; Bauer *et al.*, 2013; Aubry *et al.*, 2016). It remains therefore unclear whether the metabolic photosynthetic mode of guard cells most closely resembles that of C3, C4 or CAM cells. Alternatively, guard cells might not strictly fit into any of these classifications. If this is the case, a specific mode of regulation may be predicted in these cells. This idea is supported by the finding that illumination triggers specific responses observed in guard cells, but not in mesophyll cells, such as the degradation of lipids, starch and sugars and the activation of glycolysis (Hedrich *et al.*, 1985; Zhao and Assmann, 2011; Daloso *et al.*, 2015*a*, 2016*b*; Horrer *et al.*, 2016; McLachlan *et al.*, 2016; Robaina-Estévez *et al.*, 2017; Medeiros *et al.*, 2018; Flütsch *et al.*, 2020*b*). Additionally, the metabolic fluxes throughout the TCA cycle and associated metabolic pathways seems to be differentially regulated in illuminated guard cells, when compared to mesophyll cells (Daloso *et al.*, 2017; Robaina-Estévez *et al.*, 2017). These observations raise the question how light influences the regulation

of key metabolic pathways in guard cells. Here we addressed this question using ^{13}C-HCO_3 labelling in guard cells subjected to either dark or light conditions.

Material and methods

Plant material and growth condition

Seeds of *Nicotiana tabacum* (L.) were germinated and cultivated in a substrate composed by a mixture of vermiculite, sand and soil (2:1:0.5) for 30 days. Plants were kept well-watered and nourished with Hoagland nutrient solution every week (Hoagland and Arnon, 1950) under non-controlled greenhouse conditions with natural 12 h of photoperiod, ambient temperature 30 ± 4 °C, relative humidity 62 ± 10% and photosynthetic photon flux density (PPFD) which reached a maximum value of 500 □mol photons m^{-2} s^{-1}.

Guard cell isolation

A pool of guard cell-enriched epidermal fragments (simply referred here as guard cells) was isolated following a protocol that was optimized for metabolite profiling analysis (Daloso *et al.*, 2015*a*). Guard cells were isolated at pre-dawn by blending approximately three expanded leaves per replicate in a Waring blender (Philips, RI 2044 B.V. International Philips, Amsterdam, The Netherlands), that contains an internal filter to remove excess mesophyll cells, fibres and other cellular debris. The viability of the guard cells was analysed by staining with fluorescein diacetate and propidium iodide dyes, as described earlier (Huang *et al.*, 1986). This analysis demonstrated that only the guard cells are alive in the epidermal fragments (Daloso *et al.*, 2015*a*; Antunes *et al.*, 2017). All guard cell isolations were carried out in the dark in order to maintain closed stomata and simulate opening upon illumination, following the natural stomatal circadian rhythm (Daloso *et al.*, 2016*b*; Antunes *et al.*, 2017).

^{13}C-isotope labelling experiment

After isolation, guard cells were transferred to light or dark conditions and incubated in a solution containing 50 μM $CaCl_2$ and 5 mM MES-Tris, pH 6.15 in the presence of ^{13}C-HCO_3. Previous studies have showed that HCO_3 at a concentration of 5 mM was enough to detect ^{13}C-incorporation into primary metabolites in tobacco guard cells (Daloso *et al.*, 2015*a*, 2016*b*) and in detached Arabidopsis leaves (Porto *et al.*, 2022) with a good ^{13}C signal in the mass spectra as well as within the ranges mostly used in physiological and electrophysiological studies (Prins *et al.*, 1980; Staal *et al.*, 1989; Kolla and Raghavendra, 2007; Xue *et al.*, 2011; Tang *et al.*,

2020). Based on these observations, we decided to perform our ^{13}C-HCO_3 experiment by providing 5 mM of ^{13}C-$NaHCO_3$. The experiment was initiated at the beginning of the light period of the day and conducted with four biological replicates. Guard cell samples were rapidly harvested on a nylon membrane (220 µm) and snap-frozen in liquid nitrogen after 0, 10, 20 and 60 minutes under light or dark conditions (Supplementary Figure S1).

Metabolomics analysis

Approximately 30 mg of guard cells were disrupted and transformed into a powder by maceration using mortar, pestle and liquid nitrogen. The powder was then used for metabolite extraction. The extraction and derivatization of polar metabolites were carried out as described previously (Lisec *et al.,* 2006), except that 1 ml of the polar (upper) phase, instead of 150 µl, was collected and reduced to dryness. Metabolites were derivatized by methoxyamination, with subsequent addition of tri-methyl-silyl (TMS) and finally analysed by gas chromatography electron impact – time of flight – mass spectrometry (GC-EI-TOF-MS), as described previously (Lisec *et al.,* 2006). The mass spectral analysis were performed using the software Xcalibur® 2.1 (Thermo Fisher Scientific, Waltham, MA, USA), as described earlier (Lima *et al.*, 2018). The metabolites were identified using the Golm Metabolome Database (http://gmd.mpimp-golm.mpg.de/) (Kopka *et al.*, 2005). The metabolite content is expressed as relative to ribitol (added to each biological replicate during the extraction) on a fresh weight (FW) basis. The data is reported following recommendations for metabolomics analysis (Supplementary Dataset S1) (Fernie *et al.*, 2011; Alseekh *et al.*, 2021).

^{13}C-enrichment analysis

The relative abundance of the isotopologues (RIA) (M, M1, M2…Mn) and the fractional ^{13}C-enrichment ($F^{13}C$) was calculated as described previously (Lima *et al.*, 2018). For instance, in a fragment of three carbons, the sum of the intensity of the isotopologues M, M1, M2 and M3 was set to 100%, and the intensity of each isotopologue is then relative to this sum. In this hypothetical fragment, the $F^{13}C$ is calculated according to the following equation: $F^{13}C$ = ((M1*1)+(M2*2)+(M3*3))/3. The relative ^{13}C-enrichment ($R^{13}C$) was obtained by normalizing the $F^{13}C$ by the time 0 of the experiment.

Metabolic network analysis

Correlation-based metabolic networks were created using metabolite profiling data, in which the nodes correspond to the metabolites and the links to the strength of correlation between a pair of metabolites. The correlation was calculated using debiased sparse partial correlation (DSPC) analysis using the Java-based CorrelationCalculator software (Basu *et al.*, 2017). The networks were designed by restricting the strength of the connections to a specific limit of DSPC coefficient (r) ($-0.5 > r > 0.5$) using Metscape on CYTOSCAPE v.3.7.2 software (Shannon *et al.*, 2003; Karnovsky *et al.*, 2012). Network-derived parameters such as clustering coefficient, network heterogeneity, network density and network centralization were obtained as described previously (Assenov *et al.*, 2008). We further determined the preferential attachment and the appearance of new hubs, which highlight the nodes that are considered hubs before the start of the experiment (time 0) and maintain its degree of connection and demonstrate nodes that become highly connected after the beginning of the treatments, respectively (Freire *et al.*, 2021).

Statistical analysis

All data are expressed as the mean of four replicates ± standard error (SE). Significant difference in the content or relative ^{13}C-enrichment throughout the time was determined by one-way analysis of variance (ANOVA) and Dunnet test ($P < 0.05$), using the time 0 min as control. The difference between dark and light treatments in each time point was determined by Student's t test ($P < 0.05$). These statistical analyses were carried out using SIGMAPLOT12 (Systat Software Inc., San Jose, CA, USA) or Minitab 18 statistical software (State College, PA: Minitab, Inc.). Principal component analysis (PCA) was carried out in square root transformed and auto-scaled (mean-centred and divided by the standard deviation of each variable) data using the Metaboanalyst platform (Chong *et al.*, 2018).

Results

To distinguish dark and light-mediated metabolic changes in guard cells, we performed a ^{13}C-HCO_3 labelling experiment. Guard cells were harvested pre-dawn and subjected to 0, 10, 20 and 60 minutes of continuous darkness or following transfer to white light conditions (400 µmol photons m^{-2} s^{-1}). Primary metabolites were identified and used to compare the changes at both metabolite content and ^{13}C-enrichment. Whilst changes in the content of metabolites indicate alterations in the pool of them throughout the experiment, the ^{13}C-enrichment analysis

demonstrates the ^{13}C distribution derived from CO_2 assimilation mediated by PEPc in the dark and by both PEPc and RuBisCO in the light.

The changes in metabolite content were similar between dark-exposed and illuminated guard cells

Overall, the metabolic changes were similar between dark-exposed and illuminated guard cells. Under both dark and light conditions, the accumulation of fumarate, pyruvate, aspartate and lactate and the degradation of sucrose, glucose, gamma-aminobutyric acid (GABA) and different amino acids was observed (Fig. 1). However, also differential behaviour of specific metabolites was observed. After 60 min of illumination the content of both glutamate (Glu) and urea increased as compared to the time 0 of the experiment and fructose, sorbose and citrate levels decreased (Fig. 1). Comparing dark and light treatments in each time point, decreased content of alanine, citrate, glucose, *myo*-inositol, sorbose and sucrose was observed in illuminated samples. Interestingly, the content of malate is lower at 10 and 60 min and higher at 20 min in the light, as compared to dark-exposed guard cells (Supplementary Fig. S2). This analysis highlights that the dynamic of relative metabolite accumulation/degradation throughout time is slightly altered by light imposition. This idea is further supported by principal component analysis (PCA), in which no clear separation of dark and light treatments was observed (Fig. 2).

Illumination triggers re-modelling of metabolic network topology in guard cells

We have recently shown that light-induced stomatal opening involves changes in the density and topology of the guard cell metabolic network (Freire *et al.*, 2021). Here, no general pattern of increasing or decreasing network parameters such as clustering coefficient, centralization, density and heterogeneity was observed over time in metabolic networks created using metabolite content data (Supplementary Table S1). However, the number of hub-like nodes, the preferential attachment and the appearance of hub-like nodes differ between dark and light samples. Whilst these parameters reduced to zero after 60 min in the dark, they increased in the light metabolic network over time (Supplementary Table S1), in which malate, fumarate, GABA and glucose appear as important hubs of the metabolic network of illuminated guard cells (Fig. 3). These results suggest that illumination alter the metabolic network structure of guard cells, with particularly strong impact on the pathways associated to the TCA cycle and sugar metabolism.

Guard cells have a highly active metabolism in the dark

Similar to the described for metabolite content data, dark-exposed and illuminated guard cells display similar trends in the relative ^{13}C-enrichment ($R^{13}C$) data. Alanine, fumarate, glucose, glycine, sucrose and valine were labelled with statistical significance ($P < 0.05$) under both conditions in at least one time point, as compared to the time 0 of the experiment (Fig. 4). However, comparing light and dark treatments in each time point, increased ^{13}C-labelling in sucrose, fructose, sorbose, malate, pyruvate, succinate and glutamate was observed in illuminated guard cells, especially at 60 min of labelling (Supplementary Fig. S3). In fact, PCA indicates that dark and light treatments differ mainly at 60 min, as evidenced by the separation by the first component (Fig. 5). Analysis of the contribution of each metabolite for the PCA highlights that certain sugars (sucrose, fructose and glucose), organic acids (citrate and pyruvate), amino acids (Glu, Ile) and *myo*-inositol are those that mostly contributed to the separation observed in PCA of 60 min (Supplementary Fig. S4). These results indicate that several metabolic pathways are redirected following PEPc-mediated CO_2 assimilation in the dark, including gluconeogenesis and the TCA cycle. However, the combination of CO_2 assimilation catalysed by both PEPc and RuBisCO leads to more dramatic changes in ^{13}C-distribution over these and other metabolic pathways in illuminated guard cells.

Fumarate is equally and strongly labelled under both dark and light conditions, but succinate labelling is increased by light exposure

We investigated the $R^{13}C$ in the fragments *m/z* 245 of malate, *m/z* 245 of fumarate and *m/z* 247 of succinate, that contain the four carbons (1,2,3,4-C) of these metabolites. Increased $R^{13}C$ in fumarate *m/z* 245 under both dark and light conditions was observed (Fig. 4) and no difference in the $F^{13}C$ of this fragment was noticed after 60 min of labelling between dark and light conditions (Fig. 6). By contrast, light exposure leads to higher $F^{13}C$ in succinate *m/z* 247, when compared to dark-exposed guard cells (Fig. 6). Relative isotopologue analysis (RIA) suggests the incorporation of four ^{13}C into succinate under light conditions (Supplementary Fig. S5). No significant ^{13}C-enrichment in malate *m/z* 245 was observed in either light or dark conditions, when compared to the time 0 of the experiment (Fig. 4). However, the $F^{13}C$-enrichment in malate *m/z* 245 was higher after 60 min in the light, when compared to guard cells kept in the dark (Fig. 6). Intriguingly, the labelling in malate does not match those observed in fumarate and succinate. We have previously shown that only the 4-C of malate was labelled

under either dark or light conditions (Lima *et al.*, 2021), which contributes to explain the lack of significant $R^{13}C$ in malate *m/z* 245. The labelling in malate could be also interpreted by a dilution in the ^{13}C-labelling from previously stored, non-labelled malate, which corroborates the role of malate as a counter-ion of potassium (K^+) in the vacuole of guard cells (Outlaw and Lowry, 1977; Tallman and Zeiger, 1988; Talbott and Zeiger, 1993).

Glutamate synthesis in illuminated guard cells likely depends on PEPc CO_2 assimilation and previously stored citrate

Illumination leads to increased $R^{13}C$ in glutamate *m/z* 156 (Fig. 4). This fragment contains the 2,3,4,5-C of the Glu backbone, which are derived from the TCA cycle (2,3-C) and from pyruvate dehydrogenase (PDH) activity (4,5-C) (Abadie *et al.*, 2017). We next investigated the sources of carbon for Glu synthesis in illuminated guard cells by analysing both $R^{13}C$ and RIA data of Glu and metabolites of, or associated to, the TCA cycle. Increased $R^{13}C$ in pyruvate *m/z* 174 (1,2,3-C) was only observed in the light (Fig. 4). However, increases in the M3 isotopologue (*m/z* 177) of pyruvate was observed at 10 min of labelling in dark-exposed guard cells, indicating the incorporation of three carbons labelled at this time point (Supplementary Fig. S6). After 60 min of labelling, the $F^{13}C$ in pyruvate was 2.5-fold higher in the light, when compared to dark-exposed guard cells (Fig. 6).

No substantial difference was noticed in the intensity of citrate isotopologues of the *m/z* 273 fragment (1,2,3,4,5-C) in both dark and light samples over time. Although a slight but significant increase in the intensity of *m/z* 274 was noticed (Supplementary Fig. S7), this neither led to an increased $R^{13}C$ over time in the dark nor in the light (Fig. 4). Furthermore, no difference in the $R^{13}C$ of *m/z* 273 between dark-exposed and illuminated guard cells after 60 min of labelling was observed (Fig. 6). This fragment contains the 1,2,3,4,5-C of the citrate backbone (Okahashi *et al.*, 2019). Interestingly, the labelling in citrate does not match those observed in Glu. RIA data of the fragment *m/z* 156 (2,3,4,5-C) indicates that four ^{13}C were incorporated into Glu after 60 min in the light, as evidenced by the increases in the isotopologues M1-M4 (*m/z* 157-160) of this fragment (Supplementary Fig. S8). This leads to a higher $F^{13}C$ in Glu in the light, when compared to dark-exposed guard cells (Fig. 6). These results suggest that the carbon labelled in citrate is probably derived from PEPc activity (Abadie *et al.*, 2017) and that the labelling in citrate is diluted by the incorporation of stored, non-labelled compounds, as previously suggested in leaves (Cheung *et al.*, 2014).

Given that Glu could be synthesized by the activity of both Ala and Asp aminotransferases (AlaAT and AspAT) and degraded toward GABA synthesis, we additionally investigated the ^{13}C-enrichment in these metabolites. An increased R^{13}C in Ala was observed in both conditions, whilst Asp was only labelled in the light, when compared to the time 0 of the experiment (Fig. 4). However, no difference in the fractional ^{13}C-enrichment (F^{13}C) of these metabolites between dark and light conditions after 60 min of labelling was observed (Fig. 6). Furthermore, no ^{13}C-enrichment in GABA *m/z* 174 was observed (Fig. 4). However, assessment of recent data from Arabidopsis guard cells fed with ^{13}C-sucrose (Medeiros *et al.*, 2018), showed an increased F^{13}C in this metabolite during dark-to-light transition (Supplementary Fig. S9). Taken together, these results suggest that whilst both AlaAT and AspAT might contribute to the synthesis of Glu, the reactions catalysed by these enzymes do not fully explain the labelling found in Glu. It seems likely that Glu synthesis in illuminated guard cells mostly depends on carbons from both PEPc-mediated CO_2 assimilation and previously stored citrate.

Sugars are labelled in the dark, but light exposure increase the ^{13}C-labelling into these metabolites

Despite the presence of PEPc and RuBisCO-mediated CO_2 assimilation in guard cells (Daloso *et al.*, 2015*a*), the photorespiratory and gluconeogenic activity of these cells remains insufficiently understood. To shed light on the relative importance of photosynthesis and photorespiration in guard cells, we next evaluated the ^{13}C-enrichment into sugars as metabolites of successful photosynthetic assimilation, and glycine, serine and glycerate as photorespiratory metabolites. Increased R^{13}C in sucrose *m/z* 319 (3,4,5,6-C) was observed under both dark and light conditions. However, increased R^{13}C in sucrose *m/z* 361 (1,2,3,4,5,6-C) was only observed in the light, when compared to time 0 (Fig. 4). This resulted in a higher F^{13}C in both sucrose *m/z* 319 and *m/z* 361 in illuminated guard cells, as compared to dark-exposed guard cells after 60 min of labelling. Similarly, sorbose and fructose, but not glucose, were preferentially labelled in the light (Fig. 7). Increased R^{13}C in glycine *m/z* 102 was observed in both illuminated and dark-exposed guard cells, whilst increased R^{13}C in serine *m/z* 204 over time was only observed in the light (Fig. 4). However, no difference in the F^{13}C of these metabolites between the treatments after 60 min of labelling was observed. Additionally, glycerate was not labelled in either condition (Fig. 7), suggesting particularly low photorespiratory activity in guard cells.

Discussion

Guard cell metabolism is highly active in the dark, but light exposure triggers more drastic metabolic changes

Although signalling and metabolic pathways that regulate light-induced stomatal opening have been widely investigated (Inoue and Kinoshita, 2017; Lawson and Matthews, 2020), the metabolic pathways activated following PEPc-mediated CO_2 assimilation in the dark remains unclear. Here, we provide unprecedented information regarding the metabolic dynamics downstream of CO_2 assimilation by using a ^{13}C-labelling approach and tobacco guard cells subjected to darkness or during the dark-to-light transition. Our results highlight that the trends observed in both metabolite level and ^{13}C-enrichment were similar between dark-exposed and illuminated guard cells. For instance, sucrose breakdown and fumarate synthesis were observed under both dark and light conditions (Fig. 1). However, the metabolic changes were generally more pronounced in illuminated guard cells. This idea is supported by the higher degradation rate of sugars observed in the light, the separation observed in the PCA at 60 min of labelling (Fig. 5c), and the differences in the metabolic networks between dark-exposed and illuminated guard cells (Fig. 3). This is likely associated to the fact that certain processes such as RuBisCO-mediated CO_2 assimilation and the degradation of starch and lipids are induced by light exposure in guard cells (Horrer *et al.*, 2016; McLachlan *et al.*, 2016; Flütsch *et al.*, 2020*b*).

Interestingly, the diel course of starch synthesis and degradation differ substantially among mesophyll and guard cells (Santelia and Lunn, 2017). Whilst the degradation of this compound occurs in the dark period of the day in mesophyll cells (Martins *et al.*, 2013), starch is rapidly degraded in guard cells upon light exposure (Horrer *et al.*, 2016; Antunes *et al.*, 2017). Furthermore, evidence suggests that the PEPc-mediated anaplerotic CO_2 assimilation is higher in guard cells than mesophyll cells under dark (Gotow *et al.*, 1988) or light conditions (Robaina-Estévez *et al.*, 2017), which is related to the higher protein level of PEPc found in guard cells (Lim *et al.*, 2022). Indeed, *PPC2* mutation, considered as the major leaf PEPc gene, did not show significant effects on amino acids or organic acid leaf contents under ambient CO_2 conditions (You *et al.*, 2020). These discrepancies are associated to the function of these cells. Recent evidence suggests that the metabolic fluxes throughout the guard cell TCA cycle resemble those of sink rather than source leaves in the light (Daubermann *et al.*, 2023), in which a higher use of sucrose to the synthesis of metabolites of, or associated to, the TCA cycle such as glutamate and glutamine is observed (Dethloff *et al.*, 2017; Medeiros *et al.*, 2018). Taken together, these results highlight that the light-dependent metabolic regulation differs

substantially between mesophyll and guard cells. However, although several omics studies have been carried out in guard cells, none of them have explored the dark side of guard cell metabolism. In this context, our study raises unprecedent information regarding the functioning of these cells in the dark, which may pave the way to improve our understating concerning the metabolism of these cells in the dark. Further omics studies are needed to better understand the differences between dark-exposed and illuminated guard cells and how this is comparable with other cell types.

On the complex interplay among photosynthesis, glycolysis and gluconeogenesis for the homeostasis of sugars and organic acids in guard cells

Although initial studies did not detect RuBisCO in guard cells (Outlaw *et al.*, 1979), more recent proteomics and metabolomics analyses have confirmed the presence of RuBisCO and that guard cells are able to assimilate CO_2 by both RuBisCO and PEPc (Daloso *et al.*, 2015*a*; Robaina-Estévez *et al.*, 2017; Lawrence *et al.*, 2020; Balmant *et al.*, 2021). Indeed, the $F^{13}C$ into sugars was higher in illuminated than dark-exposed guard cells (Fig. 7), evidencing that the RuBisCO-mediated CO_2 assimilation contribute to sugar synthesis in illuminated guard cells. The ^{13}C-labelling incorporation into sugars in the dark suggests that gluconeogenesis is active in guard cells. This corroborates the high ^{13}C-enrichment observed in the 3,4-C of glucose under either dark or light conditions (Lima *et al.*, 2021), which are proposed to be the glucose carbons preferentially labelled by gluconeogenesis (Leegood and ap Rees, 1978; Beylot *et al.*, 1993). These results highlight that gluconeogenesis may be another metabolic pathway that contributes to sugar homeostasis in guard cells, an elusive source of carbon for sugar synthesis in guard cells that has long been debated (Willmer and Dittrich, 1974; Outlaw and Kennedy, 1978; Talbott and Zeiger, 1998; Zeiger *et al.*, 2002; Outlaw, 2003; Vavasseur and Raghavendra, 2005; Daloso *et al.*, 2016*a*).

Relative isotopologue analysis indicates that three ^{13}C were incorporated into pyruvate in both dark-exposed and illuminated guard cells, as evidenced by the significant increases in pyruvate *m/z* 177 after 10 min of exposure to continuous dark or after dark-to-light transition (Supplementary Fig. S6). The labelling in pyruvate in the light might occurs by a combination of ^{13}C derived from both RuBisCO and PEPc CO_2 assimilation, while the labelling in this metabolite in the dark suggests the activity of phospho*enol*pyruvate carboxykinase (PEPCK) and/or malic enzyme (ME), in which labelled OAA and malate would be rapidly converted into PEP and pyruvate, respectively (Fig. 7). Additionally, glycolysis and the activity of pyruvate

kinase (PK), that converts PEP to pyruvate, could also contribute to pyruvate labelling. Given the labelling observed in sugars in the dark, it seems that the carbon assimilated by PEPc is used to create a substrate cycle between gluconeogenesis and glycolysis, allowing the circulation of carbon between sugars and organic acids without importantly loss of assimilated carbon. Thus, PEPc activity would be important to re-assimilate the CO_2 lost by several decarboxylation reactions that occurs in chloroplast, mitochondria and cytosol (Sweetlove *et al.*, 2013). Indeed, previous modelling results suggest that the flux of CO_2 from the chloroplast to the cytosol is 17-fold higher in guard cells than mesophyll cells and is largely re-assimilated by PEPc in the cytosol (Robaina-Estévez *et al.*, 2017). According to this model, part of the carbon assimilated by PEPc is transported back to the chloroplast as malate, resulting in a net production of NADPH (Robaina-Estévez *et al.*, 2017). These results collectively suggest that PEPc activity is important for both the carbon re-assimilation and the homeostasis of sugars and organic acids in guard cells. The maintenance of a flux of carbon between sugars and organic acids (gluconeogenesis and glycolysis) could be a mechanism to rapidly provide carbons for starch synthesis or for the TCA cycle and associated pathways during stomatal closure and opening conditions, respectively (Outlaw and Manchester, 1979; Medeiros *et al.*, 2018).

Regulation of the TCA cycle and associated metabolic pathways in guard cells

Several lines of evidence point to restricted metabolic fluxes through the TCA cycle in illuminated leaves (Tcherkez *et al.*, 2009; Gauthier *et al.*, 2010; Daloso *et al.*, 2015*b*; Abadie *et al.*, 2017; Florez-Sarasa *et al.*, 2019). By contrast, our results indicate that illumination increased the metabolic fluxes throughout the TCA cycle and associated pathways in guard cells. This idea is supported by the higher $F^{13}C$ observed in malate, succinate, pyruvate and Glu in the light, when compared to dark-exposed guard cells (Fig. 6). It is noteworthy that the ^{13}C-enrichment observed in malate in illuminated guard cells was low, as compared to previous analysis (Daloso *et al.*, 2015*a*). This is likely associated to the fact that the results obtained here are from guard cells subjected to a solution without K^+ in the medium, given that the presence of this ion strongly increased the ^{13}C-enrichment in malate (Daloso *et al.*, 2015*a*). Thus, one would expect that the light-induced, PEPc-derived ^{13}C-incorporation into malate may be higher *in vivo*, given that light stimulates the influx of K^+ to guard cells (Hills *et al.*, 2012; Wang *et al.*, 2014*a*,*c*).

Interestingly, high ^{13}C-enrichment into glutamine and no ^{13}C-enrichment in malate were observed in Arabidopsis guard cells following ^{13}C-sucrose provision (Medeiros *et al.*, 2018). This suggests that the carbons derived from sucrose breakdown are either not directed to malate during the dark-to-light transition or the presence of previously stored, non-labelled carbons contribute to the synthesis of malate. Here, the ^{13}C-enrichment in citrate and malate was lower than in metabolites of the following steps of the pathway such as fumarate, succinate and Glu, suggesting that previously stored, non-labelled organic acids are used to underpin the metabolic requirements of guard cell metabolism in the light. Beyond contributing to explain the low ^{13}C-enrichment in malate and citrate observed in our study, the use of previously stored non-labelled organic acids is supported by modelling analysis predicting that malate accumulates at high rate in the vacuole of guard cells when K^+ accumulation was restricted by the model (Tan and Cheung, 2020). Taken together, modelling and ^{13}C-labelling results indicate the importance of previously stored organic acids to support the TCA cycle and Glu synthesis in illuminated guard cells, resembling the mechanism of TCA cycle regulation observed in leaves (Cheung *et al.*, 2014; Abadie *et al.*, 2017; da Fonseca-Pereira *et al.*, 2021).

On the source of carbons for glutamate synthesis in illuminated guard cells

The connection between the TCA cycle and Glu metabolism is well-established (Araújo *et al.*, 2012, 2013; O'Leary and Plaxton, 2020). ^{13}C-NMR studies indicate that the synthesis of Glu in illuminated leaves strongly depends on stored compounds (Tcherkez *et al.*, 2009; Gauthier *et al.*, 2010; Abadie *et al.*, 2017), which are presumably accumulated in the previous night period (Cheung *et al.*, 2014). This is likely an alternative to overcome the light-inhibition of PDH (Tovar-Méndez *et al.*, 2003; Zhang *et al.*, 2021), an important source of carbons for the TCA cycle and associated pathways (Reid *et al.*, 1977). The degradation of labelled pyruvate by PDH or PC would provide two and three labelled carbons into acetyl-CoA and OAA, respectively. Once synthesized, the acetyl-CoA could be used for citrate synthesis or exported from the mitochondria for fatty acid synthesis (Lonien and Schwender, 2009). However, export of citrate for fatty acid synthesis is unlikely to hold true given that light exposure triggers fatty acid degradation in guard cells (McLachlan *et al.*, 2016). It seems likely that fully labelled OAA is synthesized by the activity of both PEPc and PC, which is in turn simultaneously used to the synthesis of succinate through the activity of MDH and fumarase through the C4-branch of the TCA cycle and the synthesis of Glu through the C6(5)-branch of the TCA cycle. In parallel, PDH-derived acetyl-CoA would also contribute to the labelling of Glu through the C6(5)-

branch of the TCA cycle. This labelling pattern throughout the TCA cycle and associated pathways consider the incorporation of non-labelled carbons into malate and citrate. Therefore, our results collectively suggest that the carbon derived from PEPc-mediated CO_2 assimilation is simultaneously used to support gluconeogenesis, the TCA cycle and Glu synthesis and that previously stored citrate and malate may be an important source of carbons for the TCA cycle and associated pathways.

Acknowledgments

This work was partially supported by the National Institute of Science and Technology in Plant Physiology under Stress Conditions (INCT Plant Stress Physiology – Grant: 406455/2022-8) and the National Council for Scientific and Technological Development (CNPq, Grant No. 404817/2021-1). We also thank the research fellowship granted by CNPq to D.M.D and the scholarships granted by CNPq to F.B.S.F and by the Brazilian Federal Agency for Support and Evaluation of Graduate Education (CAPES-Brazil) to V.F.L. and N.P.P.

Conflict of interest

The authors declare no potential conflict of interest.

Author contributions

VFL and DMD designed the experiment. VFL, FBSF, NPP and SACS performed the ^{13}C-labelling experiment. Mass spectrometry analysis was performed by DBM under the supervision of ARF. Data analysis was performed by VFL, FBSF, SACS, AE, JK and DMD. All authors contributed to write the final manuscript. DMD obtained funding and is responsible for this article.

Data availability

All data supporting the findings of this study are available within the paper and within its supplementary materials published online.

References

Abadie C, Lothier J, Boex-Fontvieille E, Carroll A, Tcherkez G. 2017. Direct assessment of the metabolic origin of carbon atoms in glutamate from illuminated leaves using ^{13}C-NMR. New Phytologist **216**, 1079–1089.

Abadie C, Tcherkez G. 2019. In vivo phosphoenolpyruvate carboxylase activity is controlled by CO_2 and O_2 mole fractions and represents a major flux at high photorespiration rates. New Phytologist **221**, 1843–1852.

Alseekh S, Aharoni A, Brotman Y, *et al.* 2021. Mass spectrometry-based metabolomics: a guide for annotation, quantification and best reporting practices. Nature Methods **18**, 747–756.

Ando E, Kinoshita T. 2018. Red light-induced phosphorylation of plasma membrane H^+-ATPase in stomatal guard cells. Plant Physiology **178**, 838–849.

Antunes WC, Daloso DM, Pinheiro DP, Williams TCR, Loureiro ME. 2017. Guard cell-specific down-regulation of the sucrose transporter SUT1 leads to improved water use efficiency and reveals the interplay between carbohydrate metabolism and K^+ accumulation in the regulation of stomatal opening. Environmental and Experimental Botany **135**, 73–85.

Antunes WC, Provart NJ, Williams TCR, Loureiro ME. 2012. Changes in stomatal function and water use efficiency in potato plants with altered sucrolytic activity. Plant, Cell and Environment **35**, 747–759.

Apelt F, Breuer D, Olas JJ, Annunziata MG, Flis A, Nikoloski Z, Kragler F, Stitt M. 2017. Circadian, carbon, and light control of expansion growth and leaf movement. Plant Physiology **174**, 1949–1968.

Araújo WL, Nunes-Nesi A, Nikoloski Z, Sweetlove LJ, Fernie AR. 2012. Metabolic control and regulation of the tricarboxylic acid cycle in photosynthetic and heterotrophic plant tissues. Plant, Cell and Environment **35**, 1–21.

Araújo WL, Nunes-Nesi A, Osorio S, *et al.* 2011. Antisense Inhibition of the Iron-Sulphur Subunit of Succinate Dehydrogenase Enhances Photosynthesis and Growth in Tomato via an Organic Acid–Mediated Effect on Stomatal Aperture. The Plant Cell **23**, 600–627.

Araújo WL, Trofimova L, Mkrtchyan G, Steinhauser D, Krall L, Graf A, Fernie AR, Bunik VI. 2013. On the role of the mitochondrial 2-oxoglutarate dehydrogenase complex in amino acid metabolism. Amino Acids **44**, 683–700.

Assenov Y, Ramírez F, Schelhorn S-E, Lengauer T, Albrecht M. 2008. Computing topological parameters of biological networks. Bioinformatics **24**, 282–284.

Aubry S, Aresheva O, Reyna-Llorens I, Smith-Unna RD, Hibberd JM, Genty B. 2016. A Specific Transcriptome Signature for Guard Cells from the C4 Plant Gynandropsis gynandra. Plant Physiology **170**, 1345–1357.

Balmant KM, Lawrence SR, Duong B V., Zhu F, Zhu N, Nicklay J, Chen S. 2021. Guard cell redox proteomics reveals a role of lipid transfer protein in plant defense. Journal of

Proteomics **242**, 104247.

Basu S, Duren W, Evans CR, Burant CF, Michailidis G, Karnovsky A. 2017. Systems biology Sparse network modeling and metscape-based visualization methods for the analysis of large-scale metabolomics data. **33**, 1545–1553.

Bates GW, Rosenthal DM, Sun J, Chattopadhyay M, Peffer E, Yang J, Ort DR, Jones AM. 2012. A Comparative study of the Arabidopsis thaliana guard-cell transcriptome and its modulation by sucrose. PLoS ONE **7**.

Bauer H, Ache P, Wohlfart F, Al-Rasheid KAS, Sonnewald S, Sonnewald U, Kneitz S, Hetherington AM, Hedrich R. 2013. How do stomata sense reductions in atmospheric relative humidity? Molecular Plant **6**, 1703–1706.

Beylot M, Previs SF, David F, Brunengraber H. 1993. Determination of the ^{13}C-labeling pattern of glucose by gas chromatography-mass spectrometry. Analytical Biochemistry **212**, 526–531.

Buchanan BB. 2016. The carbon (formerly dark) reactions of photosynthesis. Photosynthesis Research **128**, 215–217.

Caird MA, Richards JH, Donovan LA. 2007. Nighttime stomatal conductance and transpiration in C3 and C4 plants. Plant Physiology **143**, 4–10.

Cheung CYM, Poolman MG, Fell DA, Ratcliffe RG, Sweetlove LJ. 2014. A diel flux balance model captures interactions between light and dark metabolism during day-night cycles in C3 and Crassulacean Acid Metabolism leaves. Plant physiology **165**, 917–929.

Chong J, Soufan O, Li C, Caraus I, Li S, Bourque G, Wishart DS, Xia J. 2018. MetaboAnalyst 4.0: Towards more transparent and integrative metabolomics analysis. Nucleic Acids Research **46**, W486–W494.

Cockburn W. 1983. Stomatal mechanism as the basis of the evolution of CAM and C4 photosynthesis. Plant, Cell & Environment **6**, 275–279.

Costa JM, Monnet F, Jannaud D, Leonhardt N, Ksas B, Reiter IM, Pantin F, Genty B. 2015. Open all night long: The Dark Side of Stomatal Control. Plant Physiology **167**, 289–294.

Daloso DM, dos Anjos L, Fernie AR. 2016*a*. Roles of sucrose in guard cell regulation. New Phytologist **211**, 809–818.

Daloso DM, Antunes WC, Pinheiro DP, Waquim JP, Araújo WL, Loureiro ME, Fernie AR, Williams TCR. 2015*a*. Tobacco guard cells fix CO2 by both Rubisco and PEPcase while sucrose acts as a substrate during light-induced stomatal opening. Plant Cell and Environment **38**, 2353–2371.

Daloso DM, Medeiros DB, dos Anjos L, Yoshida T, Araújo WL, Fernie AR. 2017. Metabolism within the specialized guard cells of plants. New Phytologist **216**, 1018–1033.

Daloso DM, Müller K, Obata T, *et al.* 2015*b*. Thioredoxin, a master regulator of the tricarboxylic acid cycle in plant mitochondria. Proceedings of the National Academy of Sciences of the United States of America **112**, E1392-400.

Daloso DM, Williams TCR, Antunes WC, Pinheiro DP, Müller C, Loureiro ME, Fernie AR. 2016*b*. Guard cell-specific upregulation of sucrose synthase 3 reveals that the role of sucrose in stomatal function is primarily energetic. New Phytologist **209**, 1470–1483.

Daubermann AG, Lima VF, Schwarzländer M, Erban A, Kopka J, Fernie AR, Anjos L dos, Daloso DM. 2023. Distinct metabolic flux modes through the tricarboxylic acid cycle in mesophyll and guard cells revealed by GC-MS-based ^{13}C-positional isotopomer analysis. bioRxiv.

Dethloff F, Orf I, Kopka J. 2017. Rapid in situ ^{13}C tracing of sucrose utilization in Arabidopsis sink and source leaves. Plant Methods **13**, 1–19.

Fernie AR, Aharoni A, Willmitzer L, Stitt M, Tohge T, Kopka J, Carroll AJ, Saito K, Fraser PD, DeLuca V. 2011. Recommendations for Reporting Metabolite Data. The Plant Cell **23**, 2477–2482.

Fischer R. 1968. Stomatal Opening: Role of Potassium Uptake by Guard Cells. Science **160**, 784–785.

Florez-Sarasa I, Obata T, Del-Saz NF, Reichheld J-P, Meyer EH, Rodriguez-Concepcion M, Ribas-Carbo M, Fernie AR. 2019. The Lack of Mitochondrial Thioredoxin TRXo1 Affects In Vivo Alternative Oxidase Activity and Carbon Metabolism under Different Light Conditions. Plant and Cell Physiology **60**, 2369–2381.

Flütsch S, Nigro A, Conci F, Fajkus J, Thalmann M, Trtílek M, Panzarová K, Santelia D. 2020*a*. Glucose uptake to guard cells via STP transporters provides carbon sources for stomatal opening and plant growth. EMBO reports **21**, 1–13.

Flütsch S, Santelia D. 2021. Mesophyll-derived sugars are positive regulators of light-driven stomatal opening. New Phytologist **230**, 1754–1760.

Flütsch S, Wang Y, Takemiya A, Vialet-Chabrand SRM, Klejchová M, Nigro A, Hills A, Lawson T, Blatt MR, Santelia D. 2020*b*. Guard Cell Starch Degradation Yields Glucose for Rapid Stomatal Opening in Arabidopsis. The Plant Cell **32**, 2325–2344.

da Fonseca-Pereira P, Souza PVL, Fernie AR, Timm S, Daloso DM, Araújo WL. 2021. Thioredoxin-mediated regulation of (photo)respiration and central metabolism (T Lawson,

Ed.). Journal of Experimental Botany **72**, 5987–6002.

Freire FBS, Bastos RLG, Bret RSC, Cândido-Sobrinho SA, Medeiros DB, Antunes WC, Fernie AR, Daloso DM. 2021. Mild reductions in guard cell sucrose synthase 2 expression leads to slower stomatal opening and decreased whole plant transpiration in Nicotiana tabacum L. Environmental and Experimental Botany **184**, 104370.

Fujita T, Noguchi K, Ozaki H, Terashima I. 2019. Confirmation of mesophyll signals controlling stomatal responses by a newly devised transplanting method. Functional Plant Biology **46**, 467–481.

Gago J, Daloso DM, Carriquí M, Nadal M, Morales M, Araújo WL, Nunes-Nesi A, Perera-Castro AV, Clemente-Moreno MJ, Flexas J. 2020. The photosynthesis game is in the 'inter-play': Mechanisms underlying CO_2 diffusion in leaves. Environmental and Experimental Botany **178**, 104174.

Gauthier PPG, Bligny R, Gout E, Mahé A, Nogués S, Hodges M, Tcherkez GGB. 2010. In folio isotopic tracing demonstrates that nitrogen assimilation into glutamate is mostly independent from current CO_2 assimilation in illuminated leaves of Brassica napus. New Phytologist **185**, 988–999.

Gotow K, Taylor S, Zeiger E. 1988. Photosynthetic Carbon Fixation in Guard Cell Protoplasts of Vicia faba L . 1. , 700–705.

Granot D, Kelly G. 2019. Evolution of Guard-Cell Theories: The Story of Sugars. Trends in Plant Science **24**, 507–518.

Hedrich R, Marten I. 1993. Malate-induced feedback regulation of plasma membrane anion channels could provide a CO2 sensor to guard cells. The EMBO journal **12**, 897–901.

Hedrich R, Raschke K, Stitt M. 1985. A role for fructose 2,6-bisphosphate in regulating carbohydrate metabolism in guard cells. Plant physiology **79**, 977–982.

Hills A, Chen Z-H, Amtmann A, Blatt MR, Lew VL. 2012. OnGuard, a Computational Platform for Quantitative Kinetic Modeling of Guard Cell Physiology. Plant Physiology **159**, 1026–1042.

Hite DRC, Outlaw WH, Tarczynski MC. 1993. Elevated levels of both sucrose-phosphate synthase and sucrose synthase in Vicia guard cells indicate cell-specific carbohydrate interconversions. Plant physiology **101**, 1217–1221.

Hoagland DR, Arnon DI. 1950. The water-culture method for growing plants without soil. California Agricultural Experiment Station Circular **347**, 1–32.

Hohmann-Marriott MF, Blankenship RE. 2011. Evolution of Photosynthesis. Annual

Review of Plant Biology **62**, 515–548.

Horrer D, Flütsch S, Pazmino D, Matthews JSA, Thalmann M, Nigro A, Leonhardt N, Lawson T, Santelia D. 2016. Blue light induces a distinct starch degradation pathway in guard cells for stomatal opening. Current Biology **26**, 362–370.

Huang C-N, Cornejo MJ, Bush DS, Jones RL. 1986. Estimating viability of plant protoplasts using double and single staining. Protoplasma **135**, 80–87.

Inoue S, Kinoshita T. 2017. Blue Light Regulation of Stomatal Opening and the Plasma Membrane H^+-ATPase. Plant Physiology **174**, 531–538.

Karnovsky A, Weymouth T, Hull T, *et al.* 2012. Metscape 2 bioinformatics tool for the analysis and visualization of metabolomics and gene expression data. Bioinformatics **28**, 373–380.

Kelly G, Moshelion M, David-Schwartz R, Halperin O, Wallach R, Attia Z, Belausov E, Granot D. 2013. Hexokinase mediates stomatal closure. Plant Journal **75**, 977–988.

Kinoshita T, Doi M, Suetsugu N, Kagawa T, Wada M, Shimazaki K. 2001. Phot1 and phot2 mediate blue light regulation of stomatal opening. Nature **414**, 656–660.

Kolla VA, Raghavendra AS. 2007. Nitric oxide is a signaling intermediate during bicarbonate-induced stomatal closure in Pisum sativum. Physiologia Plantarum **130**, 91–98.

Kopka J, Schauer N, Krueger S, *et al.* 2005. GMD@CSB.DB: The Golm metabolome database. Bioinformatics **21**, 1635–1638.

Lawrence SR, Gaitens M, Guan Q, Dufresne C, Chen S. 2020. S-nitroso-proteome revealed in stomatal guard cell response to flg22. International Journal of Molecular Sciences **21**.

Lawson T, Matthews J. 2020. Guard Cell Metabolism and Stomatal Function. Annual Review ofPlant Biology **71**, 273–302.

Leegood RC, ap Rees T. 1978. Dark fixation of CO_2 during gluconeogenesis by the cotyledons of Cucurbita pepo L. Planta **140**, 275–282.

Lima VF, Erban A, Daubermann AG, *et al.* 2021. Establishment of a GC-MS-based ^{13}C-positional isotopomer approach suitable for investigating metabolic fluxes in plant primary metabolism. The Plant Journal.

Lima VF, de Souza LP, Williams TCR, Fernie AR, Daloso DM. 2018. Gas Chromatography–Mass Spectrometry-Based ^{13}C-Labeling Studies in Plant Metabolomics. Plant Metabolomics.47–58.

Lim SL, Flütsch S, Liu J, Distefano L, Santelia D, Lim BL. 2022. Arabidopsis guard cell chloroplasts import cytosolic ATP for starch turnover and stomatal opening. Nature

Communications **13**, 1–13.

Lloyd F. E. 1908. The physiology of stomata. Publications of the Carnegie Institution of Washington **82**, 1–42.

Lonien J, Schwender J. 2009. Analysis of Metabolic Flux Phenotypes for Two Arabidopsis Mutants with Severe Impairment in Seed Storage Lipid Synthesis. Plant Physiology **151**, 1617–1634.

Lugassi N, Kelly G, Lena Fidel, *et al.* 2015. Expression of Arabidopsis Hexokinase in Citrus Guard Cells Controls Stomatal Aperture and Reduces Transpiration. **6**, 1–11.

Martins MCM, Hejazi M, Fettke J, *et al.* 2013. Feedback Inhibition of Starch Degradation in Arabidopsis Leaves Mediated by Trehalose 6-Phosphate. Plant Physiology **163**, 1142–1163.

Matthews JSA, Vialet-Chabrand S, Lawson T. 2020. Role of blue and red light in stomatal dynamic behaviour. Journal of Experimental Botany **71**, 2253–2269.

McLachlan DH, Lan J, Geilfus CM, *et al.* 2016. The Breakdown of Stored Triacylglycerols is Required during Light-Induced Stomatal Opening. Current Biology **26**, 707–712.

Medeiros DB, Martins SCV, Cavalcanti JHF, Daloso DM, Martinoia E, Nunes-Nesi A, DaMatta FM, Fernie AR, Araújo WL. 2016. Enhanced Photosynthesis and Growth in *atquac1* Knockout Mutants Are Due to Altered Organic Acid Accumulation and an Increase in Both Stomatal and Mesophyll Conductance. Plant Physiology **170**, 86–101.

Medeiros DB, Perez Souza L, Antunes WC, Araújo WL, Daloso DM, Fernie AR. 2018. Sucrose breakdown within guard cells provides substrates for glycolysis and glutamine biosynthesis during light-induced stomatal opening. The Plant Journal **94**, 583–594.

Mengin V, Pyl ET, Alexandre Moraes T, Sulpice R, Krohn N, Encke B, Stitt M. 2017. Photosynthate partitioning to starch in Arabidopsis thaliana is insensitive to light intensity but sensitive to photoperiod due to a restriction on growth in the light in short photoperiods. Plant, cell & environment **40**, 2608–2627.

Mott KA. 2009. Opinion: Stomatal responses to light and CO_2 depend on the mesophyll. Plant, Cell & Environment **32**, 1479–1486.

Ni DA. 2012. Role of vacuolar invertase in regulating Arabidopsis stomatal opening. Acta Physiologiae Plantarum **34**, 2449–2452.

Nunes-Nesi A, Carrari F, Gibon Y, Sulpice R, Lytovchenko A, Fisahn J, Graham J, Ratcliffe RG, Sweetlove LJ, Fernie AR. 2007. Deficiency of mitochondrial fumarase activity in tomato plants impairs photosynthesis via an effect on stomatal function. Plant Journal **50**, 1093–1106.

O'Leary B, Park J, Plaxton WC. 2011. The remarkable diversity of plant PEPC (phosphoenolpyruvate carboxylase): recent insights into the physiological functions and post-translational controls of non-photosynthetic PEPCs. Biochemical Journal **436**, 15–34.

O'Leary B, Plaxton WC. 2020. Multifaceted functions of post-translational enzyme modifications in the control of plant glycolysis. Current Opinion in Plant Biology **55**, 28–37.

Okahashi N, Kawana S, Iida J, Shimizu H, Matsuda F. 2019. Fragmentation of Dicarboxylic and Tricarboxylic Acids in the Krebs Cycle Using GC-EI-MS and GC-EI-MS/MS. Mass Spectrometry **8**, A0073–A0073.

Outlaw WHJ. 2003. Critical Reviews in Plant Sciences Integration of Cellular and Physiological Functions of Guard Cells Integration of Cellular and Physiological Functions of Guard Cells. Critical Reviews in Plant Sciences **22**, 503–5229.

Outlaw WH, Kennedy J. 1978. Enzymic and substrate basis for the anaplerotic step in guard cells. Plant physiology **62**, 648–652.

Outlaw WH, Lowry OH. 1977. Organic acid and potassium accumulation in guard cells during stomatal opening. **74**, 4434–4438.

Outlaw WH, Manchester J. 1979. Guard cell starch concentration quantitatively related to stomatal aperture. Plant physiology **64**, 79–82.

Outlaw WH, Manchester J, Dicamelli CA, Randall DD, Rapp B, Veith GM. 1979. Photosynthetic carbon reduction pathway is absent in chloroplasts of Vicia faba guard cells. Proceedings of the National Academy of Sciences of the United States of America **76**, 6371–5.

Porto NP, Bret RSC, Souza PVL, Cândido-Sobrinho SA, Medeiros DB, Fernie AR, Daloso DM. 2022. Thioredoxins regulate the metabolic fluxes throughout the tricarboxylic acid cycle and associated pathways in a light-independent manner. Plant Physiology and Biochemistry **193**, 36–49.

Prins HBA, Snel JFH, Helder RJ, Zanstra PE. 1980. Photosynthetic HCO_3^- utilization and OH^- excretion in aquatic angiosperms . Plant Physiology **66**, 818–822.

Ranson SL, Thomas M. 1960. Crassulacean Acid Metabolism. Annual Review of Plant Physiology **11**, 81–110.

Reid EE, Thompson P, Lyttle CR, Dennis DT. 1977. Pyruvate dehydrogenase complex from higher plant mitochondria and proplastids. Plant Physiology **59**, 854–858.

Resco de Dios V, Chowdhury FI, Granda E, Yao Y, Tissue DT. 2019. Assessing the potential functions of nocturnal stomatal conductance in C3 and C4 plants. New Phytologist **223**, 1696–1706.

Ritte G, Rosenfeld J, Rohrig K, Raschke K. 1999. Rates of sugar uptake by guard cell protoplasts of Pisum sativum L. related to the solute requirement for stomatal opening. Plant physiology **121**, 647–656.

Robaina-Estévez S, Daloso DM, Zhang Y, Fernie AR, Nikoloski Z. 2017. Resolving the central metabolism of Arabidopsis guard cells. Scientific Reports **7**, 1–13.

Santelia D, Lunn JE. 2017. Transitory starch metabolism in guard cells: unique features for a unique function. Plant Physiology **174**, 539–549.

Shannon P, Markiel A, Owen Ozier 2, Baliga NS, Wang JT, Ramage D, Amin N, Schwikowski B, Ideker T. 2003. Cytoscape: a software environment for integrated models of biomolecular interaction networks. Genome Research **13**, 2498–2504.

Staal M, Elzenga JTM, Prins HBA. 1989. ^{14}C fixation by leaves and leaf cell protoplasts of the submerged aquatic angiosperm potamogeton lucens: Carbon dioxide or bicarbonate? Plant Physiology **90**, 1035–1040.

Sulpice R, Flis A, Ivakov AA, Apelt F, Krohn N, Encke B, Abel C, Feil R, Lunn JE, Stitt M. 2014. Arabidopsis coordinates the diurnal regulation of carbon allocation and growth across a wide range of Photoperiods. Molecular Plant **7**, 137–155.

Sweetlove LJ, Williams TCR, Cheung M, Ratcliffe RG. 2013. Modelling metabolic CO_2 evolution - a fresh perspective on respiration. Plant, Cell & Environment **36**, 1631–1640.

Talbott LD, Zeiger E. 1993. Sugar and organic acid accumulation in guard cells of Vicia faba in response to red and blue light. Plant Physiology **102**, 1163–1169.

Talbott L, Zeiger E. 1998. The role of sucrose in guard cell osmoregulation. Journal of Experimental Botany **49**, 329–337.

Tallman G, Zeiger E. 1988. Light quality and osmoregulation in vicia guard cells : evidence for involvement of three metabolic pathways. Plant physiology **88**, 887–895.

Tan XLJ, Cheung CYM. 2020. A multiphase flux balance model reveals flexibility of central carbon metabolism in guard cells of C3 plants. The Plant Journal **104**, 1648–1656.

Tang M, Zhao X, Hu Y, Zeng M, Wang K, Dong N, Ma X, Bai L, Song CP. 2020. Arabidopsis guard cell CO_2/HCO_3- response mutant screening by an aequorin-based calcium imaging system. Plant Methods **16**, 1–10.

Tcherkez G, Mahé A, Gauthier P, Mauve C, Gout E, Bligny R, Cornic G, Hodges M. 2009. In folio respiratory fluxomics revealed by ^{13}C isotopic labeling and H/D isotope effects highlight the noncyclic nature of the tricarboxylic acid ‘cycle’ in illuminated leaves. Plant Physiology **151**, 620–630.

Tovar-Méndez A, Miernyk JA, Randall DD. 2003. Regulation of pyruvate dehydrogenase complex activity in plant cells. European Journal of Biochemistry **270**, 1043–1049.

Vavasseur A, Raghavendra AS. 2005. Guard cell metabolism and CO_2 sensing. New Phytologist **165**, 665–682.

Vialet-Chabrand S, Matthews JSA, Lawson T. 2021. Light, power, action! Interaction of respiratory energy- and blue light-induced stomatal movements. New Phytologist **231**, 2231–2246.

Wang Y, Hills A, Blatt MR. 2014*a*. Systems analysis of guard cell membrane transport for enhanced stomatal dynamics and water use eficiency. Plant Physiology **164**, 1593–1599.

Wang FF, Lian HL, Kang CY, Yang HQ. 2010. Phytochrome B is involved in mediating red light-induced stomatal opening in arabidopsis thaliana. Molecular Plant **3**, 246–259.

Wang SW, Li Y, Zhang XL, *et al.* 2014*b*. Lacking chloroplasts in guard cells of crumpled leaf attenuates stomatal opening: Both guard cell chloroplasts and mesophyll contribute to guard cell ATP levels. Plant, Cell and Environment **37**, 2201–2210.

Wang Y, Noguchi K, Ono N, Inoue S, Terashima I, Kinoshita T. 2014*c*. Overexpression of plasma membrane H^+-ATPase in guard cells promotes light-induced stomatal opening and enhances plant growth. Proceedings of the National Academy of Sciences of the United States of America **111**, 533–8.

Wang RS, Pandey S, Li S, Gookin TE, Zhao Z, Albert R, Assmann SM. 2011. Common and unique elements of the ABA-regulated transcriptome of Arabidopsis guard cells. BMC Genomics **12**, 216.

Wang H, Yan S, Xin H, *et al.* 2019. A subsidiary cell-localized glucose transporter promotes stomatal conductance and photosynthesis. The Plant cell **31**, 1328–1343.

Willmer CM, Dittrich P. 1974. Carbon dioxide fixation by epidermal and mesophyll tissues of Tulipa and Commelina. Planta **117**, 123–132.

Xue S, Hu H, Ries A, Merilo E, Kollist H, Schroeder JI. 2011. Central functions of bicarbonate in S-type anion channel activation and OST1 protein kinase in CO_2 signal transduction in guard cell. EMBO Journal **30**, 1645–1658.

You L, Zhang J, Li L, Xiao C, Feng X, Chen S, Guo L, Hu H. 2020. Involvement of abscisic acid, ABI5, and PPC2 in plant acclimation to low CO_2. Journal of Experimental Botany **71**, 4093–4108.

Zeiger E, Talbott LD, Frechilla S, Srivastava A, Zhu J. 2002. The guard cell chloroplast: A perspective for the twenty-first century. New Phytologist **153**, 415–424.

Zhang Y, Giese J, Mae-Lin Kerbler S, *et al.* 2021. Two mitochondrial phosphatases, PP2c63 and Sal2, are required for posttranslational regulation of the TCA cycle in Arabidopsis. Molecular Plant **14**, 1104–1108.

Zhao Z, Assmann SM. 2011. The glycolytic enzyme, phosphoglycerate mutase, has critical roles in stomatal movement, vegetative growth, and pollen production in Arabidopsis thaliana. Journal of Experimental Botany **62**, 5179–5189.

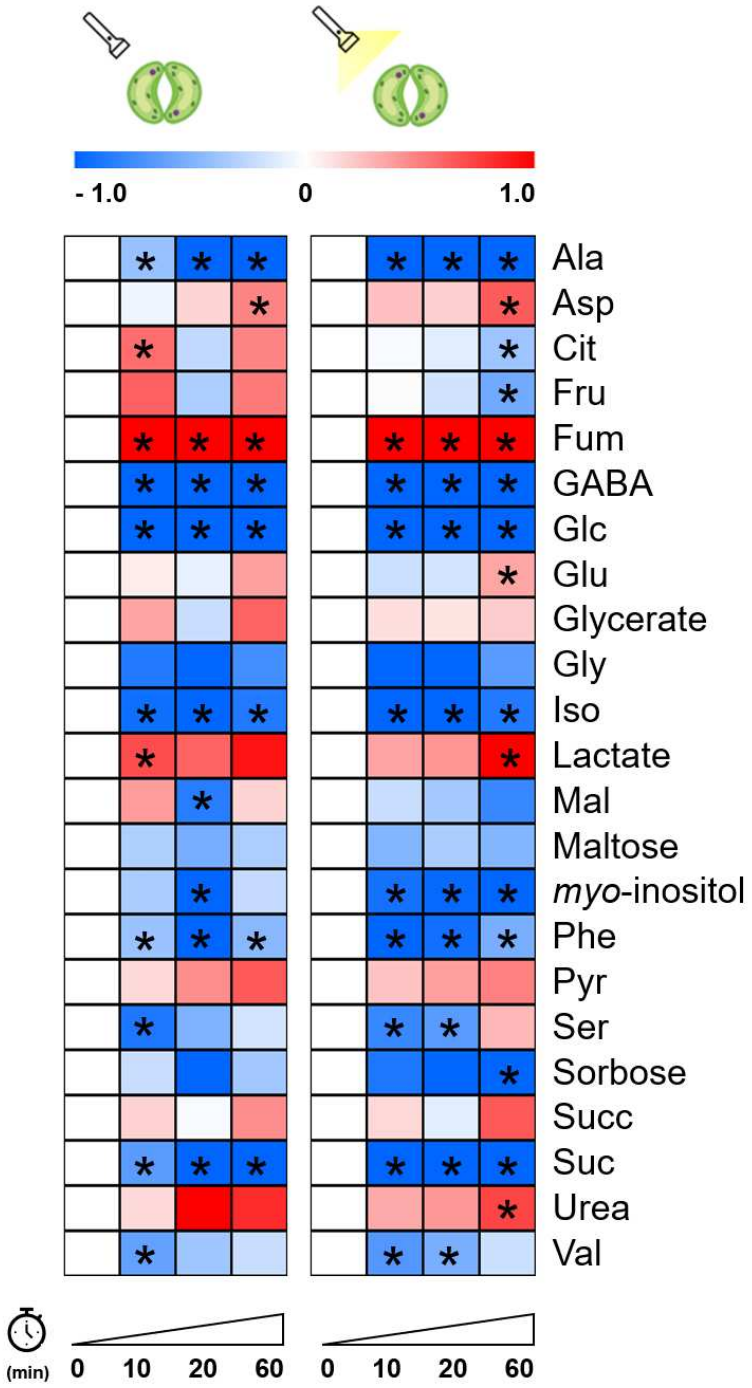

Fig. 1. Heat map representation of the metabolite content in guard cells fed with 5 mM of ^{13}C-HCO_3 for 0, 10, 20 and 60 min under dark (left) or light conditions (right). Metabolite content refers to the level of the metabolite normalized by ribitol and the fresh weight used during extraction. The data was further normalized by the values found at the time 0 of the experiment and log_2-transformed for heat map representation. Asterisks (*) indicate significant difference from dark (0 min) by Student's *t* test ($P < 0.05$) ($n = 4$). The abbreviation used in this figure correspond to: metabolites: Cit, citrate, Fru, fructose, Fum, fumarate, GABA, gamma-aminobutyric acid, Glc, glucose, Mal, malate, Pyr, pyruvate, Succ, succinate, Suc, sucrose. Amino acids are abbreviated using the standard three-letters code.

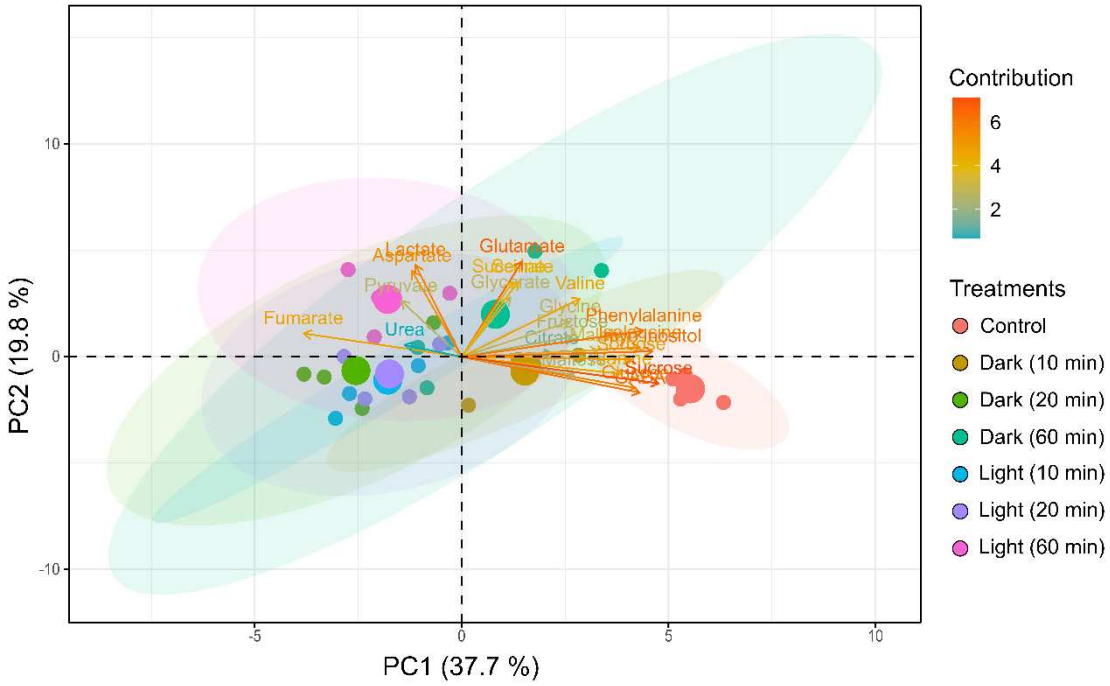

Fig. 2. Biplots of the principal component analysis (PCA) of the content of primary metabolites identified from guard cells fed with 5 mM of ^{13}C-HCO_3 for 10 min, 20 min and 60 min under dark or light conditions. The percentage variation explained by the components 1 (PC1) and 2 (PC2) is highlighted between parentheses in each axis. Ellipses surrounding circles of the same colour are the confidence interval of PCA of that treatment. Each colour represents a treatment, as indicated at the right bottom of the figure ($n = 4$). The contribution of each metabolite for the distinction between the samples is highlighted according to the colour scale at the upper right of each figure. The contribution of a variable (metabolite) to a given component (PC1 or PC2) is the $\cos^2\theta$ of the variable divided by the $\cos^2$ of the component ×100.

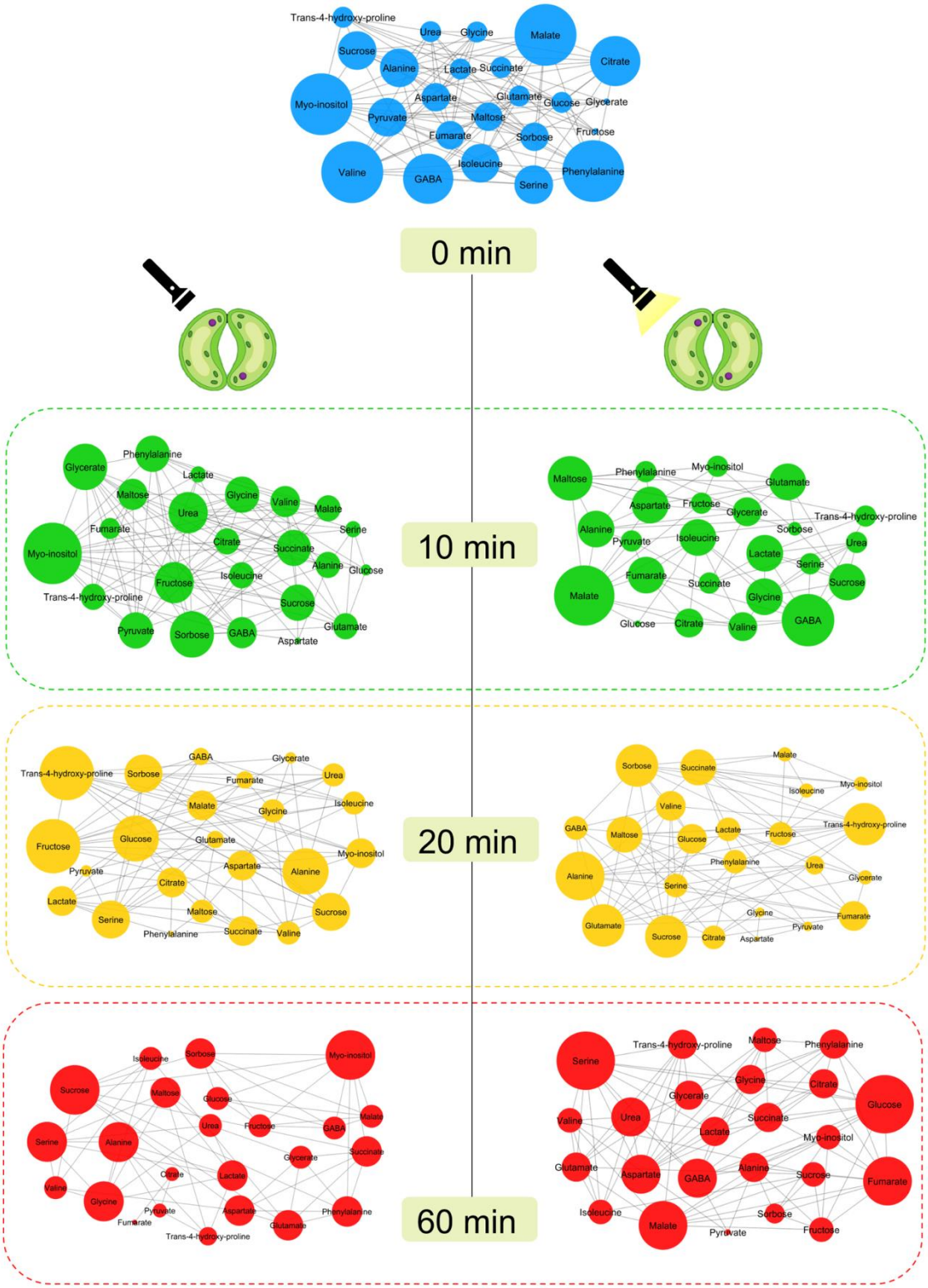

Fig. 3. Correlation-based metabolic networks of guard cells fed with 5 mM of ^{13}C-HCO_3 for 0, 10 min, 20 min and 60 min under dark or light conditions. The networks were created using data from relative metabolite content (n = 4). Nodes are metabolites and links denote debiased sparse partial correlation (-0.5 > r > 0.5) between two metabolites. Bigger nodes indicate higher degree of connection, i.e., have more links. These analyses were performed using CorrelationCalculator® and MetScape on Cytoscape®.

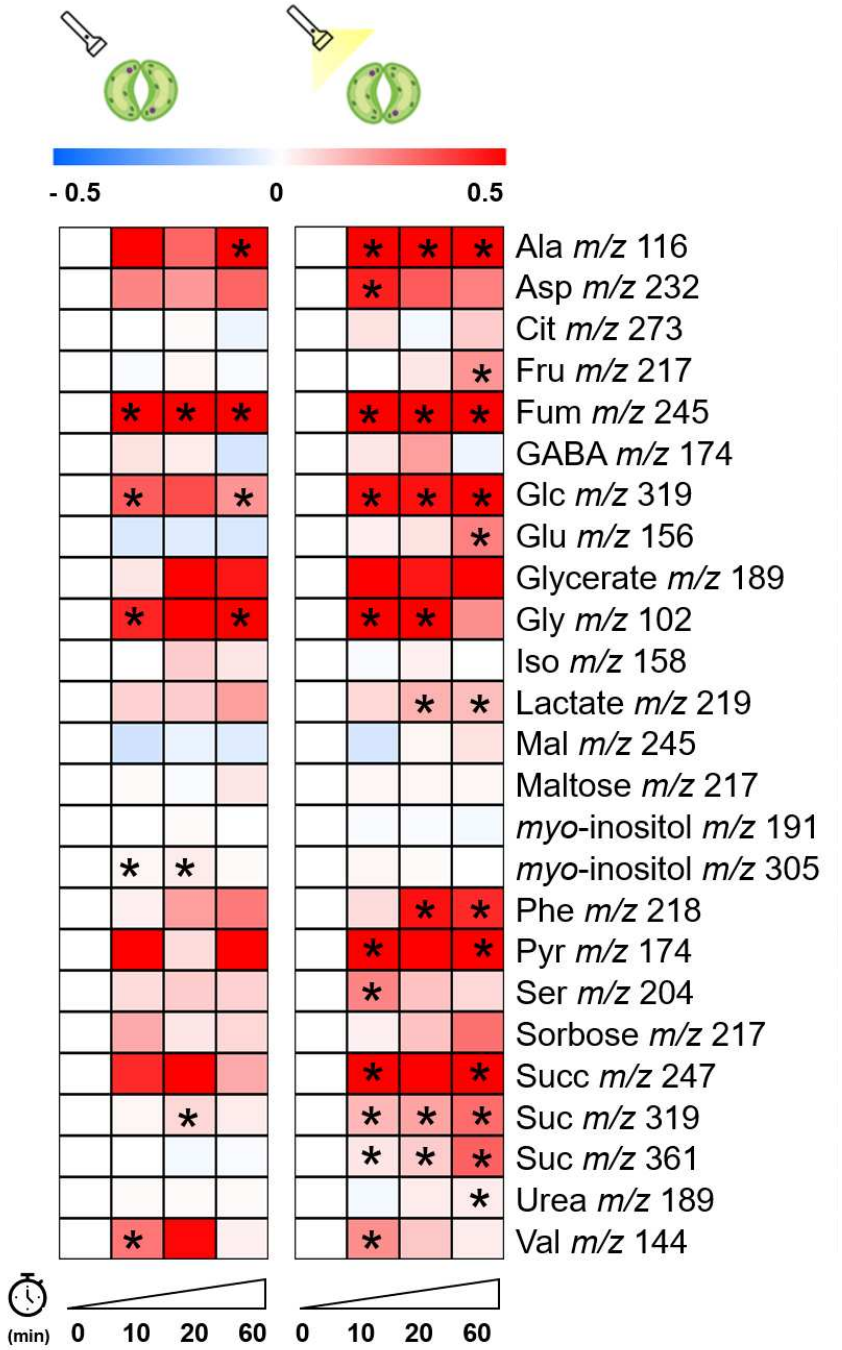

Fig. 4. Heat map representation of the relative ^{13}C-enrichment ($R^{13}C$) in guard cells fed with 5 mM of ^{13}C-HCO_3 for 0, 10, 20 and 60 min under dark or light conditions. The data was normalized by the values found at the time 0 of the experiment and $\log_2$-transformed for heat map representation. Asterisks (*) indicate significant difference from dark (0 min) by Student's *t* test ($P < 0.05$) ($n = 4$). Abbreviations: metabolites: Cit, citrate, Fru, fructose, Fum, fumarate, GABA, gamma-aminobutyric acid, Glc, glucose, Mal, malate, Pyr, pyruvate, Succ, succinate, Suc, sucrose. Amino acids are abbreviated using the standard three-letters code.

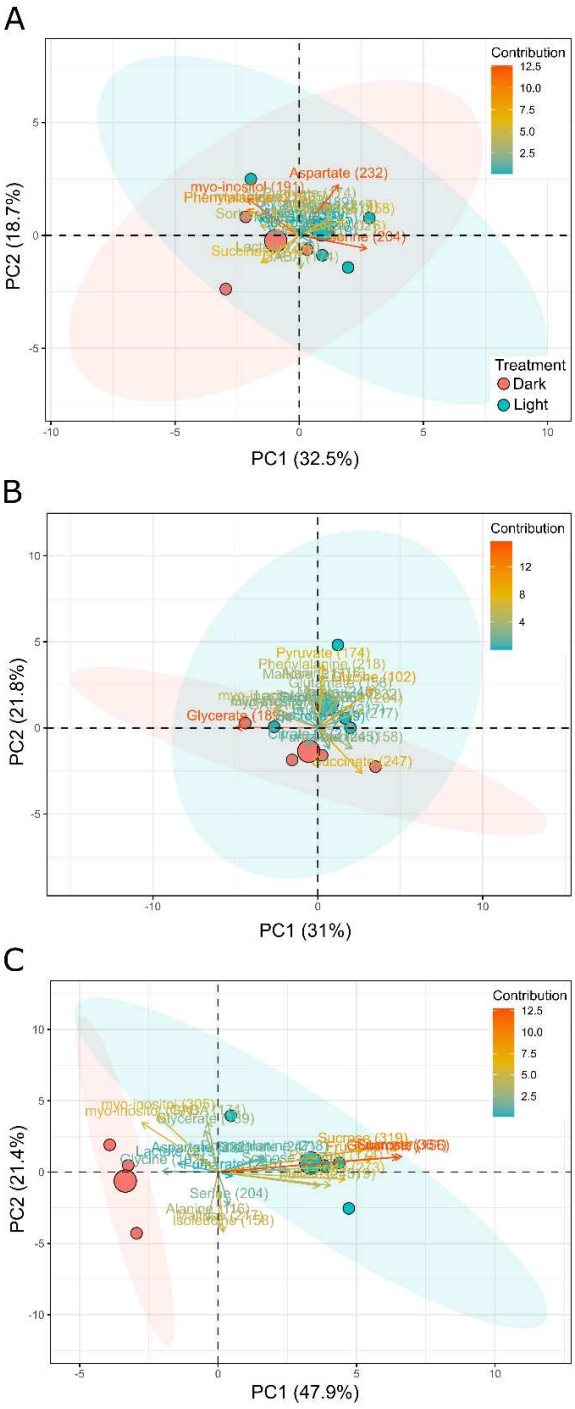

Fig. 5. Biplots of the principal component analysis (PCA) of fractional ^{13}C-enrichment ($F^{13}C$) in primary metabolites identified from guard cells fed with 5 mM of ^{13}C-HCO_3 for 10 min (A), 20 min (B) and 60 min (C) under dark (red circles) or light (blue circles) conditions. The percentage variation explained by the components 1 (PC1) and 2 (PC2) is highlighted between parentheses in each axis. Red and blue ellipses are the confidence interval of PCA of dark and light samples, respectively (n = 4). The contribution of each metabolite for dark and light distinction is highlighted according to the colour scale at the upper right of each figure. The contribution of a variable (metabolite) to a given component (PC1 or PC2) is the $\cos^2\theta$ of the variable divided by the $\cos^2$ of the component ×100.

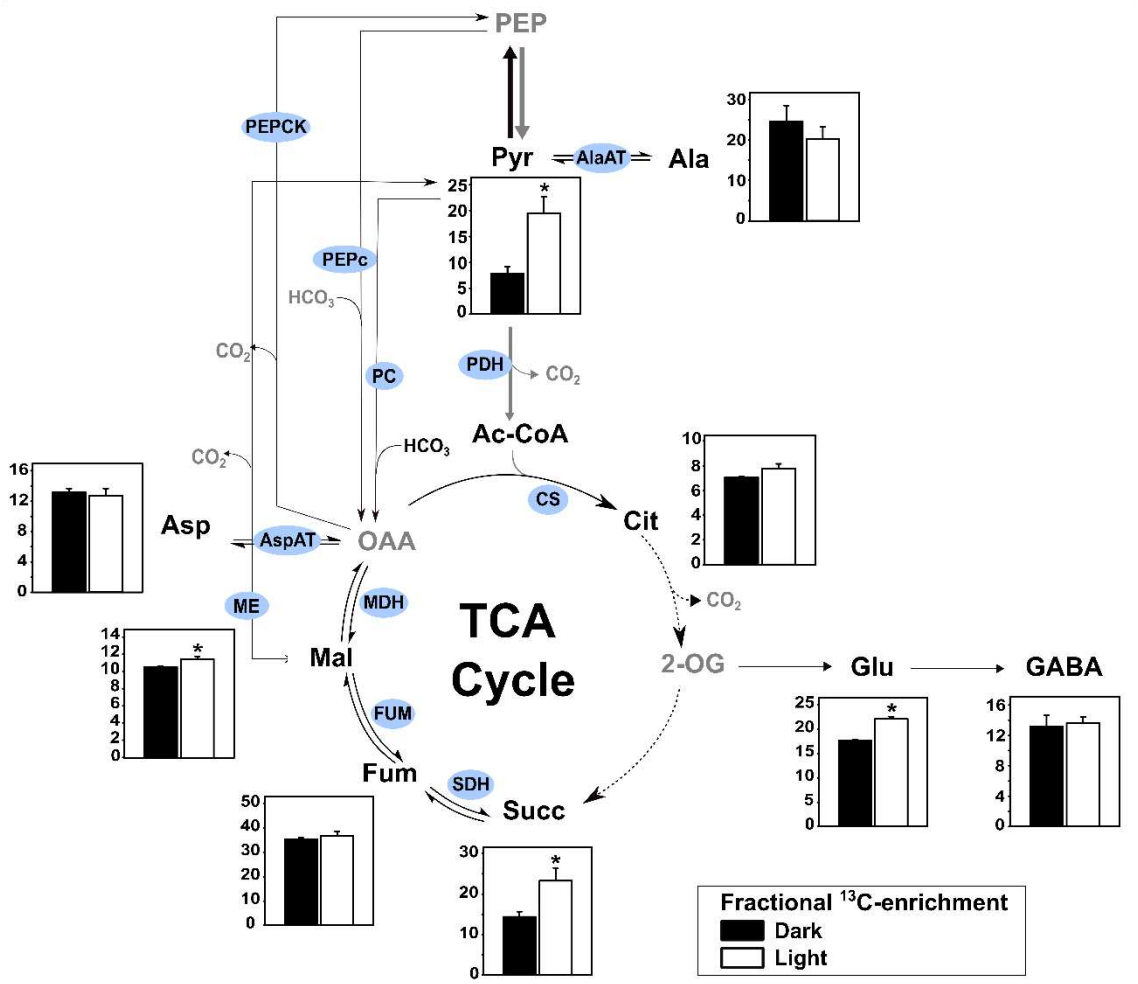

Fig. 6. Schematic representation of the fractional ^{13}C-enrichment ($F^{13}C$) in metabolites of, or associated to, the tricarboxylic acid (TCA) cycle. Bar graphs demonstrate the $F^{13}C$ found after 60 min of 5 mM of ^{13}C-HCO_3 labelling under dark (black bars) or light (white bars) conditions. Asterisks (*) indicate significant difference between dark and light conditions by Student's *t* test ($P < 0.05$) ($n = 4$). Abbreviations: metabolites: Ac-CoA, acetyl-CoA, Cit, citrate, Fum, fumarate, GABA, gamma-aminobutyric acid, Mal, malate, OAA, oxaloacetate, PEP, phospho*enol*pyruvate, Pyr, pyruvate, Succ, succinate, 2-OG, 2-oxoglutarate. Enzymes: AlaAT, alanine aminotransferase, AspAT, aspartate aminotransferase, CS, citrate synthase, FUM, fumarase, ME, malic enzyme, MDH, malate dehydrogenase, PC, pyruvate carboxylase, PDH, pyruvate dehydrogenase, PEPc, phospho*enol*pyruvate carboxylase, PEPCK, phospho*enol*pyruvate carboxykinase, SDH, succinate dehydrogenase. Amino acids are abbreviated using the standard three-letters code.

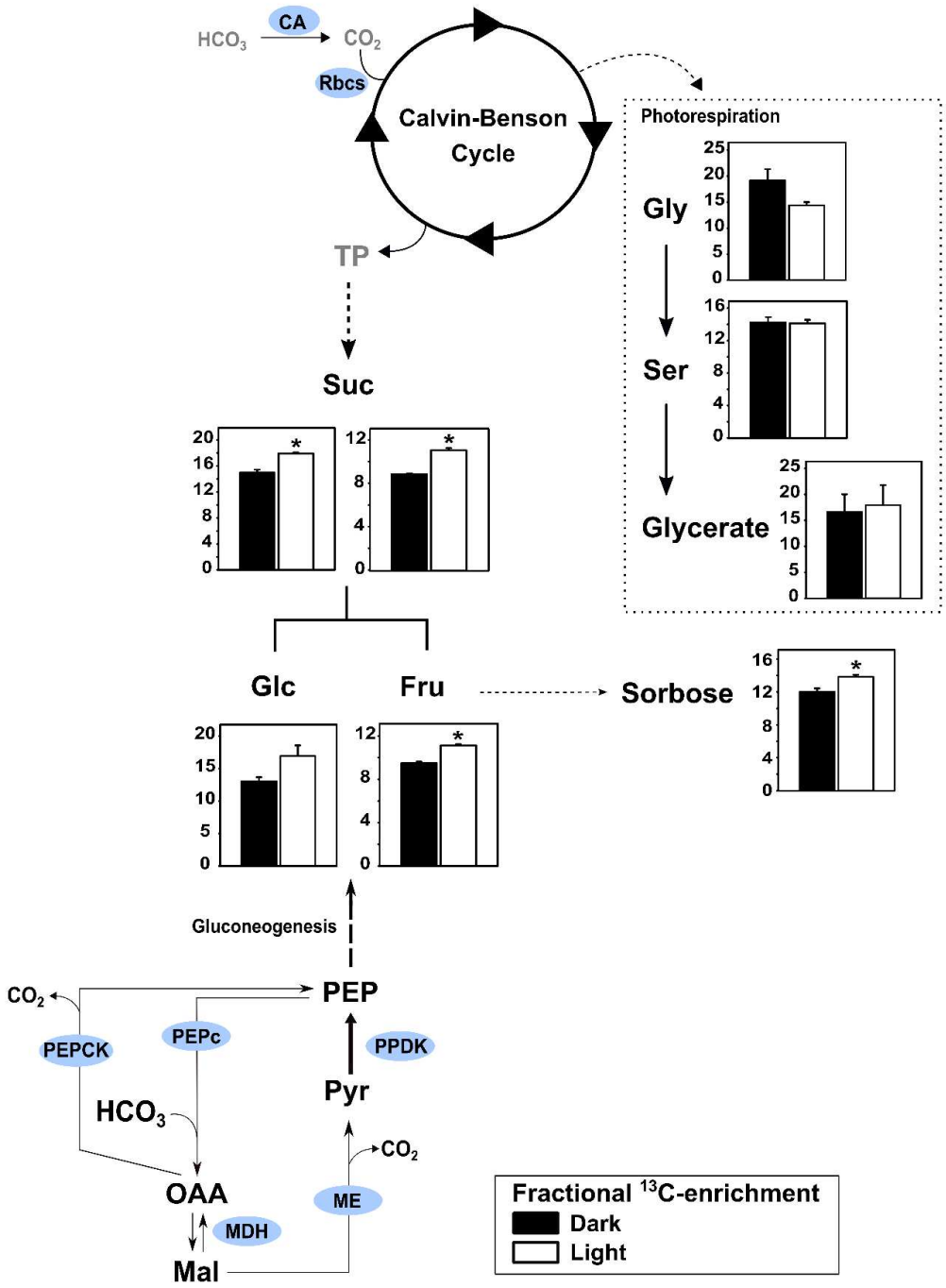

Fig. 7. Schematic representation of the fractional ^{13}C-enrichment ($F^{13}C$) in sugars and photorespiratory metabolites. Bar graphs demonstrate the $F^{13}C$ found after 60 min of ^{13}C-HCO_3 labelling under dark (black bars) or light (white bars) conditions. Asterisks (*) indicate significant difference between dark and light conditions by Student's *t* test ($P < 0.05$) ($n = 4$). Abbreviations: metabolites: Fru, fructose, Glc, glucose, Mal, malate, OAA, oxaloacetate, PEP, phospho*enol*pyruvate, Pyr, pyruvate, Suc, sucrose, TP, triose-phosphates. Enzymes: CA, carbonic anhydrase, ME, malic enzyme, MDH, malate dehydrogenase, PEPc, phospho*enol*pyruvate carboxylase, PEPCK, phospho*enol*pyruvate carboxykinase, PPDK, pyruvate phosphate dikinase, Rbcs, ribulose-1,5-biphosphate carboxylase/oxygenase. Amino acids are abbreviated using the standard three-letters code.

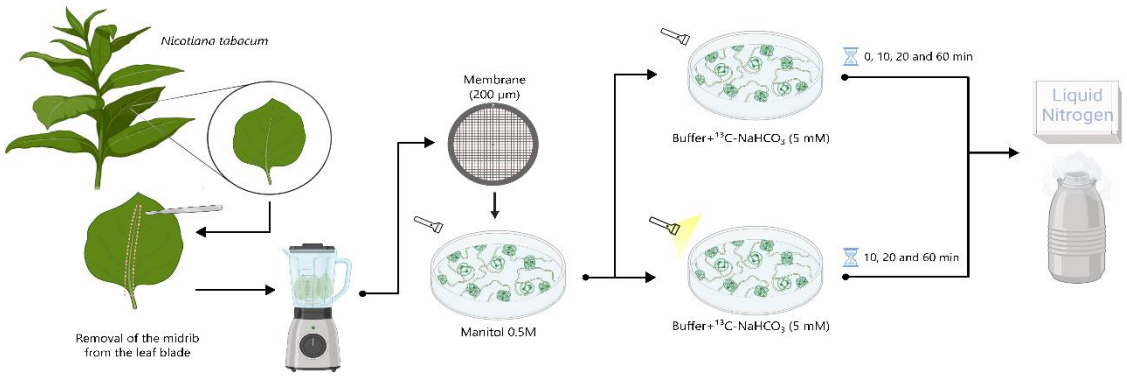

Supplementary Figure S1. Experimental procedure for ^{13}C-HCO_3 isotope labelling with guard cell-enriched epidermal fragments (referred as guard cells) isolated from tobacco plants. The guard cell isolation was performed using approximately three fully expanded non-midrib leaves per replicate, which were blended in a Waring blender. The resulting solution was filtered in a 200 mm nylon membrane and stored in 0.5 M mannitol in order to collect enough material for further metabolomic analysis. After isolation, guard cells were transferred to light or dark conditions and incubated in a buffer containing 50 µM $CaCl_2$ and 5 mM MES-Tris, pH 6.15 in the presence of 5 mM ^{13}C-HCO_3. Guard cell samples were harvested and snap-frozen in liquid nitrogen after 0, 10, 20 and 60 minutes under continuous dark or during the dark-to-light transition.

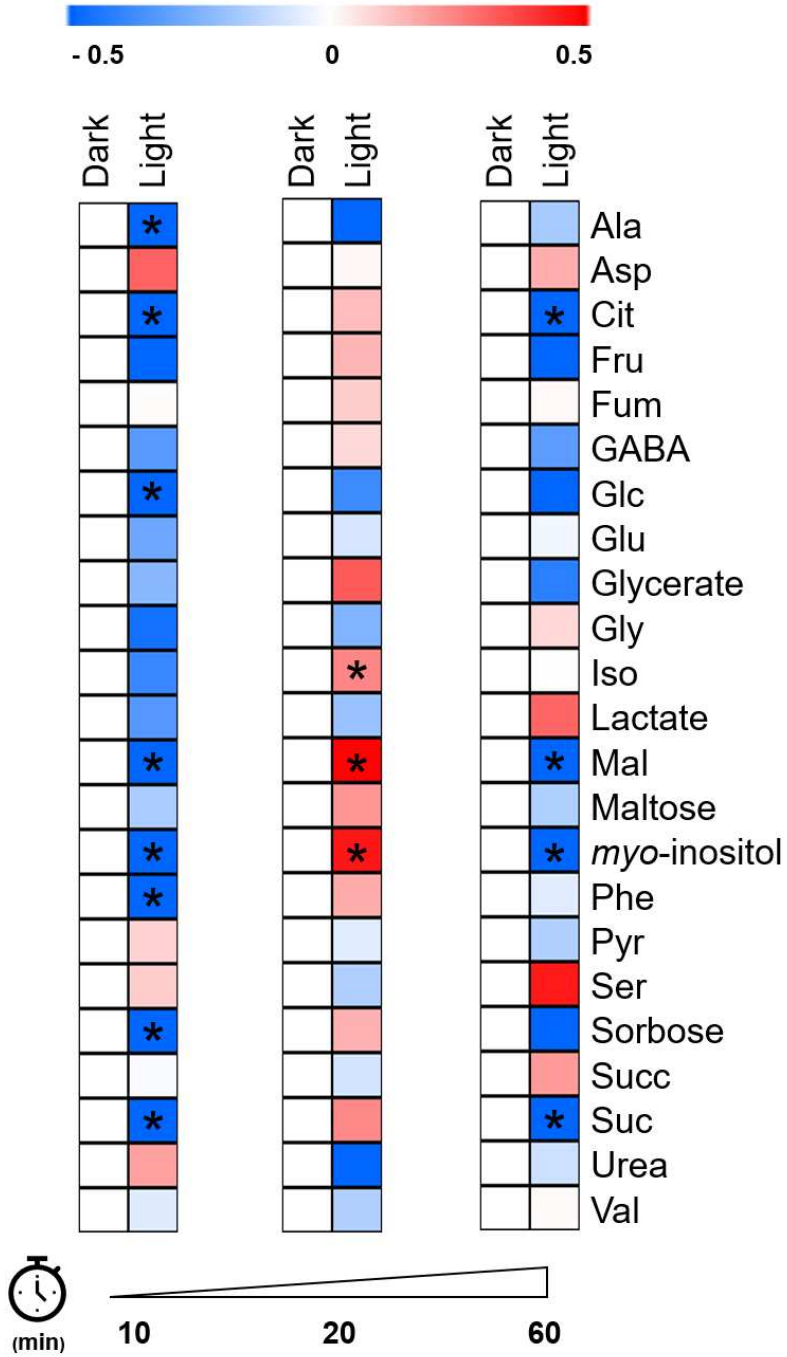

Supplementary Figure S2. Heat map representation of the metabolite content in guard cells fed with ^{13}C-HCO_3 for 10, 20 or 60 min under dark or light conditions. Metabolite content refers to the level of metabolites normalized by ribitol and the fresh weight used during extraction. The data was further normalized by the values found under dark conditions at each time point of the experiment and Log2 transformed for heat map representation. Asterisks (*) indicate significant difference between dark and light treatments in each time point by Student's *t* test ($P < 0.05$) ($n = 4$). The abbreviation used in this figure correspond to: metabolites: Cit, citrate, Fru, fructose, Fum, fumarate, GABA, gamma-aminobutyric acid, Glc, glucose, Mal, malate, Pyr, pyruvate, Succ, succinate, Suc, sucrose. Amino acids are abbreviated using the standard three-letters code.

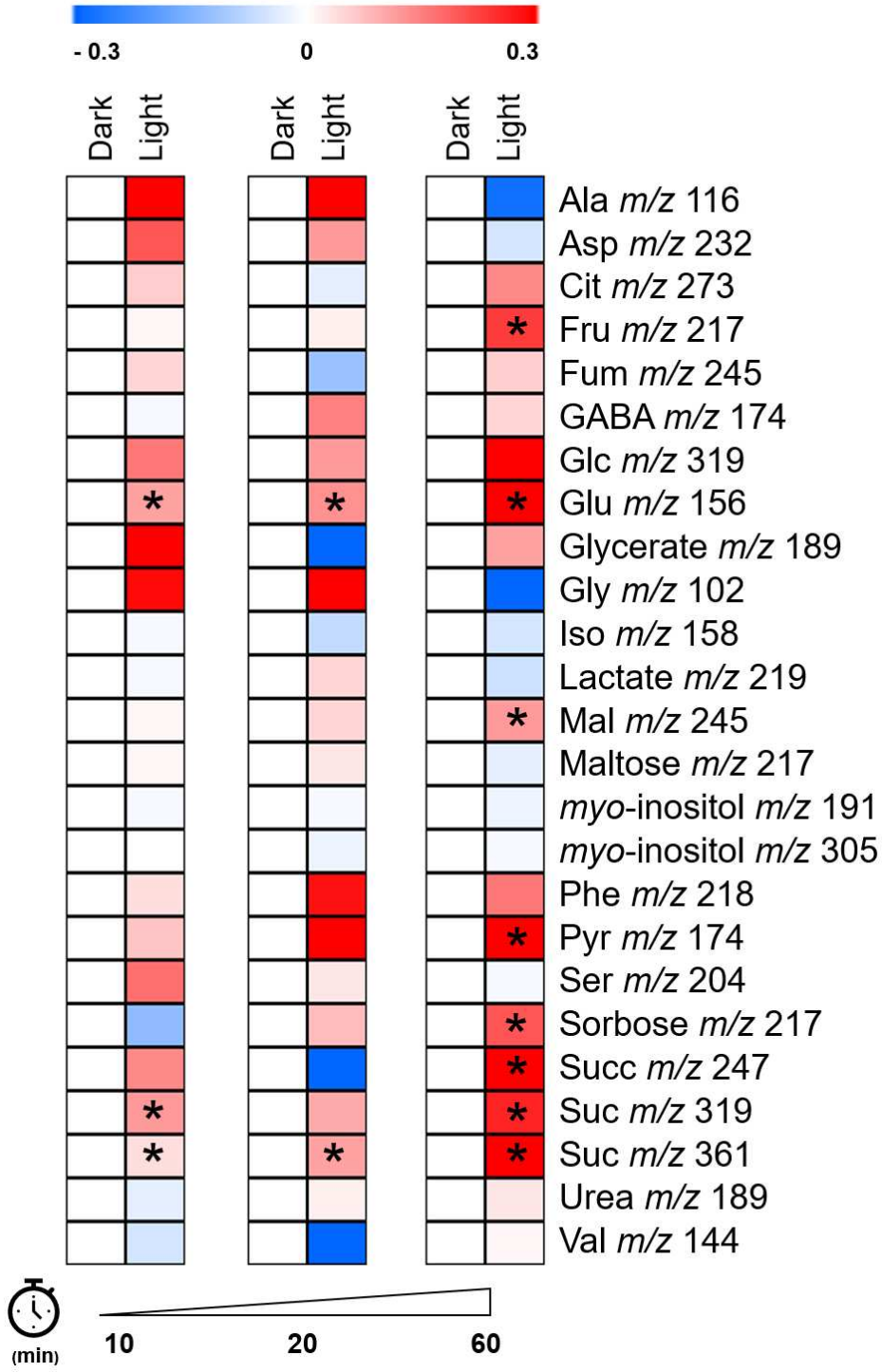

Supplementary Figure S3. Heat map representation of the relative ^{13}C-enrichment ($R^{13}C$) in guard cells fed with ^{13}C-HCO_3 for 10, 20 or 60 min under dark or light conditions. The data was normalized by the values found under dark conditions at each time point of the experiment and Log2 transformed for heat map representation. Asterisks (*) indicate significant difference between dark and light treatments in each time point by Student's *t* test ($P < 0.05$) ($n = 4$). Abbreviations: metabolites: Cit, citrate, Fru, fructose, Fum, fumarate, GABA, gamma-aminobutyric acid, Glc, glucose, Mal, malate, Pyr, pyruvate, Succ, succinate, Suc, sucrose. Amino acids are abbreviated using the standard three-letters code.

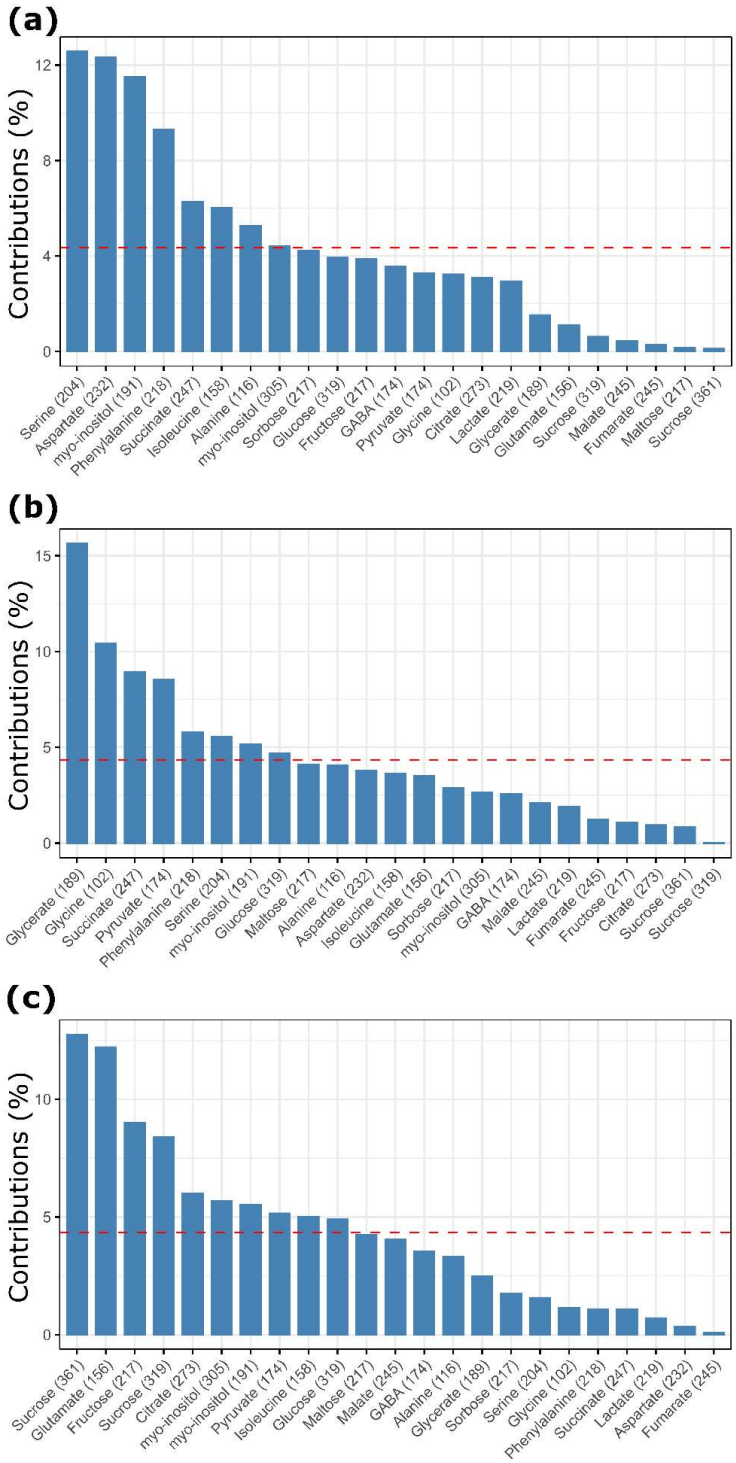

Supplementary Figure S4. Relative contribution (%) of the variables (metabolites) for the distinction observed in the fractional ^{13}C-enrichment ($F^{13}C$) observed in primary metabolites from guard cells fed with 5 mM of ^{13}C-HCO_3 for 10 min (A), 20 min (B) and 60 min (C) under dark or light conditions. The contribution of a variable to a given component (PC1 or PC2) is the $\cos^2\theta$ of the variable divided by the $\cos^2$ of the component ×100. The red line points for the average contribution. Numbers between brackets refer to the mass-to-charge ratio of the fragment analysed in the respective metabolite. This data is related to the principal component analysis of the Fig. 5 (n = 4)**.**

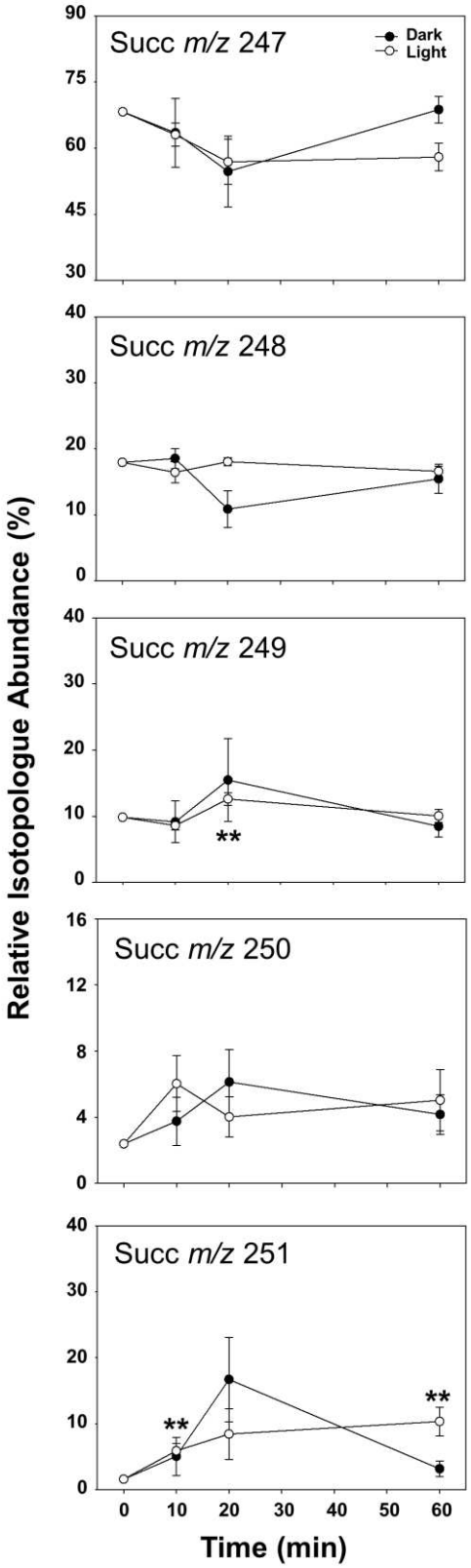

Supplementary Figure S5. Relative isotopologue abundance (RIA) of the fragment *m/z* 247 of Succ, succinate. One (*) and two (**) asterisks indicate significant difference of dark and light treatments from the time 0 of the experiment by Student's *t* test ($P < 0.05$), respectively ($n = 4$).

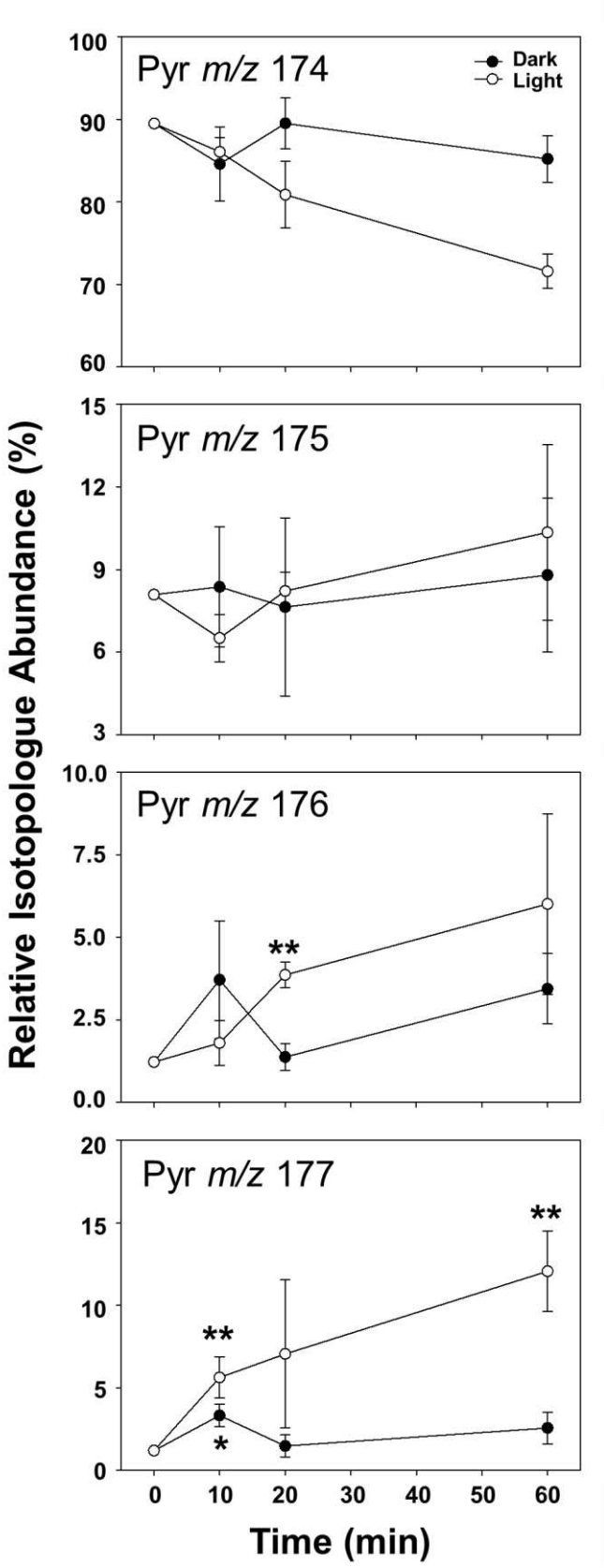

Supplementary Figure S6. Relative isotopologue abundance (RIA) of the fragment *m/z* 174 of Pyr, pyruvate. One (*) and two (**) asterisks indicate significant difference of dark and light treatments from the time 0 of the experiment by Student's *t* test ($P < 0.05$), respectively ($n = 4$).

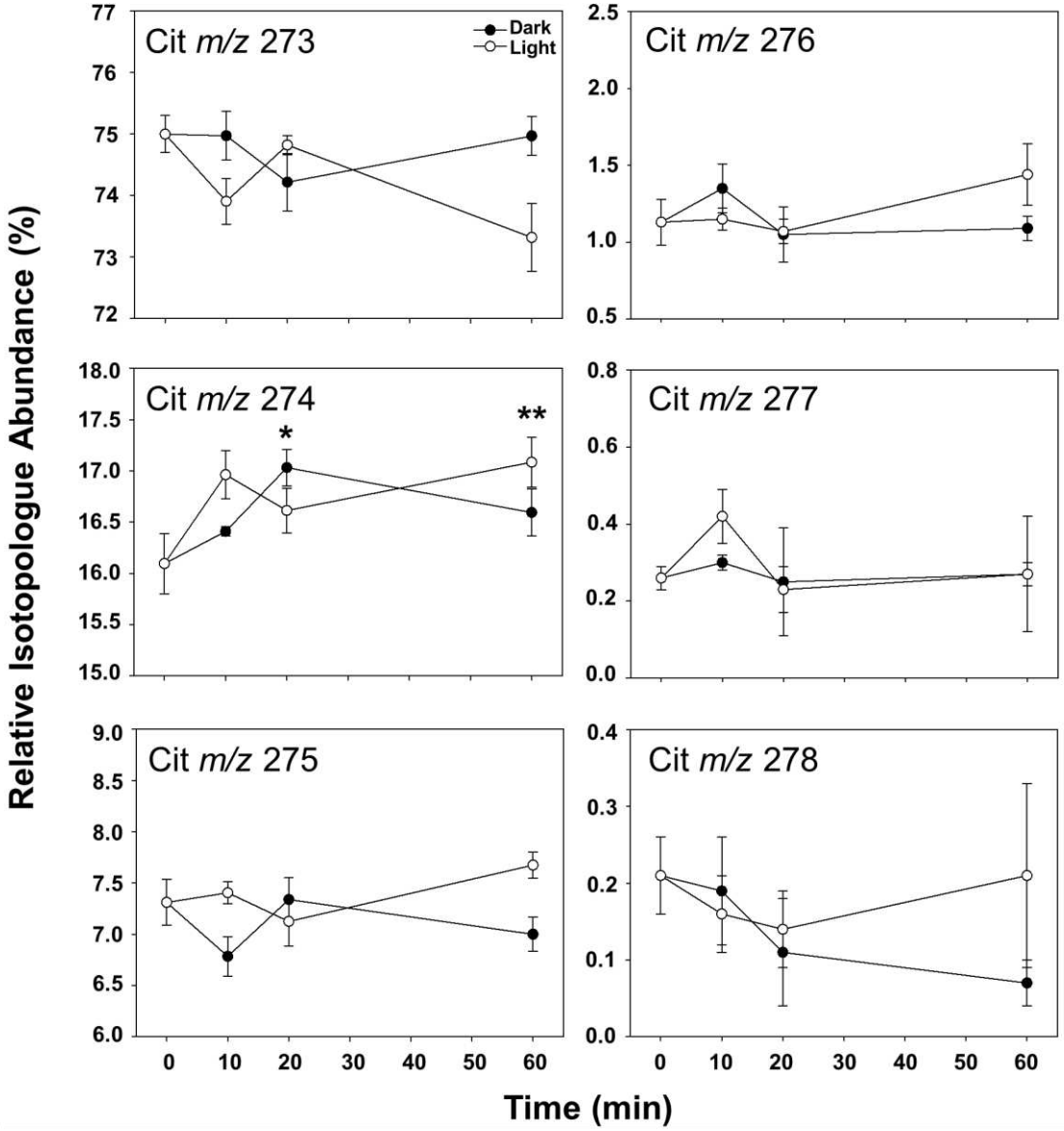

Supplementary Figure S7. Relative isotopologue abundance (RIA) of the fragment *m/z* 273 of Cit, citrate. One (*) and two (**) asterisks indicate significant difference of dark and light treatments from the time 0 of the experiment by Student's *t* test ($P < 0.05$), respectively ($n = 4$).

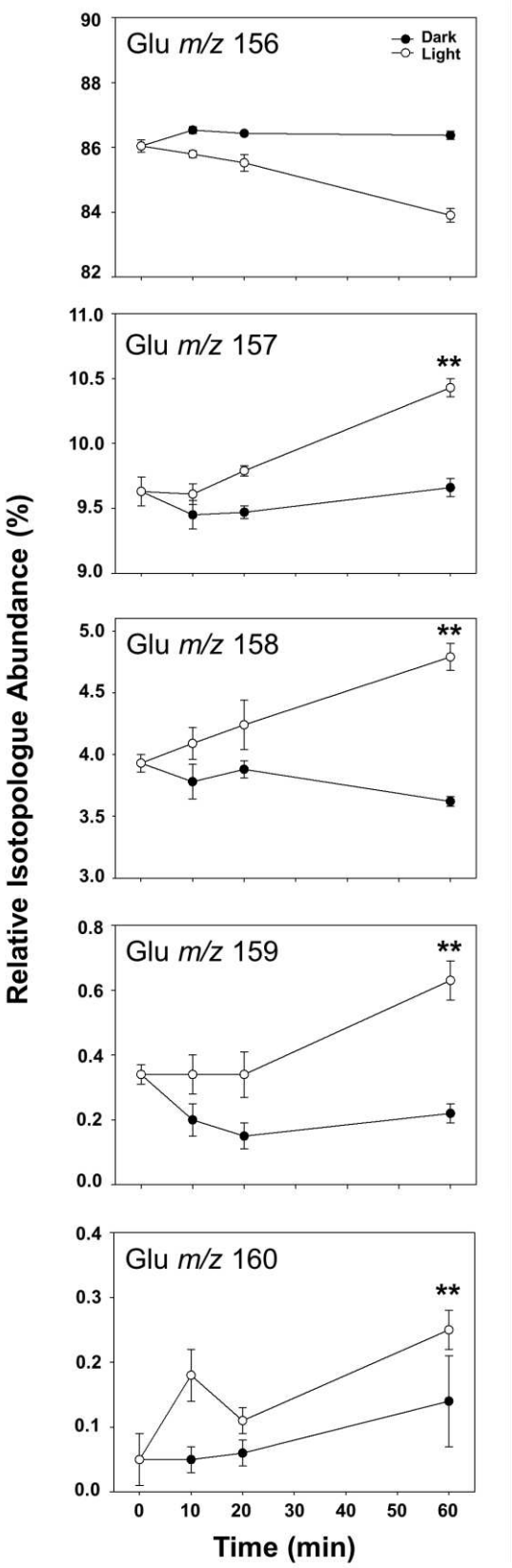

Supplementary Figure S8. Relative isotopologue abundance (RIA) of the fragment *m/z* 156 of Glu, glutamate. One (*) and two (**) asterisks indicate significant difference of dark and light treatments from the time 0 of the experiment by Student's *t* test ($P < 0.05$), respectively ($n = 4$).

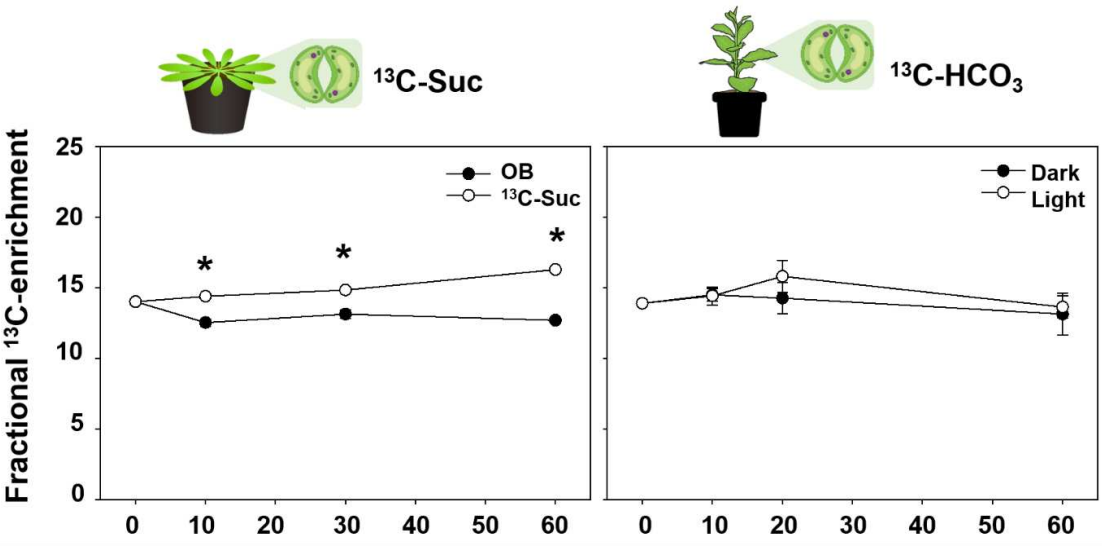

Supplementary Figure S9. Fractional ^{13}C-enrichment (F^{13}C) in GABA from guard cells fed with ^{13}C-sucrose for 0, 10, 20 and 60 min in the light (left) or with ^{13}C-HCO_3 for 0, 10, 20 and 60 min under dark or light conditions (right). Asterisks (*) indicate significant difference from dark (0 min) by Student's *t* test ($P < 0.05$) ($n = 4$).

Supplementary Table S1. Parameters derived from correlation-based metabolic network analysis. The network was built as described in the Figure 3. Hub-like nodes indicate nodes with degree of connection higher than 8, which is the average of connection found at the time 0 of the experiment. Preferential attachment corresponds the number of nodes that were considered as hub at the time 0 and maintain its degree of connection or become more connected after the beginning of the treatments (Freire *et al.*, 2021). Hub-like nodes and the preferential attachment were calculated as described previously (Freire *et al.*, 2021). The other parameters were obtained by Network Analysis in Cytoscape (Assenov *et al.*, 2008) (n = 4).

		Dark			Light		
	0 min	10 min	20 min	60 min	10 min	20 min	60 min
Number of hub-like nodes	11	13	7	0	2	7	7
Number of new hub-like nodes	-	7	4	0	0	5	4
Preferential attachment	-	6	3	0	2	2	3
Custering coefficient	0.604	0.627	0.651	0.642	0.571	0.642	0.577
Network centralization	0.126	0.289	0.158	0.123	0.182	0.182	0.142
Network density	0.362	0.388	0.333	0.236	0.268	0.312	0.348
Network heterogeneity	0.207	0.267	0.234	0.287	0.251	0.303	0.204

CHAPTER IV

The fern *Nephrolepis exaltata* is largely unresponsive to climate change conditions at physiological and metabolic levels

8 CHAPTER IV – THE FERN *NEPHROLEPIS EXALTATA* IS LARGELY UNRESPONSIVE TO CLIMATE CHANGE CONDITIONS AT PHYSIOLOGICAL AND METABOLIC LEVELS

Valéria F. Lima[1,2,#], Jorge Gago[2,#,*], Iker Aranjuelo[3], Yariv Brotman[4], Asdrúbal Burgos[5], Marc Carriquí[2,6], Alisdair R. Fernie[7], Carlos María Figueroa[8], Juan José Irigoyen[9], Iván Jáuregui[3], Mónica Oyarzun[9], Inmaculada Pascual[9], Miquel Ribas-Carbo[2], Manuel Sánchez-Díaz[9], Héctor Santesteban[9], Julia Smirnova[7,10], Amadeo Urdiain[9], Danilo Daloso[1,¥], Fermín Morales[3,¥], Jaume Flexas[2,¥]

[1]LabPlant, Departamento de Bioquímica e Biologia Molecular, Universidade Federal do Ceará, 60451-970, Fortaleza, Ceará, Brasil.
[2]Research Group on Plant Biology Under Mediterranean Conditions; Universitat de les Illes Balears – Agro-Environmental and Water Economics Institute (UIB-INAGEA). Carretera de Valldemossa Km 7.5; 07122 Palma, Illes Balears, Spain.
[3]Instituto de Agrobiotecnología (IdAB), CSIC-Gobierno de Navarra, Avda. de Pamplona 123, 31192 Mutilva, Navarra, Spain.
[4]Department of Life Sciences, Ben-Gurion University of the Negev, 8410501 Beer-Sheva, Israel.
[5]Laboratorio de Biotecnología, CUCBA, Universidad de Guadalajara, Guadalajara, Mexico
[6]Instituto de Ciencias Forestales (ICIFOR-INIA), CSIC, Carretera de La Coruña km. 7.5.; 28040 Madrid, Madrid, Spain
[7]Max Planck Institute of Molecular Plant Physiology, Am Mühlenberg 1, 14476 Potsdam-Golm, Germany
[8]Instituto de Agrobiotecnología del Litoral, UNL, CONICET, FBCB, 3000 Santa Fe, Argentina.
[9]Instituto BIOMA-Universidad de Navarra, Plant Stress Physiology Group (associated Unit to CSIC, EEAD, Zaragoza). Irunlarrea 1, 31008, Pamplona, Navarra, Spain.
[10]Present address: Structural Biology, Max Delbrück Center for Molecular Medicine in the Helmholtz Association (MDC), 13125 Berlin, Germany.
[#]These two authors contributed equally to the present work
[¥]These three authors contributed equally to the present work
*Corresponding author.

Running title: The fern *Nephrolepis exaltata* does not care about climate change

Submitted to *Journal of Experimental Botany*.

Abstract

Climate change is impacting the performance of plants worldwide. However, the impact on ferns, a relevant phylogenetic group among land plants, has received little attention. Here, we investigated the effects of drought, high temperature (HT) and high CO_2 concentration (HC) on a fern (*Nephrolepis exaltata*) and a typical angiosperm (*Brassica oleracea*) at photosynthetic, anatomical and metabolic levels. Leaf anatomical parameters were slightly affected by stress conditions in both species. *B. oleracea* physiological responses to HC differed substantially, independently of HT and/or drought. In contrast, the fern was mostly unresponsive to all stress conditions at the physiological level. Lipids and primary metabolites levels differed in response to stress factors in *B. oleracea*. Notably, the combination of all stresses exacerbated changes in primary metabolites, resulting in reduced amino and organic acids levels. Interestingly, phosphatidylcholine and phosphatidylethanolamine levels showed varied responses, increasing under HT and decreasing under HC or the combination of drought, HT and HC in *B. oleracea*. These metabolic responses were not observed in the fern. Beyond providing important information concerning the trade-off between carbon uptake and stress tolerance mechanisms, our study indicates minor fern responses to drought, HT and HC, suggesting differential impacts of climate change on ferns and angiosperms.

Keywords: Angiosperms, climate change, ferns, metabolomics, photosynthesis, stress tolerance.

Introduction

Ferns are an ancient lineage of vascular plants, first appearing in the Palaeozoic, during the Devonian > 400 million years ago (Mya) (Pryer *et al*., 2004). Subsequently, they colonized all of Earth's landscapes before the emergence of seed plants, and the appearance of angiosperms in the Mesozoic, during the Late Cretaceous period, about 100-65 Mya (Haworth *et al*., 2011; Flexas and Keeley, 2012). Although ferns are currently represented by over 10,000 species distributed worldwide (Kenrick and Crane, 1997; Smith *et al*., 2006; Schuettpelz and Pryer, 2009), angiosperms are the dominant plant group in terrestrial habitats, accounting for nearly 90% of extant vascular plant species (Schuettpelz and Pryer, 2009; Condamine *et al*., 2020). Ferns and angiosperms originated under different atmospheric conditions and selective pressures (Brodribb *et al*., 2009; Haworth *et al*., 2011; Flexas and Keeley, 2012; Franks *et al*., 2014). This might have resulted in different regulatory mechanisms for acclimation and adaptation to different environmental constraints, some of which have not been elucidated yet. Thus, ferns represent an important genetic resource to improve our understanding of the evolution of plants to cope with adverse conditions, especially considering the current climate change scenario, in which drought periods associated with high temperatures are expected to be frequently observed in an atmosphere with a continuously increasing CO_2 concentration.

Ferns generally have a lower photosynthetic rate (A_N), reduced stomatal (g_s) and mesophyll (g_m) conductances to CO_2, and slower stomatal responses to different environmental and endogenous signals than angiosperms (McAdam and Brodribb, 2012; Franks and Britton-Harper, 2016; Tosens *et al*., 2016; Haworth *et al*., 2018; Gago *et al*., 2019; Lima *et al*., 2019; Cândido-Sobrinho *et al*., 2022). Several studies have reported that the photosynthetic capacity of ferns is typically lower than 10 μmol CO_2 m^{-2} s^{-1}, whereas values for angiosperms usually vary between 10 and 50 μmol CO_2 m^{-2} s^{-1} (Carriquí *et al*., 2015; Tosens *et al*., 2016; Xiong *et al*., 2018; Gago *et al*., 2019). Although research investigating the mechanisms that coordinate gas exchange across land plants is increasing, the anatomical, physiological and biochemical bases that explain this discrepancy in A_N between ferns and angiosperms are not totally resolved. The kinetic constants of Rubisco (ribulose 1,5-bisphosphate carboxylase/oxygenase) and the patterns of carbon/nitrogen allocation in the photosynthetic apparatus between ferns and angiosperms are similar (Yeoh *et al*., 1981; Bird *et al*., 1982; Jordan and Ogren, 1983; Karst and Lechowicz, 2007; Gago *et al*., 2013); therefore, they are not expected to explain the differences in A_N between these plant groups. In contrast, it is known that photosynthesis is largely constrained by biochemical limitations and by both g_s and g_m in most angiosperms

(Gago *et al*., 2019), whereas CO_2 diffusion resistance is the major constrainer of the photosynthetic capacity of ferns (Carriquí *et al*., 2015; Xiong *et al*., 2018).

The low values of g_s would be expected based on the characteristics of fern stomata, which are larger but fewer in number, and have low sensitivity to changes in cell turgor and in response to different environmental cues, when compared with angiosperms (Franks and Farquhar, 2007; Franks and Beerling, 2009; Jordan *et al*., 2015). The low g_m values in ferns have been related to thicker cell walls and lower chloroplast surface areas exposed to intercellular airspaces, two important cell anatomical features driving A_N and g_m (Flexas and Keeley, 2012; Carriquí *et al*., 2015; Tosens *et al*., 2016; Veromann-Jurgenson *et al*., 2017; Xiong *et al*., 2018; Yiotis and McElwain, 2019; Evans *et al*., 2009; Hassiotou *et al*., 2009; Scafaro *et al*., 2011; Peguero-Pina *et al*., 2012; Tosens *et al*., 2012; Tomás *et al*., 2013). Despite these advances, the biochemical changes and their physiological consequences in terms of diffusional conductance regulation in ferns are still unclear. Interestingly, a multi-species meta-analysis revealed a positive relationship between A_N and leaf sugars in angiosperms (Gago *et al*., 2016), which strongly agrees with reported data showing that angiosperms have higher levels of sugars as well as higher A_N than ferns (Lima *et al*., 2019). These results suggest that metabolism-mediated mechanisms could be the elusive link that tightly coordinates the A_N-g_s trade-off in angiosperms (Cândido-Sobrinho *et al*., 2022), which would allow this plant group to have not only higher g_s and g_m than ferns, and consequently higher A_N, but also faster stomatal closure responses to drought and high CO_2, contributing to explain the success of this plant group in land plant colonization.

Several other pieces of evidence suggest that the metabolism of leaves and guard cells is important to explain the differences in A_N and g_s between ferns and angiosperms. It is known that the content of flavonols, a class of secondary metabolites that remove the excess of reactive oxygen species (ROS), is negatively associated with the speed of stomatal closure (Watkins *et al*., 2014; Watkins *et al*., 2017). This idea is based on the fact that increased flavonol content leads to a lower level of ROS in guard cells, which are well-established signalling molecules that induce stomatal closure in response to abscisic acid (ABA), ethylene and other signals (Mittler *et al*., 2011). Interestingly, ferns have lower levels of ROS in their guard cells (Watkins *et al*., 2014) and a higher investment of the daily CO_2 assimilated toward secondary rather than primary metabolism (Lima *et al*., 2019). On the other hand, leaf sucrose content was positively correlated with a faster high CO_2-induced stomatal closure in angiosperms, consistently with their higher A_N and thus higher capacity to produce sugars under high CO_2, as compared to

ferns (Lima *et al*., 2019). These results strongly agree with the fact that ferns have greater tolerance to different abiotic stress conditions when compared to angiosperms (Proctor and Tuba, 2002; Salachna and Piechocki, 2021). Furthermore, given that fern stomata have no ABA-responsiveness and a reduced capacity to respond to mesophyll-derived sucrose (Cândido-Sobrinho *et al*., 2022), the differential carbon allocation between primary and secondary metabolism could be a mechanism to improve stress tolerance in ferns, at the expense of lower gas-exchange rates, slower stomatal responses and consequently, reduced growth.

Although the discrepancies between ferns and angiosperms in A_N, hydraulic characteristics and stomatal responses to drought, light/dark and high CO_2 concentration have been investigated recently (Auler *et al*., 2022; Lobo *et al*., 2022), no studies have simultaneously compared fern and angiosperm species growing under multiple stress conditions. Furthermore, evidence indicates that the metabolic responses to drought combined with high temperature differ substantially from these types of stress acting separately (Vital *et al*., 2022). Thus, it is reasonable to assume that to fully understand the mechanisms that aid plants to acclimate to the current and foreseen climate change we need to perform experiments simulating the major stressful conditions of this scenario, such as the combination of drought, high CO_2 and elevated temperatures. Information from such studies assumes a paramount importance to improve our understanding not only on how crops will adapt to the climate changes, but especially on how ferns will respond to these conditions. In fact, to the best of our knowledge, very few studies have analysed the performance of any fern species growing under high CO_2 concentrations, and none of them has studied the combination of high CO_2 with other foreseen climate change factors (Caporn *et al*., 1999; Yiotis *et al*., 2017). Based on current knowledge about their respective photosynthetic and diffusional properties, Flexas *et al*. (2014) modelled that photosynthesis of ferns is expected to increase more than that of angiosperms under high CO_2 conditions, but there have been few previous attempts to demonstrate this empirically (Yiotis *et al*., 2017). Here, we compared the photosynthetic, anatomic and metabolic responses among a fern (*Nephrolepis exaltata* - Nephrolepis) and an angiosperm (*Brassica oleracea L.* - cauliflower), used as reference, under one of the most claimed scenarios of the climatic change: drought and increased temperature and CO_2.

Material and methods

Plant material and growth conditions

We used two species from different plant groups, a fern (*Nephrolepis exaltata* - Nephrolepis), and an angiosperm (*Brassica oleracea L.* - cauliflower). Cauliflower plantlets (2-3 expanded leaves) and ferns were cultivated in 8 L plastic pots filled with peat:perlite (2:1 v/v). Plants were placed in research-oriented facilities, the Temperature Gradient Greenhouses (TGG) (Morales *et al*., 2014), installed at the University of Navarra (42°48'9.3" N, 1°40'6.9" W) in Pamplona (Navarra, Spain). They were established with a modular design with three temperature modules, which constitutes a temperature gradient ranging from near-ambient temperature in module 1 to ambient temperature +4°C in module 3. CO_2 can be flushed into the TGG to increase the air CO_2 concentration as desired (see details in Morales *et al*., 2014). Both species were subjected to different conditions: a non-stressful environment (well-watered plants with ambient CO_2 concentration of approximately 400 ppm ($_ACO_2$) and ambient temperature (temperature diurnal cycle) (AT)) or to different stress conditions, including drought (D), high temperature (HT) (ambient temperature +4°C), high CO_2 concentration ($_HCO_2$) (700 ppm of CO_2) and the combination between them. All plants were watered every day both with water and Hoagland's nutrient solution, with exception of plants under drought. Drought was imposed in the short term (20 days) by withholding irrigation until the substrate reached a water content corresponding to the 60% of field capacity, then it was maintained at this level until de end of the experiment. After 20 days, fern and cauliflower plants were able to develop new leaves, which were used for the analysis described below. Fully expanded leaves were used for the different analytical techniques performed, except when indicated.

Gas exchange analysis

Gas exchange analysis was carried out in four to six fully expanded leaves using portable infrared gas analysers (Li6400-XT, Li-Cor Inc., Lincon, Nebraska, USA; and GFS-3000, Walz, Effeltrich, Germany) with an integrated fluorescence chamber. All measurements were performed at block temperature (25°C), air vapor pressure deficit (VPD) varying between 1 and 2 kPa, atmospheric CO_2 conditions (400 ppm - 700 ppm) and light-saturating photosynthetic active radiation (PAR) of 1500 μmol photon m^{-2} s^{-1}. After stabilization of net CO_2 assimilation (A_N) and steady-state fluorescence (F_S), an intense light flash (8000 μmol m^{-2} s^{-1}) was used to determine the maximum fluorescence (F_m') and the real quantum efficiency of photosystem II (ΦPSII) following the procedures of Genty *et al*. (1989), in which ΦPSII = (F_m'-F_s)/F_m'. The electron transport rate (ETR) was estimated as ETR = PAR*ΦPSII*α*β, in which PAR is the quantum flux density of photosynthetically active radiation (PAR), α the leaf absorbance and β

the electrons partitioning between photosystems I and II. The α*β parameter was estimated following Valentini *et al*. (1995), from the relationship between ϕPSII and ϕCO_2 under non-photorespiratory conditions through low O_2-light curves, in which α*β = 4/*b*, where *b* is the slope of the ϕPSII~ϕCO_2 relationship. Day respiration (R_{day}) was estimated as half the dark-adapted mitochondrial respiration (R_d) after placing plants 30 min under dark conditions (Niinemets *et al*., 2005). Then, the maximum potential PSII efficiency (F_vF_m) was simultaneously determined by chlorophyll fluorescence (Genty *et al*., 1989). The CO_2 response curves (A_N-C_i) were performed at varying atmospheric CO_2 concentrations in a cuvette to further estimate the maximum velocity of Rubisco carboxylation (V_{cmax}) and maximum electron transport rate (J_{max}), according to the models of Farquhar *et al*. (1980) and Sharkey *et al*. (2007). For all measurements, the chloroplastic CO_2 concentration (C_c) and the mesophyll conductance to CO_2 (g_m) were estimated from leaf chlorophyll fluorescence following Harley *et al*. (1992). The ratio between electron transport rate and assimilation ratio (ETR / A_N) was used to check for both proper well-functioning of the equipment and optimal photosynthetic status of control plants at the onset of the experiment (Flexas *et al*., 2002; Perera-Castro and Flexas, 2023).

Plant water status, leaf mass per area and □^{13}C composition

Leaf mass per area (LMA) and relative water content (RWC) were estimated for each species after gas exchange measurements. RWC was calculated as [(FW - DW)/(TW - DW)] x 100, where FW, TW and DW are fresh, turgor and dry leaf weights, respectively. The FW was determined immediately after excising leaves from the plants, TW was obtained after rehydration in distilled water for 24h in the dark at 4°C until reaching a constant weight, and DW was subsequently determined after 72h at 70°C in an oven until constant weight was reached. Leaf pieces were also photographed before drying to estimate the leaf area using ImageJ software (Schneider *et al*. 2012). The LMA was calculated from leaf dry weight and leaf area.

Leaf dry matter was used to analyse $\delta^{13}C$ composition by isotope ratio mass spectrometry (GC-IRMS) (Deltaplus; Thermo Finnigan, Palm Beach, Florida, USA) as described in Tomás *et al*. (2012). $\delta^{13}C$ values were referred to a Pee Dee Belemnite standard. For cauliflower, the last fully-expanded leaf was sampled, while in fern plants, young leaves not yet fully expanded were sampled, as most of their mature leaves had been fully developed prior to bringing the plants into the Temperature Gradient Greenhouses used for the experiment.

Since a compressed CO_2 tank was used to generate the high CO_2 treatment, air $\delta^{13}C$ was determined for each Temperature Gradient Greenhouse. Air samples were collected using 50-mL syringes (SGE International PTY Ltd., Ringwood, Australia), kept in 10-mL vacutainers (BD Vacutainers, Plymouth, UK). The air samples were analysed by gas chromatography–combustion–isotope ratio mass spectrometry (GC–C–IRMS). Briefly, water vapour and oxygen from gas samples were removed and the carbon dioxide, argon, and nitrogen gases were separated by GC (model 6890 gas chromatograph; Agilent, Santa Clara, California, USA) coupled to an isotope ratio mass spectrometer (Deltaplus; Thermo Finnigan, Palm Beach, Florida, USA) via a GC-C Combustion III interface (Thermo Finnigan). The column used was a GS-GASPRO (30 m x 0.32 mm i.d.; J.W. Scientific Inc., Folsom, California, USA).

From leaf and air $\delta^{13}C$, carbon isotope discrimination $\Delta^{13}C$ was calculated as described by Farqyhar, O'Leary and Berry (1982):

$$\Delta^{13}C = \frac{\delta_{substrate} - \delta_{product}}{1 + \delta_{product} / 1000}$$

Anatomical traits

Light and electron transmission microscopy techniques were used for leaf anatomic analysis. Four to six leaves were collected immediately after gas exchange measurements, and small leaf pieces (2 mm x 1 mm) were cut avoiding major veins and fixed in paraformaldehyde (2%) and glutaraldehyde (4%) in 0.1 M phosphate buffer solution (pH 7.4) under vacuum pressure and processed as in Carriqui *et al*. (2021). Transversal semi-thin (0.8 □m) and ultra-thin (90 nm) sections of mesophyll were cut with an ultramicrotome (Leica UC6, Vienna, Austria). Semi-thin preparations were dyed with 1% toluidine blue and observed at 200x magnifications under a light microscopy (Olympus, Tokyo, Japan) and photographed with a Moticam 3 digital camera (Motic Electric Group Co., Xiamen, China), while ultra-thin sections were contrasted with uranyl acetate and lead citrate and were observed at 1500x and 30000x magnifications with a transmission electron microscopy (TEM H600, Hitachi, Tokyo, Japan). All images were analysed using the ImageJ software (Schneider *et al*. 2012). The following parameters were obtained from light microscopy images: leaf thickness (T_L), mesophyll thickness (T_{MES}), upper and lower epidermis thickness (T_{UE} and T_{LE}, respectively), and mesophyll fraction of intercellular air spaces (f_{ias}). Images at 1500x magnification were used to calculate chloroplast thickness (T_{chl}), chloroplast length (L_{chl}), distance between chloroplasts (L_{betchl}), cytosol thickness (T_{cyt}) mesophyll and chloroplast surface area exposed to intercellular

air spaces per area (S_m and S_c, respectively), and the S_c/S_m ratio. Cell wall thickness of mesophyll cells (T_{cw}) was measured from images at 30000x magnification. The curvature correction factor was determined performing an average length-width ratio of five cells per mesophyll type (palisade or spongy), as described previously (Thain, 1983). Finally, g_m was calculated based on anatomical particularities (Tomás *et al*., 2013). Ten measurements were made for each anatomical characteristic. Nail polish imprints were taken from both abaxial and adaxial surfaces of fully developed leaves from both species and stomatal density (*SD*) was determined in both leaf epidermis of the species studied here by light microscopy, as previously described (Daloso *et al*., 2016).

Metabolite and lipid profiling analysis

Metabolite analysis was performed in the same leaves used for gas exchange measurements. Leaf samples (five biological replicates) were collected avoiding the midrib, and immediately frozen in liquid nitrogen and stored at -80°C for subsequent analysis. About 50 mg of frozen material were quickly ground using liquid nitrogen. The extraction of polar metabolites was carried out exactly as described earlier (Lisec *et al*., 2006).The metabolites were derivatized and analysed by gas chromatography coupled to time-of-flight mass spectrometry (GC-TOF-MS) following a well-established approach (Lisec *et al*., 2006). Both chromatogram and mass spectral analyses were performed using TagFinder software (Luedemann *et al*., 2008). The lipophilic phase of the extraction was suspended in acetonitrile/isopropanol and used for lipid analysis according to Hummel *et al*. (2011). Lipid metabolism was analysed exactly as described in Liu *et al*. (2017). The extraction, solubilization and hydrolysis of starch followed by enzymatic assay of glucose was done as in Ruzanski *et al*. (2013).

Statistical analysis

All data are expressed as the mean of four-seven replicates ± standard error (SE). Significant differences between stress conditions in each species were determined using ANOVA and Tukey test ($P < 0.05$), while the differences in the heatmaps were determined using Student's *t*-test with AT_ACO_2 as control ($P < 0.05$). The relationships between gas exchange and anatomical parameters were examined by the Pearson correlation coefficient (*r*) and by linear regression analyses. We used the modified Thompson τ technique to check data outliers in the datasets. All data were analysed using the SIGMAPLOT 14 (Systat Software Inc., San

Jose, California, USA) or R software (R Development Core Team, http://www.R-project.org). The metabolic data were subjected to multivariate analysis, such as principal components analysis (PCA) and partial least square-discriminant analysis (PLS-DA) using the MetaboAnalyst platform (Chong *et al*., 2018).

Results

How much is fern physiology affected by abiotic factors compared to an angiosperm?

Aiming to investigate how ferns and angiosperms respond to climate change conditions, we grew plants from two representative species (*Nephrolepis exaltata* – Nephrolepis and *Brassica oleracea* – cauliflower) of these groups under ambient CO_2 concentration ($_ACO_2$), high CO_2 ($_HCO_2$) and different stress conditions (high temperature (HT), drought (D), and all combinations between them).

No changes in LMA were observed in Nephrolepis (*Nephrolepis exaltata*), while significant increases were observed in this parameter in cauliflower (*Brassica oleracea*) in response to drought (Fig. 1A; Supplementary Tables S1 and S2). When drought was combined with high temperatures, small reductions in RWC were observed in both genotypes (Fig. 1B), but RWC was only significantly altered in cauliflower in response to the three stimuli ($_HCO_2$, HT and D) combined (Supplementary Tables S1 and S2). Similarly, the effect of drought was exacerbated when combined with high temperatures in some gas-exchange parameters, as evidenced by the lowest average values of A_N in both species (Fig. 2A). By contrast, the effect of both high temperature and drought stresses seems to be alleviated by high CO_2, as evidenced by the higher A_N found under AT_HCO_2, ATD_HCO_2, HT_HCO_2 and HTD_HCO_2, when compared to their respective controls (Fig. 2A; Supplementary Table S1). Beyond high CO_2, drought also had a significant influence on A_N in both species and on the ETR of Nephrolepis (Fig. 2B; Supplementary Table S2), while this parameter was only influenced by the combination of high CO_2 and high temperatures in cauliflower, having the lowest absolute values under HTD_ACO_2 (Supplementary Table S1 and S2).

Stomatal and mesophyll conductances were sensitive to drought in both species, but only sensitive to changes in temperature in cauliflower. Nephrolepis changed significantly g_s in response to drought and the combination of drought and high CO_2, and curiously g_m just in response to drought. On the other hand, cauliflower changed g_s influenced by drought and the combination of drought and high temperature, being the latter, the only condition affecting g_m (Fig. 2C and D; Supplementary Table S2). Interestingly, g_s and g_m from both plant groups

responded to drought. However, g_s and g_m in Nephrolepis was substantially reduced under ATD_ACO_2 as compared to AT_ACO_2, whilst no statistical difference between AT_ACO_2 and ATD_ACO_2 was observed in cauliflower (Supplementary Table S1).

At the same time, R_d and photorespiration (P_r) in Nephrolepis were altered in response to the combination of drought and high CO_2, albeit they were unresponsive to changes in CO_2 alone (Supplementary Table S2). However, no statistical differences among the treatments were observed in both parameters in Nephrolepis (Fig. 3A and B; Supplementary Table S1). By contrast, in cauliflower, R_d was only influenced by drought, and P_r by high CO_2 (Supplementary Table S2). The reduction in R_d was greater under ATD_ACO_2, highlighting that high CO_2 and/or high temperatures increased the R_d up to the values observed in the AT_ACO_2 treatment (Fig. 3A; Supplementary Table S1). Also, as expected, P_r was inhibited by high CO_2, but this was mainly observed in the absence of drought (Fig. 3B; Supplementary Table S1). Additionally, Nephrolepis increased internal CO_2 concentration (C_i) only in response to CO_2, but to a lesser extent than cauliflower, in which C_i was the most responsive parameter to high CO_2, high temperature and drought treatments, acting separately as well as to the combinations of HTD_ACO_2 and HTD_HCO_2 (Fig. 3C; Supplementary Table S1 and S2). High CO_2 and drought as single factors changed chloroplastic CO_2 concentration (C_c) in Nephrolepis, whilst C_c in cauliflower was altered in response to high CO_2, high temperatures and drought separately, but not to the combination of them for both species (Fig. 3D; Supplementary Table S2). Interestingly, despite all the differences observed, V_{cmax} did not change in response to the treatments in both species. Regarding the J_{max}, no changes were observed in the Nephrolepis, whilst cauliflower changed solely in response to high CO_2 (Fig. 3E-H; Supplementary Table S1 and S2).

$\Delta^{13}C$ values for both species at AT_ACO_2 treatment were typical of C_3 species (i.e., on average -32.00 ± 0.08 ‰ for cauliflower and -24.59 ± 0.05 ‰ for Nephrolepis, data not shown). This difference resulted from a much larger discrimination $\Delta^{13}C$ in cauliflower than Nephrolepis (Supplementary Table S3), reflecting the much larger assimilation rate of the former species. A slight yet significant effect of temperature and/or drought was found in $\Delta^{13}C$ for any of the two species, whereas high CO_2 resulted in increased $\Delta^{13}C$ in both species (Supplementary Table S3).

Nephrolepis physiology is slightly affected by climate change conditions, while high CO_2 strongly drives physiological performance in cauliflower

Multivariate analysis, such as principal component analysis (PCA) and partial least squares discriminant analysis (PLS-DA) are efficient approaches to discriminate stressed from non-stressed plants at both physiological and metabolic levels (Cardoso *et al*., 2022; Vital *et al*., 2022). Therefore, we carried out a PLS-DA using all physiological data described above (Supplementary Table S1) to identify which environmental condition mostly impacted the physiological responses of Nephrolepis and cauliflower. Nephrolepis showed no group separation by the PLS-DA, either under stress conditions acting separately or combined (Fig. 4A and B). This result indicates that the physiological performance of the fern is highly unresponsive to high temperature, high CO_2, drought and their combinations. Contrarily, cauliflower plants under high CO_2 were clearly separated by the component 1 of the PLS-DA from all other treatments in the absence of stress (Fig. 4C). Similarly, all combinations containing high CO_2 were separated from treatments under ambient CO_2 by the component 1 (Fig. 4D). Thus, the overall physiological status of cauliflower plants to high CO_2 differs substantially from plants under ambient CO_2, despite the presence of high temperature or drought. This was not the case for the fern, suggesting that the acclimation to high temperature and drought differs between these species in an enriched CO_2 atmosphere.

Leaf anatomical parameters were little affected by stress conditions in both species

Leaf anatomical analyses were performed to investigate whether the structural traits related to the physiological parameters measured here were affected by the treatments. Nephrolepis leaves were hypostomatic, while cauliflower leaves were amphystomatic but showed higher values of abaxial *SD*, almost four times the number in Nephrolepis, with the exception of plants under high CO_2 conditions (Fig. 5A). Moreover, *SD* in abaxial epidermis was higher altered in response to high CO_2 and high temperature in the Nephrolepis, whereas this parameter was slightly altered by the combination of high CO_2 and high temperature in cauliflower (Supplementary Table S2). In Nephrolepis, T_{UE} was significantly higher under AT_ACO_2 than stress conditions, but f_{ias}, T_{chl} and T_{cyt} increased mostly under high CO_2 and decreased under high temperature (Supplementary Table S4), which leads to a significant alteration of these parameters in response to the combination of high CO_2 and high temperature (Supplementary Table S5). Similarly, increases in T_{MES_spo}, T_{cw}, and L_{chl} were observed under high CO_2 in cauliflower, with reductions under high temperature and drought, while $g_{m\_anatomy}$ was significantly higher under control conditions. High CO_2 and high temperature combined with drought greatly affected anatomical parameters in cauliflower; conversely, no significant

changes were observed in any of the other parameters measured (Supplementary Table S4 and S5). We further investigated the relationships between gas-exchange and anatomical parameters. We observed that *SD* was significantly correlated with A_N and C_C, and C_i-C_c with f_{ias} and T_{chl} in Nephrolepis. On the other hand, in cauliflower, C_i-C_c was positively correlated with T_L, T_{UE}, T_{LE}, T_{MES}, T_{cw}, T_{chl}, L_{chl}, L_{betchl}, T_{cyt} and S_m. Additionally, g_m was positively correlated with T_{chl}, but negatively with L_{betchl} in cauliflower. Interestingly, A_N was positively correlated with C_c in both species, but positively correlated with *SD* and both conductances (g_s and g_m) only in Nephrolepis (Fig. 5B).

Nephrolepis has lower contents of starch and protein than cauliflower

Nephrolepis showed lower contents of both starch and protein than cauliflower under all conditions tested, especially under non-stressed conditions (AT_ACO_2). However, although both species showed changes in different directions, high CO_2 (AT_HCO_2) did not significantly increase the amount of leaf starch and total protein neither in Nephrolepis nor in cauliflower, when compared to the AT_ACO_2 treatment of each species (Fig. 6A and B). The content of starch was higher altered in response to the high CO_2 and high temperatures in Nephrolepis, whereas this parameter decreased in response to drought, to the combination of drought and high temperatures and the combination of them at high CO_2 conditions in cauliflower (Fig. 6A; Supplementary Table S1). Interestingly, the level of leaf protein did not respond to any treatment in Nephrolepis, while it decreased in response to drought, to the combination of drought and high temperature, and the combination of drought and high CO_2 in cauliflower (Fig. 6B; Supplementary Table S1).

Primary and lipid metabolism are not affected in Nephrolepis, but are responsive to high CO_2, high temperature and drought in cauliflower

To further explore the role of primary and lipid metabolism in driving the measured physiological responses, we performed primary and lipid profiling, annotating 60 different primary metabolites from different compound classes, such as amino and organic acids, sugar and sugar alcohols, as well as 80 membrane and storage lipids. Despite specific differences in the gas-exchange parameters under stress conditions in Nephrolepis, PCA revealed that neither primary metabolites nor lipids changed under stress conditions (Fig. 7A). In contrast, cauliflower metabolism was highly responsive to the imposed treatments (Fig. 7B). PCA using primary metabolism data showed a clear separation between the treatments, which together

explained about 71% of the variability. PC1 (45.4%) and PC2 (26%) separated most high temperature and drought treatments from their respective controls, with the exception of HTD_ACO_2 and HTD_HCO_2, which were clustered separately from AT_ACO_2 and the other high temperature and drought treatments, respectively. Regarding the lipid metabolism, with the exception of HT_ACO_2 and AT_HCO_2, all other treatments were clustered separated from the AT_ACO_2 control by the PC2 in cauliflower. Among them, HTD_ACO_2 was the most discrepant, being separated from ATD_ACO_2 and HT_ACO_2 by PC1 (41.2%) and PC2 (22.2%), respectively (Fig. 7B).

Leaf primary metabolites diverge substantially in Nephrolepis and cauliflower

We next investigated the changes in the level of specific lipids and primary metabolites in both species. In general, Nephrolepis displayed fewer significant differences in the level of lipids and primary metabolites between the treatments and the control, compared to cauliflower (Fig. 8A and B). In general, stress treatments and their combination induced significant alteration in the levels of only 21% of metabolites and 16% of lipids in Nephrolepis, whereas cauliflower displayed significant changes of around 32% of the measured primary metabolites and lipids.

However, most of the stress treatments in Nephrolepis shared some common response patterns in primary metabolites, such as increases in fructose, glucose and caffeic acid and decreases in malate, citrate, glucoheptose and Val (Fig. 8A). Higher levels of antioxidant and secondary metabolism precursors, such as caffeic acid, hydroxycinnamic acid, dehydroascorbate, putrescine, GABA, Met and Phe were also observed in Nephrolepis under certain stress conditions. By contrast, cauliflower plants differentially accumulated several metabolites in comparison with the control, mainly in response to HTD_ACO_2 and ATD_HCO_2 treatments (Fig. 8A). Interestingly, while high CO_2 mainly influenced the physiological changes, drought seemed to be the major factor modulating the metabolic responses, particularly when drought is analysed in combination with high temperature and/or high CO_2. The combination of high temperature, drought and high CO_2 (HTD_HCO_2) showed a pronounced decrease in relative metabolite content, which resembled either HT_HCO_2 and/or ATD_ACO_2 treatments (Fig. 8A). Certain amino acids (Ala, Asp, Gln, Gly, Ser and Thr), and metabolites associated to the TCA cycle (citrate, fumarate, malate, succinate, 2-OG and Pyr) have reduced levels in HTD_HCO_2, when compared to the control. At the same time, most sugars were increased under drought (ATD_ACO_2), a typical response showed by other plant species

(Fàbregas and Fernie, 2019). Increased raffinose and galactinol contents were also observed under HTD_ACO_2 and ATD_HCO_2 treatments, whereas glucose, fructose, mannose and *myo*-inositol increased only under ATD_HCO_2.

The levels of certain lipids are antagonistically altered in Nephrolepis and cauliflower

Interestingly, stress conditions, especially high temperature (HT_ACO_2), led to increased levels of chloroplast membrane lipids, digalactosyl diacylglycerol (DGDG; 34:0, 34:3, 34:6) and monogalactosyl diacylglycerol (MGDG; 34:1, 34:2, 34:3, 34:5, 34:6, 36:3, 36:4, 36:5, 36:6, 36:7, 38:6) in Nephrolepis (Fig. 8B). Increased content in storage lipids (triacylglycerols; TAG) was also observed in the fern, although the significance was observed solely in specific lipids and in particular conditions (Fig. 8B). Cauliflower plants displayed several lipids with a differential accumulation in comparison with the control (AT_ACO_2) (Fig. 8B). In general, the levels of most lipids decreased under drought treatments and increased under the HT_ACO_2 treatment. However, the high temperature-induced increases in cell membrane lipids, phosphatidylcholine (PC; 34:2, 34:3, 36:2, 36:4, 36:5, 36:6) and phosphatidyl ethanolamine (PE; 34:2, 34:3, 36:2, 36:3, 36:4, 36:5) were abolished by the combination with high CO_2 and/or drought or high CO_2 and drought acting separately (Fig. 8B).

Discussion

This fern does not care: Nephrolepis exaltata responds differently to foreseen climate change stress conditions than Brassica oleracea, a typical angiosperm

Global climate change is expected to cause unprecedented challenges to both natural and agriculture ecosystems in the upcoming decades, due to the predicted increases in atmospheric CO_2 concentration and temperature associated to more frequent drought periods (Lobell and Gourdji, 2012; Ripple *et al*., 2021; IPCC, 2022). It is thus important to understand how plants will acclimate to these conditions. However, although certain regulatory mechanisms that aid crop plants to acclimate to these adverse conditions have been revealed in the last decade, how basal lineages of plants, such as ferns, respond to these conditions is less understood. Ferns and angiosperms differ substantially at morphological, physiological and genetic levels (Gago *et al*., 2019; Lima *et al*., 2019; Sussmilch *et al*., 2019; Harris *et al*., 2020; Gong *et al*., 2021). The results obtained here indicate that these plant groups further differ in the way by which they acclimate to the combination of drought, high temperature and high CO_2

concentration. This suggests that climate change conditions may differently affect these plant groups, which can lead to alterations in the dynamics of natural ecosystems.

Elevated CO_2 concentration, high temperature and drought have already been documented to trigger several changes in plant functionality, including alterations in the photosynthetic process. The harmful effects of the combination of these stress conditions on photosynthesis can induce oxidative stress within plant cells, leading to biochemical imbalances and ultimately resulting in reduced plant growth (Chaves *et al*., 2009; Fernández-Marín *et al*., 2020; Lobo *et al*., 2022; Vital *et al*., 2022). In the current study, the fern and the angiosperm showed different responses to each stress condition applied separately or in combination. In absolute terms, Nephrolepis had much lower values of A_N, g_s and g_m than cauliflower, consistent with previous studies (Gago *et al*., 2013; Flexas *et al*., 2014; Carriquí *et al*., 2015; Lima *et al*., 2019; Cândido-Sobrinho *et al*., 2022). Drought and high temperature combined imposed reductions in A_N of both species, mostly driven by reductions in g_s and g_m rather than photochemistry/biochemistry (Fig. 2). These results suggest that A_N was mostly restricted by diffusion rather than photochemical limitation at the stress level imposed to the plants, consistent with previous reports in other plant species, highlighting an important role for g_s and g_m in driving photosynthetic responses to environmental and stress conditions (Flexas *et al*., 2009; Hu *et al*., 2010; Carriquí *et al*., 2015).

Generally speaking, the $\delta^{13}C$ values, as well as their variations among treatments, were much lower for Nephrolepis than cauliflower, which contradicts the proposal of Porter *et al*. (2017) that discrimination is inherently larger in spore-bearing than seed-bearing plants - although this was concluded based on a comparison of relatively few species. In this sense, average $\delta^{13}C$ in cauliflower was larger than in any fern, while average $\delta^{13}C$ in Nephrolepis was lower than in any angiosperm included in their study, suggesting that there might be a large variability in $\delta^{13}C$ among species of both groups. Drought had only a slight effect on the $\Delta^{13}C$, likely due to its short duration and indicating that the majority of leaf dry matter was formed prior to the its onset. In addition, there was no significant impact of temperature alone on photosynthesis in both species. However, CO_2 has a large effect on $\delta^{13}C$, provided that the sampled leaves were fully unfolded once the differential CO_2 treatments had been established. Again, in general, the response was much larger in cauliflower than in Nephrolepis, highlighting the substantial disparity in assimilation between these two species. In cauliflower, $\delta^{13}C$ followed a pattern among treatments that resembled that of A_N, as expected (e.g. Porter *et al*., 2017). In Nephrolepis, $\delta^{13}C$ increased from AT_ACO_2 to AT_HCO_2, in agreement with a large

increase in A_N, but it also increased from AT_ACO_2 to HT_ACO_2 despite decreased photosynthesis, in this case likely reflecting the strong increase in leaf respiration (Fig. 3A). Also, $\Box^{13}C$ did not increase from HT_ACO_2 to HT_HCO_2 despite increased photosynthesis.

Increased photosynthesis in ferns grown at high CO_2 has been already reported (Caporn *et al*., 1999; Yiotis *et al*., 2017), and the prediction of Flexas *et al*. (2014) of larger response of photosynthesis to increased CO_2 in ferns than angiosperms seemed supported by Yiotis *et al*. (2017), whose study in plants grown at very large CO_2 (1900 ppm) showed an average increase in photosynthesis of 32% in two fern species, while one angiosperm species showed an increase of 30% and two angiosperm species showed no increase. Interestingly, this was not evidenced in Nephrolepis in the present study. Although at ambient temperature, high CO_2 resulted in a slightly – but non-significant – larger % increase of A_N in Nephrolepis than in cauliflower, the opposite occurred at high temperatures. Moreover, due to larger effects of drought on A_N in Nephrolepis, in most stress and high CO_2 combinations, A_N was less enhanced in Nephrolepis than cauliflower, to the extent that, in the fern, photosynthesis was even lower than in AT_ACO_2, under ATD_HCO_2 and HTD_HCO_2, while in the angiosperm all high CO_2 treatments, including those with drought, resulted in larger assimilation than in AT_HCO_2. This is coincident with what is typically found in C3 angiosperm species (Robredo *et al*., 2007; Robredo *et al*., 2010), while this is, to the best of our knowledge, the first report of simulated multi-factorial climate change conditions in a fern species. Although we cannot extrapolate the behaviour of a single species to the whole group of ferns, the present results aware that it could happen that the combination of stress factors associated to climate change resulted in low increases or even decreases in fern photosynthesis. Studies with more fern species are necessary to confirm this point.

On the relationship among stomatal conductance, photosynthesis and metabolism

It has been shown that stomatal movement is finely regulated by the accumulation of mesophyll derived-metabolites in the apoplast and symplast of guard cells (Flütsch and Santelia, 2021). Metabolites are thus important molecules to modulate stomatal opening or closure according to the prevailing environmental condition (Lawson and Blatt, 2014). Moreover, it has been reported that specific metabolites associated to low g_m can directly impact CO_2 diffusion and consequently photosynthesis (Carriquí *et al*., 2015; Gago *et al*., 2016; Clemente-Moreno *et al*., 2019). However, it is still unclear how metabolism-mediated mechanisms regulate both g_s and g_m under stress conditions. Plant metabolism is highly responsive to stress conditions. Notably, changes in the level of lipids, sugars and amino acids

have been documented for a wide range of stressful conditions (Obata and Fernie, 2012; Fàbregas and Fernie, 2019; Liu *et al*., 2019; Cardoso *et al*., 2022; Zandalinas *et al*., 2022). Here, primary metabolites and lipids showed distinct stress responses between the two species belonging to different phylogenetic groups, as evidenced by the separation of cauliflower and Nephrolepis in the PCA (Fig. 7). While the changes in Nephrolepis were minor in response to high temperature, high CO_2 concentration and/or drought, the metabolism of cauliflower was substantially altered, which could be either associated with a better acclimation capacity or a higher level of stress in cauliflower, when compared to Nephrolepis.

Both species shared the accumulation of osmolytes and compatible solutes, and decreased levels of organic acids (mainly TCA cycle intermediates) and amino acids under stress, as described in previous studies (Obata and Fernie, 2012; Keunen *et al*., 2013). However, we observed specific responses for each stress condition. For instance, drought imposition elevated the levels of sugars and sugar alcohols (Fru, Glc, raffinose and galactinol) and reduced the levels of organic acids (fumarate, malate and citrate), in parallel to the stronger reductions in g_s values. The accumulation of sugars, especially sucrose, has been reported as an important mechanism for the regulation of the water use efficiency (WUE) (Antunes *et al*., 2012; Daloso *et al*., 2016; Antunes *et al*., 2017; Freire *et al*., 2021). This idea relies in the fact that high sucrose content induces stomatal closure (Kelly *et al*., 2013; Kottapalli *et al*., 2018; Medeiros *et al*., 2018), as a mechanism to reduce transpiration and thus improve WUE in periods of high A_N or under stress conditions (Lugassi *et al*., 2015; Kelly *et al*., 2019). Furthermore, the ratio between sugars and organic acids, especially sucrose and malate, has been suggested to be key for the differential regulation of stomatal closure speediness among ferns and angiosperms (Gago *et al*., 2016; Lima *et al*., 2019). Taken together, these results highlight that the balance between sugar and organic acids might coordinate the magnitude of stomatal responses by connecting mesophyll photosynthetic activity with stomatal movement regulation, which in turn could modulate the differential stomatal, photosynthetic, and metabolic responses of ferns and angiosperms to stress conditions, especially drought.

Beyond sugars and organic acids, other metabolites might be also associated with the different physiological and anatomical responses observed between the plant species studied here. For example, metabolites associated with protein and membrane stabilization (raffinose, galactinol, trehalose, xylose) (Hincha *et al*., 2003), osmoprotection (Pro) (Hayat *et al*., 2012), protection against reactive oxygen species (ascorbate) (Das and Roychoudhury, 2014), and related to antioxidant responses or precursors of phenolic compounds (Met, Phe, Trp) were

highly affected by stress imposition but showed different responses in Nephrolepis and cauliflower, suggesting that they might be related to stress acclimation and the differential metabolic plasticity of these species (Zhao *et al*., 1998). Besides their importance in osmoregulation and the balance between supply and utilization of C and energy, monosaccharides can also act as signalling molecules (Sheen *et al*., 1999). In turn, reduction in amino acid content could be related to changes in N metabolism and ATP limitation (Batista-Silva *et al*., 2019), given that the degradation of amino acids is an alternative source of carbons for the mitochondrial respiratory metabolism (Araújo *et al*., 2011; Batista-Silva *et al*., 2019).

The role of lipid remodelling in enhancing plant adaptation mechanisms to different abiotic stresses

High temperature increased the levels of DGDG and MGDG in Nephrolepis and PC and PE in cauliflower, both mainly presenting a low degree of unsaturation. Increases in these membrane lipids may be a mechanism to compensate changes in membrane fluidity triggered by heat stress, given that high temperature considerably alters membrane fluidity and its function (Balogh *et al*., 2013; Zhang *et al*., 2019; Shiva *et al*., 2020; Zoong Lwe *et al*., 2021). Moreover, increased levels of TAG after stress conditions, mostly observed in Nephrolepis (Fig. 8B), may constitute a strategy to reduce oxidative membrane damage through the elimination of toxic lipid intermediates. This idea is supported by studies showing that abiotic stresses can result in the accumulation of toxic lipids intermediates (including diacylglycerols and free fatty acids), while key genes involved in TAG biosynthesis are up-regulated under stress conditions, which catalyse the conversion of diacylglycerols or free fatty acids into TAG (Lu *et al*., 2020). These results indicate that lipid metabolism is slightly altered in Nephrolepis, whereas substantially changed in cauliflower, likely as a mechanism to maintain their membrane integrity. However, the pattern and the magnitude of lipids accumulation differ between Nephrolepis and cauliflower, suggesting that the climate change scenario may differentially affect the metabolism of lipids in ferns and angiosperms.

Taken together, our results indicate that Nephrolepis is highly unresponsive to the stress conditions associated to the climate change scenario tested here. Given that leaf anatomical parameters were not clearly influenced by high temperature, high CO_2 or drought in both species, it seems likely that the alterations observed in g_s and g_m may be associated to metabolic changes rather than with leaf morpho-anatomical rearrangements (Lehmann *et al*., 2009; Lawson *et al*., 2014; Gago *et al*., 2017; Verbancic *et al*., 2018). The low Nephrolepis stress

responsiveness can be associated to a lack of plant stress acclimation mechanisms of ferns. For instance, it has been shown that ferns have slower stomatal responses to several stomatal closure stimuli, including slower responses to dark, high CO_2 and exogenous application of sucrose, and a lack of stomatal response to ABA (Franks and Britton-Harper, 2016; Lima *et al*., 2019; Sussmilch *et al*., 2019; Cândido-Sobrinho *et al*., 2022). Beyond a well-described regulator of stomatal movement, ABA is key for the expression of drought-related genes and the activation of several other mechanisms associated to plant drought acclimation (Raghavendra *et al*., 2010). Thus, several plant stress acclimation mechanisms regulated by ABA may be disrupted in ferns, consequently affecting the manner and the magnitude by which these plants respond to stress conditions. Alternatively, the evidence suggests that carbon assimilated during the diel course is preferentially used to the synthesis of secondary rather primary metabolites in ferns, and the opposite is observed in angiosperms (Lima *et al*., 2019; Cândido-Sobrinho *et al*., 2022). This observation implies that ferns may have a higher resilience associated to a higher investment of assimilated carbon in defence-related rather than growth-related metabolic pathways, which could explain the low plasticity of Nephrolepis under stress conditions. Our study highlights that the predicted climate change scenario may differentially affect ferns and angiosperms. However, further studies using more species are needed to better understand how plants from different evolutionary lineages will acclimate to the predicted stress conditions.

Acknowledgements

VFL thanks the scholarship granted by the Brazilian Federal Agency for Support and Evaluation of Graduate Education (CAPES-Brazil), and with JG also publicly thank MCIN/AEI for the research project PID2019-107434GA-100 (Spain). DMD thanks the resources obtained by the National Institute of Science and Technology in Plant Physiology under Stress Conditions (INCT Plant Stress Physiology – Grant: 406455/2022-8) and the research fellowship granted by the National Council for Scientific and Technological Development (CNPq). CMF is funded by the Max Planck Society (Partner Group for Plant Biochemistry).

Author contributions

Conceptualization, methodology and investigation were designed by JF, FM and MS-D; MS-D, FM, JJI, IP, MO, HS and AU implemented the experimental set-up, grew plants, applied treatments and performed the whole set-up maintenance; JF, FM and IP performed all gas exchange and chlorophyll fluorescence measurements; IA, MO and HS collected samples for the different analyses; MC performed the whole leaf anatomy analyses; IJ, IA and MRC

performed the isotopic analyses; metabolomic analysis were performed by JG, JS and AB; statistical data analysis and modelling was performed by VFL, JG and AB; writing and editing was done by VFL, DD, CF, FM, YB, AB, AF, IA, JG and JF. All authors have read and agreed to the published version of the manuscript.

Conflict of interest

The authors declare no potential conflict of interest.

Funding

This research was supported by the projects CTM2014-53902-C2-1-P from the Ministerio de Economía y Competitividad (MINECO, Spain), PGC2018-093824-B-C41 from the Ministerio de Ciencia, Innovación y Universidades, and the ERDF (FEDER), and PID2019-107434GA-100 funded by MCIN/AEI/10.13039/501100011033 and by the European Union 'NextGenerationEU/PRTR'.

Data availability

All data supporting the findings of this study are available within the article and within its supplementary material published online.

References

Antunes WC, Daloso DM, Pinheiro DP, Williams TCR, Loureiro ME. 2017. Guard cell-specific down-regulation of the sucrose transporter SUT1 leads to improved water use efficiency and reveals the interplay between carbohydrate metabolism and K^+ accumulation in the regulation of stomatal opening. Environmental and Experimental Botany **135**, 73–85.

Antunes WC, Provart NJ, Williams TCR, Loureiro ME. 2012. Changes in stomatal function and water use efficiency in potato plants with altered sucrolytic activity. Plant, Cell and Environment **35**, 747–759.

Araújo WL, Tohge T, Ishizaki K, Leaver CJ, Fernie AR. 2011. Protein degradation - an alternative respiratory substrate for stressed plants. Trends in Plant Science **16**, 489–498.

Auler PA, Freire FBS, Lima VF, Daloso DM. 2022. On the role of guard cells in sensing environmental signals and memorising stress periods. Theoretical and Experimental Plant Physiology **34**, 277–299.

Balogh G, Péter M, Glatz A, Gombos I, Török Z, Horváth I, Harwood JL, Vígh L. 2013.

Key role of lipids in heat stress management. FEBS Letters **587**, 1970–1980.

Batista-Silva W, Heinemann B, Braun HP, Araújo WL, Rugen N, Nunes A, Hildebrandt TM. 2019. The role of amino acid metabolism during abiotic stress release. Plant, Cell and Environment **42**, 1630–1644.

Bird IF, Cornelius MJ, Keys AJ, Station RE, Al H. 1982. Affinity of RuBP carboxylases for carbon dioxide and inhibition of the enzymes by oxygen. Journal of Experimental Botany **33**, 1004–1013.

Brodribb TJ, McAdam SAM, Jordan GJ, Feild TS. 2009. Evolution of stomatal responsiveness to CO_2 and optimization of water-use efficiency among land plants. New Phytologist **183**, 839–847.

Cândido-Sobrinho SA, Lima VF, Freire FBS, Souza LP, Gago J, Fernie AR, Daloso DM. 2022. Metabolism-mediated mechanisms underpin the differential stomatal speediness regulation among ferns and angiosperms. Plant, Cell and Environment **45**, 296–311.

Caporn SJM, Brooks AL, Press MC, Lee JA. 1999. Effects of long-term exposure to elevated CO_2 and increased nutrient supply on bracken (Pteridium aquilinum). Functional Ecology **13**, 107–115.

Cardoso LL, Freire FBS, Daloso DM. 2022. Plant Metabolic Networks Under Stress: a Multi-species/Stress Condition Meta-analysis. Journal of Soil Science and Plant Nutrition **23**, 4–21.

Carriquí M, Cabrera HM, Conesa M, Coopman RE, Douthe C, Gago J, Gallé A, Galmés J, Ribas-Carbo M, Tomás M, *et al*. 2015. Diffusional limitations explain the lower photosynthetic capacity of ferns as compared with angiosperms in a common garden study. Plant, Cell and Environment **38**, 448–460.

Carriquí M, Nadal M, Flexas J. 2021. Acclimation of mesophyll conductance and anatomy to light during leaf aging in Arabidopsis thaliana. Physiologia Plantarum **172**, 1894-1907.

Chaves MM, Flexas J, Pinheiro C. 2009. Photosynthesis under drought and salt stress: Regulation mechanisms from whole plant to cell. Annals of Botany **103**, 551–560.

Chong J, Soufan O, Li C, Caraus I, Li S, Bourque G, Wishart DS, Xia J, 2018. MetaboAnalyst 4.0: Towards more transparent and integrative metabolomics analysis. Nucleic Acids Research **46**, W486–W494.

Clemente-Moreno MJ, Gago J, Díaz-Vivancos P, Bernal A, Miedes E, Bresta P, Liakopoulos G, Fernie AR, Hernández JA, Flexas J. 2019. The apoplastic antioxidant system and altered cell wall dynamics influence mesophyll conductance and the rate of photosynthesis. The Plant Journal **99**, 1031–1046.

Condamine FL, Silvestro D, Koppelhus EB, Antonelli A. 2020. The rise of angiosperms pushed conifers to decline during global cooling. Proceedings of the National Academy of Sciences **117**, 28867–28875.

Daloso DM, Williams TCR, Antunes WC, Pinheiro DP, Müller C, Loureiro ME, Fernie AR. 2016. Guard cell-specific upregulation of sucrose synthase 3 reveals that the role of sucrose in stomatal function is primarily energetic. New Phytologist **209**, 1470–1483.

Das K, Roychoudhury A. 2014. Reactive oxygen species (ROS) and response of antioxidants as ROS-scavengers during environmental stress in plants. Frontiers in Environmental Science **2**, 1–13.

Evans JR, Kaldenhoff R, Genty B, Terashima I. 2009. Resistances along the CO_2 diffusion pathway inside leaves. Journal of Experimental Botany **60**, 2235–2248.

Fàbregas N, Fernie AR. 2019. The metabolic response to drought. Journal of Experimental Botany **70**, 1077–1085.

Farquhar GD, Caemmerer S, Berry JA. 1980. A biochemical model of photosynthetic CO_2 assimilation in leaves of C_3 species. Planta **149**, 78-90–90.

Farquhar GD, O'Leary MH, Berry JA. 1982. On the relationship between carbon isotope discrimination and the intercellular carbon dioxide concentration in leaves. Functional Plant Biology **9**, 121-137.

Fernández-Marín B, Gulías J, Figueroa CM, Iñiguez C, Clemente-Moreno MJ, Nunes-Nesi A, Fernie AR, Cavieres LA, Bravo LA, García-Plazaola JI, *et al*. 2020. How do vascular plants perform photosynthesis in extreme environments? An integrative ecophysiological and biochemical story. The Plant Journal **101**, 979–1000.

Flexas J, Bota J, Escalona JM, Sampol B, Medrano H. 2002. Effects of drought on photosynthesis in grapevines under field conditions: an evaluation of stomatal and mesophyll limitations. Functional Plant Biology **29**, 461–471.

Flexas J, Barón M, Bota J, Ducruet JM, Gallé A, Galmés J, Jiménez M, Pou A, Ribas-Carbó M, Sajnani C, *et al*. 2009. Photosynthesis limitations during water stress acclimation and recovery in the drought-adapted Vitis hybrid Richter-110 (V. berlandieri×V. rupestris). Journal of Experimental Botany **60**, 2361–2377.

Flexas J, Carriquí M, Coopman RE, Gago J, Galmés J, Martorell S, Morales F, Diaz-Espejo A. 2014. Stomatal and mesophyll conductances to CO_2 in different plant groups: Underrated factors for predicting leaf photosynthesis responses to climate change? Plant Science **226**, 41–48.

Flexas J, Keeley JE. 2012. Evolution of photosynthesis I: Basic leaf morphological traits and diffusion and photosynthetic structures. Terrestrial Photosynthesis in a Changing Environment **24**, 373–385.

Flütsch S, Santelia D. 2021. Mesophyll-derived sugars are positive regulators of light-driven stomatal opening. New Phytologist **230**, 1754–1760.

Franks PJ, Beerling DJ. 2009. Maximum leaf conductance driven by CO_2 effects on stomatal size and density over geologic time. Proceedings of the National Academy of Sciences **106**, 10343–10347.

Franks PJ, Britton-Harper ZJ. 2016. No evidence of general CO_2 insensitivity in ferns: one stomatal control mechanism for all land plants? New Phytologist **211**, 819–827.

Franks PJ, Farquhar GD. 2007. The mechanical diversity of stomata and its significance in gas-exchange control. Plant Physiology **143**, 78–87.

Franks PJ, Royer DL, Beerling DJ, Van De Water PK, Cantrill DJ, Barbour MM, Berry JA. 2014. New constraints on atmospheric CO_2 concentration for the Phanerozoic. Geophysical Research Letters **41**, 4685–4694.

Freire FBS, Bastos RLG, Bret RSC, Cândido-Sobrinho SA, Medeiros DB, Antunes WC, Fernie AR, Daloso DM. 2021. Mild reductions in guard cell sucrose synthase 2 expression leads to slower stomatal opening and decreased whole plant transpiration in Nicotiana tabacum L. Environmental and Experimental Botany **184**, 104370.

Gago J, Carriquí M, Nadal M, Clemente-Moreno MJ, Coopman RE, Fernie AR, Flexas J. 2019. Photosynthesis Optimized across Land Plant Phylogeny. Trends in Plant Science **24**, 947–958.

Gago J, Coopman RE, Cabrera HM, Hermida C, Molins A, Conesa MÀ, Galmés J, Ribas-Carbó M, Flexas J. 2013. Photosynthesis limitations in three fern species. Physiologia Plantarum **149**, 599–611.

Gago J, Daloso DDM, Figueroa CM, Flexas J, Fernie AR. 2016. Relationships of Leaf Net Photosynthesis, Stomatal Conductance, and Mesophyll Conductance to Primary Metabolism: A Multispecies Meta-Analysis Approach. Plant Physiology **171**, 265–279.

Gago J, Fernie AR, Nikoloski Z, Tohge T, Martorell S. 2017. Integrative field scale phenotyping for investigating metabolic components of water stress within a vineyard. Plant Methods **13**, 90.

Genty B, Briantais JM, Baker NR. 1989. The relationship between the quantum yield of photosynthetic electron transport and quenching of chlorophyll fluorescence. Biochimica et

Biophysica Acta - General Subjects **990**, 87–92.

Gong L, Liu XD, Zeng YY, Tian XQ, Li YL, Turner NC, Fang XW. 2021. Stomatal morphology and physiology explain varied sensitivity to abscisic acid across vascular plant lineages. Plant Physiology **186**, 782–797.

Harley PC, Loreto F, Di Marco G, Sharkey TD. 1992. Theoretical considerations when estimating the mesophyll conductance to CO_2 flux by analysis of the response of photosynthesis to CO_2. Plant Physiology **98**, 1429–1436.

Harris BJ, Harrison CJ, Hetherington AM, Williams TA. 2020. Phylogenomic evidence for the monophyly of bryophytes and the reductive evolution of stomata. Current Biology **30**, 2001–2012.e2.

Hassiotou F, Ludwig M, Renton M, Veneklaas EJ, Evans JR. 2009. Influence of leaf dry mass per area, CO_2, and irradiance on mesophyll conductance in sclerophylls. Journal of Experimental Botany **60**, 2303–2314.

Haworth M, Elliott-Kingston C, McElwain JC. 2011. Stomatal control as a driver of plant evolution. Journal of Experimental Botany **62**, 2419–2423.

Haworth M, Scutt CP, Douthe C, Marino G, Thiago M, Gomes G, Loreto F, Flexas J, Centritto M. 2018. Allocation of the epidermis to stomata relates to stomatal physiological control: Stomatal factors involved in the evolutionary diversification of the angiosperms and development of amphistomaty. Environmental and Experimental Botany **151**, 55–63.

Hayat S, Hayat Q, Alyemeni MN, Wani AS, Pichtel J, Ahmad A. 2012. Role of proline under changing environments: A review. Plant Signaling & Behavior **7**, 1456–1466.

Hincha DK, Zuther E, Heyer AG. 2003. The preservation of liposomes by raffinose family oligosaccharides during drying is mediated by effects on fusion and lipid phase transitions. Biochimica et Biophysica Acta - Biomembranes **1612**, 172–177.

Hu L, Wang Z, Huang B. 2010. Diffusion limitations and metabolic factors associated with inhibition and recovery of photosynthesis from drought stress in a C3 perennial grass species. Physiologia Plantarum **139**, 93–106.

Hummel J, Segu S, Li Y, Irgang S, Jueppner J, Giavalisco P. 2011. Ultra performance liquid chromatography and high resolution mass spectrometry for the analysis of plant lipids. Frontiers in Plant Science **2**, 1–17.

IPCC (2022) Climate Change 2022: Impacts, Adaptation and Vulnerability. Work Gr II Contrib to Sixth Assess Rep Intergovernamental Panel Clim Chang. doi: 10.1017/9781009325844.Front.

Jordan B, Ogren LT. 1983. Species variation in kinetic properties of Ribulose Carboxylase/Oxygenase. Archives of Biochemistry and Biophysics **227**, 425–433.

Jordan GJ, Carpenter RJ, Koutoulis A, Price A, Brodribb TJ, Jordan GJ. 2015. Environmental adaptation in stomatal size independent of the effects of genome size. New Phytologist **205**, 608–617.

Karst AL, Lechowicz MJ. 2007. Are correlations among foliar traits in ferns consistent with those in the seed plants? New Phytologist **173**, 306–312.

Kelly G, Egbaria A, Khamaisi B, Lugassi N, Attia Z, Moshelion M, Granot D. 2019. Guard-cell hexokinase increases water-use efficiency under normal and drought conditions. Frontiers in Plant Science **10**, 1–12.

Kelly G, Moshelion M, David-Schwartz R, Halperin O, Wallach R, Attia Z, Belausov E, Granot D. 2013. Hexokinase mediates stomatal closure. The Plant Journal **75**, 977–988.

Kenrick P, Crane PR. 1997. The origin and early evolution of plants on land. Nature **389**, 33–39.

Keunen E, Peshev D, Vangronsveld J, Van Den Ende W, Cuypers A. 2013. Plant sugars are crucial players in the oxidative challenge during abiotic stress: Extending the traditional concept. Plant, Cell and Environment **36**, 1242–1255.

Kottapalli J, David-Schwartz R, Khamaisi B, Brandsma D, Lugassi N, Egbaria A, Kelly G, Granot D. 2018. Sucrose-induced stomatal closure is conserved across evolution. PLoS One **13**, 1–17.

Lawson T, Blatt MR. 2014. Stomatal size, speed, and responsiveness impact on photosynthesis and water use efficiency. Plant Physiology **164**, 1556–1570.

Lawson T, Simkin AJ, Kelly G, Granot D. 2014. Mesophyll photosynthesis and guard cell metabolism impacts on stomatal behaviour. New Phytologist **203**, 1064–1081.

Lehmann M, Schwarzländer M, Obata T, Sirikantaramas S, Burow M, Olsen CE, Tohge T, Fricker MD, Møller BL, Fernie AR, *et al*. 2009. The metabolic response of Arabidopsis roots to oxidative stress is distinct from that of heterotrophic cells in culture and highlights a complex relationship between the levels of transcripts, metabolites, and flux. Molecular Plant **2**, 390–406.

Lima VF, Anjos L dos, Medeiros DB, Cândido-Sobrinho SA, Souza LP, Gago J, Fernie AR, Daloso DM. 2019. The sucrose-to-malate ratio correlates with the faster CO_2 and light stomatal responses of angiosperms compared to ferns. New Phytologist **223**, 1873–1887.

Lisec J, Schauer N, Kopka J, Willmitzer L, Fernie AR. 2006. Gas chromatography mass

spectrometry-based metabolite profiling in plants. Nature Protocols **1**, 387–396.

Liu MY, Burgos A, Ma L, Zhang Q, Tang D, Ruan J. 2017. Lipidomics analysis unravels the effect of nitrogen fertilization on lipid metabolism in tea plant (Camellia sinensis L.). BMC Plant Biology **17**, 1-10.

Liu X, Ma D, Zhang Z, Wang S, Du S, Deng X, Yin L. 2019. Plant lipid remodeling in response to abiotic stresses. Environmental and Experimental Botany **165**, 174–184.

Lobell DB, Gourdji SM. 2012. The influence of climate change on global crop productivity. Plant Physiology **160**, 1686–1697.

Lobo AKM, Catarino ICA, Silva EA, Centeno DC, Domingues DS. 2022. Physiological and molecular responses of woody plants exposed to future atmospheric CO_2 levels under abiotic stresses. Plants **11**, 1880.

Lu J, Xu Y, Wang J, Singer SD, Chen G. 2020. The role of triacylglycerol in plant stress response. Plants **9**, 472.

Luedemann A, Strassburg K, Erban A, Kopka J. 2008. TagFinder for the quantitative analysis of gas chromatography-mass spectrometry (GC-MS)-based metabolite profiling experiments. Bioinformatics **24**, 732–737.

Lugassi N, Kelly G, Lena Fidel, Yaniv Y, Attia Z, Levi A, Alchanatis V, Menachem Moshelion, Raveh E, Carmi N, *et al*. 2015. Expression of Arabidopsis hexokinase in citrus guard cells controls stomatal aperture and reduces transpiration. Frontiers in Plant Science **6**, 1–11.

McAdam SAM, Brodribb TJ. 2012. Fern and lycophyte guard cells do not respond to endogenous abscisic acid. The Plant Cell **24**, 1510–1521.

Medeiros DB, Perez Souza L, Antunes WC, Araújo WL, Daloso DM, Fernie AR . 2018. Sucrose breakdown within guard cells provides substrates for glycolysis and glutamine biosynthesis during light-induced stomatal opening. The Plant Journal **94**, 583–594.

Mittler R, Vanderauwera S, Suzuki N, Miller G, Tognetti VB, Vandepoele K, Gollery M, Shulaev V, Van Breusegem F. 2011. ROS signaling: The new wave? Trends in Plant Science **16**, 300–309.

Morales F, Pascual I, Sánchez-Díaz M, Aguirreolea J, Irigoyen JJ, Goicoechea N, Antolín MC, Oyarzun M, Urdiain A. 2014. Methodological advances: Using greenhouses to simulate climate change scenarios. Plant Science **226**, 30–40.

Niinemets Ü, Cescatti A, Rodeghiero M, Tosens T. 2005. Leaf internal diffusion conductance limits photosynthesis more strongly in older leaves of Mediterranean evergreen broad-leaved

species. Plant, Cell and Environment **28**, 1552–1566.

Obata T, Fernie AR. 2012. The use of metabolomics to dissect plant responses to abiotic stresses. Cellular and Molecular Life Sciences **69**, 3225–3243.

Peguero-Pina JJ, Flexas J, Galmés J, Niinemets ÜLO, Sancho-knapik D, Barredo G, Villarroya D, Gil-pelegrín E. 2012. Leaf anatomical properties in relation to differences in mesophyll conductance to CO_2 and photosynthesis in two related Mediterranean Abies species. Plant, Cell and Environment **35**, 2121–2129.

Perera-Castro A, Flexas J. 2023. The ratio of electron transport to assimilation (ETR/AN): underutilized but essential for assessing both equipment's proper performance and plant status. Planta **257**, 29.

Porter AS, Yiotis C, Montañez IP, McElwain JC. 2017. Evolutionary differences in $\Delta^{13}C$ detected between spore and seed bearing plants following exposure to a range of atmospheric O_2:CO_2 ratios; implications for paleoatmosphere reconstruction. Geochimica et Cosmochimica Acta **213**, 517–533.

Proctor MCF, Tuba Z. 2002. Poikilohydry and homoihydry: Antithesis or spectrum of possibilities? New Phytologist **156**, 327–349.

Pryer KM, Schuettpelz E, Wolf PG, Schneider H, Smith AR, Cranfill R. 2004. Phylogeny and evolution of ferns (monilophytes) with a focus on the early leptosporangiate divergences. American Journal of Botany **91**, 1582–1598.

Raghavendra AS, Gonugunta VK, Christmann A, Grill E. 2010. ABA perception and signalling. Trends in Plant Science **15**, 395–401.

Ripple WJ, Wolf C, Newsome TM, Gregg JW, Lenton TM, Palomo I, Eikelboom JAJ, Law BE, Huq S, Duffy PB, *et al*. 2021. World scientists' warning of a climate emergency 2021. Bioscience **71**, 894–898.

Robredo A, Pérez-López U, de la Maza HS, González-Moro B, Lacuesta M, Mena-Petite A, Muñoz-Rueda A. 2007. Elevated CO_2 alleviates the impact of drought on barley improving water status by lowering stomatal conductance and delaying its effects on photosynthesis. Environmental and Experimental Botany **59**, 252–263.

Robredo A, Pérez-López U, Lacuesta M, Mena-Petite A, Muñoz-Rueda A. 2010. Influence of water stress on photosynthetic characteristics in barley plants under ambient and elevated CO_2 concentrations. Biologia Plantarum **54**, 285–292.

Ruzanski C, Smirnova J, Rejzek M, Cockburn D, Pedersen HL, Pike M, Willats WGT, Svensson B, Steup M, Ebenhöh O, *et al*. 2013. A bacterial glucanotransferase can replace the

complex maltose metabolism required for starch to sucrose conversion in leaves at night. Journal of Biological Chemistry **288**, 28581-28598.

Salachna P, Piechocki R. 2021. Salinity tolerance of four hardy ferns from the genus dryopteris adans grown under different light conditions. Agronomy **11**, 49.

Scafaro AP, Caemmerer SVON, Evans JR, Atwell BJ. 2011. Temperature response of mesophyll conductance in cultivated and wild Oryza species with contrasting mesophyll cell wall thickness. Plant, Cell and Environment **34**, 1999–2008.

Schneider CA, Rasband WS, Eliceiri KW. 2012. NIH Image to ImageJ: 25 years of image analysis. Nature Methods **9**, 671-675.

Schuettpelz E, Pryer KM. 2009. Evidence for a Cenozoic radiation of ferns in an angiosperm-dominated canopy. Proceedings of the National Academy of Sciences **106**, 11200–11205.

Sharkey TD, Bernacchi CJ, Farquhar GD, Singsaas EL. 2007. Fitting photosynthetic carbon dioxide response curves for C3 leaves. Plant, Cell and Environment **30**, 1035–1040.

Sheen J, Zhou L, Jang J. 1999. Sugars as signaling molecules. Current Opinion in Plant Biology **2**, 410–419.

Shiva S, Samarakoon T, Lowe KA, Roach C, Vu HS, Colter M, Porras H, Hwang C, Roth MR, Tamura P, *et al*. 2020. Leaf lipid alterations in response to heat stress of Arabidopsis thaliana. Plants **9**, 1–22.

Smith AR, Pryer KM, Schuettpelz E, Korall P, Schneider H, Wolf PG. 2006. A classification for extant ferns. Taxon **55**, 705–731.

Sussmilch FC, Schultz J, Hedrich R, Roelfsema MRG. 2019. Acquiring control: the evolution of stomatal signalling pathways. Trends in Plant Science **24**, 342–351.

Thain JF. 1983. Curvature correction factors in the measurement of cell surface areas in plant tissues. Journal of Experimental Botany **34**, 87–94.

Tomás M, Medrano H, Pou A, Escalona JM, Martorell S, Ribas-Carbó M, Flexas J. 2012. Water-use efficiency in grapevine cultivars grown under controlled conditions: effects of water stress at the leaf and whole-plant level. Australian Journal of Grape and Wine Research **18**, 164-172.

Tomás M, Flexas J, Copolovici L, Galmés J, Hallik L, Medrano H, Ribas-Carbó M, Tosens T, Vislap V, Niinemets Ü. 2013. Importance of leaf anatomy in determining mesophyll diffusion conductance to CO_2 across species: Quantitative limitations and scaling up by models. Journal of Experimental Botany **64**, 2269–2281.

Tosens T, Niinemets LO, Vislap V, Eichelmann H, Castro P. 2012. Developmental changes

in mesophyll diffusion conductance and photosynthetic capacity under different light and water availabilities in Populus tremula: how structure constrains function. Plant, Cell and Environment **35**, 839–856.

Tosens T, Nishida K, Gago J, Coopman RE, Cabrera M, Carriqu M, Laanisto L, Morales L, Nadal M, Rojas R, *et al*. 2016. The photosynthetic capacity in 35 ferns and fern allies: mesophyll CO_2 diffusion as a key trait. New Phytologist **209**, 1576–1590.

Valentini R, Gamon JA, Field CB. 1995. Ecosystem gas exchange in a California grassland: seasonal patterns and implications for scaling. Ecology **76**, 1940–1952.

Verbancic J, Lunn JE, Stitt M, Persson S. 2018. Carbon supply and the regulation of cell wall synthesis. Molecular Plant **11**, 75–94.

Veromann-Jurgenson LL, Tosens T, Laanisto L, Niinemets Ü. 2017. Extremely thick cell walls and low mesophyll conductance: welcome to the world of ancient living! Journal of Experimental Botany **68**, 1639–1653.

Vital RG, Müller C, Freire FBS, Silva FB, Batista PF, Fuentes D, Rodrigues AA, Moura LMF, Daloso DM, Silva AA, *et al*. 2022. Metabolic, physiological and anatomical responses of soybean plants under water deficit and high temperature condition. Scientific Reports **12**, 16467.

Watkins JM, Chapman JM, Muday GK. 2017. Abscisic acid-induced reactive oxygen species are modulated by flavonols to control stomatal aperture. Plant Physiology **175**, 1807–1825.

Watkins JM, Hechler PJ, Muday GK, Carolina N. 2014. Ethylene-induced flavonol accumulation in guard cells suppresses reactive oxygen species and moderates stomatal aperture. Plant Physiology **164**, 1707–1717.

Xiong D, Douthe C, Flexas J. 2018. Differential coordination of stomatal conductance, mesophyll conductance, and leaf hydraulic conductance in response to changing light across species. Plant, Cell and Environment **41**, 436–450.

Yeoh H, Badger MR, Watson L. 1981. Variations in Kinetic Properties of Ribulose-1 , 5-bisphosphate Carboxylases among Plants. Plant Physiology **2**, 1151–1155.

Yiotis C, Evans-Fitzgerald C, McElwain JC. 2017. Differences in the photosynthetic plasticity of ferns and Ginkgo grown in experimentally controlled low $[O_2]$:$[CO_2]$ atmospheres may explain their contrasting ecological fate across the Triassic-Jurassic mass extinction boundary. Annals of Botany **119**, 1385–1395.

Yiotis C, McElwain JC. 2019. A novel hypothesis for the role of photosynthetic physiology in

shaping macroevolutionary patterns. Plant Physiology **181**, 1148–1162.

Zandalinas SI, Balfagón D, Gómez-Cadenas A, Mittler R. 2022. Plant responses to climate change: Metabolic changes under combined abiotic stresses. Journal of Experimental Botany **73**, 3339–3354.

Zhang X, Xu Y, Huang B. 2019. Lipidomic reprogramming associated with drought stress priming-enhanced heat tolerance in tall fescue (Festuca arundinacea). Plant, Cell and Environment **42**, 947–958.

Zhao J, Williams CC, Last RL. 1998. Induction of Arabidopsis tryptophan pathway enzymes and camalexin by amino acid starvation, oxidative stress, and an abiotic elicitor. The Plant Cell **10**, 359–370.

Zoong Lwe Z, Sah S, Persaud L, Li J, Gao W, Raja Reddy K, Narayanan S. 2021. Alterations in the leaf lipidome of Brassica carinata under high-temperature stress. BMC Plant Biology **21**, 1–15.

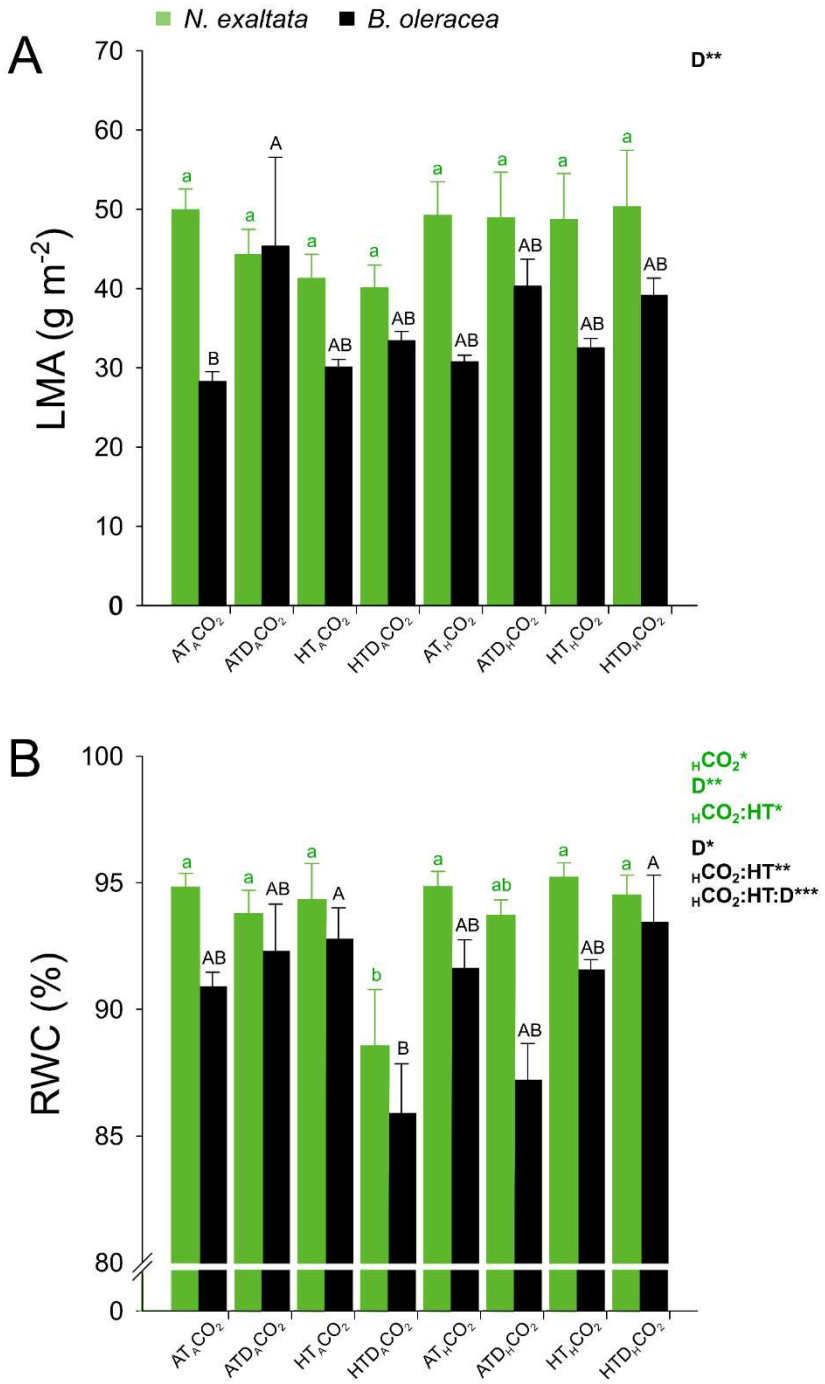

Fig. 1. Leaf mass per area (LMA) (A), and relative water content (RWC) (B) of *Nephrolepis exaltata* (fern) and *Brassica oleracea* (angiosperm) under different conditions, including ambient temperature (AT) or high temperature (HT), ambient CO_2 concentration ($_ACO_2$) or high CO_2 concentration ($_HCO_2$), drought (D) and combined conditions. Mean ± SE values are shown (n = 4–6). Different lowercase and uppercase letters indicate treatments that have significant difference in fern and cauliflower, respectively, by Tukey's test ($P < 0.05$). Significance in $_HCO_2$, HT, D treatments and $_HCO_2$:HT, $_HCO_2$:D, HT:D and $_HCO_2$:HT:D interactions are symbolized by: *$P < 0.05$; **$P < 0.01$; ***$P < 0.001$.

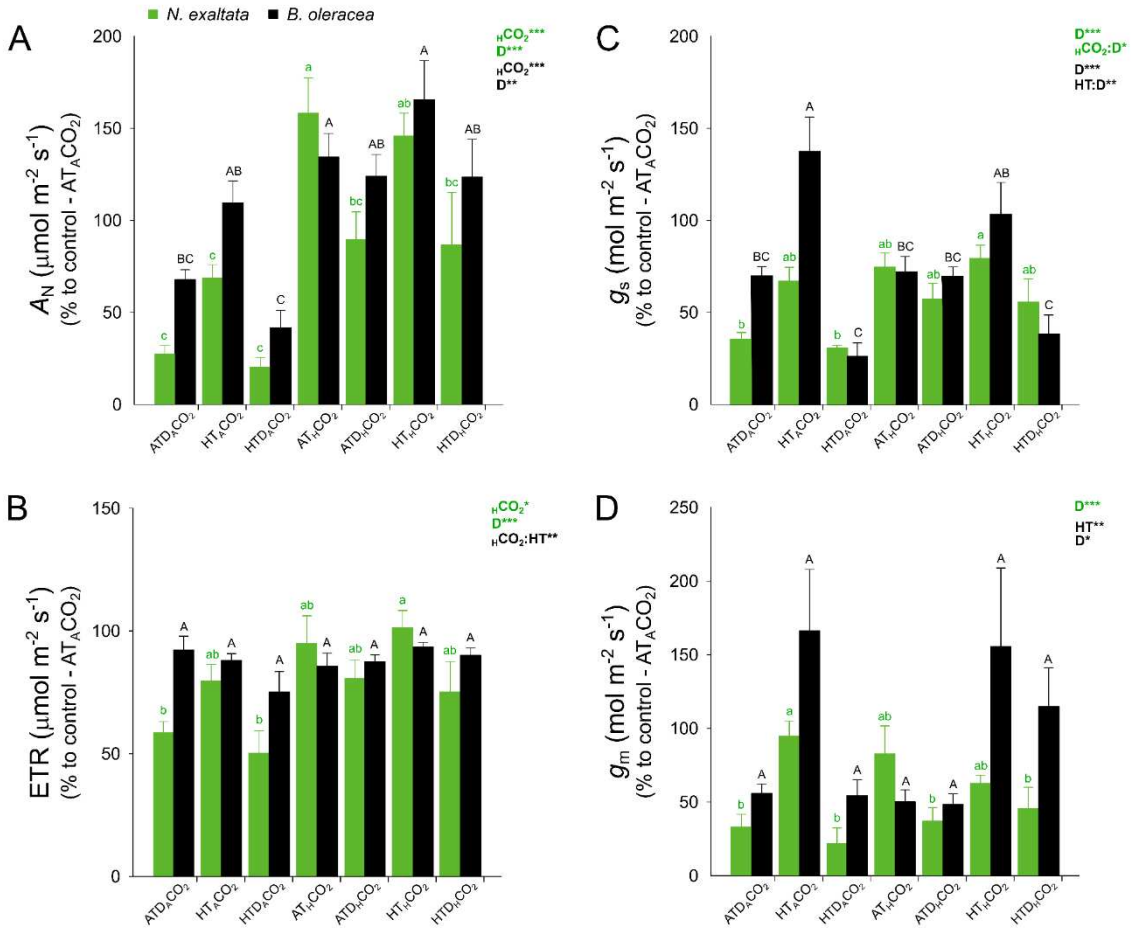

Fig. 2. Effects of stress treatments on the physiological parameters of *Nephrolepis exaltata* (fern) and *Brassica oleracea* (angiosperm). A, net photosynthetic rate (A_N), B, electron transport rate (ETR), C, stomatal conductance (g_s), and D, mesophyll conductance (g_m) under different conditions, including ambient temperature (AT) or high temperature (HT), ambient CO_2 concentration ($_ACO_2$) or high CO_2 concentration ($_HCO_2$), drought (D) and combined conditions. Data are presented as the mean percentage relative to control (AT_ACO_2) ± SE (n = 4–6). Different lowercase and uppercase letters indicate treatments that have significant difference in fern and cauliflower, respectively, by Tukey's test ($P < 0.05$). Significance in $_HCO_2$, HT, D treatments and $_HCO_2$:HT, $_HCO_2$:D, HT:D and $_HCO_2$:HT:D interactions are symbolized by: *$P <$ 0.05; **$P < 0.01$; ***$P < 0.001$.

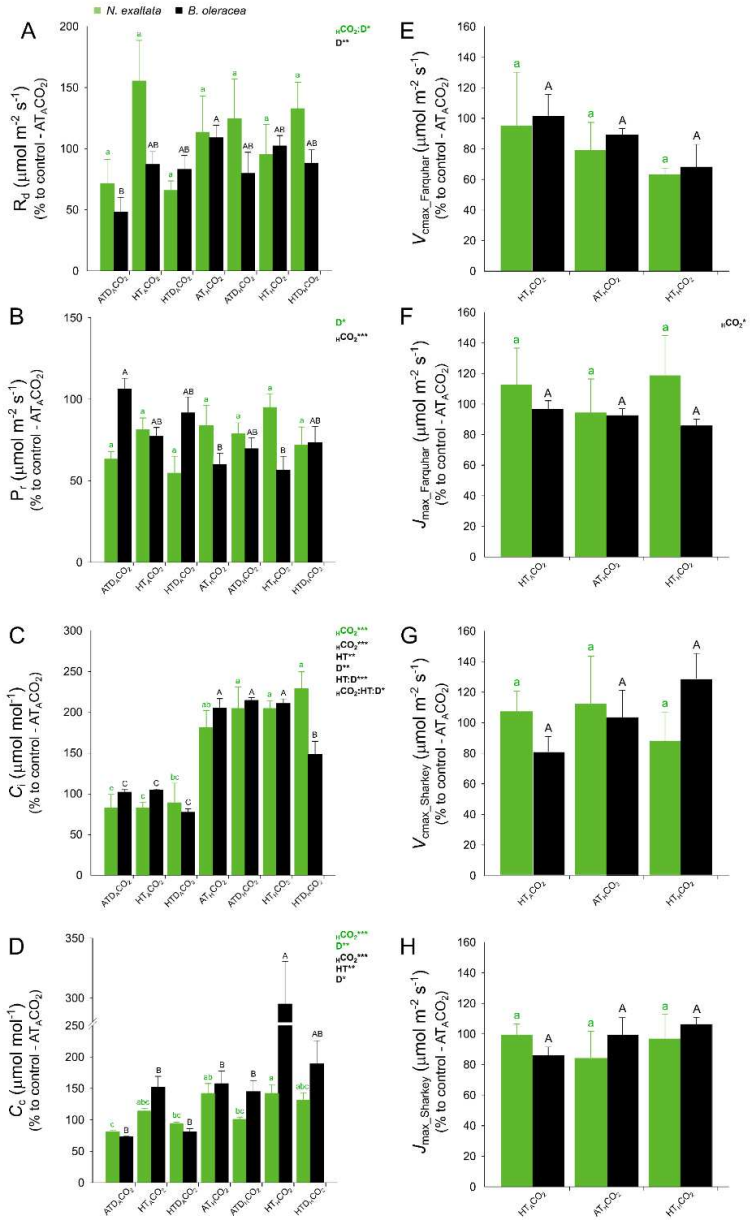

Fig. 3. Effects of stress treatments on the physiological parameters of *Nephrolepis exaltata* (fern) and *Brassica oleracea* (angiosperm) under different conditions, including ambient temperature (AT) or high temperature (HT), ambient CO_2 concentration ($_ACO_2$) or high CO_2 concentration ($_HCO_2$), drought (D) and combined conditions. A, dark respiration (R_d), B, photorespiration (P_r), C, sub-stomatal CO_2 concentration (C_i), D, chloroplastic CO_2 concentration (C_c), E, Maximum velocity of Rubisco carboxylation (V_{cmax}) and F, maximum electron transport rate (J_{max}) determined using curve-fitting method of Farhquar *et al*. (1980). G, Maximum velocity of Rubisco carboxylation (V_{cmax}) and H, maximum electron transport rate (J_{max}) determined using curve-fitting method of Sharkey *et al.* (2007). Data are presented as the mean percentage relative to control (AT_ACO_2) ± SE (n = 4–6). Different lowercase and uppercase letters indicate treatments that have significant difference in fern and cauliflower, respectively, by Tukey's test ($P < 0.05$). Significance in $_HCO_2$, HT, D treatments and $_HCO_2$:HT, $_HCO_2$:D, HT:D and $_HCO_2$:HT:D interactions are symbolized by: *$P < 0.05$; **$P < 0.01$; ***$P <$ 0.001.

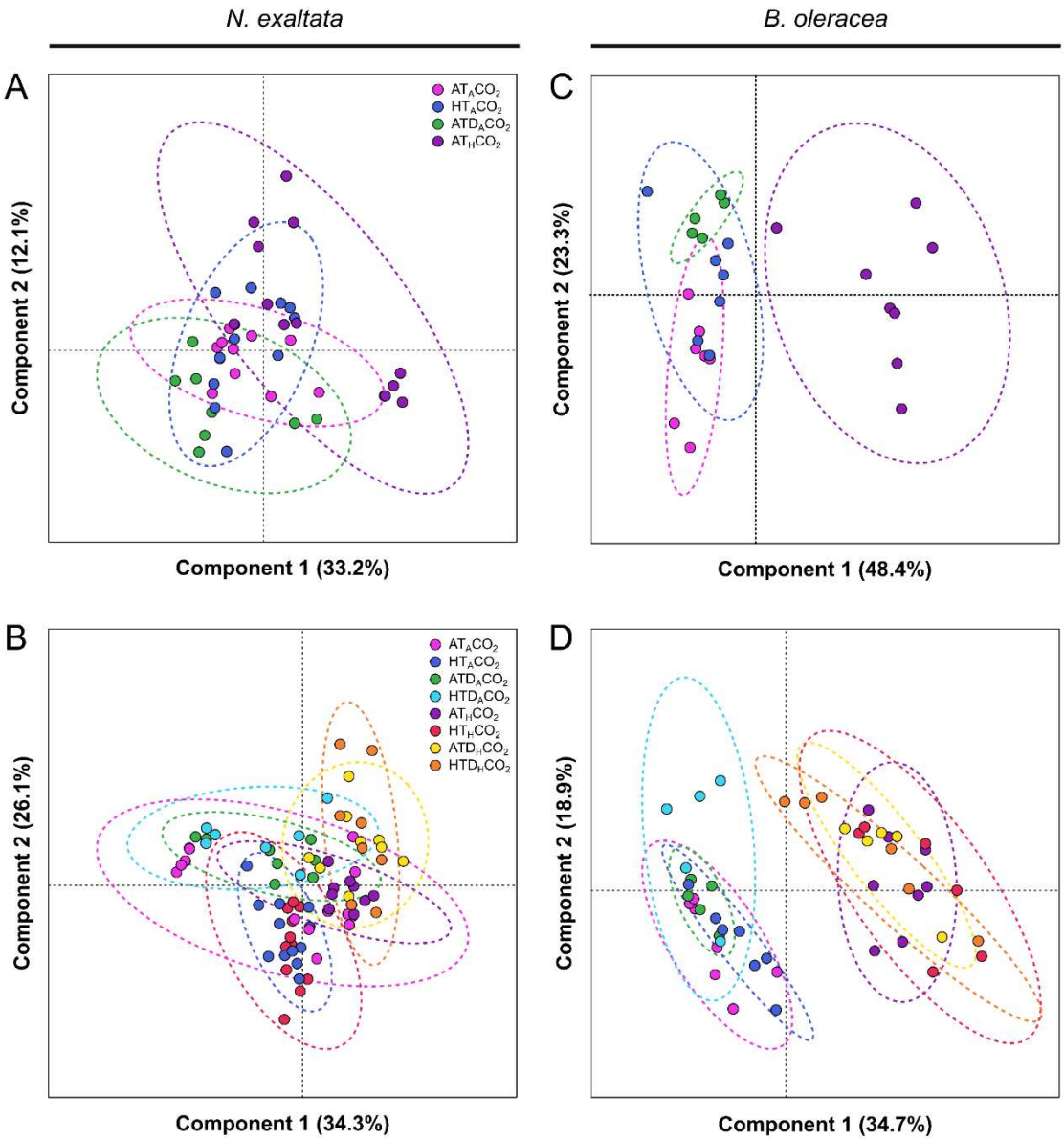

Fig. 4. Partial least square discriminant analysis (PLS-DA) using physiological data from *Nephrolepis exaltata* (fern) and *Brassica oleracea* (angiosperm) under different conditions, including ambient temperature (AT) or high temperature (HT), ambient CO_2 concentration ($_ACO_2$) or high CO_2 concentration ($_HCO_2$), drought (D) and combined conditions. A, PLS-DA using physiological data from fern leaves in optimum conditions and under single stress conditions. B, PLS-DA using physiological data from fern leaves under all treatment combinations. C, PLS-DA using physiological data from cauliflower leaves in optimum conditions and under single stress conditions. D, PLS-DA using physiological data from cauliflower leaves under all treatment combinations. The percentage variation explained by the components 1 and 2 is highlighted between parenthesis in each axis of each figure.

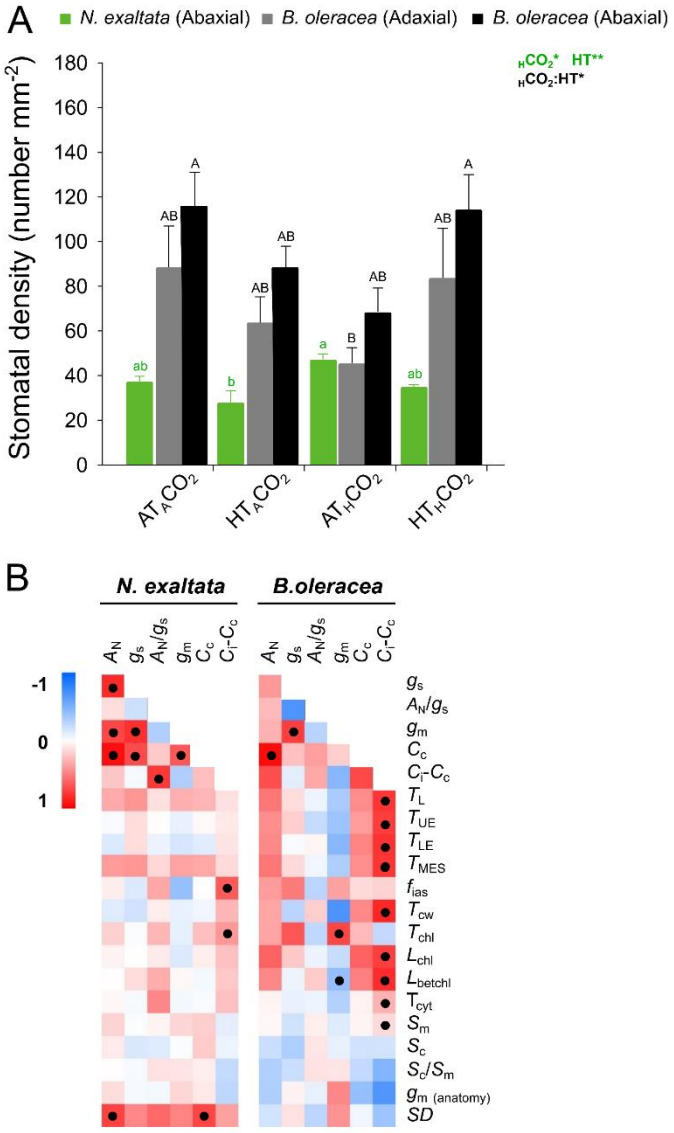

Fig. 5. Leaf anatomical characterization of *Nephrolepis exaltata* (fern) and *Brassica oleracea* (angiosperm) under different conditions, including ambient temperature (AT) or high temperature (HT), ambient CO_2 concentration ($_ACO_2$) or high CO_2 concentration ($_HCO_2$), and combined conditions. A, Stomatal density (*SD*) of abaxial and adaxial leaf epidermis. Mean ± SE values are shown (n = 4–6). Different lowercase and uppercase letters indicate treatments that have significant difference in fern and cauliflower, respectively, by Tukey's test ($P < 0.05$). Significance in $_HCO_2$, HT, D treatments and $_HCO_2$:HT, $_HCO_2$:D, HT:D and $_HCO_2$:HT:D interactions are symbolized by: *$P < 0.05$; **$P < 0.01$; ***$P < 0.001$. B, Fold-change heatmap of the relationship between physiological and leaf anatomical parameters. Significant correlations were represented with dots ($P < 0.05$). Physiological parameters: A_N, net photosynthetic rate, g_s, stomatal conductance, g_m, mesophyll conductance, C_i, sub-stomatal CO_2 concentration, and C_c, chloroplastic CO_2 concentration. Anatomical parameters: T_L, leaf thickness, T_{UE}, upper epidermis thickness, T_{LE}, lower epidermis thickness, T_{MES}, mesophyll thickness, f_{ias}, fraction of mesophyll intercellular air spaces, T_{cw}, cell wall thickness, T_{chl}, chloroplast thickness, L_{chl}, chloroplast length, L_{betch}, distance between chloroplasts, T_{cyt}, cytosol thickness, S_m, mesophyll area exposed to intercellular air spaces per area, S_c, chloroplast surface area exposed to intercellular air spaces per area, S_c/S_m, ratio between chloroplasts and mesophyll surface areas exposed to intercellular air spaces.

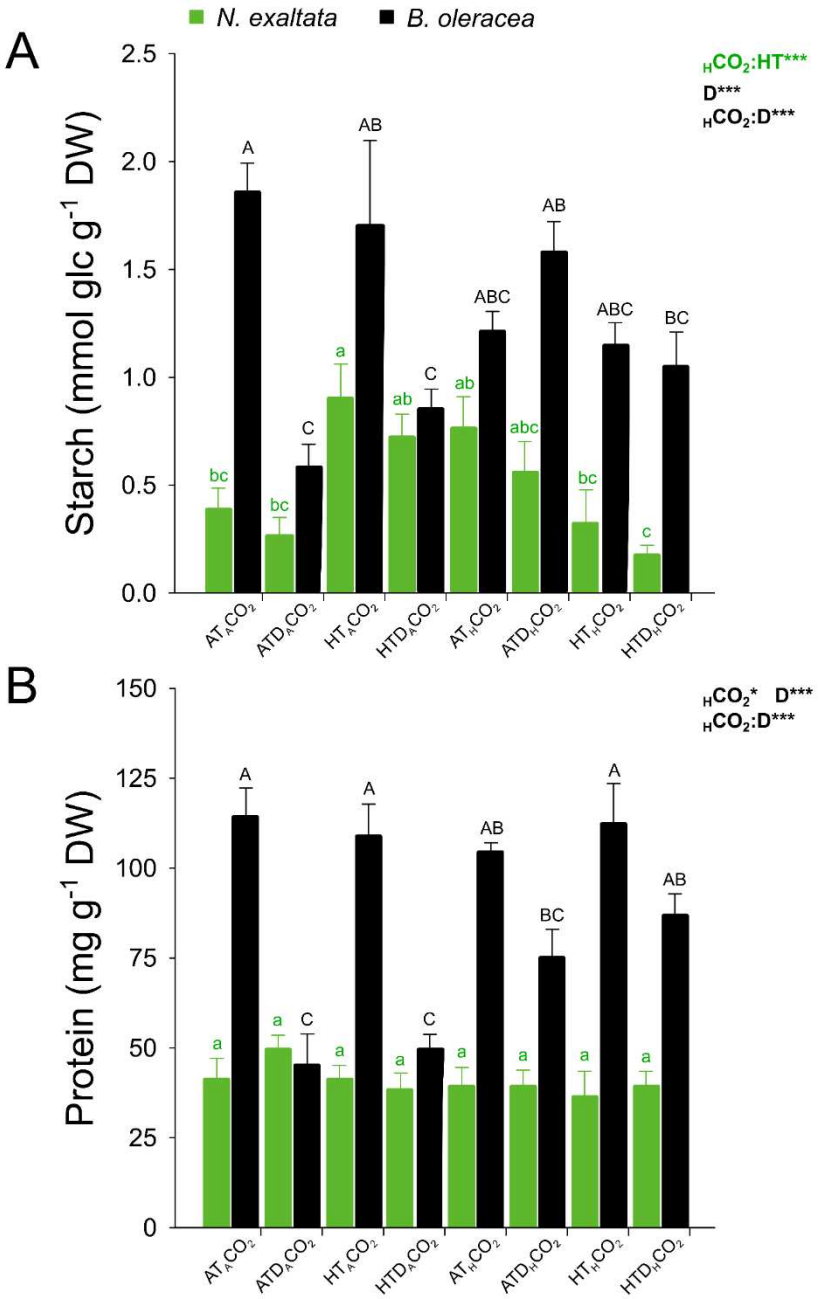

Fig. 6. Levels of starch (A) and protein (B) in *Nephrolepis exaltata* (fern) and *Brassica oleracea* (angiosperm) under different conditions, including ambient temperature (AT) or high temperature (HT), ambient CO_2 concentration ($_{A}CO_2$) or high CO_2 concentration ($_{H}CO_2$), drought (D) and combined conditions. Mean ± SE values are shown (n = 4–6). Different lowercase and uppercase letters indicate treatments that have significant difference in fern and cauliflower, respectively, by Tukey's test ($P < 0.05$). Significance in $_{H}CO_2$, HT, D treatments and $_{H}CO_2$:HT, $_{H}CO_2$:D, HT:D and $_{H}CO_2$:HT:D interactions are symbolized by: *$P < 0.05$; **$P < 0.01$; ***$P < 0.001$.

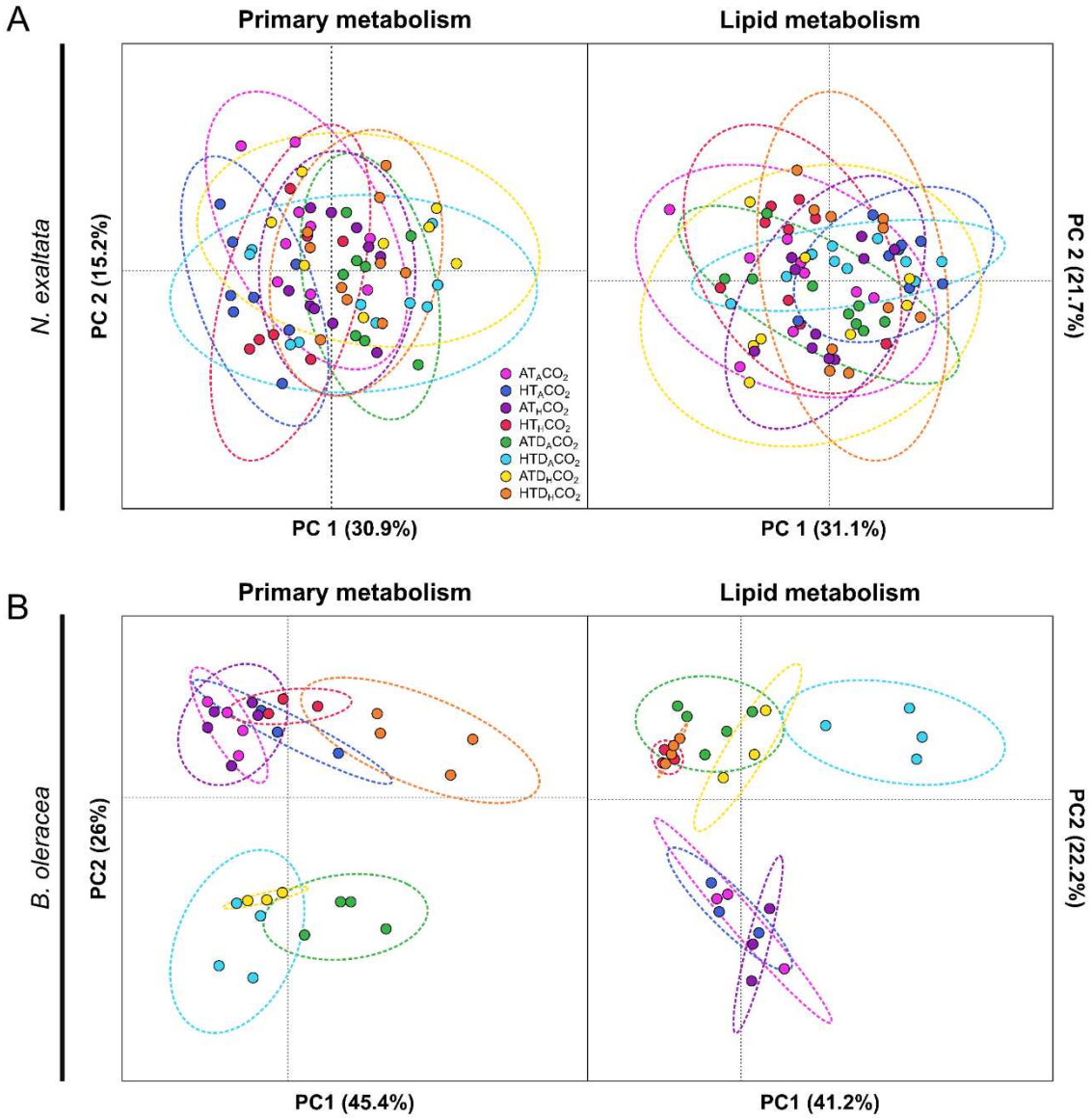

Fig. 7. Principal component analysis (PCA) using leaf metabolic and lipid levels data from *Nephrolepis exaltata* (fern) and *Brassica oleracea* (angiosperm) under different conditions, including ambient temperature (AT) or high temperature (HT), ambient CO_2 concentration ($_ACO_2$) or high CO_2 concentration ($_HCO_2$), drought (D) and combined conditions. A, PCA of the primary metabolites and all lipids differently accumulated under the different treatments imposed in the fern. B, PCA of the primary metabolites and all lipids differently accumulated under the different treatments imposed in cauliflower. The percentage variation explained by PC 1 and 2 is highlighted between parenthesis in each axis of each figure.

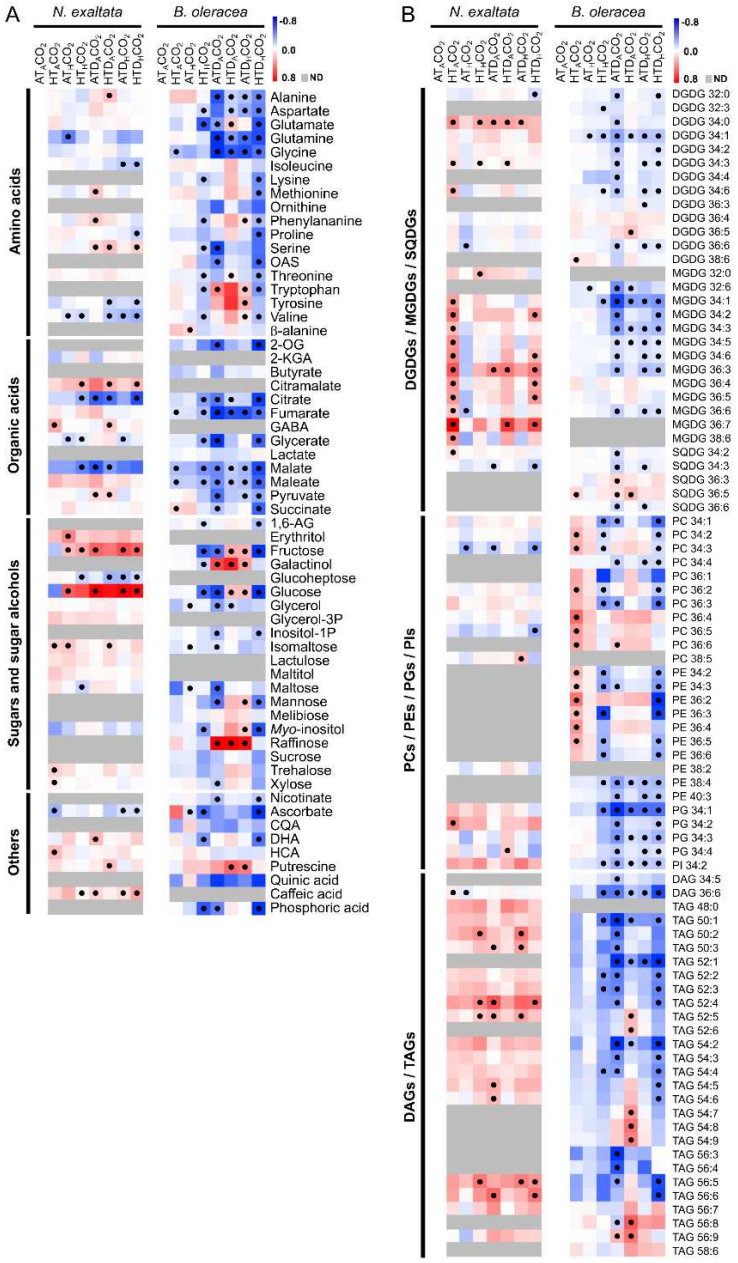

Fig. 8. Effects of different stress conditions on the metabolic and lipid levels in leaves of *Nephrolepis exaltata* (fern) and *Brassica oleracea* (angiosperm) under different conditions, including ambient temperature (AT) or high temperature (HT), ambient CO_2 concentration ($_{A}CO_2$) or high CO_2 concentration ($_{H}CO_2$), drought (D) and combined conditions. A, Profile of primary metabolites identified by GC-MS analysis. B, Profile of lipids identified by UPLC-MS analysis. Scales represent the log2 fold change relative to the control treatment (AT_ACO_2). Gray colour indicates metabolites or lipids no detected in the species. Dots mean significant differences by Student's *t*-test ($P < 0.05$). ND, no detected. Metabolites: CQA, caffeoylquinic acid; DHA, dehydroascorbate; GABA, gamma-aminobutyric acid; HCA, hydroxycinnamic acid; OAS, o-acetylserine; 1,6-AG, 1,6-anhydroglucose; 2-KGA, *2-ketogluconate*; 2-OG, 2-oxoglutarate. Lipids: DAG, diacylglycerol; DGDG, digalactosyl diacylglycerol; MGDG, monogalactosyl diacylglycerol; PC, phosphatidyl choline; PE, Phosphatidyl ethanolamine; PG, phosphatidyl glycerol; PI, phosphatidyl inositol; SQDG, sulfoquinovosyl diacylglycerol; TAG, triacylglycerol. Lipid names were describes as (number of carbons in the fatty acid chain):(number of double bonds in the fatty acid chain).

Table S1. Summary table for the data variables measured in *Nephrolepis exaltata* (fern) and *Brassica oleracea* (angiosperm) under different combinations of ambient temperature (AT) or high temperature (HT), ambient CO_2 concentration ($_ACO_2$) or high CO_2 concentration ($_HCO_2$) and drought (D). Mean ± SE values are shown (n = 4–6). Letters denote a significant difference ($P < 0.05$). LMA – leaf mass per area, RWC – relative water content, A_N – net photosynthetic rate, ETR – electron transport rate, g_s – stomatal conductance, g_m – mesophyll conductance, R_d – dark respiration, P_r – photorespiration, C_i – sub-stomatal CO_2 concentration, C_c - chloroplastic CO_2 concentration, V_{cmax} – maximum velocity of Rubisco carboxylation, J_{max} – maximum electron transport rate and *SD* – stomatal density.

N. exaltata

	AT_ACO_2	ATD_ACO_2	HT_ACO_2	HTD_ACO_2	AT_HCO_2	ATD_HCO_2	HT_HCO_2	HTD_HCO_2
LMA (g m^{-2})	49.95 ± 2.62^{a}	44.30 ± 3.19^{a}	41.25 ± 3.07^{a}	40.10 ± 2.85^{a}	49.25 ± 4.23^{a}	48.93 ± 5.76^{a}	48.70 ± 5.83^{a}	50.32 ± 7.13^{a}
RWC (%)	94.81 ± 0.56^{a}	93.75 ± 0.96^{a}	94.32 ± 1.44^{a}	88.53 ± 2.25^{b}	94.83 ± 0.62^{a}	93.69 ± 0.63^{ab}	95.20 ± 0.59^{a}	94.50 ± 0.80^{a}
A_N (μmol CO_2 m^{-2} s^{-1})	2.92 ± 0.36^{abc}	0.80 ± 0.13^{d}	2.00 ± 0.21^{cd}	0.59 ± 0.16^{d}	4.62 ± 0.55^{a}	2.61 ± 0.45^{bcd}	4.25 ± 0.36^{ab}	2.53 ± 0.83^{bcd}
ETR (μmol m^{-2} s^{-1})	91.43 ± 10.46^{a}	53.59 ± 4.06^{a}	72.80 ± 6.18^{a}	45.83 ± 8.40^{a}	86.64 ± 10.47^{a}	73.79 ± 6.91^{a}	92.54 ± 6.54^{a}	68.61 ± 11.44^{a}
g_s (mol m^{-2} s^{-1})	0.030 ± 0.003^{a}	0.010 ± 0.001^{c}	0.020 ± 0.002^{abc}	0.009 ± 0.000^{c}	0.022 ± 0.002^{abc}	0.017 ± 0.003^{bc}	0.024 ± 0.002^{ab}	0.016 ± 0.004^{bc}
g_m (mol m^{-2} s^{-1})	0.021 ± 0.004^{a}	0.007 ± 0.002^{b}	0.020 ± 0.002^{a}	0.005 ± 0.002^{b}	0.018 ± 0.004^{ab}	0.008 ± 0.002^{b}	0.013 ± 0.001^{ab}	0.010 ± 0.003^{ab}
R_d (μmol CO_2 m^{-2} s^{-1})	-0.51 ± 0.14^{a}	-0.37 ± 0.10^{a}	-0.79 ± 0.17^{a}	-0.34 ± 0.04^{a}	-0.58 ± 0.15^{a}	-0.64 ± 0.17^{a}	-0.49 ± 0.13^{a}	-0.68 ± 0.11^{a}
P_r (μmol m^{-2} s^{-1})	6.46 ± 0.77^{a}	4.08 ± 0.31^{a}	5.25 ± 0.46^{a}	3.53 ± 0.67^{a}	5.42 ± 0.80^{a}	5.08 ± 0.45^{a}	6.14 ± 0.53^{a}	4.63 ± 0.72^{a}
C_i (μmol mol^{-1})	190.76 ± 9.43^{b}	158.33 ± 30.77^{b}	157.84 ± 12.78^{b}	170.30 ± 44.93^{b}	345.19 ± 40.30^{a}	390.27 ± 50.61^{a}	390.44 ± 17.69^{a}	436.80 ± 39.09^{a}
C_c (μmol mol^{-1})	59.13 ± 1.62^{cd}	47.74 ± 0.58^{d}	67.34 ± 2.63^{abcd}	55.31 ± 1.70^{cd}	84.27 ± 9.01^{ab}	59.48 ± 2.29^{bcd}	84.31 ± 7.97^{a}	77.46 ± 7.06^{abc}
V_{cmax} Farquhar (μmol m^{-2} s^{-1})	114.86 ± 15.49^{a}		109.17 ± 40.27^{a}		90.98 ± 20.81^{a}		72.97 ± 4.45^{a}	
J_{max} Farquhar (μmol m^{-2} s^{-1})	78.33 ± 4.99^{a}		88.33 ± 18.68^{a}		74.01 ± 17.19^{a}		93.06 ± 20.41^{a}	
V_{cmax} Sharkey (μmol m^{-2} s^{-1})	59.55 ± 4.67^{a}		64.00 ± 7.86^{a}		66.97 ± 18.60^{a}		52.41 ± 11.29^{a}	
J_{max} Sharkey (μmol m^{-2} s^{-1})	77.21 ± 8.61^{a}		76.71 ± 5.49^{a}		65.36 ± 13.16^{a}		74.66 ± 12.59^{a}	
SD Abaxial (number mm^{-2})	36.90 ± 2.82^{ab}		33.33 ± 4.55^{b}		46.83 ± 2.33^{a}		34.92 ± 1.07^{ab}	
Starch (mmol glc g^{-1} DW)	0.39 ± 0.09^{bc}	0.27 ± 0.08^{bc}	0.91 ± 0.15^{a}	0.73 ± 0.10^{ab}	0.77 ± 0.14^{ab}	0.56 ± 0.14^{abc}	0.33 ± 0.15^{bc}	0.18 ± 0.05^{c}
Protein (mg g^{-1} DW)	41.69 ± 5.39^{a}	49.86 ± 3.65^{a}	41.33 ± 3.82^{a}	38.75 ± 4.27^{a}	39.81 ± 4.77^{a}	39.40 ± 4.41^{a}	36.60 ± 6.93^{a}	39.47 ± 4.01^{a}

B. oleracea

	AT_ACO_2	ATD_ACO_2	HT_ACO_2	HTD_ACO_2	AT_HCO_2	ATD_HCO_2	HT_HCO_2	HTD_HCO_2
LMA (g m^{-2})	28.27 ± 1.24^{b}	45.36 ± 11.22^{a}	30.07 ± 0.99^{ab}	33.43 ± 1.16^{ab}	30.74 ± 0.87^{ab}	40.30 ± 3.41^{ab}	32.51 ± 1.20^{ab}	39.14 ± 2.18^{ab}
RWC (%)	90.88 ± 0.58^{ab}	92.27 ± 1.89^{ab}	92.75 ± 1.26^{a}	85.88 ± 1.97^{b}	91.59 ± 1.15^{ab}	87.18 ± 1.49^{ab}	91.55 ± 0.42^{ab}	93.41 ± 1.90^{a}
A_N (μmol CO_2 m^{-2} s^{-1})	19.43 ± 1.39^{bcd}	13.17 ± 1.05^{cd}	21.27 ± 2.31^{bcd}	8.11 ± 1.82^{d}	26.11 ± 2.49^{ab}	24.06 ± 2.34^{abc}	32.17 ± 4.13^{a}	23.99 ± 4.00^{abc}
ETR (μmol m^{-2} s^{-1})	238.74 ± 9.56^{a}	219.91 ± 13.82^{ab}	210.26 ± 6.39^{ab}	179.36 ± 19.94^{b}	204.07 ± 13.04^{ab}	209.00 ± 6.47^{ab}	223.08 ± 4.56^{ab}	214.98 ± 7.25^{ab}
g_s (mol m^{-2} s^{-1})	0.41 ± 0.05^{a}	0.29 ± 0.02^{ab}	0.57 ± 0.08^{a}	0.11 ± 0.03^{b}	0.30 ± 0.04^{ab}	0.29 ± 0.02^{ab}	0.42 ± 0.07^{a}	0.16 ± 0.04^{b}
g_m (mol m^{-2} s^{-1})	0.11 ± 0.01^{a}	0.06 ± 0.01^{a}	0.18 ± 0.05^{a}	0.06 ± 0.01^{a}	0.06 ± 0.01^{a}	0.05 ± 0.01^{a}	0.17 ± 0.06^{a}	0.13 ± 0.03^{a}
R_d (μmol CO_2 m^{-2} s^{-1})	-1.74 ± 0.13^{ab}	-0.84 ± 0.21^{b}	-1.51 ± 0.19^{ab}	-1.45 ± 0.20^{ab}	-1.86 ± 0.18^{a}	-1.39 ± 0.30^{ab}	-1.78 ± 0.15^{a}	-1.53 ± 0.19^{ab}
P_r (μmol m^{-2} s^{-1})	12.84 ± 1.04^{a}	13.65 ± 0.82^{a}	9.93 ± 0.69^{ab}	11.76 ± 1.25^{ab}	7.67 ± 0.91^{b}	8.93 ± 0.87^{ab}	7.27 ± 1.07^{b}	9.41 ± 1.28^{ab}
C_i (μmol mol^{-1})	289.12 ± 4.06^{c}	294.20 ± 9.01^{c}	301.05 ± 4.48^{c}	222.92 ± 12.36^{c}	593.12 ± 32.98^{a}	619.54 ± 10.00^{a}	609.11 ± 16.55^{a}	428.26 ± 46.67^{b}
C_c (μmol mol^{-1})	108.21 ± 10.87^{b}	78.70 ± 1.28^{b}	164.82 ± 18.25^{b}	87.57 ± 5.42^{b}	170.59 ± 21.65^{b}	156.55 ± 19.26^{b}	319.12 ± 62.09^{a}	204.85 ± 39.77^{ab}
V_{cmax} Farquhar (μmol m^{-2} s^{-1})	295.67 ± 14.17^{a}		299.25 ± 42.81^{a}		263.15 ± 12.97^{a}		201.43 ± 43.61^{a}	
J_{max} Farquhar (μmol m^{-2} s^{-1})	256.95 ± 3.61^{a}		249.10 ± 13.35^{a}		237.70 ± 11.39^{a}		220.11 ± 11.56^{a}	
V_{cmax} Sharkey (μmol m^{-2} s^{-1})	197.77 ± 25.30^{a}		160.27 ± 19.47^{a}		204.20 ± 35.57^{a}		255.06 ± 32.18^{a}	
J_{max} Sharkey (μmol m^{-2} s^{-1})	228.80 ± 14.44^{a}		196.26 ± 13.06^{a}		227.80 ± 25.61^{a}		243.00 ± 10.78^{a}	
SD Adaxial (number mm^{-2})	88.10 ± 18.88^{ab}		63.49 ± 11.49^{b}		45.24 ± 6.71^{ab}		83.33 ± 22.56^{ab}	
SD Abaxial (number mm^{-2})	115.87 ± 15.19^{a}		88.10 ± 9.74^{ab}		68.25 ± 10.48^{ab}		114.29 ± 15.75^{a}	
Starch (mmol glc g^{-1} DW)	1.87 ± 0.13^{a}	0.59 ± 0.10^{c}	1.71 ± 0.39^{ab}	0.86 ± 0.09^{c}	1.22 ± 0.09^{abc}	1.59 ± 0.13^{ab}	1.15 ± 0.10^{abc}	1.06 ± 0.16^{bc}
Protein (mg g^{-1} DW)	114.80 ± 7.52^{a}	45.53 ± 8.35^{c}	109.32 ± 8.50^{a}	49.67 ± 4.15^{c}	101.72 ± 3.59^{ab}	75.26 ± 7.74^{bc}	112.86 ± 10.64^{a}	87.03 ± 5.81^{ab}

Table S2. Three-way ANOVA summary table for the data variables measured in *Nephrolepis exaltata* (fern) and *Brassica oleracea* (angiosperm) under different combinations of ambient temperature (AT) or high temperature (HT), ambient CO_2 concentration ($_ACO_2$) or high CO_2 concentration ($_HCO_2$) and drought (D). Bold and underlined values indicate significant influence ($P < 0.05$). LMA – leaf mass per area, RWC – relative water content, A_N – net photosynthetic rate, ETR – electron transport rate, g_s – stomatal conductance, g_m – mesophyll conductance, R_d – dark respiration, P_r – photorespiration, C_i – sub-stomatal CO_2 concentration, C_c - chloroplastic CO_2 concentration, V_{cmax} – maximum velocity of Rubisco carboxylation, J_{max} – maximum electron transport rate and *SD* – stomatal density.

N. exaltata							
	$_HCO_2$	HT	D	$_HCO_2$:HT	$_HCO_2$:D	HT:D	$_HCO_2$:HT:D
LMA (g m^{-2})	0.102	0.359	0.675	0.296	0.536	0.623	0.844
RWC (%)	**0.028**	0.142	**0.006**	**0.027**	0.105	0.165	0.095
A_N mol CO_2 m^{-2} s^{-1})	**<0.001**	0.248	**<0.001**	0.614	0.878	0.466	0.758
ETR mol m^{-2} s^{-1})	**0.031**	0.330	**<0.001**	0.304	0.288	0.993	0.405
g_s mol m^{-2} s^{-1})	0.233	0.213	**<0.001**	0.148	**0.035**	0.426	0.221
g_m mol m^{-2} s^{-1})	0.597	0.516	**<0.001**	0.902	0.073	0.594	0.418
R_d mol CO_2 m^{-2} s^{-1})	0.357	0.620	0.380	0.454	**0.040**	0.657	0.271
P_r mol m^{-2} s^{-1})	0.310	0.441	**0.003**	0.292	0.240	0.788	0.342
C_i mol mol^{-1})	**<0.001**	0.437	0.433	0.218	0.223	0.612	0.632
C_c mol mol^{-1})	**<0.001**	0.055	**0.002**	0.897	0.635	0.320	0.286
V_{cmax} Farquhar mol m^{-2} s^{-1})	0.206	0.610		0.791			
J_{max} Farquhar mol m^{-2} s^{-1})	0.991	0.437		0.807			
V_{cmax} Sharkey mol m^{-2} s^{-1})	0.679	0.505		0.564			
J_{max} Sharkey mol m^{-2} s^{-1})	0.434	0.726		0.562			
SD Abaxial (number mm^{-2})	**0.012**	**0.002**		0.673			
Starch (mmol glc g^{-1} DW)	0.162	0.668	0.052	**<0.001**	0.870	0.989	0.725
Protein (mg g^{-1} DW)	0.222	0.274	0.545	0.531	0.814	0.574	0.293
B. oleracea							
	$_HCO_2$	HT	D	$_HCO_2$:HT	$_HCO_2$:D	HT:D	$_HCO_2$:HT:D
LMA (g m^{-2})	0.593	0.364	**0.001**	0.306	0.683	0.116	0.302
RWC (%)	0.610	0.659	**0.040**	**0.008**	0.439	0.599	**<0.001**
A_N mol CO_2 m^{-2} s^{-1})	**<0.001**	0.912	**0.001**	0.176	0.377	0.178	0.877
ETR mol m^{-2} s^{-1})	0.825	0.153	0.146	**0.005**	0.204	0.520	0.896
g_s mol m^{-2} s^{-1})	0.390	0.505	**<0.001**	0.559	0.171	**0.003**	0.986
g_m mol m^{-2} s^{-1})	0.910	**0.009**	**0.023**	0.127	0.200	0.230	0.810
R_d mol CO_2 m^{-2} s^{-1})	0.074	0.472	**0.005**	0.533	0.705	0.063	0.312
P_r mol m^{-2} s^{-1})	**<0.001**	0.139	0.064	0.126	0.705	0.617	0.933
C_i mol mol^{-1})	**<0.001**	**0.001**	**0.007**	0.139	0.138	**<0.001**	**0.041**
C_c mol mol^{-1})	**<0.001**	**0.006**	**0.013**	0.104	0.697	0.120	0.455
V_{cmax} Farquhar mol m^{-2} s^{-1})	0.062	0.384		0.330			
J_{max} Farquhar mol m^{-2} s^{-1})	**0.031**	0.231		0.640			
V_{cmax} Sharkey mol m^{-2} s^{-1})	0.096	0.819		0.143			
J_{max} Sharkey mol m^{-2} s^{-1})	0.192	0.614		0.174			
SD Adaxial (number mm^{-2})	0.485	0.681		0.067			
SD Abaxial (number mm^{-2})	0.422	0.493		**0.010**			
Starch (mmol glc g^{-1} DW)	0.987	0.286	**<0.001**	0.128	**<0.001**	0.929	0.055
Protein (mg g^{-1} DW)	**0.010**	0.312	**<0.001**	0.256	**<0.001**	0.628	0.671

Table S3. Discrimination against $^{13}CO_2$ measured in *Nephrolepis exaltata* (fern) and *Brassica oleracea* (angiosperm) under different combinations of ambient temperature (AT) or high temperature (HT), ambient CO_2 concentration ($_ACO_2$) or high CO_2 concentration ($_HCO_2$) and drought (D). Mean ± SE values are shown (n = 4–6). Letters denote a significant difference ($P < 0.05$). Each variable effect for the ^{13}C isotope discrimination were quantified by Three-way ANOVA. Bold and underlined values indicate significant influence ($P < 0.05$).

Treatments	***N. exaltata***	***B. oleracea***
AT_ACO_2	17.00 ± 0.02^c	24.80 ± 0.03^d
ATD_ACO_2	18.25 ± 0.02^b	24.47 ± 0.04^e
HT_ACO_2	18.01 ± 0.11^b	24.55 ± 0.06^e
HTD_ACO_2	18.07 ± 0.07^b	24.20 ± 0.03^f
AT_HCO_2	18.95 ± 0.08^a	28.19 ± 0.03^a
ATD_HCO_2	14.92 ± 0.09^e	26.79 ± 0.03^c
HT_HCO_2	16.32 ± 0.03^d	27.59 ± 0.02^b
HTD_HCO_2	16.56 ± 0.01^d	27.47 ± 0.05^b
$_HCO_2$	**<0.001**	**<0.001**
HT	**0.009**	**<0.001**
D	**<0.001**	**<0.001**
$_HCO_2$:HT	**<0.001**	**0.005**
$_HCO_2$:D	**<0.001**	**<0.001**
HT:D	**<0.001**	**<0.001**
$_HCO_2$:HT:D	**<0.001**	**<0.001**

Table S4. Leaf anatomical parameters measured from light and electron microscopic images of semi-thin and ultra-thin sections of *Nephrolepis exaltata* (fern) and *Brassica oleracea* (angiosperm) under different combinations of ambient temperature (AT) or high temperature (HT), ambient CO_2 concentration ($_ACO_2$) or high CO_2 concentration ($_HCO_2$) and drought (D). Mean ± SE values are shown (n = 4–6). Letters denote a significant difference ($P < 0.05$). T_L, leaf thickness, T_{UE}, upper epidermis thickness, T_{LE}, lower epidermis thickness, T_{MES}, mesophyll thickness, T_{MES_pal}, palisade mesophyll thickness, T_{MES_spo}, spongy mesophyll thickness, f_{ias}, fraction of mesophyll intercellular air spaces, T_{cw}, cell wall thickness, T_{chl}, chloroplast thickness, L_{chl}, chloroplast length, L_{betch}, distance between chloroplasts, T_{cyt}, cytosol thickness, S_m, mesophyll area exposed to intercellular air spaces per area, S_c, chloroplast surface area exposed to intercellular air spaces per area, S_c/S_m, ratio between chloroplasts and mesophyll surface areas exposed to intercellular air spaces.

N. exaltata

	AT_ACO_2	ATD_ACO_2	HT_ACO_2	HTD_ACO_2	AT_HCO_2	ATD_HCO_2	HT_HCO_2	HTD_HCO_2
T_L (µm)	134.98 ± 9.32^a	114.75 ± 8.22^a	105.28 ± 9.84^a	98.80 ± 8.53^a	120.23 ± 10.02^a	115.15 ± 10.72^a	120.56 ± 8.61^a	124.57 ± 8.58^a
T_{UE} (µm)	23.91 ± 1.55^a	18.89 ± 1.54^{ab}	16.60 ± 1.15^b	15.07 ± 1.30^b	17.85 ± 1.17^{ab}	20.11 ± 2.22^{ab}	18.33 ± 1.35^{ab}	20.09 ± 1.69^{ab}
T_{LE} (µm)	20.20 ± 1.82^a	15.81 ± 1.57^a	15.93 ± 1.18^a	15.87 ± 0.66^a	15.52 ± 1.07^a	18.16 ± 2.01^a	15.99 ± 0.97^a	17.06 ± 1.65^a
T_{MES} (µm)	91.60 ± 6.56^a	79.36 ± 5.59^a	73.80 ± 8.63^a	69.52 ± 8.12^a	86.13 ± 9.72^a	79.36 ± 8.03^a	87.10 ± 7.29^a	87.47 ± 6.74^a
f_{ias} (%)	13.89 ± 1.61^{ab}	17.58 ± 2.56^{ab}	12.22 ± 1.87^b	12.89 ± 2.21^{ab}	15.68 ± 1.23^{ab}	17.44 ± 2.28^{ab}	21.67 ± 1.78^a	19.51 ± 1.94^{ab}
T_{cw} (µm)	0.16 ± 0.03^a	0.17 ± 0.01^a	0.22 ± 0.02^a	0.19 ± 0.02^a	0.18 ± 0.01^a	0.27 ± 0.05^a	0.23 ± 0.01^a	0.19 ± 0.02^a
T_{chl} (µm)	3.50 ± 0.50^{ab}	2.87 ± 0.42^{ab}	2.46 ± 0.22^b	3.04 ± 0.28^{ab}	3.67 ± 0.51^{ab}	4.83 ± 0.24^a	3.75 ± 0.15^{ab}	3.53 ± 0.21^{ab}
L_{chl} (µm)	7.16 ± 0.48^a	6.87 ± 0.60^a	5.78 ± 0.34^a	5.55 ± 0.34^a	6.21 ± 0.47^a	7.44 ± 0.11^a	7.33 ± 0.32^a	6.73 ± 0.38^a
L_{betchl} (µm)	1.68 ± 0.19^a	1.27 ± 0.14^a	1.09 ± 0.10^a	1.35 ± 0.17^a	1.34 ± 0.43^a	1.01 ± 0.21^a	1.42 ± 0.19^a	1.83 ± 0.42^a
T_{cyt} (µm)	0.16 ± 0.03^{ab}	0.19 ± 0.02^{ab}	0.20 ± 0.02^{ab}	0.23 ± 0.03^{ab}	0.15 ± 0.02^{ab}	0.13 ± 0.02^b	0.27 ± 0.02^{ab}	0.28 ± 0.04^a
S_m (µm)	16.68 ± 1.66^a	18.20 ± 2.15^a	11.03 ± 1.22^a	14.66 ± 2.82^a	17.41 ± 0.94^a	17.26 ± 1.10^a	16.66 ± 0.44^a	15.40 ± 0.57^a
S_c (µm)	8.71 ± 0.87^a	11.91 ± 1.69^a	7.47 ± 0.73^a	7.39 ± 1.30^a	9.82 ± 1.07^a	11.52 ± 0.56^a	10.85 ± 0.65^a	8.73 ± 1.40^a
S_c/S_m (µm)	0.53 ± 0.03^a	0.66 ± 0.04^a	0.69 ± 0.02^a	0.52 ± 0.03^a	0.60 ± 0.07^a	0.67 ± 0.02^a	0.65 ± 0.04^a	0.56 ± 0.08^a
$g_{m\_anatomy}$	65.74 ± 5.18^a	97.68 ± 9.74^a	54.50 ± 6.33^a	80.49 ± 14.79^a	89.21 ± 6.10^a	66.69 ± 4.04^a	73.45 ± 2.33^a	72.43 ± 2.62^a

B. oleracea

	AT_ACO_2	ATD_ACO_2	HT_ACO_2	HTD_ACO_2	AT_HCO_2	ATD_HCO_2	HT_HCO_2	HTD_HCO_2
T_L (µm)	252.12 ± 17.63^a	323.64 ± 28.13^a	223.33 ± 24.71^a	177.62 ± 13.33^a	310.87 ± 69.89^a	350.94 ± 32.35^a	315.96 ± 24.67^a	240.79 ± 40.32^a
T_{UE} (µm)	20.82 ± 1.82^a	29.82 ± 2.67^a	20.41 ± 2.85^a	15.89 ± 2.12^a	31.15 ± 7.43^a	31.29 ± 2.95^a	28.28 ± 3.03^a	17.28 ± 1.55^a
T_{LE} (µm)	14.90 ± 0.78^a	20.97 ± 1.93^a	16.04 ± 1.21^a	15.06 ± 1.45^a	21.00 ± 4.45^a	21.08 ± 0.65^a	21.20 ± 0.75^a	16.65 ± 2.55^a
T_{MES_pal} (µm)	103.78 ± 11.02^a	133.68 ± 19.70^a	89.94 ± 15.79^a	70.25 ± 9.61^a	145.11 ± 41.40^a	153.76 ± 18.27^a	139.80 ± 22.63^a	105.28 ± 23.85^a
T_{MES_spo} (µm)	108.98 ± 7.20^{ab}	138.07 ± 9.65^{ab}	99.00 ± 13.70^{ab}	73.61 ± 3.92^b	111.70 ± 19.04^{ab}	155.35 ± 17.05^a	124.19 ± 5.30^{ab}	99.66 ± 13.36^{ab}
T_{MES} (µm)	212.76 ± 16.86^a	271.74 ± 24.91^a	188.94 ± 28.28^a	143.86 ± 13.52^a	256.81 ± 59.75^a	309.11 ± 25.57^a	264.00 ± 20.29^a	204.94 ± 37.19^a
f_{ias} (%)	26.88 ± 1.41^a	25.90 ± 1.28^a	23.19 ± 2.74^a	15.20 ± 2.36^a	21.35 ± 1.95^a	25.43 ± 4.89^a	22.37 ± 1.89^a	23.24 ± 2.98^a
T_{cw} (µm)	0.08 ± 0.01^b	0.14 ± 0.01^{ab}	0.10 ± 0.01^b	0.13 ± 0.01^{ab}	0.18 ± 0.00^a	0.18 ± 0.01^a	0.17 ± 0.01^a	0.11 ± 0.02^b
T_{chl} (µm)	2.59 ± 0.22^a	2.71 ± 0.31^a	2.99 ± 0.35^a	2.45 ± 0.12^a	2.75 ± 0.39^a	2.40 ± 0.01^a	2.71 ± 0.08^a	2.68 ± 0.11^a
L_{chl} (µm)	6.03 ± 0.03^{ab}	7.70 ± 0.10^{ab}	6.52 ± 0.57^{ab}	5.44 ± 0.13^b	7.58 ± 0.65^{ab}	7.93 ± 0.42^{ab}	8.52 ± 0.13^a	6.22 ± 0.89^{ab}
L_{betchl} (µm)	0.40 ± 0.15^a	0.55 ± 0.18^a	0.61 ± 0.04^a	0.56 ± 0.00^a	0.81 ± 0.37^a	1.79 ± 1.11^a	1.10 ± 0.22^a	0.68 ± 0.27^a
T_{cyt} (µm)	0.19 ± 0.06^a	0.39 ± 0.09^a	0.25 ± 0.02^a	0.23 ± 0.01^a	0.22 ± 0.06^a	0.34 ± 0.08^a	0.33 ± 0.07^a	0.26 ± 0.06^a
S_m (µm)	50.73 ± 2.06^a	53.54 ± 4.22^a	38.58 ± 5.26^a	43.57 ± 2.81^a	38.04 ± 0.00^a	51.51 ± 6.57^a	54.34 ± 2.11^a	48.62 ± 3.79^a
S_c (µm)	36.86 ± 0.67^a	41.10 ± 3.63^a	29.37 ± 4.79^a	33.97 ± 2.10^a	29.98 ± 0.00^a	33.11 ± 7.18^a	38.21 ± 2.15^a	37.14 ± 2.29^a
S_c/S_m (µm)	0.73 ± 0.03^a	0.77 ± 0.04^a	0.75 ± 0.03^a	0.78 ± 0.00^a	0.79 ± 0.00^a	0.63 ± 0.05^a	0.73 ± 0.03^a	0.77 ± 0.04^a
$g_{m\_anatomy}$	268.91 ± 2.99^a	215.74 ± 13.29^{ab}	200.95 ± 26.11^{ab}	208.48 ± 4.73^{ab}	173.46 ± 0.00^b	174.65 ± 5.46^b	194.97 ± 9.03^{ab}	230.32 ± 12.54^{ab}

Table S5. Three-way ANOVA summary table for the anatomical data measured in *Nephrolepis exaltata* (fern) and *Brassica oleracea* (angiosperm) under different combinations of ambient temperature (AT) or high temperature (HT), ambient CO_2 concentration ($_ACO_2$) or high CO_2 concentration ($_HCO_2$) and drought (D). Bold and underlined values indicate significant influence ($P < 0.05$). T_L, leaf thickness, T_{UE}, upper epidermis thickness, T_{LE}, lower epidermis thickness, T_{MES}, mesophyll thickness, T_{MES_pal}, palisade mesophyll thickness, T_{MES_spo}, spongy mesophyll thickness, f_{ias}, fraction of mesophyll intercellular air spaces, T_{cw}, cell wall thickness, T_{chl}, chloroplast thickness, L_{chl}, chloroplast length, L_{betch}, distance between chloroplasts, T_{cyt}, cytosol thickness, S_m, mesophyll area exposed to intercellular air spaces per area, S_c, chloroplast surface area exposed to intercellular air spaces per area, S_c/S_m, ratio between chloroplasts and mesophyll surface areas exposed to intercellular air spaces.

N. exaltata

	$_HCO_2$	HT	D	$_HCO_2$:HT	$_HCO_2$:D	HT:D	$_HCO_2$:HT:D
T_L (µm)	0.335	0.196	0.316	**0.048**	0.354	0.409	0.866
T_{UE} (µm)	0.656	0.016	0.556	**0.009**	**0.016**	0.487	0.355
T_{LE} (µm)	0.792	0.243	0.859	0.384	0.052	0.504	0.155
T_{MES} (µm)	0.266	0.421	0.322	0.115	0.661	0.513	0.972
f_{ias} (%)	**0.004**	0.772	0.498	**0.016**	0.416	0.237	0.876
T_{cw} (µm)	0.089	0.604	0.639	0.158	0.391	**0.045**	0.207
T_{chl} (µm)	**0.002**	0.088	0.459	0.764	0.408	0.882	**0.035**
L_{chl} (µm)	0.115	0.125	0.944	**0.040**	0.433	0.234	0.201
L_{betchl} (µm)	0.809	0.651	0.940	0.117	0.795	0.119	0.943
T_{cyt} (µm)	0.538	**<0.001**	0.555	**0.045**	0.365	0.722	0.647
S_m (µm)	0.290	**0.049**	0.517	0.259	0.262	0.865	0.577
S_c (µm)	0.231	0.100	0.546	0.375	0.430	0.120	0.903
S_c/S_m (µm)	0.643	0.825	0.767	0.735	0.873	**0.023**	0.507
$g_{m\_anatomy}$	0.904	0.177	0.226	0.512	**0.007**	0.580	0.331

B. oleracea

	$_HCO_2$	HT	D	$_HCO_2$:HT	$_HCO_2$:D	HT:D	$_HCO_2$:HT:D
T_L (µm)	**0.045**	**0.022**	0.935	0.544	0.596	0.053	0.986
T_{UE} (µm)	0.079	**0.012**	0.583	0.826	0.192	**0.042**	0.837
T_{LE} (µm)	0.063	0.187	0.926	0.937	0.162	0.091	0.718
T_{MES_pal} (µm)	**0.049**	0.075	0.825	0.740	0.611	0.199	0.928
T_{MES_spo} (µm)	0.088	**0.008**	0.573	0.441	0.702	**0.006**	0.734
T_{MES} (µm)	**0.041**	**0.021**	0.944	0.589	0.838	**0.043**	0.942
f_{ias} (%)	0.887	0.081	0.639	0.134	0.116	0.242	0.658
T_{cw} (µm)	**<0.001**	**0.041**	0.386	**0.033**	**0.001**	**0.013**	0.354
T_{chl} (µm)	**0.011**	0.126	0.393	0.530	0.123	**0.004**	0.953
L_{chl} (µm)	0.792	0.628	0.314	0.891	0.956	0.673	0.226
L_{betchl} (µm)	**0.046**	0.565	0.537	0.331	0.659	0.141	0.255
T_{cyt} (µm)	0.661	0.741	0.222	0.476	0.508	**0.049**	0.870
S_m (µm)	0.614	0.474	0.210	**0.011**	0.997	0.173	0.094
S_c (µm)	0.788	0.824	0.315	**0.024**	0.526	0.719	0.668
S_c/S_m (µm)	0.254	0.321	0.711	0.573	0.096	0.073	0.060
$g_{m\_anatomy}$	**0.016**	0.964	0.836	**0.004**	0.081	**0.048**	0.550

9 GENERAL CONCLUSIONS

From the results presented in the Chapters 1, 2, 3 and 4, the following conclusion have been drawn to respond the General and Specific Objectives of this Thesis:

General Objective 4.1.1: To establish a GC-MS-based ^{13}C-positional isotopomer approach to improve the resolution of flux maps from ^{13}C-metabolic flux analysis (^{13}C-MFA).

Specific Objective 4.2.1: *To evaluate the accuracy and limitations of mass spectrometry-based ^{13}C-metabolic flux analysis (^{13}C-MFA) compared to ^{13}C-isotope labelling experiments (^{13}C-ILE) in assessing metabolic fluxes in plant primary metabolism.*

Conclusion 1: The enhancement of the atomic resolution of mass spectrometry-based ^{13}C-MFA offered more accurate metabolite fragment structure deciphering, a crucial step to ensure the precision of metabolic flux calculations and eliminate potential errors associated with ^{13}C-ILE.

Specific Objective 4.2.2: *To develop and validate an approach based on gas chromatography coupled to mass spectrometry (GC-MS) to obtain information on the ^{13}C-positional labeling in key metabolites of plant systems.*

Conclusion 2: The developed and validated GC-MS-based ^{13}C-positional isotopomer approach enables the determination of ^{13}C-positional labelling information in key metabolites of primary metabolism, which can provide detailed insights into metabolic pathways involved and their regulation.

Conclusion 3: The established approach can be integrated into existing GC-EI-MS-based ^{13}C-MFA methodologies without requiring experimental modifications, improving our understanding of plant metabolic networks compared to traditional methods.

Conclusion 4: The approach provides a way to explore ^{13}C-positional labelling in glucose, malate and glutamate. Our findings indicates that specific carbon atoms within glucose were identified to be preferentially labelled by photosynthesis and gluconeogenesis; gluconeogenesis and phosphoenolpyruvate carboxylase (PEPc)-mediated CO_2 assimilation into malate are activated in a manner not dependent on light conditions in guard cells, and mitochondrial thioredoxin system acts on restricting fluxes from glycolysis and PEPc towards glutamate during illuminated leaf conditions.

General Objective 4.1.2: To unveil the metabolic changes following PEPc-mediated CO_2 assimilation in dark-exposed guard cells as well as to identify those associated to the transition from dark-to-light condition.

Specific Objective 4.2.3: *To apply ^{13}C-MFA to investigate metabolic carbon fluxes in guard cells and leaves in response different light conditions, identifying redirected metabolic fluxes following phosphoenolpyruvate carboxylase (PEPc)-mediated CO_2 assimilation.*

Conclusion 5: Dark-exposed and illuminated guard cells shared most metabolic change responses, however, illumination induced greater alterations in the metabolic network structure of guard cells, leading to higher ^{13}C-enrichment in sugars and metabolites linked to the tricarboxylic acid (TCA) cycle.

Conclusion 6: PEPc-mediated CO_2 assimilation redirected gluconeogenesis and TCA cycle in the dark-exposed guard cells, at the same time, provides carbons for gluconeogenesis, TCA cycle, and glutamate synthesis, while previously stored malate and citrate are used to underpin specific metabolic requirements in illuminated guard cells.

General Objective 4.1.3: To investigate ecophysiological and metabolic responses of angiosperms and ferns subjected to conditions associated to the climate change scenario, such as increased CO_2, high temperatures and drought.

Specific Objective 4.2.4: *To evaluate the physiological, anatomical and metabolic responses of one fern and one angiosperm to climate change conditions, including drought, high temperatures and high CO_2 concentrations.*

Conclusion 7: Varied responses to the applied stress conditions were observed in *Nephrolepis exaltata* (fern) and *Brassica oleracea* (angiosperm). Leaf anatomical parameters exhibited slight changes under stress conditions in both species. *B. oleracea* showed significant physiological to high CO_2, regardless of high temperature and drought, in contrast to the fern which displayed minimal physiological responsiveness. Moreover, stress factors induced several changes in lipid and primary metabolite levels in *B. oleracea*, that were not observed in the fern. Overall, our results suggest differential impacts of climate change on these species, from distinct plant groups.

REFERENCES

ABADIE, C.; BATHELLIER, C.; TCHERKEZ, G. Carbon allocation to major metabolites in illuminated leaves is not just proportional to photosynthesis when gaseous conditions (CO_2 and O_2) vary. **New Phytologist**, v. 218, p. 94–106, 2018.

ABADIE, C.; LOTHIER, J.; BOEX-FONTVIEILLE, E.; CARROLL, A.; TCHERKEZ, G. Direct assessment of the metabolic origin of carbon atoms in glutamate from illuminated leaves using ^{13}C-NMR. **New Phytologist**, v. 216, p. 1079–1089, 2017.

ABADIE, C.; TCHERKEZ, G. In vivo phosphoenolpyruvate carboxylase activity is controlled by CO_2 and O_2 mole fractions and represents a major flux at high photorespiration rates. **New Phytologist**, v. 221, p. 1843–1852, 2019.

ADEBIYI, A. O.; JAZMIN, L. J.; YOUNG, J. D. ^{13}C-flux analysis of cyanobacterial metabolism. **Photosynthesis Research**, v. 126, p. 19–32, 2015.

ALLEN, D. K.; LIBOUREL, I. G. L.; SHACHAR-HILL, Y. Metabolic flux analysis in plants: coping with complexity. **Plant Journal**, v. 58, p. 1241–1257, 2009a.

ALLEN, D. K.; OHLROGGE, J. B.; SHACHAR-HILL, Y. The role of light in soybean seed filling metabolism. **Plant Journal**, v. 58, p. 220–234, 2009b.

ALONSO, A. P.; VAL, D. L.; SHACHAR-HILL, Y. Central metabolic fluxes in the endosperm of developing maize seeds and their implications for **Metabolic Engineering**. **Metabolic Engineering**, v. 13, p. 96–107, 2011.

ALSEEKH, S.; AHARONI, A.; BROTMAN, Y.; *et al*. Mass spectrometry-based metabolomics: a guide for annotation, quantification and best reporting practices. **Nature Methods**, v. 18, p. 747–756, 2021.

ANDO, E.; KINOSHITA, T. Red light-induced phosphorylation of plasma membrane H^+-ATPase in stomatal guard cells. **Plant Physiology**, v. 178, p. 838–849, 2018.

ANTONIEWICZ, M. R. Tandem mass spectrometry for measuring stable-isotope labeling. **Current Opinion in Biotechnology**, v. 24, p. 48–53, 2013a.

ANTONIEWICZ, M. R. ^{13}C metabolic flux analysis: Optimal design of isotopic labeling experiments. **Current Opinion in Biotechnology**, v. 24, p. 1116–1121, 2013b.

ANTONIEWICZ, M. R. Methods and advances in metabolic flux analysis: a mini-review. **Journal of Industrial Microbiology and Biotechnology**, v. 42, p. 317–325, 2015.

ANTONIEWICZ, M. R.; KELLEHER, J. K.; STEPHANOPOULOS, G. Accurate assessment of amino acid mass isotopomer distributions for metabolic flux analysis. **Analytical Chemistry**, v. 79, p. 7554–7559, 2007.

ANTUNES, W. C.; DALOSO, D. M.; PINHEIRO, D. P.; WILLIAMS, T. C. R.; LOUREIRO, M. E. Guard cell-specific down-regulation of the sucrose transporter SUT1 leads to improved

water use efficiency and reveals the interplay between carbohydrate metabolism and K^+ accumulation in the regulation of stomatal opening. **Environmental and Experimental Botany**, v. 135, p. 73–85, 2017.

ANTUNES, W. C.; PROVART, N. J.; WILLIAMS, T. C. R.; LOUREIRO, M. E. Changes in stomatal function and water use efficiency in potato plants with altered sucrolytic activity. **Plant, Cell and Environment**, v. 35, p. 747–759, 2012.

APELT, F.; BREUER, D.; OLAS, J. J.; *et al*. Circadian, carbon, and light control of expansion growth and leaf movement. **Plant Physiology**, v. 174, p. 1949–1968, 2017.

ARAÚJO, W. L.; NUNES-NESI, A.; NIKOLOSKI, Z.; SWEETLOVE, L. J.; FERNIE, A. R. Metabolic control and regulation of the tricarboxylic acid cycle in photosynthetic and heterotrophic plant tissues. **Plant, Cell and Environment**, v. 35, p. 1–21, 2012.

ARAÚJO, W. L.; NUNES-NESI, A.; OSORIO, S.; *et al*. Antisense inhibition of the iron-sulphur subunit of succinate dehydrogenase enhances photosynthesis and growth in tomato via an organic acid–mediated effect on stomatal aperture. **The Plant Cell**, v. 23, p. 600–627, 2011.

ARAÚJO, W. L.; TOHGE, T.; ISHIZAKI, K.; LEAVER, C. J.; FERNIE, A. R. Protein degradation - an alternative respiratory substrate for stressed plants. **Trends in Plant Science**, v. 16, p. 489–498, 2011.

ARAÚJO, W. L.; TROFIMOVA, L.; MKRTCHYAN, G.; *et al*. On the role of the mitochondrial 2-oxoglutarate dehydrogenase complex in amino acid metabolism. **Amino Acids**, v. 44, p. 683–700, 2013.

ARRIVAULT, S.; OBATA, T.; SZECÓWKA, M.; *et al*. Metabolite pools and carbon flow during C4 photosynthesis in maize: $^{13}CO_2$ labeling kinetics and cell type fractionation. **Journal of Experimental Botany**, v. 68, p. 283–298, 2017.

ASSENOV, Y.; RAMÍREZ, F.; SCHELHORN, S.-E.; LENGAUER, T.; ALBRECHT, M. Computing topological parameters of biological networks. **Bioinformatics**, v. 24, p. 282–284, 2008.

AU, J.; CHOI, J.; JONES, S. W.; VENKATARAMANAN, K. P. Parallel labeling experiments validate Clostridium acetobutylicum metabolic network model for ^{13}C-metabolic flux analysis. **Metabolic Engineering**, v. 26, p. 23–33, 2014.

AUBRY, S.; ARESHEVA, O.; REYNA-LLORENS, I.; SMITH-UNNA, R. D.; HIBBERD, J. M.; GENTY, B. A specific transcriptome signature for guard cells from the C4 plant Gynandropsis gynandra. **Plant Physiology**, v. 170, p. 1345–1357, 2016.

AULER, P. A.; FREIRE, F. B. S.; LIMA, V. F.; DALOSO, D. M. On the role of guard cells in sensing environmental signals and memorising stress periods. **Theoretical and Experimental Plant Physiology**, v. 34, p. 277–299, 2022.

BALOGH, G. *et al*. Key role of lipids in heat stress management. **FEBS Letters**, v. 587, p. 1970–1980, 2013.

BAKER, J. M. *et al*. A metabolomic study of substantial equivalence of field-grown genetically modified wheat. **Plant Biotechnology Journal**, v. 4, p. 381–392, 2006.

BALMANT, K. M. *et al*. Guard cell redox proteomics reveals a role of lipid transfer protein in plant defense. **Journal of Proteomics**, v. 242, p. 104247, 2021.

BALMER, Y. ***et al***. Thioredoxin links redox to the regulation of fundamental processes of plant mitochondria. **Proceedings of the National Academy of Sciences**, v. 101, p. 2642–2647, 2004.

BASU, S. *et al*. Systems biology sparse network modeling and metscape-based visualization methods for the analysis of large-scale metabolomics data. **Bioinformatics**, v. 33, p. 1545–1553, 2017.

BATES, G. W. *et al*. A comparative study of the Arabidopsis thaliana guard-cell transcriptome and its modulation by sucrose. **PLoS ONE**, v. 7, p. e49641, 2012.

BATISTA-SILVA, W. *et al*. The role of amino acid metabolism during abiotic stress release. **Plant, Cell and Environment**, v. 42, p. 1630–1644, 2019.

BAUER, H. *et al*. How do stomata sense reductions in atmospheric relative humidity? **Molecular Plant**, v. 6, p. 1703–1706, 2013.

BEYLOT, M. *et al*. Determination of the ^{13}C-labeling pattern of glucose by gas chromatography-mass spectrometry. **Analytical Biochemistry**, v. 212, p. 526–531, 1993.

BINO, R. J. *et al*. Potential of metabolomics as a functional genomics tool. **Trends in Plant Science**, v. 9, p. 418–425, 2004.

BIRD, I. F. *et al*. Affinity of RuBP carboxylases for carbon dioxide and inhibition of the enzymes by oxygen. **Journal of Experimental Botany**, v. 33, p. 1004–1013, 1982.

BOWYER, J. R.; LEEGOOD, R. C. Photosynthesis. In: Plant **Biochemistry**. Elsevier, 1997. p. 49-74.

BRODRIBB, T. J. *et al*. Evolution of stomatal responsiveness to CO_2 and optimization of water-use efficiency among land plants. **New Phytologist**, v. 183, p. 839–847, 2009.

BROWN, P. H.; OUTLAW, W. H. Effect of fusicoccin on dark 14CO2 fixation by Vicia faba guard-cell protoplasts. **Plant Physiology**, v. 70, p. 1700–1703, 1982.

BUCHANAN, B. B. The carbon (formerly dark) reactions of photosynthesis. **Photosynthesis Research**, v. 128, p. 215–217, 2016.

CAIRD, M. A.; RICHARDS, J. H.; DONOVAN, L. A. Nighttime stomatal conductance and transpiration in C3 and C4 plants. **Plant Physiology**, v. 143, p. 4–10, 2007.

CALDANA, C. *et al*. High-density kinetic analysis of the metabolomic and transcriptomic response of Arabidopsis to eight environmental conditions. The **Plant Journal**, v. 67, p. 869–884, 2011.

CÂNDIDO-SOBRINHO, S. A. *et al*. Metabolism-mediated mechanisms underpin the differential stomatal speediness regulation among ferns and angiosperms. **Plant, Cell & Environment**, v. 45, p. 296–311, 2022.

CAPORN, S. J. M. *et al*. Effects of long-term exposure to elevated CO_2 and increased nutrient supply on bracken (Pteridium aquilinum). **Functional Ecology**, v. 13, p. 107–115, 1999.

CARDOSO, L. L.; FREIRE, F. B. S.; DALOSO, D. M. Plant metabolic networks under stress: a multi-species/stress condition meta-analysis. **Journal of Soil Science and Plant Nutrition**, v. 23, p. 4–21, 2022.

CARRIQUÍ, M. *et al*. Diffusional limitations explain the lower photosynthetic capacity of ferns as compared with angiosperms in a common garden study. **Plant, Cell and Environment**, v. 38, p. 448–460, 2015.

CARRIQUÍ, M.; NADAL, M.; FLEXAS, J. Acclimation of mesophyll conductance and anatomy to light during leaf aging in Arabidopsis thaliana. **Physiologia Plantarum**, v. 172, p. 1894-1907, 2021.

CHAVES, M. M.; FLEXAS, J.; PINHEIRO, C. Photosynthesis under drought and salt stress: Regulation mechanisms from whole plant to cell. **Annals of Botany**, v. 103, p. 551–560, 2009.

CHEN, W. *et al*. Comparative and parallel genome-wide association studies for metabolic and agronomic traits in cereals. **Nature Communications**, v. 7, p. 12767, 2016.

CHEUNG, C. Y. M. *et al*. A diel flux balance model captures interactions between light and dark metabolism during day-night cycles in C3 and Crassulacean Acid Metabolism leaves. **Plant Physiology**, v. 165, p. 917–929, 2014a.

CHOI, J.; GROSSBACH, M. T.; ANTONIEWICZ, M. R. Measuring complete isotopomer distribution of aspartate using gas chromatography/tandem mass spectrometry. **Analytical Chemistry**, v. 84, p. 4628–4632, 2012.

CHONG, J. *et al*. MetaboAnalyst 4.0: Towards more transparent and integrative metabolomics analysis. **Nucleic Acids Research**, v. 46, p. W486–W494, 2018.

CHUNG, S. T.; CHACKO, S. K.; SUNEHAG, A. L.; HAYMOND, M. W. Measurements of gluconeogenesis and glycogenolysis: A methodological review. **Diabetes**, v. 64, p. 3996–4010, 2015.

CLARK, T. J. *et al*. Modeling plant metabolism: from network reconstruction to mechanistic models. **Annual Review of Plant Biology**, v. 71, p. 1–24, 2020.

CLEMENTE-MORENO, M. J. *et al*. The apoplastic antioxidant system and altered cell wall dynamics influence mesophyll conductance and the rate of photosynthesis. **Plant Journal**, v.

99, p. 1031–1046, 2019.

COCKBURN, W. Stomatal mechanism as the basis of the evolution of CAM and C4 photosynthesis. **Plant, Cell & Environment**, v. 6, p. 275–279, 1983.

CONDAMINE, F. L.; SILVESTRO, D.; KOPPELHUS, E. B.; ANTONELLI, A. The rise of angiosperms pushed conifers to decline during global cooling. **Proceedings of the National Academy of Sciences**, v. 117, p. 28867–28875, 2020.

CORNAH, J. E. *et al*. Lipid utilization, gluconeogenesis, and seedling growth in Arabidopsis mutants lacking the glyoxylate cycle enzyme malate synthase. **Journal of Biological Chemistry**, v. 279, p. 42916–42923, 2004.

COSTA, J. M. *et al*. Open all night long: the dark side of stomatal control. **Plant Physiology**, v. 167, p. 289–294, 2015.

DALOSO, D. M.; DOS ANJOS, L.; FERNIE, A. R. Roles of sucrose in guard cell regulation. **New Phytologist**, v. 211, p. 809–818, 2016a.

DALOSO, D. M. *et al*. Tobacco guard cells fix CO_2 by both Rubisco and PEPcase while sucrose acts as a substrate during light-induced stomatal opening. **Plant Cell and Environment**, v. 38, p. 2353–2371, 2015a.

DALOSO, D. M. *et al*. Metabolism within the specialized guard cells of plants. **New Phytologist**, v. 216, p. 1018–1033, 2017.

DALOSO, D. M. *et al*. Thioredoxin, a master regulator of the tricarboxylic acid cycle in plant mitochondria. **Proceedings of the National Academy of Sciences of the United States of America**, v. 112, p. E1392-400, 2015b.

DALOSO, D. M. *et al*. Guard cell-specific upregulation of sucrose synthase 3 reveals that the role of sucrose in stomatal function is primarily energetic. **New Phytologist**, v. 209, p. 1470–1483, 2016b.

DAS, K.; ROYCHOUDHURY, A. Reactive oxygen species (ROS) and response of antioxidants as ROS-scavengers during environmental stress in plants. **Frontiers in Environmental Science**, v. 2, p. 1–13, 2014.

DAUBERMANN, A. G. *et al*. Distinct metabolic flux modes through the tricarboxylic acid cycle in mesophyll and guard cells revealed by GC-MS-based ^{13}C-positional isotopomer analysis. **bioRxiv**, 2023.

DESAGE, M. *et al*. Positional isotopic analysis of ^{13}C-labelled glucose by mass spectrometry: Applications to the study of gluconeogenesis in liver cells. **Biomedical & Environmental Mass Spectrometry**, v. 18, p. 1010–1015, 1989.

DETHLOFF, F.; ORF, I.; KOPKA, J. Rapid in situ ^{13}C tracing of sucrose utilization in Arabidopsis sink and source leaves. **Plant Methods**, v. 13, p. 1–19, 2017.

DETTMER, K.; ARONOV, P. A.; HAMMOCK, B. D. Mass spectrometry-based

metabolomics. **Mass Spectrometry Reviews**, v. 26, p. 51–78, 2007.

DIXON, R.; STRACK, D. Phytochemistry meets genome analysis, and beyond. **Phytochemistry**, v. 62, p. 815–816, 2003.

DUNN, W. B. Current trends and future requirements for the mass spectrometric investigation of microbial, mammalian and plant metabolomes. **Physical Biology**, v. 5, p. 011001, 2008.

DUNNETT, C. W. A Multiple Comparison Procedure for Comparing Several Treatments with a Control. **Journal of the American Statistical Association**, v. 50, p. 1096–1121, 1955.

EASTMOND, P. J. *et al*. Arabidopsis uses two gluconeogenic gateways for organic acids to fuel seedling establishment. **Nature Communications**, v. 6, p. 1–8, 2015.

EISENREICH, W.; BACHER, A. Advances of high-resolution NMR techniques in the structural and metabolic analysis of plant biochemistry. **Phytochemistry**, v. 68, p. 2799–2815, 2007.

ERBAN, A. *et al*. Multiplexed profiling and data processing methods to identify temperature-regulated using gas chromatography coupled to mass spectrometry. In: HINCHA, D. K.; ZUTHER, E. (eds.). **Plant Cold Acclimation**. New York, NY: Humana Press, p. 203–239, 2020.

ESPINOZA, C. *et al*. Interaction with diurnal and circadian regulation results in dynamic metabolic and transcriptional changes during cold acclimation in Arabidopsis. **PLoS ONE**, v. 5, e14101, 2010.

EVANS, J. R.; KALDENHOFF, R.; GENTY, B.; TERASHIMA, I. Resistances along the CO_2 diffusion pathway inside leaves. **Journal of Experimental Botany**, v. 60, p. 2235–2248, 2009.

FÀBREGAS, N.; FERNIE, A. R. The metabolic response to drought. **Journal of Experimental Botany**, v. 70, p. 1077–1085, 2019.

FANG, C.; FERNIE, A. R.; LUO, J. Exploring the Diversity of Plant Metabolism. **Trends in Plant Science**, v. 24, p. 83–98, 2019.

FARQUHAR, G. D.; CAEMMERER, S.; BERRY, J. A. A biochemical model of photosynthetic CO_2 assimilation in leaves of C3 species. **Planta**, v. 149, p. 78-90, 1980.

FARQUHAR, G. D.; O'LEARY, M. H.; BERRY, J. A. On the relationship between carbon isotope discrimination and the intercellular carbon dioxide concentration in leaves. **Functional Plant Biology**, v. 9, p. 121-137, 1982.

FERNÁNDEZ-MARÍN, B. *et al*. How do vascular plants perform photosynthesis in extreme environments? An integrative ecophysiological and biochemical story. **The Plant Journal**, v. 101, p. 979–1000, 2020.

FERNIE, A. R. The future of metabolic phytochemistry: Larger numbers of metabolites, higher resolution, greater understanding. **Phytochemistry**, v. 68, p. 2861–2880, 2007.

FERNIE, A. R. *et al*. Recommendations for reporting metabolite data. **The Plant Cell**, v. 23, p. 2477–2482, 2011.

FERNIE, A. R.; MORGAN, J. A. Analysis of metabolic flux using dynamic labelling and metabolic modelling. **Plant, Cell and Environment**, v. 36, p. 1738–1750, 2013.

FERNIE, A. R.; SCHAUER, N. Metabolomics-assisted breeding: a viable option for crop improvement? **Trends in Genetics**, v. 25, p. 39–48, 2009.

FERNIE, A. R.; STITT, M. On the discordance of metabolomics with proteomics and transcriptomics: coping with increasing complexity in logic, chemistry, and network interactions scientific correspondence. **Plant Physiology**, v. 158, p. 1139–1145, 2012.

FERNIE, A. R.; TOHGE, T. The Genetics of Plant Metabolism. **Annual Review of Genetics**, v. 51, p. 287–310, 2017.

FERNIE, A. R. *et al*. Metabolite profiling: from diagnostics to systems biology. **Nature Reviews Molecular Cell Biology**, v. 5, p. 763–769, 2004.

FLEXAS, J. *et al*. Effects of drought on photosynthesis in grapevines under field conditions: an evaluation of stomatal and mesophyll limitations. **Functional Plant Biology**, v. 29, p. 461–471, 2002.

FLEXAS, J. *et al*. Photosynthesis limitations during water stress acclimation and recovery in the drought-adapted Vitis hybrid Richter-110 (V. berlandieri×V. rupestris). **Journal of Experimental Botany**, v. 60, p. 2361–2377, 2009.

FLEXAS, J. *et al*. Stomatal and mesophyll conductances to CO_2 in different plant groups: Underrated factors for predicting leaf photosynthesis responses to climate change? **Plant Science**, v. 226, p. 41–48, 2014.

FLEXAS, J.; KEELEY, J. E. Evolution of photosynthesis I: Basic leaf morphological traits and diffusion and photosynthetic structures. In: **Terrestrial Photosynthesis in a Changing Environment**, v. 24, p. 373–385, 2012.

FIEHN, O. Metabolomics - The link between genotypes and phenotypes. **Plant Molecular Biology**, v. 48, p. 155–171, 2002.

FIEHN, O. Extending the breadth of metabolite profiling by gas chromatography coupled to mass spectrometry. TrAC - **Trends in Analytical Chemistry**, v. 27, p. 261–269, 2008.

FIEHN, O. *et al*. Metabolite profiling for plant functional genomics. **Nature Biotechnology**, v. 18, p. 1157–1161, 2000.

FISCHER, R. Stomatal opening: role of potassium uptake by guard cells. **Science**, v. 160, p. 784–785, 1968.

FLOREZ-SARASA, I. *et al*. The lack of mitochondrial thioredoxin TRXo1 affects in vivo alternative oxidase activity and carbon metabolism under different light conditions. **Plant and**

Cell Physiology, v. 60, p. 2369–2381, 2019.

FLÜTSCH, S. *et al*. Glucose uptake to guard cells via STP transporters provides carbon sources for stomatal opening and plant growth. **EMBO Reports**, v. 21, p. 1–13, 2020a.

FLÜTSCH, S.; SANTELIA, D. Mesophyll-derived sugars are positive regulators of light-driven stomatal opening. **New Phytologist**, v. 230, p. 1754–1760, 2021.

FLÜTSCH, S. *et al*. Guard cell starch degradation yields glucose for rapid stomatal opening in Arabidopsis. **The Plant Cell**, v. 32, p. 2325–2344, 2020b.

FONSECA-PEREIRA, P. *et al*. Thioredoxin-mediated regulation of (photo)respiration and central metabolism. In: LAWSON, T. (ed.). **Journal of Experimental Botany**, v. 72, p. 5987–6002, 2021.

FRANKS, P. J.; BEERLING, D. J. Maximum leaf conductance driven by CO_2 effects on stomatal size and density over geologic time. **Proceedings of the National Academy of Sciences**, v. 106, p. 10343–10347, 2009.

FRANKS, P. J.; BRITTON-HARPER, Z. J. No evidence of general CO_2 insensitivity in ferns: one stomatal control mechanism for all land plants? **New Phytologist**, v. 211, p. 819–827, 2016.

FRANKS, P. J.; FARQUHAR, G. D. The mechanical diversity of stomata and its significance in gas-exchange control. **Plant Physiology**, v. 143, p. 78–87, 2007.

FRANKS, P. J. *et al*. New constraints on atmospheric CO_2 concentration for the Phanerozoic. **Geophysical Research Letters**, v. 41, p. 4685–4694, 2014.

FREIRE, F. B. S. *et al*. Mild reductions in guard cell sucrose synthase 2 expression leads to slower stomatal opening and decreased whole plant transpiration in Nicotiana tabacum L. **Environmental and Experimental Botany**, v. 184, p. 104370, 2021.

FUJITA, T. *et al*. Confirmation of mesophyll signals controlling stomatal responses by a newly devised transplanting method. **Functional Plant Biology**, v. 46, p. 467–481, 2019.

GAGO, J. *et al*. Photosynthesis optimized across land plant phylogeny. **Trends in Plant Science**, v. 24, p. 947–958, 2019.

GAGO, J. *et al*. Photosynthesis limitations in three fern species. **Physiologia Plantarum**, v. 149, p. 599–611, 2013.

GAGO, J. *et al*. The photosynthesis game is in the ‘inter-play’: Mechanisms underlying CO_2 diffusion in leaves. **Environmental and Experimental Botany**, v. 178, p. 104174, 2020.

GAGO, J. *et al*. Relationships of leaf net photosynthesis, stomatal conductance, and mesophyll conductance to primary metabolism: a multispecies meta-analysis approach. **Plant Physiology**, v. 171, p. 265–279, 2016.

GAGO, J. *et al*. Integrative field scale phenotyping for investigating metabolic components of

water stress within a vineyard. **Plant Methods**, v. 13, p. 90, 2017.

GARCIA, A.; BARBAS, C. Gas chromatography-mass spectrometry (GC-MS)-based metabolomics. In: **Methods in Molecular Biology** (Clifton, N.J.), v. 708, p. 191–204, 2011.

GAUTHIER, P. P. G. *et al*. In folio isotopic tracing demonstrates that nitrogen assimilation into glutamate is mostly independent from current CO_2 assimilation in illuminated leaves of Brassica napus. **New Phytologist**, v. 185, p. 988–999, 2010.

GENTY, B.; BRIANTAIS, J. M.; BAKER, N. R. The relationship between the quantum yield of photosynthetic electron transport and quenching of chlorophyll fluorescence. **Biochimica et Biophysica Acta - General Subjects**, v. 990, p. 87–92, 1989.

GIBON, Y. *et al*. Integration of metabolite with transcript and enzyme activity profiling during diurnal cycles in Arabidopsis rosettes. **Genome Biology**, v. 7, p. 76, 2006.

GONG, L. *et al*. Stomatal morphology and physiology explain varied sensitivity to abscisic acid across vascular plant lineages. **Plant Physiology**, v. 186, p. 782–797, 2021.

GOTOW, K.; TAYLOR, S.; ZEIGER, E. Photosynthetic carbon fixation in guard cell protoplasts of Vicia faba L. Evidence from radiolabel experiments. **Plant Physiology**, v. 86, p. 700–705, 1988.

GRANOT, D.; KELLY, G. Evolution of guard-cell theories: the story of sugars. **Trends in Plant Science**, v. 24, p. 507–518, 2019.

HAGEL, J. M.; FACCHINI, E. P. J. Plant metabolomics: analytical platforms and integration with functional genomics. **Phytochemistry**, v. 7, p. 479–497, 2008.

HALL, R. D. Plant metabolomics: from holistic hope, to hype, to hot topic. **New Phytologist**, v. 169, p. 453–468, 2006.

HALL, R. *et al*. Plant metabolomics: the missing link in functional genomics strategies. **The Plant Cell**, v. 14, p. 1437–1440, 2002.

HARLEY, P. C. *et al*. Theoretical considerations when estimating the mesophyll conductance to CO2 flux by analysis of the response of photosynthesis to CO_2. **Plant Physiology**, v. 98, p. 1429–1436, 1992.

HARRIS, B. J. *et al*. Phylogenomic evidence for the monophyly of bryophytes and the reductive evolution of stomata. **Current Biology**, v. 30, p. 2001–2012.e2, 2020.

HASSIOTOU, F. *et al*. Influence of leaf dry mass per area, CO_2, and irradiance on mesophyll conductance in sclerophylls. **Journal of Experimental Botany**, v. 60, p. 2303–2314, 2009.

HAWORTH, M. *et al*. Stomatal control as a driver of plant evolution. **Journal of Experimental Botany**, v. 62, p. 2419–2423, 2011.

HAWORTH, M. *et al*. Allocation of the epidermis to stomata relates to stomatal physiological control: Stomatal factors involved in the evolutionary diversification of the angiosperms and

development of amphistomaty. **Environmental and Experimental Botany**, v. 151, p. 55–63, 2018.

HAYAT, S. *et al*. Role of proline under changing environments: A review. **Plant Signaling & Behavior**, v. 7, p. 1456–1466, 2012.

HEATH, D. F. The interaction of glycolysis, gluconeogenesis and the tricarboxylic acid cycle in rat liver in vivo. **The Biochemical Journal**, v. 110, p. 337–362, 1968.

HEDRICH, R.; MARTEN, I. Malate-induced feedback regulation of plasma membrane anion channels could provide a CO_2 sensor to guard cells. **The EMBO Journal**, v. 12, p. 897–901, 1993.

HEDRICH, R.; RASCHKE, K.; STITT, M. A role for fructose 2,6-bisphosphate in regulating carbohydrate metabolism in guard cells. **Plant Physiology**, v. 79, p. 977–982, 1985.

HILLER, K.; METALLO, C. M. Profiling metabolic networks to study cancer metabolism. **Current Opinion in Biotechnology**, v. 24, p. 60–68, 2013.

HILLS, A. *et al*. OnGuard, a computational platform for quantitative kinetic modeling of guard cell physiology. **Plant Physiology**, v. 159, p. 1026–1042, 2012.

HINCHA, D. K.; ZUTHER, E.; HEYER, A. G. The preservation of liposomes by raffinose family oligosaccharides during drying is mediated by effects on fusion and lipid phase transitions. **Biochimica et Biophysica Acta - Biomembranes**, v. 1612, p. 172–177, 2003.

HIRAI, M. Y. *et al*. Integration of transcriptomics and metabolomics for understanding of global responses to nutritional stresses in Arabidopsis thaliana. **Proceedings of the National Academy of Sciences**, v. 101, p. 10205–10210, 2004.

HITE, D. R. C.; OUTLAW, W. H.; TARCZYNSKI, M. C. Elevated levels of both sucrose-phosphate synthase and sucrose synthase in Vicia guard cells indicate cell-specific carbohydrate interconversions. **Plant Physiology**, v. 101, p. 1217–1221, 1993.

HOAGLAND, D. R.; ARNON, D. I. The water-culture method for growing plants without soil. **California Agricultural Experiment Station Circular**, n. 347, p. 1–32, 1950.

HOHMANN-MARRIOTT, M. F.; BLANKENSHIP, R. E. Evolution of photosynthesis. **Annual Review of Plant Biology**, v. 62, p. 515–548, 2011.

HONG, J. *et al*. Plant metabolomics: an indispensable system biology tool for **Plant Science**. International Journal of Molecular Sciences, v. 17, p. 167, 2016.

HORRER, D. *et al*. Blue light induces a distinct starch degradation pathway in guard cells for stomatal opening. **Current Biology**, v. 26, p. 362–370, 2016.

HU, L.; WANG, Z.; HUANG, B. Diffusion limitations and metabolic factors associated with inhibition and recovery of photosynthesis from drought stress in a C3 perennial grass species. **Physiologia Plantarum**, v. 139, p. 93–106, 2010.

HUANG, C. N. *et al*. Estimating viability of plant protoplasts using double and single staining. **Protoplasma**, v. 135, p. 80–87, 1986.

HUEGE, J. *et al*. GC-EI-TOF-MS analysis of in vivo carbon-partitioning into soluble metabolite pools of higher plants by monitoring isotope dilution after $^{13}CO_2$ labelling. **Phytochemistry**, v. 68, p. 2258–2272, 2007.

HUMMEL, J. *et al*. Ultra performance liquid chromatography and high resolution mass spectrometry for the analysis of plant lipids. **Frontiers in Plant Science**, v. 2, p. 1–17, 2011.

INOUE, S.; KINOSHITA, T. Blue light regulation of stomatal opening and the plasma membrane H^+-ATPase. **Plant Physiology**, v. 174, p. 531–538, 2017.

IPCC. Climate Change 2022: Impacts, adaptation and vulnerability. Work Group II Contribution to the Sixth Assessment Report of the Intergovernmental Panel on Climate Change. Cambridge: **Cambridge University Press**, 2022. doi: 10.1017/9781009325844.Front.

ISHIHARA, H. *et al*. Quantifying protein synthesis and degradation in Arabidopsis by dynamic $^{13}CO_2$ labeling and analysis of enrichment in individual amino acids in their free pools and in protein. **Plant Physiology**, v. 168, p. 74–93, 2015.

JIN, E. S. *et al*. Comparison of [3,4-$^{13}C_2$]glucose to [6,6-$^{2}H_2$]glucose as a tracer for glucose turnover by nuclear magnetic resonance. **Magnetic Resonance in Medicine**, v. 53, p. 1479–1483, 2005.

JITRAPAKDEE, S. *et al*. Structure, mechanism and regulation of pyruvate carboxylase. **Biochemical Journal**, v. 413, p. 369–387, 2008.

JONGH, D. C. *et al*. Analysis of trimethylsilyl derivatives of carbohydrates by gas chromatography and mass spectrometry. **Journal of the American Chemical Society**, v. 91, p. 1728–1740, 1969.

JORDAN, B.; OGREN, L. T. Species variation in kinetic properties of Ribulose Carboxylase/Oxygenase. **Archives of Biochemistry and Biophysics**, v. 227, p. 425–433, 1983.

JORDAN, G. J. *et al*. Environmental adaptation in stomatal size independent of the effects of genome size. **New Phytologist**, v. 205, p. 608–617, 2015.

KARNOVSKY, A. *et al*. Metscape 2 bioinformatics tool for the analysis and visualization of metabolomics and gene expression data. **Bioinformatics**, v. 28, p. 373–380, 2012.

KARST, A. L.; LECHOWICZ, M. J. Are correlations among foliar traits in ferns consistent with those in the seed plants? **New Phytologist**, v. 173, p. 306–312, 2007.

KELLY, G. *et al*. Guard-cell hexokinase increases water-use efficiency under normal and drought conditions. **Frontiers in Plant Science**, v. 10, p. 1–12, 2019.

KELLY, G. *et al*. Hexokinase mediates stomatal closure. **Plant Journal**, v. 75, p. 977–988,

2013.

KENRICK, P.; CRANE, P. R. The origin and early evolution of plants on land. **Nature**, v. 389, p. 33–39, 1997.

KEUNEN, E. *et al*. Plant sugars are crucial players in the oxidative challenge during abiotic stress: Extending the traditional concept. **Plant, Cell and Environment**, v. 36, p. 1242–1255, 2013.

KIM, H. K.; CHOI, Y. H.; VERPOORTE, R. NMR-based metabolomic analysis of plants. **Nature Protocols**, v. 5, p. 536–549, 2010.

KINOSHITA, T. *et al*. Phot1 and phot2 mediate blue light regulation of stomatal opening. **Nature**, v. 414, p. 656–660, 2001.

KOLLA, V. A.; RAGHAVENDRA, A. S. Nitric oxide is a signaling intermediate during bicarbonate-induced stomatal closure in Pisum sativum. **Physiologia Plantarum**, v. 130, p. 91–98, 2007.

KOPKA, J. *et al*. Metabolite profiling in plant biology: platforms and destinations. **Genome Biology**, v. 5, p. 1–9, 2004.

KOPKA, J. *et al*. GMD@CSB.DB: The Golm metabolome database. **Bioinformatics**, v. 21, p. 1635–1638, 2005.

KOPKA, J. *et al*. Systems analysis of ethanol production in the genetically engineered cyanobacterium Synechococcus sp. PCC 7002. **Biotechnology for Biofuels**, v. 10, p. 1–21, 2017.

KOTTAPALLI, J. *et al*. Sucrose-induced stomatal closure is conserved across evolution. **PLoS ONE**, v. 13, p. 1–17, 2018.

KRISHNAN, P.; KRUGER, N. J.; RATCLIFFE, R. G. Metabolite fingerprinting and profiling in plants using NMR. **Journal of Experimental Botany**, v. 56, p. 255–265, 2005.

KRUGER, N. J.; RATCLIFFE, R. G. Whither metabolic flux analysis in plants? **Journal of Experimental Botany**, v. 72, p. 7653–7657, 2021.

KUMAR, M. *et al*. Metabolomics and molecular approaches reveal drought stress tolerance in plants. **International Journal of Molecular Sciences**, v. 22, 2021.

KUSANO, M. *et al*. Metabolomics reveals comprehensive reprogramming involving two independent metabolic responses of Arabidopsis to UV-B light. **The Plant Journal**, v. 67, p. 354–369, 2011.

LAWRENCE, S. R. *et al*. S-nitroso-proteome revealed in stomatal guard cell response to flg22. **International Journal of Molecular Sciences**, v. 21, p. 1688, 2020.

LAWSON, T. Guard cell photosynthesis and stomatal function. **New Phytologist**, v. 181, p. 13–34, 2009.

LAWSON, T.; BLATT, M. R. Stomatal size, speed, and responsiveness impact on photosynthesis and water use efficiency. **Plant Physiology**, v. 164, p. 1556–1570, 2014.

LAWSON, T.; MATTHEWS, J. Guard Cell Metabolism and Stomatal Function. **Annual Review of Plant Biology**, v. 71, p. 273–302, 2020.

LAWSON, T. *et al*. Mesophyll photosynthesis and guard cell metabolism impacts on stomatal behaviour. **New Phytologist**, v. 203, p. 1064–1081, 2014.

LEE, K. *et al*. Metabolic flux analysis: A powerful tool for monitoring tissue function. **Tissue Engineering**, v. 5, p. 347–368, 1999.

LEEGOOD, R. C.; AP REES, T. Dark fixation of CO_2 during gluconeogenesis by the cotyledons of Cucurbita pepo L. **Planta**, v. 140, p. 275–282, 1978.

LEHMANN, M. *et al*. The metabolic response of Arabidopsis roots to oxidative stress is distinct from that of heterotrophic cells in culture and highlights a complex relationship between the levels of transcripts, metabolites, and flux. **Molecular Plant**, v. 2, p. 390–406, 2009.

LEIMER, K. R.; RICE, R. H.; GEHRKE, C. W. Complete mass spectra of the per-trimethylsilylated amino acids. **Journal of Chromatography A**, v. 141, p. 355–375, 1977.

LIM, S. L. *et al*. Arabidopsis guard cell chloroplasts import cytosolic ATP for starch turnover and stomatal opening. **Nature Communications**, v. 13, p. 1–13, 2022.

LIMA, V. F. *et al*. The sucrose-to-malate ratio correlates with the faster CO_2 and light stomatal responses of angiosperms compared to ferns. **New Phytologist**, v. 223, p. 1873–1887, 2019.

LIMA, V. F. *et al*. Establishment of a GC-MS-based ^{13}C-positional isotopomer approach suitable for investigating metabolic fluxes in plant primary metabolism. **The Plant Journal**, v. 108, p. 1213–1233, 2021.

LIMA, V. F.; DE SOUZA, L. P.; WILLIAMS, T. C. R.; FERNIE, A. R.; DALOSO, D. M. Gas Chromatography–Mass Spectrometry-Based ^{13}C-Labeling Studies in Plant Metabolomics. In: **Plant Metabolomics: Methods and Protocols**. 2018. p. 47–58.

LISEC, J. *et al*. Gas chromatography mass spectrometry-based metabolite profiling in plants. **Nature Protocols**, v. 1, p. 387–396, 2006.

LIU, M. Y. *et al*. Lipidomics analysis unravels the effect of nitrogen fertilization on lipid metabolism in tea plant (Camellia sinensis L.). **BMC Plant Biology**, v. 17, p. 1–10, 2017.

LIU, Z. *et al*. Drivers of metabolic diversification: how dynamic genomic neighbourhoods generate new biosynthetic pathways in the Brassicaceae. **New Phytologist**, v. 227, p. 1109–1123, 2020.

LIU, L. *et al*. Integration of transcriptome and metabolome analyses reveals key lodging-

resistance-related genes and metabolic pathways in maize. **Frontiers in Genetics**, v. 13, p. 1–15, 2022.

LIU, X. *et al*. Plant lipid remodeling in response to abiotic stresses. **Environmental and Experimental Botany**, v. 165, p. 174–184, 2019.

LLOYD, F. E. The physiology of stomata. **Publications of the Carnegie Institution of Washington**, v. 82, p. 1–42, 1908.

LOBELL, D. B.; GOURDJI, S. M. The influence of climate change on global crop productivity. **Plant Physiology**, v. 160, p. 1686–1697, 2012.

LOBO, A. K. M. *et al*. Physiological and molecular responses of woody plants exposed to future atmospheric CO_2 levels under abiotic stresses. **Plants**, v. 11, p. 1880, 2022.

LONIEN, J.; SCHWENDER, J. Analysis of metabolic flux phenotypes for two Arabidopsis mutants with severe impairment in seed storage lipid synthesis. **Plant Physiology**, v. 151, p. 1617–1634, 2009.

LU, J. *et al*. The role of triacylglycerol in plant stress response. **Plants**, v. 9, p. 472, 2020.

LUEDERMANN, A. *et al*. TagFinder for the quantitative analysis of gas chromatography-mass spectrometry (GC-MS)-based metabolite profiling experiments. **Bioinformatics**, v. 24, p. 732–737, 2008.

LUGASSI, N. *et al*. Expression of Arabidopsis hexokinase in citrus guard cells controls stomatal aperture and reduces transpiration. **Frontiers in Plant Science**, v. 6, p. 1–11, 2015.

LUO, J. Metabolite-based genome-wide association studies in plants. **Current Opinion in Plant Biology**, v. 24, p. 31–38, 2015.

MA, F. *et al*. Isotopically nonstationary ^{13}C flux analysis of changes in Arabidopsis thaliana leaf metabolism due to high light acclimation. **Proceedings of the National Academy of Sciences of the United States of America**, v. 111, p. 16967–16972, 2014.

MA, A.; QI, X. Mining plant metabolomes: Methods, applications, and perspectives. **Plant Communications**, v. 2, p. 100238, 2021.

MCADAM, S. A. M.; BRODRIBB, T. J. Fern and lycophyte guard cells do not respond to endogenous abscisic acid. **The Plant Cell**, v. 24, p. 1510–1521, 2012.

MACLEOD, J. K.; FLANIGAN, I. L.; WILLIAMS, J. F.; GRANT COLLINS, J. Mass spectrometric studies of the path of carbon in photosynthesis: Positional isotopic analysis of ^{13}C-labelled C4 to C7 sugar phosphates. **Journal of Mass Spectrometry**, v. 36, p. 500–508, 2001.

MAIER, K.; HOFMANN, U.; REUSS, M.; MAUCH, K. Identification of metabolic fluxes in hepatic cells from transient ^{13}C-labeling experiments: Part II. Flux Estimation. **Biotechnology and Bioengineering**, v. 100, p. 355–370, 2008.

MALTESE, F.; VERPOORTE, R. Metabolomics: Novel tool for studying complex biological systems. In: **Techniques in Crop Improvement**. p. 493–510, 2010.

MARTINS, M. C. M.; HEJAZI, M.; FETTKE, J.; *et al*. Feedback inhibition of starch degradation in Arabidopsis leaves mediated by trehalose 6-phosphate. **Plant Physiology**, v. 163, p. 1142–1163, 2013.

MATTHEWS, J. S. A.; VIALET-CHABRAND, S.; LAWSON, T. Role of blue and red light in stomatal dynamic behaviour. **Journal of Experimental Botany**, v. 71, p. 2253–2269, 2020.

MCLACHLAN, D. H.; LAN, J.; GEILFUS, C. M.; *et al*. The breakdown of stored triacylglycerols is required during light-induced stomatal opening. **Current Biology**, v. 26, p. 707–712, 2016.

MEDEIROS, D. B.; DA LUZ, L. M.; DE OLIVEIRA, H. O.; ARAÚJO, W. L.; DALOSO, D. M.; FERNIE, A. R. Metabolomics for understanding stomatal movements. **Theoretical and Experimental Plant Physiology**, v. 9, p. 91–102, 2019.

MEDEIROS, D. B.; MARTINS, S. C. V.; CAVALCANTI, J. H. F.; DALOSO, D. M.; MARTINOIA, E.; NUNES-NESI, A.; DAMATTA, F. M.; FERNIE, A. R.; ARAÚJO, W. L. Enhanced photosynthesis and growth in atquac1 knockout mutants are due to altered organic acid accumulation and an increase in both stomatal and mesophyll conductance. **Plant Physiology**, v. 170, p. 86–101, 2016.

MEDEIROS, D. B.; PEREZ SOUZA, L.; ANTUNES, W. C.; ARAÚJO, W. L.; DALOSO, D. M.; FERNIE, A. R. Sucrose breakdown within guard cells provides substrates for glycolysis and glutamine biosynthesis during light-induced stomatal opening. **The Plant Journal**, v. 94, p. 583–594, 2018.

MELZER, E.; O'LEARY, M. H. Anapleurotic CO_2 fixation by phosphoenolpyruvate carboxylase in C3 Plants. **Plant Physiology**, v. 84, p. 58–60, 1987.

MENGIN, V.; PYL, E. T.; ALEXANDRE MORAES, T.; SULPICE, R.; KROHN, N.; ENCKE, B.; STITT, M. Photosynthate partitioning to starch in Arabidopsis thaliana is insensitive to light intensity but sensitive to photoperiod due to a restriction on growth in the light in short photoperiods. **Plant, Cell & Environment**, v. 40, p. 2608–2627, 2017.

MERRITT, M. E.; HARRISON, C.; SHERRY, A. D.; MALLOY, C. R.; BURGESS, S. C. Flux through hepatic pyruvate carboxylase and phosphoenolpyruvate carboxykinase detected by hyperpolarized ^{13}C magnetic resonance. **Proceedings of the National Academy of Sciences**, v. 108, p. 19084–19089, 2011.

MISRA, B. B. New software tools, databases, and resources in metabolomics: updates from 2020. **Metabolomics**, v. 17, p. 49, 2021.

MITTLER, R.; VANDERAUWERA, S.; SUZUKI, N.; MILLER, G.; TOGNETTI, V. B.; VANDEPOELE, K.; GOLLERY, M.; SHULAEV, V.; VAN BREUSEGEM, F. ROS signaling: The new wave? **Trends in Plant Science**, v. 16, p. 300–309, 2011.

MØLLER, I. M.; IGAMBERDIEV, A. U.; BYKOVA, N. V.; FINKEMEIER, I.; RASMUSSON, A. G.; SCHWARZLÄNDER, M. Matrix redox physiology governs the regulation of plant mitochondrial metabolism through posttranslational protein modifications. **The Plant Cell**, v. 32, p. 573–594, 2020.

MORALES, F.; PASCUAL, I.; SÁNCHEZ-DÍAZ, M.; AGUIRREOLEA, J.; IRIGOYEN, J. J.; GOICOECHEA, N.; ANTOLÍN, M. C.; OYARZUN, M.; URDIAIN, A. Methodological advances: Using greenhouses to simulate climate change scenarios. **Plant Science**, v. 226, p. 30–40, 2014.

MOREIRA, T. B.; SHAW, R.; LUO, X.; GANGULY, O.; KIM, H. S.; COELHO, L. G. F.; CHEUNG, C. Y. M.; WILLIAMS, T. C. R. A genome-scale metabolic model of soybean (Glycine max) highlights metabolic fluxes in seedlings. **Plant Physiology**, v. 180, p. 1912–1929, 2019.

MOTT, K. A. Opinion: Stomatal responses to light and CO_2 depend on the mesophyll. **Plant, Cell & Environment**, v. 32, p. 1479–1486, 2009.

MOXLEY, J. F.; JEWETT, M. C.; ANTONIEWICZ, M. R.; *et al*. Linking high-resolution metabolic flux phenotypes and transcriptional regulation in yeast modulated by the global regulator Gcn4p. **Proceedings of the National Academy of Sciences**, v. 106, p. 6477–6482, 2009.

MUELLER, D.; HEINZLE, E. Stable isotope-assisted metabolomics to detect metabolic flux changes in mammalian cell cultures. **Current Opinion in Biotechnology**, v. 24, p. 54–59, 2013.

NI, D. A. Role of vacuolar invertase in regulating Arabidopsis stomatal opening. **Acta Physiologiae Plantarum**, v. 34, p. 2449–2452, 2012.

NICHOLSON, J. K.; LINDON, J. C. Metabonomics. **Nature**, v. 455, p. 1054–1056, 2008.

NIELSEN, J.; KEASLING, J. D. Engineering Cellular Metabolism. **Cell**, v. 164, p. 1185–1197, 2016.

NIETZEL, T.; MOSTERTZ, J.; RUBERTI, C.; *et al*. Redox-mediated kick-start of mitochondrial energy metabolism drives resource-efficient seed germination. **Proceedings of the National Academy of Sciences of the United States of America**, v. 117, p. 741–751, 2020.

NIINEMETS, Ü.; CESCATTI, A.; RODEGHIERO, M.; TOSENS, T. Leaf internal diffusion conductance limits photosynthesis more strongly in older leaves of Mediterranean evergreen broad-leaved species. **Plant, Cell and Environment**, v. 28, p. 1552–1566, 2005.

NUNES-NESI, A.; ARAÚJO, W. L.; OBATA, T.; FERNIE, A. R. Regulation of the mitochondrial tricarboxylic acid cycle. **Current Opinion in Plant Biology**, v. 16, p. 335–343, 2013.

NUNES-NESI, A. *et al*. Deficiency of mitochondrial fumarase activity in tomato plants impairs photosynthesis via an effect on stomatal function. **Plant Journal**, v. 50, p. 1093–

1106, 2007.

OBATA, T.; FERNIE, A. R. The use of metabolomics to dissect plant responses to abiotic stresses. **Cellular and Molecular Life Sciences**, v. 69, p. 3225–3243, 2012.

O'LEARY, B.; PARK, J.; PLAXTON, W. C. The remarkable diversity of plant PEPC (phosphoenolpyruvate carboxylase): recent insights into the physiological functions and post-translational controls of non-photosynthetic PEPCs. **Biochemical Journal**, v. 436, p. 15–34, 2011.

O'LEARY, B.; PLAXTON, W. C. Multifaceted functions of post-translational enzyme modifications in the control of plant glycolysis. **Current Opinion in Plant Biology**, v. 55, p. 28–37, 2020.

OKAHASHI, N. *et al*. Fragmentation of dicarboxylic and tricarboxylic acids in the Krebs Cycle using GC-EI-MS and GC-EI-MS/MS. **Mass Spectrometry**, v. 8, p. A0073–A0073, 2019.

OKAZAKI, Y.; SAITO, K. Recent advances of metabolomics in plant biotechnology. **Plant Biotechnology Reports**, v. 6, p. 1–15, 2012.

OUTLAW, W. H. Integration of cellular and physiological functions of guard cells. **Critical Reviews in Plant Science**s, v. 22, p. 503–5229, 2003.

OUTLAW, W. H.; KENNEDY, J. Enzymic and substrate basis for the anaplerotic step in guard cells. **Plant Physiology**, v. 62, p. 648–652, 1978.

OUTLAW, W. H.; LOWRY, O. H. Organic acid and potassium accumulation in guard cells during stomatal opening. **Plant Physiology**, v. 74, p. 4434–4438, 1977.

OUTLAW, W. H.; MANCHESTER, J. Guard cell starch concentration quantitatively related to stomatal aperture. **Plant Physiology**, v. 64, p. 79–82, 1979.

OUTLAW, W. H. *et al*. Photosynthetic carbon reduction pathway is absent in chloroplasts of Vicia faba guard cells. **Proceedings of the National Academy of Sciences of the United States of America**, v. 76, p. 6371–6375, 1979.

PEGUERO-PINA, J. J. *et al*. Leaf anatomical properties in relation to differences in mesophyll conductance to CO_2 and photosynthesis in two related Mediterranean Abies species. **Plant, Cell and Environment**, v. 35, p. 2121–2129, 2012.

PENFIELD, S. *et al*. Expression and manipulation of PHOSPHOENOLPYRUVATE CARBOXYKINASE 1 identifies a role for malate metabolism in stomatal closure. **Plant Journal**, v. 69, p. 679–688, 2012.

PENFIELD, S. *et al*. Reserve mobilization in the Arabidopsis endosperm fuels hypocotyl elongation in the dark, is independent of abscisic acid, and requires phosphoenolpyruvate carboxykinase1. **Plant Cell**, v. 16, p. 2705–2718, 2004.

PERERA-CASTRO, A.; FLEXAS, J. The ratio of electron transport to assimilation

(ETR/AN): underutilized but essential for assessing both equipment's proper performance and plant status. **Planta**, v. 257, p. 29, 2023.

PEREZ DE SOUZA, L.; ALSEEKH, S.; NAAKE, T.; FERNIE, A. Mass spectrometry-based untargeted plant metabolomics. **Current Protocols in Plant Biology**, v. 4, p. e20100, 2019.

PETERSSON, G. Mass spectrometry of hydroxy dicarboxylic acids as trimethylsilyl derivatives. Rearrangement fragmentations. **Organic Mass Spectrometry**, v. 6, p. 565–576, 1972.

PICHERSKY, E.; LEWINSOHN, E. Convergent evolution in plant specialized metabolism. **Annual Review of Plant Biology**, v. 62, p. 549–566, 2011.

PORTER, A. S. *et al*. Evolutionary differences in $\Delta^{13}C$ detected between spore and seed bearing plants following exposure to a range of atmospheric O_2 ratios; implications for paleoatmosphere reconstruction. **Geochimica et Cosmochimica Acta**, v. 213, p. 517–533, 2017.

PORTO, N. P. *et al*. Thioredoxins regulate the metabolic fluxes throughout the tricarboxylic acid cycle and associated pathways in a light-independent manner. **Plant Physiology** and Biochemistry, v. 193, p. 36–49, 2022.

POTT, D.; OSORIO, S.; VALLARINO, J. G. From central to specialized metabolism: an overview of some secondary compounds derived from the primary metabolism for their role in conferring nutritional and organoleptic characteristics to fruit. **Frontiers in Plant Science**, v. 10, p. 835, 2019.

PRAMAI, P.; ASHIKIN, N.; HAMID, A.; MEDIANI, A. Metabolite profiling, antioxidant, and α-glucosidase inhibitory activities of germinated rice: nuclear magnetic resonance-based metabolomics study. **Journal of Food and Drug Analysis**, v. 26, p. 47–57, 2017.

PRINS, H. B. A.; SNEL, J. F. H.; HELDER, R. J.; ZANSTRA, P. E. Photosynthetic HCO3− Utilization and OH− excretion in aquatic angiosperms. **Plant Physiology**, v. 66, p. 818–822, 1980.

PROCTOR, M. C. F.; TUBA, Z. Poikilohydry and homoihydry: Antithesis or spectrum of possibilities? **New Phytologist**, v. 156, p. 327–349, 2002.

PRYER, K. M. *et al*. Phylogeny and evolution of ferns (monilophytes) with a focus on the early leptosporangiate divergences. **American Journal of Botany**, v. 91, p. 1582–1598, 2004.

PUTRI, S. P. *et al*. Current metabolomics: Practical applications. **Journal of Bioscience and Bioengineering**, v. 115, p. 579–589, 2012.

RAGHAVENDRA, A. S.; GONUGUNTA, V. K.; CHRISTMANN, A.; GRILL, E. ABA perception and signalling. **Trends in Plant Science**, v. 15, p. 395–401, 2010.

RANSON, S. L.; THOMAS, M. Crassulacean Acid Metabolism. **Annual Review of Plant Physiology**, v. 11, p. 81–110, 1960.

RASCHKE, K.; DITTRICH, P. [^{14}C]Carbon-dioxide fixation by isolated leaf epidermes with stomata closed or open. **Planta**, v. 134, p. 69–75, 1977.

RATCLIFFE, R. G.; SHACHAR-HILL, Y. Measuring multiple fluxes through plant metabolic networks. **Plant Journal**, v. 45, p. 490–511, 2006.

REID, E. E.; THOMPSON, P.; LYTTLE, C. R.; DENNIS, D. T. Pyruvate dehydrogenase complex from higher plant mitochondria and proplastids. **Plant Physiology**, v. 59, p. 854–858, 1977.

REINHOLDT, O. *et al*. Redox-regulation of photorespiration through mitochondrial thioredoxin o1. **Plant Physiology**, v. 181, p. 442–457, 2019.

RESCO DE DIOS, V. *et al*. Assessing the potential functions of nocturnal stomatal conductance in C3 and C4 plants. **New Phytologist**, v. 223, p. 1696–1706, 2019.

RICROCH, E.; BERGE, J. B.; KUNTZ, M. Evaluation of genetically engineered crops using transcriptomic, proteomic, and metabolomic profiling techniques. **Plant Physiology**, v. 155, p. 1752–1761, 2011.

RIPPLE, W. J. *et al*. World scientists' warning of a climate emergency 2021. **Bioscience**, v. 71, p. 894–898, 2021.

RITTE, G. *et al*. Rates of sugar uptake by guard cell protoplasts of Pisum sativum L. related to the solute requirement for stomatal opening. **Plant Physiology**, v. 121, p. 647–656, 1999.

ROBAINA-ESTÉVEZ, S. *et al*. Resolving the central metabolism of Arabidopsis guard cells. **Scientific Reports**, v. 7, p. 1–13, 2017.

ROBREDO, A. *et al*. Elevated CO_2 alleviates the impact of drought on barley improving water status by lowering stomatal conductance and delaying its effects on photosynthesis. **Environmental and Experimental Botany**, v. 59, p. 252–263, 2007.

ROBREDO, A. *et al*. Influence of water stress on photosynthetic characteristics in barley plants under ambient and elevated CO_2 concentrations. **Biologia Plantarum**, v. 54, p. 285–292, 2010.

ROESSNER, U.; BOWNE, J. What is metabolomics all about? **BioTechniques**, v. 46, p. 363–365, 2009.

ROESSNER, U. *et al*. Metabolic profiling allows comprehensive phenotyping of genetically or environmentally modified plant systems. **Plant Cell**, v. 13, p. 11–29, 2001.

RUZANSKI, C. *et al*. A bacterial glucanotransferase can replace the complex maltose metabolism required for starch to sucrose conversion in leaves at night. **Journal of Biological Chemistry**, v. 288, p. 28581–28598, 2013.

RYLOTT, E. L.; GILDAY, A. D.; GRAHAM, I. A. The gluconeogenic enzyme phosphoenolpyruvate carboxykinase in Arabidopsis is essential for seedling establishment.

Plant Physiology, v. 131, p. 1834–1842, 2003.

SAITO, K.; MATSUDA, F. Metabolomics for functional genomics, systems biology, and biotechnology. **Annual Review of Plant Biology**, v. 61, p. 463–489, 2010.

SALACHNA, P.; PIECHOCKI, R. Salinity tolerance of four hardy ferns from the genus Dryopteris Adans grown under different light conditions. **Agronomy**, v. 11, p. 49, 2021.

SANTELIA, D.; LUNN, J. E. Transitory starch metabolism in guard cells: unique features for a unique function. **Plant Physiology**, v. 174, p. 539–549, 2017.

SAUER, U. High-throughput phenomics: experimental methods for mapping fluxomes. **Current Opinion in Biotechnology**, v. 15, p. 58–63, 2004.

SAUER, U.; EIKMANNS, B. J. The PEP-pyruvate-oxaloacetate node as the switch point for carbon flux distribution in bacteria. **FEMS Microbiology Reviews**, v. 29, p. 765–794, 2005.

SCAFARO, A. P. *et al*. Temperature response of mesophyll conductance in cultivated and wild Oryza species with contrasting mesophyll cell wall thickness. **Plant, Cell and Environment**, v. 34, p. 1999–2008, 2011.

SCHNABL, H. CO_2 and malate metabolism in starch-containing and starch-lacking guard-cell protoplasts. **Planta**, v. 149, p. 52–58, 1980.

SCHNEIDER, C. A.; RASBAND, W. S.; ELICEIRI, K. W. NIH Image to ImageJ: 25 years of image analysis. **Nature Methods**, v. 9, p. 671–675, 2012.

SCHUETTPELZ, E.; PRYER, K. M. Evidence for a Cenozoic radiation of ferns in an angiosperm-dominated canopy. **Proceedings of the National Academy of Sciences**, v. 106, p. 11200–11205, 2009.

SCHWAB, W. Metabolome diversity: too few genes, too many metabolites? **Phytochemistry**, v. 62, p. 837–849, 2003.

SCHWENDER, J.; OHLROGGE, J.; SHACHAR-HILL, Y. Understanding flux in plant metabolic networks. **Current Opinion in Plant Biology**, v. 7, p. 309–317, 2004.

SHANNON, P. *et al*. Cytoscape: a software environment for integrated models of biomolecular interaction networks. **Genome Research**, v. 13, p. 2498–2504, 2003.

SHARKEY, T. D.; BERNACCHI, C. J.; FARQUHAR, G. D.; SINGSAAS, E. L. Fitting photosynthetic carbon dioxide response curves for C3 leaves. **Plant, Cell and Environment**, v. 30, p. 1035–1040, 2007.

SHEEN, J.; ZHOU, L.; JANG, J. Sugars as signaling molecules. **Current Opinion in Plant Biology**, v. 2, p. 410–419, 1999.

SHEN, S. *et al*. Metabolomics-centered mining of plant metabolic diversity and function: Past decade and future perspectives. **Molecular Plant**, v. 16, p. 43–63, 2023.

SHIVA, S. *et al*. Leaf lipid alterations in response to heat stress of Arabidopsis thaliana. **Plants**, v. 9, p. 1–22, 2020.

SILVA, W. B. *et al*. Can stable isotope mass spectrometry replace radiolabelled approaches in metabolic studies? **Plant Science**, v. 249, p. 59–69, 2016.

SMITH, A. R. *et al*. A classification for extant ferns. **Taxon**, v. 55, p. 705–731, 2006.

SOUZA, L. P. de; FERNIE, A. R.; TOHGE, T. Carbon atomic survey for identification of selected metabolic fluxes. In: **PLANT METABOLOMICS: METHODS AND PROTOCOLS**. New York, 2018. p. 59–67.

STAAL, M.; ELZENGA, J. T. M.; PRINS, H. B. A. ^{14}C fixation by leaves and leaf cell protoplasts of the submerged aquatic angiosperm Potamogeton lucens: Carbon dioxide or bicarbonate? **Plant Physiology**, v. 90, p. 1035–1040, 1989.

STARK, R. *et al*. Phosphoenolpyruvate cycling via mitochondrial phosphoenolpyruvate carboxykinase links anaplerosis and mitochondrial GTP with insulin secretion. **Journal of Biological Chemistry**, v. 284, p. 26578–26590, 2009.

STITT, M. Fructose-2,6-bisphosphate as a regulatory molecule in plants. **Annual Review of Plant Physiology and Plant Molecular Biology**, v. 41, p. 153–185, 1990.

STITT, M.; FERNIE, A. R. From measurements of metabolites to metabolomics: an 'on the fly' perspective illustrated by recent studies of carbon – nitrogen interactions. **Current Opinion in Biotechnology**, v. 14, p. 136–144, 2003.

STOLL, S. Isotopomers and isotopologues: The History behind the confusion. **Chem. Educator,** v. 12, p. 1–3, 2007.

STREHMEL, N.; KOPKA, J.; SCHEEL, D.; BÖTTCHER, C. Annotating unknown components from GC/EI-MS-based metabolite profiling experiments using GC/APCI(+)-QTOFMS. **Metabolomics**, v. 10, p. 324–336, 2014.

SULPICE, R. *et al*. Arabidopsis coordinates the diurnal regulation of carbon allocation and growth across a wide range of photoperiods. **Molecular Plant**, v. 7, p. 137–155, 2014.

SULPICE, R.; MCKEOWN, P. C. Moving toward a comprehensive map of central plant metabolism. **Annual Review of Plant Biology**, v. 66, p. 187–212, 2015.

SUMNER, L. W. *et al*. Proposed minimum reporting standards for chemical analysis. **Journal of Proteome Research**, v. 6, p. 211–221, 2007.

SUSSMILCH, F. C.; SCHULTZ, J.; HEDRICH, R.; ROELFSEMA, M. R. G. Acquiring control: the evolution of stomatal signalling pathways. **Trends in Plant Science**, v. 24, p. 342–351, 2019.

SWEETLOVE, L. J.; FERNIE, A. R. The spatial organization of metabolism within The Plant Cell. **Annual Review of Plant Biology**, v. 64, p. 723–746, 2013.

SWEETLOVE, L. J. *et al*. Modelling metabolic CO_2 evolution - a fresh perspective on respiration. **Plant, Cell & Environment**, v. 36, p. 1631–1640, 2013.

SZECOWKA, M. *et al*. Metabolic fluxes in an illuminated Arabidopsis rosette. **The Plant Cell**, v. 25, p. 694–714, 2013.

SZYPERSKI, T. ^{13}C-NMR, MS and metabolic flux balancing in biotechnology research. **Quarterly Reviews of Biophysics**, v. 31, p. 41–106, 1998.

TALBOTT, L. D.; ZEIGER, E. Sugar and organic acid accumulation in guard cells of Vicia faba in response to red and blue light. **Plant Physiology**, v. 102, p. 1163–1169, 1993.

TALBOTT, L.; ZEIGER, E. The role of sucrose in guard cell osmoregulation. **Journal of Experimental Botany**, v. 49, p. 329–337, 1998.

TALLMAN, G.; ZEIGER, E. Light quality and osmoregulation in Vicia guard cells: evidence for involvement of three metabolic pathways. **Plant Physiology**, v. 88, p. 887–895, 1988.

TAN, X. L. J.; CHEUNG, C. Y. M. A multiphase flux balance model reveals flexibility of central carbon metabolism in guard cells of C3 plants. **The Plant Journal**, v. 104, p. 1648–1656, 2020.

TANG, M. *et al*. Arabidopsis guard cell CO_2/HCO_3^- Response mutant screening by an aequorin-based calcium imaging system. **Plant Methods**, v. 16, p. 1–10, 2020.

TCHERKEZ, G. *et al*. Respiratory carbon fluxes in leaves. **Current Opinion in Plant Biology**, v. 15, p. 308–314, 2012.

TCHERKEZ, G. *et al*. In vivo respiratory metabolism of illuminated leaves. **Plant Physiology**, v. 138, p. 1596–1606, 2005.

TCHERKEZ, G. *et al*. In folio respiratory fluxomics revealed by ^{13}C isotopic labeling and H/D isotope effects highlight the noncyclic nature of the tricarboxylic acid 'cycle' in illuminated leaves. **Plant Physiology**, v. 151, p. 620–630, 2009.

THAIN, J. F. Curvature correction factors in the measurement of cell surface areas in plant tissues. **Journal of Experimental Botany**, v. 34, p. 87–94, 1983.

TOMÁS, M. *et al*. Water-use efficiency in grapevine cultivars grown under controlled conditions: effects of water stress at the leaf and whole-plant level. **Australian Journal of Grape and Wine Research**, v. 18, p. 164–172, 2012.

TOMÁS, M. *et al*. Importance of leaf anatomy in determining mesophyll diffusion conductance to CO2 across species: Quantitative limitations and scaling up by models. **Journal of Experimental Botany**, v. 64, p. 2269–2281, 2013.

TOSENS, T. *et al*. Developmental changes in mesophyll diffusion conductance and photosynthetic capacity under different light and water availabilities in Populus tremula: how structure constrains function. **Plant, Cell & Environment**, v. 35, p. 839–856, 2012.

TOSENS, T. *et al*. The photosynthetic capacity in 35 ferns and fern allies: mesophyll CO2 diffusion as a key trait. **New Phytologist**, v. 209, p. 1576–1590, 2016.

TOVAR-MÉNDEZ, A.; MIERNYK, J. A.; RANDALL, D. D. Regulation of pyruvate dehydrogenase complex activity in plant cells. **European Journal of Biochemistry**, v. 270, p. 1043–1049, 2003.

VALENTINI, R.; GAMON, J. A.; FIELD, C. B. Ecosystem gas exchange in a California grassland: seasonal patterns and implications for scaling. **Ecology**, v. 76, p. 1940–1952, 1995.

VAVASSEUR, A.; RAGHAVENDRA, A. S. Guard cell metabolism and CO_2 sensing. **New Phytologist**, v. 165, p. 665–682, 2005.

VENEGAS-MOLINA, J. *et al*. Why and how to dig into plant metabolite – protein interactions. Trends in **Plant Science**, v. 26, p. 472–483, 2021.

VERBANCIC, J.; LUNN, J. E.; STITT, M.; PERSSON, S. Carbon supply and the regulation of cell wall synthesis. **Molecular Plant**, v. 11, p. 75–94, 2018.

VEROMANN-JURGENSON, L. L.; TOSENS, T.; LAANISTO, L.; NIINEMETS, Ü. Extremely thick cell walls and low mesophyll conductance: welcome to the world of ancient living! **Journal of Experimental Botany**, v. 68, p. 1639–1653, 2017.

VERSLUES, P. E.; JUENGER, T. E. Drought, metabolites, and Arabidopsis natural variation: a promising combination for understanding adaptation to water-limited environments. **Current Opinion in Plant Biology**, v. 14, p. 240–245, 2011.

VIALET-CHABRAND, S.; MATTHEWS, J. S. A.; LAWSON, T. Light, power, action! Interaction of respiratory energy- and blue light-induced stomatal movements. **New Phytologist**, v. 231, p. 2231–2246, 2021.

VITAL, R. G. *et al*. Metabolic, physiological and anatomical responses of soybean plants under water deficit and high temperature condition. **Scientific Reports**, v. 12, p. 16467, 2022.

WALKER, R. P. *et al*. Gluconeogenesis and nitrogen metabolism in maize. **Plant Physiology and Biochemistry**, v. 130, p. 324–333, 2018.

WANG, S. *et al*. The structure and function of major plant metabolite modifications. **Molecular Plant**, p. 899–919, 2019a.

WANG, Y.; HILLS, A.; BLATT, M. R. Systems analysis of guard cell membrane transport for enhanced stomatal dynamics and water use efficiency. **Plant Physiology**, v. 164, p. 1593–1599, 2014a.

WANG, S. W. *et al*. Lacking chloroplasts in guard cells of crumpled leaf attenuates stomatal opening: Both guard cell chloroplasts and mesophyll contribute to guard cell ATP levels. **Plant, Cell and Environment**, v. 37, p. 2201–2210, 2014b.

WANG, F. F. *et al*. Phytochrome B is involved in mediating red light-induced stomatal opening in Arabidopsis thaliana. **Molecular Plant**, v. 3, p. 246–259, 2010.

WANG, Y. *et al*. Overexpression of plasma membrane H^+-ATPase in guard cells promotes light-induced stomatal opening and enhances plant growth. **Proceedings of the National Academy of Sciences of the United States of America**, v. 111, p. 533–538, 2014c.

WANG, R. S. *et al*. Common and unique elements of the ABA-regulated transcriptome of Arabidopsis guard cells. **BMC Genomics**, v. 12, p. 216, 2011.

WANG, H. *et al*. A subsidiary cell-localized glucose transporter promotes stomatal conductance and photosynthesis. **The Plant Cell**, v. 31, p. 1328–1343, 2019b.

WATKINS, J. M.; CHAPMAN, J. M.; MUDAY, G. K. Abscisic acid-induced reactive oxygen species are modulated by flavonols to control stomatal aperture. **Plant Physiology**, v. 175, p. 1807–1825, 2017.

WATKINS, J. M. *et al*. Ethylene-induced flavonol accumulation in guard cells suppresses reactive oxygen species and moderates stomatal aperture. **Plant Physiology**, v. 164, p. 1707–1717, 2014.

WECKWERTH, W. *et al*. Differential metabolic networks unravel the effects of silent plant phenotypes. **Proceedings of the National Academy of Sciences of the United States of America**, v. 101, p. 7809–7814, 2004.

WENG, J. The evolutionary paths towards complexity: a metabolic perspective. **New Phytologist**, v. 201, p. 1141–1149, 2013.

WENG, J. *et al*. The rise of chemodiversity in plants. **Science**, v. 336, p. 1667–1670, 2014.

WIECHERT, W. 13C-Metabolic flux analysis. **Metabolic Engineering**, v. 3, p. 195–206, 2001.

WIELOCH, T. The next phase in the development of 13C isotopically non-stationary metabolic flux analysis. **Journal of Experimental Botany**, v. 72, p. 6087–6090, 2021.

WIELOCH, T. *et al*. Intramolecular 13C analysis of tree rings provides multiple plant ecophysiology signals covering decades. **Scientific Reports**, v. 8, p. 1–10, 2018.

WIELOCH, T.; SHARKEY, T. D.; WERNER, R. A.; SCHLEUCHER, J. Intramolecular carbon isotope signals reflect metabolite allocation in plants. **Journal of Experimental Botany**, v. 73, p. 2558–2575, 2022.

WIELOCH, T.; WERNER, R. A.; SCHLEUCHER, J. Carbon flux around leaf-cytosolic glyceraldehyde-3-phosphate dehydrogenase introduces a ^{13}C signal in plant glucose. **Journal of Experimental Botany**, v. 72, p. 7136–7144, 2021.

WILLIAMS, T. C. R. *et al*. Metabolic network fluxes in heterotrophic Arabidopsis cells: Stability of the flux distribution under different oxygenation conditions. **Plant Physiology**, v. 148, p. 704–718, 2008.

WILLMER, C. M.; DITTRICH, P. Carbon dioxide fixation by epidermal and mesophyll

tissues of Tulipa and Commelina. **Planta**, v. 117, p. 123–132, 1974.

WITTMANN, C. Metabolic flux analysis using mass spectrometry. In: **Tools and Applications of Biochemical Engineering Science**. v. 39, p. 39–64, 2001.

XIONG, D.; DOUTHE, C.; FLEXAS, J. Differential coordination of stomatal conductance, mesophyll conductance, and leaf hydraulic conductance in response to changing light across species. **Plant, Cell and Environment**, v. 41, p. 436–450, 2018.

XU, Y. *et al*. The metabolic origins of non-photorespiratory CO_2 release during photosynthesis: A metabolic flux analysis. **Plant Physiology**, v. 186, p. 297–314, 2021.

XU, Z.; JIANG, Y.; ZHOU, G. Response and adaptation of photosynthesis, respiration, and antioxidant systems to elevated CO_2 with environmental stress in plants. **Frontiers in Plant Science**, v. 6, p. 1–17, 2015.

XUE, S. *et al*. Central functions of bicarbonate in S-type anion channel activation and OST1 protein kinase in CO2 signal transduction in guard cell. **EMBO Journal**, v. 30, p. 1645–1658, 2011.

YEOH, H.; BADGER, M. R.; WATSON, L. Variations in kinetic properties of ribulose-1,5-bisphosphate carboxylases among plants. **Plant Physiology**, v. 2, p. 1151–1155, 1981.

YIOTIS, C.; EVANS-FITZGERALD, C.; MCELWAIN, J. C. Differences in the photosynthetic plasticity of ferns and Ginkgo grown in experimentally controlled low $[O_2]$:$[CO_2]$ atmospheres may explain their contrasting ecological fate across the Triassic-Jurassic mass extinction boundary. **Annals of Botany**, v. 119, p. 1385–1395, 2017.

YIOTIS, C.; MCELWAIN, J. C. A novel hypothesis for the role of photosynthetic physiology in shaping macroevolutionary patterns. **Plant Physiology**, v. 181, p. 1148–1162, 2019.

YOSHIDA, K.; HISABORI, T. Mitochondrial isocitrate dehydrogenase is inactivated upon oxidation and reactivated by thioredoxin-dependent reduction in Arabidopsis. **Frontiers in Environmental Science**, v. 2, p. 1–7, 2014.

YOSHIDA, K.; HISABORI, T. Adenine nucleotide-dependent and redox-independent control of mitochondrial malate dehydrogenase activity in Arabidopsis thaliana. **Biochimica et Biophysica Acta (BBA) - Bioenergetics**, v. 1857, p. 810–818, 2016.

YOU, L. *et al*. Involvement of abscisic acid, ABI5, and PPC2 in plant acclimation to low CO2. **Journal of Experimental Botany**, v. 71, p. 4093–4108, 2020.

YOUNG, J. D. Metabolic flux rewiring in mammalian cell cultures. **Current Opinion in Biotechnology**, v. 24, p. 1–8, 2013.

YUAN, H. *et al*. Development of a widely targeted volatilomics method for profiling volatilomes in plants. **Molecular Plant**, v. 15, p. 189–202, 2022.

ZAMBONI, N. 13C metabolic flux analysis in complex systems. **Current Opinion in Biotechnology**, v. 22, p. 103–108, 2011.

ZAMBONI, N.; FENDT, S.-M.; RÜHL, M.; SAUER, U. ^{13}C-based metabolic flux analysis. **Nature Protocols**, v. 4, p. 878–892, 2009.

ZANDALINAS, S. I. *et al*. Plant responses to climate change: Metabolic changes under combined abiotic stresses. **Journal of Experimental Botany**, v. 73, p. 3339–3354, 2022.

ZAYNAB, M. *et al*. Role of secondary metabolites in plant defense against pathogens. **Microbial Pathogenesis**, v. 124, p. 198–202, 2018.

ZEIGER, E.; TALBOTT, L. D.; FRECHILLA, S.; SRIVASTAVA, A.; ZHU, J. The guard cell chloroplast: A perspective for the twenty-first century. **New Phytologist**, v. 153, p. 415–424, 2002.

ZHANG, Y. *et al*. Two mitochondrial phosphatases, PP2c63 and Sal2, are required for posttranslational regulation of the TCA cycle in Arabidopsis. **Molecular Plant**, v. 14, p. 1104–1118, 2021.

ZHANG, X.; XU, Y.; HUANG, B. Lipidomic reprogramming associated with drought stress priming-enhanced heat tolerance in tall fescue (Festuca arundinacea). **Plant, Cell and Environment**, v. 42, p. 947–958, 2019.

ZHAO, Z.; ASSMANN, S. M. The glycolytic enzyme, phosphoglycerate mutase, has critical roles in stomatal movement, vegetative growth, and pollen production in Arabidopsis thaliana. **Journal of Experimental Botany**, v. 62, p. 5179–5189, 2011.

ZHAO, J.; WILLIAMS, C. C.; LAST, R. L. Induction of Arabidopsis tryptophan pathway enzymes and camalexin by amino acid starvation, oxidative stress, and an abiotic elicitor. **The Plant Cell**, v. 10, p. 359–370, 1998.

ZOONG LWE, Z. *et al*. Alterations in the leaf lipidome of Brassica carinata under high-temperature stress. **BMC Plant Biology**, v. 21, p. 1–15, 2021.

ANNEX A – LIST OF PUBLICATIONS

Publications derived from the present Thesis

This PhD Thesis is presented as a compendium of four manuscripts, either published or submitted to scientific journals:

1. **Lima VF** & Daloso DM. Mass spectrometry-based ^{13}C-metabolic flux analysis should go deeper at atomic level. Submitted to *Journal of Experimental Botany*.

2. **Lima VF**, Erban A, Daubermann AG, Freire FBS, Porto NP, Cândido-Sobrinho SA, Medeiros DB, Schwarzländer M, Fernie AR, dos Anjos L, Kopka J, Daloso, DM. (2021). Establishment of a GC-MS-based ^{13}C-positional isotopomer approach suitable for investigating metabolic fluxes in plant primary metabolism. *The Plant Journal*, 108(4), 1213-1233.

3. **Lima VF**, Freire FBS, Cândido-Sobrinho SA, Porto NP, Medeiros DB, Erban A, Kopka J, Schwarzländer M, Fernie AR, Daloso, DM. (2023). Unveiling the dark side of guard cell metabolism. *Plant Physiology and Biochemistry*, 107862.

4. **Lima VF***, Gago J*, Aranjuelo I, Brotman Y, Burgos A, Carriquí M, Fernie AR, Figueroa CM, Irigoyen JJ, Jáuregui I, Oyarzun M, Pascual I, Ribas-Carbo M, Sánchez-Díaz M, Santesteban H, Smirnova J, Urdiain A, Daloso DM, Morales F, Flexas J. The fern *Nephrolepis exaltata* is largely unresponsive to climate change conditions at physiological and metabolic levels. Submitted to *Journal of Experimental Botany*.

*Both authors contributed equally to this paper.

ANNEX B – PUBLISHED AND SUBMITTED ARTICLES DURING THE DOCTORATE PERIOD

Lima, V. F., Anjos, L. D., Medeiros, D. B., Cândido-Sobrinho, S. A., Souza, L. P., Gago, J., ... & Daloso, D. M. (2019). The sucrose-to-malate ratio correlates with the faster CO_2 and light stomatal responses of angiosperms compared to ferns. *New Phytologist*, *223*(4), 1873-1887.

Auler, P. A., Freire, F. B. S., Lima, V. F., & Daloso, D. M. (2022). On the role of guard cells in sensing environmental signals and memorising stress periods. *Theoretical and Experimental Plant Physiology*, *34*(3), 277-299.

Cândido-Sobrinho, S. A., Lima, V. F., Freire, F. B., de Souza, L. P., Gago, J., Fernie, A. R., & Daloso, D. M. (2022). Metabolism-mediated mechanisms underpin the differential stomatal speediness regulation among ferns and angiosperms. *Plant, Cell & Environment*, *45*(2), 296-311.

Daubermann, A. G.*, Lima, V. F.*, Schwarzländer, M., Erban, A., Kopka, J., Fernie, A. R., dos Anjos, L., Daloso, D. M. (2023). Distinct metabolic flux modes through the tricarboxylic acid cycle in mesophyll and guard cells revealed by GC-MS-based ^{13}C-positional isotopomer analysis. *Theoretical and Experimental Plant Physiology*, *submitted manuscript.*

Nadal M., Quintanilla L.G., Pons-Perpinyà, J., Lima, V.F., Gago, J., Aranda, I. (2023). Leaf structure and water relations of an allotetraploid Mediterranean fern and its diploid parents. *Physiologia Plantarum*, *submitted manuscript.*

Cândido-Sobrinho, S. A., Lima, V. F., & Daloso, D. M. (2019). Guard Cell Metabolism. *eLS*, 1-8. [Book chapter].

*Both authors contributed equally to this paper.